Université du Québec
Institut national de la recherche scientifique
Centre Eau-Terre-Environnement

Évaluation des effets de pompage sur la subsidence: une approche par des relevés de terrain, la télédétection et la modélisation numérique

(Pumping effects on land subsidence: assessment using field data, remote sensing and numerical modeling)

Par Angus I. Calderhead

Thèse présentée pour l'obtention du grade
de Philosophiae Doctor (Ph. D.)
en Sciences de la Terre et Environnement

Jury d'évaluation

Président de jury de thèse et examinateur interne :	Dr. Claudio Paniconi INRS-ETE
Examinateur externe :	Dr. David Rudolph The University of Waterloo
Examinateur externe :	Dr. Vern Singhroy Centre canadien de télédétection
Directeur de recherche :	Dr. Richard Martel INRS-ETE
Co-directeur de recherche :	Dr. Alfonso Rivera Commission géologique du Canada
Co-directeur de recherche :	Dr. Jaime Garfías Universidad Autónoma del Estado de México
Co-directeur de recherche :	Dr. René Therrien Université Laval

© droits réservés de *Angus Ian Calderhead*, 2009

Résumé

Dans plusieurs villes du monde (e.g. Venise, Las Vegas, Shanghai, Mexico), la surexploitation de l'eau souterraine entraîne la compaction de couches argileuses et crée de multiples problèmes dont l'effondrement des sols, des dommages importants aux infrastructures, et la création de fractures dans les sédiments en surface.

L'objectif de cette thèse est de présenter une méthodologie multidisciplinaire, combinant les méthodes utilisées dans les domaines de l'hydrogéologie et de la télédétection, pour mieux quantifier et prédire l'affaissement régional des sols dans un aquifère hétérogène intercalé de couches argileuses.

La zone d'étude est localisé dans la vallée de Toluca, Mexique, une zone ayant les critères propices à l'affaissement : soient un pompage excessif avec un bilan d'eau souterraine déficitaire, et la présence de couches argileuses compressibles. Contrairement aux autres villes mentionnées ci-haut, ce bassin a peu de donnés historiques sur l'affaissement régional.

La méthodologie entreprise comprend : (1) une revue de la littérature et une revue de rapports avec des données utiles à l'étude de cas, (2) des travaux de terrain (puits, extensomètres, et prélèvement de sol), (3) l'évaluation détaillée du bilan en eau à l'aide d'un modèle numérique de recharge multi-paramètres, (4) la génération d'un modèle géologique 3D, (5) l'utilisation de l'interférométrie radar (InSAR) pour obtenir des données de subsidence, (6) le couplage (compaction instantanée + écoulement d'eau souterraine), la vérification, et la mise en œuvre d'un modèle numérique, (7) la simulation de plusieurs scénarios pour prédire l'affaissement futur.

Les travaux détaillés avec les modèles de recharge et la géologie 3D permettent d'avoir une plus grande confiance dans les simulations. De plus, l'utilisation des techniques d'interférométrie radar permettent de localiser et mesurer les zones en affaissement. Aussi, en combinant les données InSAR, les données du bilan d'eau, le modèle géologique, et les données d'affaissement avec les

extensomètres, il est possible de mieux estimer les propriétés d'emmagasinement spécifique squelettique et de mieux caler le modèle numérique.

Plus spécifiquement, le travail démontre qu'il y a un déficit en eau souterraine dans la vallée de Toluca depuis environ 1962. Des scénarios de recharge (utilisant le modèle HELP3) et de pompage, incluant l'impact des changements climatiques, démontrent une diminution de la recharge et une augmentation du pompage dans les 50 prochaines années. Le déficit continuera à augmenter jusqu'à une moyenne de 292 Mm^3/année (million de mètres cubes par année) ou un maximum de 456 Mm^3/année en 2050.

D'après les simulations, depuis 1950 l'affaissement maximal a atteint près de 2 m. Les taux de compaction sont variables dans le temps et dans l'espace et dépendent du taux de pompage et des caractéristiques géo-mécaniques des sols. Le taux d'affaissement maximum dans la vallée est environ 15 cm/an. Les prévisions moyennes estiment que l'affaissement maximal dans la vallée sera d'environ 1,2 m dans les prochaines 40 années. La subsidence totale maximale en 2050 atteint 2,2 m pour le pire des scénarios, 1,4 m pour le meilleur scénario, et 1,6 m pour la subsidence moyenne attendue. Diminuer les exportations du bassin de 50% et déplacer les centres de pompage à des endroits avec une faible épaisseur d'argile, engendre un effet positif sur le bilan global de l'eau et ralentit la subsidence.

Cette étude a permis de contribuer à une meilleure compréhension du bilan en eau, de la structure géologique, et le processus d'affaissement du sol dans la vallée de Toluca. L'utilisation de cette approche multidisciplinaire pour quantifier les processus et les paramètres de compaction d'argile pourrait être appliquée à d'autres bassins ayant des problèmes semblables.

Resumen

En varias ciudades del mundo (por ejemplo, Venecia, Las Vegas, Shanghai, México), la sobreexplotación de las aguas subterráneas provoca la compactación de las capas de arcilla y crea muchos problemas, incluyendo problemas de colapso, daño a la infraestructura, y fractura en los sedimentos de la superficie.

El objetivo de esta tésis es presentar una metodología multidisciplinaria, combinando los métodos utilizados en las disciplinas de la hidrogeología y la teledetección, para tener la capacidad de cuantificar mejor y predecir la subsidencia regional en un acuífero heterogéneo con capas intercaladas de arcilla.

El área de estudio se centra en el valle de Toluca, México, una zona con criterios favorables a la subsidencia: el bombeo excesivo de agua con un déficit de las aguas subterráneas, y la presencia de capas de arcilla compresible. A diferencia de las ciudades antes mencionadas, la cuenca del valle de Toluca tiene pocos estudios históricos sobre la subsidencia regional, haciendo la tarea más difícil.

La metodología incluye: (1) una revisión bibliográfica y una revisión de los reportes para obtener los datos disponibles del estudio de caso (2) trabajo de campo (construcción de pozos, extensómetros, caracterización de los arcillas) (3) una evaluación detallada del balance de agua utilizando un modelo digital con varios parámetros, (4) la generación de un modelo 3D geológico, (5) el uso de interferometría radar (InSAR) para obtener los datos de subsidencia regionales, (6) acoplamiento (compactación instantánea + flujo de aguas subterráneas), la verificación y la aplicación de un modelo numérico (7) la simulación de diferentes escenarios para predecir la subsidencia futura.

El trabajo detallado sobre los modelos de la geología 3D y la recarga permiten una mayor confianza en las simulaciones. El uso de las técnicas de interferometría radar permite localizar y medir la subsidencia. Además, con los datos InSAR combinado con los datos de la balanza de agua, el modelo geológico, y los datos de compactación de los extensómetros, es posible estimar mejor las propiedades de almacenamiento específico del esqueleto y calibrar mejor el modelo numérico.

Concretamente, el trabajo demuestra que existe una escasez de aguas subterráneas en el valle de Toluca, desde alrededor de 1962. Escenarios de la recarga (utilizando el modelo de HELP3) y de bombeo, incluyendo el impacto del cambio climático, muestran una disminución en la recarga y el aumento de bombeo de agua en los próximos 50 años. Este déficit aumentará a un promedio de 292 Mm^3/año (millones de metros cúbicos por año) o un máximo de 456 Mm^3/año en 2050.

Según las simulaciones, desde 1950 la subsidencia máxima ha alcanzado casi los 2 m. La tasa de compactamiento es variable en el tiempo y el espacio y dependen del ritmo de bombeo y las características géo-mecánicas de los suelos. El porcentaje máximo de hundimiento de la tierra en el valle son de unos 15 cm/año. Las previsiones estiman que el promedio máximo de subsidencia en el valle es de 1.2 m en los próximos 40 años. La subsidencia máxima total en 2050 alcanzó el 2.2 m en el peor de los casos, 1.4 m en el mejor de los casos, y 1.6 m para el caso promedio. Reducir las exportaciones de la cuenca de 50% y desplazar de los centros de bombeo en áreas con bajo contenido de arcilla, crea un efecto positivo en el balance global de agua y la subsidencia disminuye.

Este estudio contribuirá a una mejor comprensión del balance hídrico, la estructura geológica y el proceso de subsidencia en el Valle de Toluca. El uso de este enfoque multidisciplinario para la cuantificación de los parámetros del proceso y la compactación de la arcilla podría aplicarse a otras cuencas con problemas similares.

Abstract

Excessive pumping of groundwater from compressible clay layers causes land subsidence. Many cities around the world (eg, Venice, Las Vegas, Shanghai, Mexico) experience subsidence in the form of collapsing ground, the formation of fractures in the surface sediments, and damages to infrastructure.

The objective of this thesis is to present a multidisciplinary approach, combining the methods used in the fields of hydrogeology and remote sensing, to better quantify and predict regional land subsidence in a heterogeneous aquifer interbedded with layers of clay.

The study area focuses on the Toluca Valley, Mexico where excessive pumping and compressible clay layers are found. Unlike the cities mentioned above, the basin has few historical studies or data on regional subsidence.

The methodology includes: (1) a literature review and a review of reports with data of the case study (2) fieldwork (installing wells, extensometers, and consolidation tests on clays), (3) a detailed assessment of the water budget using a multi-parameter recharge numerical model (HELP3), (4) generating a 3D geological model, (5) the use of radar interferometry (InSAR) to obtain regional subsidence data, (6) coupling the numerical model (instantaneous compaction + groundwater flow), verification, and implementation of the model, and (7) simulating various scenarios to predict future subsidence.

Detailed work on the recharge and 3D geology models lead to more confidence in the simulations. Moreover, the use of radar interferometry techniques assists in locating and measuring subsiding areas. Also, combining InSAR data, water budget data, the geological model, and extensometer data, it is possible to better estimate skeletal specific storage parameters and to better calibrate the numerical model.

More specifically, the work shows that there has been a groundwater deficit in the Toluca Valley

since about 1962. Recharge scenarios (using the HELP3 model) and pumping estimates, including climate change predictions, show a decrease in recharge and increased pumping in the next 50 years. The deficit will increase to an average of 292 Mm^3/year (million cubic meters per year) or a maximum of 456 Mm^3/year in 2050.

According to the simulations, since 1950 the maximum subsidence has reached nearly 2 m. The compaction rate is variable in time and space and depends on pumping rates and geo-mechanical characteristics of soils. The maximum subsidence rate in the valley is about 15 cm/year. The average estimates show that the maximum subsidence in the valley will be approximately 1.2 m in the next 40 years. The total maximum subsidence in 2050 reached 2.2 m for the worst case, 1.4 m for the best scenario, and 1.6 m for the average expected scenario. Reducing exports by 50% and moving the pumping centers to areas with low clay content creates a positive effect on the overall balance of water and slow subsidence.

This study contributes to a better understanding of the water balance, the geological structure, and the process of land subsidence in the Toluca Valley, Mexico. Using this multidisciplinary approach for quantifying clay compaction parameters and processes could be applied to other basins with similar problems.

Remerciements

Je désire d'abord remercier mon directeur de recherche, monsieur Richard Martel, qui a bien su me guider dans mes travaux, tout en me laissant la liberté d'explorer les voies qui me passionnent. Son savoir-faire, ses encouragements à publier les résultats, son enthousiasme, son support dans les temps difficiles, et son attitude face aux obstacles sont une source d'inspiration pour tous ceux qui l'entourent.

Alors que ce n'est pas toujours facile d'avoir plus d'un directeur, chaque co-directeur a été quintessentiel au produit final de cette thèse. Les trois co-directeurs de recherche ont contribué à ce projet pour le rendre d'une envergure importante dont nous pouvons être fiers.

Monsieur Alfonso Rivera qui, par ses précieux conseils, patience, et enthousiasme à partager son savoir, m'a supporté tout au long de mes recherches. Dans les moments d'incertitude j'apprécie qu'il ait sue me pointer dans la bonne direction. Sa grande vision de la science ainsi que sa rigueur ont été une source d'inspiration. Je le remercie beaucoup.

J'en dois également à Jaime Garfias, sans lui ce projet que j'ai vraiment apprécié n'aurait jamais existé. La réception que j'ai reçu au Mexique ainsi que l'aide avec les travaux de terrain ont grandement étés appréciés. Il m'a permis de mieux apprendre une culture pas très loin de nous et de développer mon vocabulaire espagnol. Muchas gracias!! De plus son soin avec les suggestions et corrections ont grandement contribué à une amélioration du produit final.

Le dernier co-directeur, mais non le moindre, René Therrien a toujours eu des commentaires pertinents et des suggestions forts enrichissantes. Non seulement ses habilités en modélisation, mais aussi sa capacité de fusionner et reformuler les idées et les concepts d'une façon élégante sont une source d'inspiration. C'était un plaisir de travailler avec lui. Merci beaucoup.

Je souhaite également remercier les examinateurs qui ont gentiment accepté de participer à l'évaluation de cette thèse : messieurs Vern Singhroy, David Rudolph, Claudio Paniconi, et Normand Tassé. Je les remercie grandement pour l'intérêt porté à mes recherches.

Cette thèse aurait été impossible à réaliser sans le support financier du Ministère des Relations Internationales du Québec, l'Institut national de recherche scientifique Eau Terre et Environnement (INRS-ETE), CRSNG (subvention de découverte tenu par Richard Martel), CONACyT, L'Université Autonome de l'Etat de México (UAEM), Association des Universités et Collèges du Canada (AUCC)/Centre de recherche pour le développement International (CRDI), et le Ministère d'Éducation du Québec.

Je remercie aussi l'Agence Spatiale Canadienne et la Commission Géologique du Canada pour l'accès aux images RADARSAT-1 et nous remercions l'Agence Spatiale Européenne pour la contribution des images ERS-1, ERS-2 et ENVISAT aux prix de reproduction sous le projet C1P 3821.

De plus, cette thèse aurait été impossible à réaliser sans le support scientifique, technique et administratif des gens qui travaillent à l'INRS-ETE, à l'UAEM, au Comission Geologique du Canada (CGC), au Centre Canadien de Teledetection (CCRS), la Comision National del Agua (CNA), l'Université Laval, et le United States Geological Survey (USGS). Pour en nommer que quelques un, j'aimerais remercier : *INRS-ETE* : Suzanne Dussault, Claude Blanchette, Josée Pozadski, Linda Aubert, Alain Gravel, Johanne Desrosiers ; *CGC* : Ruth Boivin, Miroslav Nastev; *UAEM* : Javier Salas, Emmanuelle Quentin, Marcela Magallón Andalón; *CNA* : Sergio Murillo; *CCRS* : Pierre-Jean Allaset, Vern Singhroy; *Université Laval :* Geoffrey Edwards, Daniela Blessent; et *USGS* : Stan Leake.

Je tiens à offrir mes derniers remerciements à mes amis, et à ma famille, c'est-à-dire ma sœur, mes grands parents, et mes parents, pour leur support et encouragement à travers mes études. Finalement un remerciement spécial à ma copine, Laurence, pour son encouragement, sa compréhension, et son soutien pendant plus de 4 ans à travers les weekends et les soirées où je devais travailler.

Avant-propos

L'ensemble de cette thèse se concentre sur l'affaissement des sols dû au pompage d'eau souterraine. Le document suivant s'articule en deux parties distinctes. La première partie (chapitre 1), une synthèse, permet de faire le point sur la contribution des travaux et des publications dans le domaine de l'affaissement des sols dû à l'extraction de l'eau souterraine. Elle comprend également des informations complémentaires aux écrits de la partie suivante. La deuxième partie (chapitres 2 à 5) présente 4 articles soumis ou sur le point d'être soumis à des revues scientifiques avec comité de lecture (nommées en A de cette section). Plus précisément, le chapitre 2 focalise sur le bilan d'eau, nécessaire pour quantifier l'affaissement. Le chapitre 3 examine la télédétection comme méthode pour quantifier l'affaissement des sols. Le chapitre 4 présente un modèle numérique couplant la compaction à l'écoulement d'eau souterraine ainsi qu'une représentation de l'affaissement dans la vallée de Toluca. Enfin, le dernier chapitre (chapitre 5) propose des scénarios afin de prédire l'affaissement futur des sols dans la vallée de Toluca.

Trois articles publiés dans le cadre de conférences nationales et internationales avec comité de lecture (présenté en B de cette section; voir Annexe A pour les articles complètes) et deux communications orales accepté sur résumé et publier dans les actes de colloques (section C) complètent la contribution de l'étudiant a ce projet. Bien que ces articles fournissent des informations pertinentes sur l'affaissement des sols dans la vallee de Toluca, les résultats présentés sont considérés comme complémentaires. Par conséquent, ces documents ne sont pas intégrés dans la deuxième partie afin d'éviter certaines répétitions, mais incorporé a l'annexe A.

Dans le cadre de sa thèse, l'auteur a pu apporter des contributions pertinentes au domaine choisi à travers des articles de revues scientifiques publiés ou soumis et des articles et/ou communications réalisés dans le cadre de conférences internationales. Il faut cependant mentionner que les communications sans arbitrage ne sont pas rapportées ici. Dans tous les cas, le premier auteur est l'auteur correspondant. En qualité de premier auteur,

l'étudiant a rédigé entièrement tous les articles après révisions et suggestions pertinentes des co-auteurs : Dr. Richard Martel, Dr Alfonso Rivera, Dr. Jaime Garfias, Dr René Therrien et Dr Pierre-Jean Allasset (voir section D).

De plus, l'auteur a pu apprendre une troisième langue au cours de cette thèse (voir section E).

A. Articles de périodique composant la seconde partie :

Calderhead A. I., Martel, R. Rivera, A., Garfias, J., Therrien, R., An increasing groundwater budget deficit induced by urbanization, industrialization, and climate change in the Toluca Valley, Mexico. *Hydrological Processes* (to submit in October 2009a)

Calderhead, A. I., Martel, R., Allasset, P-J., Rivera, A., Garfias, J, Land subsidence induced by groundwater pumping, monitored by C-band D-InSAR and field data in the Toluca Valley, Mexico. *Canadian Journal of Remote Sensing* (accepted 2009b)

Calderhead A. I., Therrien, R, Rivera, A., Martel, R. Garfias, J., Simulating pumping-induced regional land subsidence in a complex aquifer system *Advances in Water Resources* (to submit in October 2009c)

Calderhead A. I., Martel, A., Garfias, J., R. Rivera, Therrien, R., Groundwater pumping scenarios for minimizing land subsidence in the Toluca Valley, Mexico: tools for policy design. *Water Resources Management* (to submit in October 2009d)

B. Articles de conférences avec comité de lecture :

Calderhead, A I; Martel, R; Rivera, A; Therrien, R.; Garfias, J, Pumping-induced regional land subsidence: calibrating a flow and compaction model with remote sensors and field data. 62nd annual and 10th Joint International Association of Hydrogeologists

/Canadian Geotechnical Conference, Canadian Geotechnical Society, Halifax, NS, Canada, GeoHalifax 2009, September 20-24, 2009, pp 1400-1407

Calderhead, A I; Martel, R; Rivera, A; Garfias, J; P-J Alasset' C-BAND D-INSAR AND FIELD DATA FOR CALIBRATING A GROUNDWATER FLOW AND LAND SUBSIDENCE MODEL. In: IEEE International Geoscience & Remote Sensing Symposium, Cape Town, South Africa, July 12-17, 2009

Calderhead, A. I.; Martel, R.; Garfias, J. (2006) A STUDY OF GROUNDWATER RESOURCES AND LAND SUBSIDENCE IN THE TOLUCA VALLEY, MEXICO In: 59th annual and 7th Joint International Association of Hydrogeologists /Canadian Geotechnical Conference, Canadian Geotechnical Society, Vancouver, BC, Canada, Sea to sky Geotechnique 2006, pp 848-855.

C. Communication avec résumé dans acte de colloque

Calderhead, A I; Martel, R; Rivera, A; Garfias, J; Therrien, R. Interférométrie Radar: Une application à la subsidence des sols due à l'extraction de l'eau souterraine dans la Vallée de Toluca, Mexique. Conférencier invité au 13e CONGRÈS DE L'ASSOCIATION QUÉBÉCOISE DE TÉLÉDÉTECTION, Trois-Rivières Québec. April, 2008.

Calderhead, A I; Martel, R; Rivera, A; Garfias, J; Therrien, R. Groundwater Resources and Land Subsidence investigations in the Toluca Valley, Mexico. Presentation at the American Geophysical Union (AGU), Joint Assembly Acapulco Mexico. May 2007.

D. Contribution de l'auteur pour les travaux et la rédaction des articles

La compilation des données et la revue de littérature ont été entièrement réalisées par l'étudiant. L'ensemble des travaux décrits dans les articles Calderhead et al., (2009a); (2009b); (2009c); et (2009d) ont été réalisés par l'étudiant. Les travaux de terrains ont été

effectués ou supervisés par l'étudiant avec la participation du Dr. Jaime Garfias, Dr. Richard Martel et le Dr Alfonso Rivera et aussi avec l'aide de Monsieur Javier Salas, Mme Marcela Magallón Andalón et le Dr Ondra Stacek. Deux stagiaires d'été à l'INRS ont contribué à la compilation des données du modèle HELP et la géologie 3D: Mr. Alain Gravel et Mme Geneviève Parent. La conception du couplage de module de compaction a été faite par l'étudiant tandis que le Dr. René Therrien a fait le travail de couplage. Le Dr Pierre-Jean Allaset a contribué à l'interprétation des images interférométriques.

E. Apprentissage de l'espagnol par l'auteur

Pendant plus d'un an, l'auteur a séjourné au Mexique et s'est donc exposé à la riche culture mexicaine en plus d'apprendre une troisième langue, l'espagnol. L'auteur peut donc communiquer dans cette langue autant à l'écrit qu'à l'oral.

Table des matières

Résumé ..... *iii*
Resumen ..... *v*
Abstract ..... *vii*
Remerciements ..... *ix*
Avant-propos ..... *xi*

PARTIE 1 ..... **1**

CHAPITRE 1: SYNTHÈSE **3**
1 Introduction 5
2 Mise en contexte de la Vallée de Toluca 6
Situation géographique 6
Population 7
Climat, réseau hydrique et géologie 7
Utilisation de l'eau 8
Exportations vers Mexico 9
3 Travaux de terrain 9
3.1 Cueillette de données en provenance de la littérature 9
3.2 Installation de deux extensomètres 10
3.3 Mesures d'affaissement dans les extensomètres 12
3.4 Récupération des données de niveau d'eau 12
3.5 Forages pour obtenir des données sur les paramètres géomécaniques 13
4 Bilan en eau 13
5 Géologie 16
6 Télédétection 19
Introduction à InSAR 19
L'utilisation des techniques InSAR dans la Vallée de Toluca 20
7 Modélisation 25
7.1 Couplage d'un module de compaction 27
7.2 Validation du nouveau modèle 28
7.3 Conception et mise en œuvre du modèle numérique dans la Valle de Toluca 30
7.4 Calage 32
Charge hydraulique 32
Estimer S'_{sk} pour une couche individuelle 33
Compaction 34
7.5 Résultats des simulations de compaction 35
8 Gestion de l'aquifère 37
9 Conclusions et perspectives 42
Bilan en eau 42
InSAR 43
Modélisation 43
Gestion de l'aquifère 43
10 Les aspects innovateurs de la thèse. 44
Références *45*
Liste des Tableaux *51*
Liste des figures *53*

PARTIE 2 ..... **57**

CHAPITRE 2: AN INCREASING GROUNDWATER BUDGET DEFICIT INDUCED BY URBANIZATION, INDUSTRIALIZATION, AND CLIMATE CHANGE IN THE TOLUCA VALLEY, MEXICO **59**
Résumé *61*
Abstract *63*
1 Introduction 64
2 The Toluca Valley 66
3 Methodology 68
3.1 Total Recharge (Q_{on}) 71

Recharge Domain for HELP3 74
Historical Climate data approach used with HELP3 75
Climate change 76
Calibration of the HELP3 Model 78
R_{ART} and ΔR_0 79
3.2 Discharge (Q_{off}): 79
Groundwater extraction from pumping wells (P): 80
Groundwater flow (GW_{flow}) 81
4 Results 83
4.1 Recharge simulations 83
4.2 Discharge results 85
Natural groundwater flow (GW_{flow}), Change in Virgin Discharge Rate due to Pumping (ΔD_0), and yearly Change in Virgin Discharge Rate due to Pumping (ΔD_{yi}): 85
Spring discharge (Sp) 87
Groundwater pumping (P): 88
4.3 Deficit 88
5 Discussion and Conclusion 91
6 Acknowledgements 94
References *95*
List of tables *101*
List of figures *103*
CHAPITRE 3: LAND SUBSIDENCE INDUCED BY GROUNDWATER PUMPING, MONITORED BY C-BAND D-INSAR AND FIELD DATA IN THE TOLUCA VALLEY, MEXICO **105**
Résumé *107*
Abstract *109*
1 INTRODUCTION 110
2 Study Area 112
Geological setting 113
Groundwater resources 115
3 Methods and Materials 116
3.1 Brief description of D-InSAR 116
3.2 Image data and processing 117
Image Data for the Toluca Valley 117
D-InSAR processing and selected parameters 118
3.3 Field data acquisition 118
Water levels 119
Extensometer measurements 119
4 Results 121
5 Discussion and Conclusion 132
Acknowledgments *134*
References *135*
List of tables *141*
List of figures *143*
CHAPITRE 4: SIMULATING PUMPING-INDUCED REGIONAL LAND SUBSIDENCE IN A COMPLEX AQUIFER SYSTEM **145**
Résumé *147*
Abstract *148*
1 Introduction 149
2 Background 151
3 Methodology 157
3.1 Coupling compaction to the groundwater flow equation 157
Discretization 159
3.2 HGS model verification 160
4 Toluca Valley Background 162
Geology 163
Water budget 166
Subsidence measurements 167
Borehole extensometers 168
InSAR 168
5 Model setup and Calibration 168

5.1 Model setup 168
5.2 Calibration 172
The model was set up by using field data for assigning the aquifer and aquitard physical properties (Table 2), initial hydraulic head conditions, and boundary conditions. Several points, or numerical observation wells, were used to monitor the calibration process. Namely, the points used were located at Extensometer-1, Extensometer-2 and the Pecuario well, located in the region where most of the compaction is observed. This is also where a significant amount of InSAR work was focused. 172
Initial simulations showed that the hydraulic heads were not decreasing and compaction was not increasing as rapidly as measured in the field. Certain parameters of the model were adjusted to achieve an acceptable degree of calibration. 172
Head calibration 173
Estimating S'_{sk} for an individual clay layer 173
6 Results 177
7 Discussion and Conclusion 182
Acknowledgements *185*
References *185*
List of tables *191*
List of figures *193*
CHAPITRE 5: GROUNDWATER PUMPING SCENARIOS FOR MINIMIZING LAND SUBSIDENCE IN THE TOLUCA VALLEY, MEXICO: TOOLS FOR POLICY DESIGN 195
Résumé *197*
Abstract *199*
1 Introduction 200
Geographic Setting 201
Population growth 202
Hydrogeology and Groundwater pumping 203
2 Methodology 204
Model setup 204
Scenarios 210
3 Results 211
4 Discussion 216
Acknowledgements *218*
References *218*
List of tables *223*
List of figures *225*
ANNEXES 227
Annexe A : Articles de conférences 229
Annexe A 1 – IAH/CNC 2006, VANCOUVER 231
Annexe A 2 – IEEE IGARSS 2009, Cape Town 241
Annexe A 3 – IAH/CNC 2009, HALIFAX 247
Annexe B: Résumé des modèles numériques couplés 261
Annexe C : Autres travaux de terrain 269
Annexe D : Résultats des tests de consolidation 275
Annexe E : Modèles d'évapotranspiration 299
Annexe F : D-InSAR description and discussion on limitations 303
Annexe G : Supplementary data for the HELP3 Model 309
Annexe H: Sources of uncertainty 312

Partie 1

Chapitre 1:

Synthèse

1 INTRODUCTION

Les ressources souterraines en eau potable de la vallée de Toluca connaissent une forte demande de la part des secteurs industriel et agricole, mais surtout de la part de la population urbaine, ce qui inclut non seulement les habitants de la vallée, mais aussi ceux de la populeuse capitale nationale, la ville de Mexico. Par conséquent, un grand pourcentage de l'eau souterraine est exporté à l'extérieur du bassin. Le bassin subit un déficit en eau souterraine, c'est-à-dire qu'il y a plus de pompage qu'il y en a de recharge. Cette surexploitation de l'aquifère entraîne la réduction du stockage de l'eau, ce qui cause une subsidence régionale importante dont les symptômes sont des effondrements superficiels du sol et de l'infrastructure, ainsi que la formation de fractures dans ceux-ci.

La subsidence due au pompage de l'eau a été bien documentée dans d'autres bassins aux États-Unis (Helm, 1975; Amelung et al., 1999; Galloway and Hoffman, 2007), en Italie (Gambolati, 1972; Teatini, et al., 2005; Ferronato et al., 2006), en Chine (Shearer, 1998; Li et al., 2006) ainsi qu'au Mexique (Ortega et al., 1993; Rudolph et Frind, 1991; Rivera et al., 1991; et Ortega et al., 1999), mais aucune étude a comme point de mire la Vallée de Toluca; bien qu'on y observe d'importants déplacements de terrain et l'apparition de fractures.

Depuis les années 1970, l'évaluation de l'affaissement des sols dû au pompage d'eau souterraine a surtout été étudiée par voie de modèles numériques calés avec des données de terrain (voir Annexe B). Généralement, les modèles, de plus en plus sophistiqués, couplent les principes d'écoulement de l'eau et la théorie de consolidation 1D de Terzhaghi (1925) ou 3D de Biot (1941). Jusqu'à présent cette approche demeure la meilleure pour représenter et prédire l'affaissement. La précision de ces modèles couplés dépend grandement des données de terrain qui sont souvent déficientes, dispendieuses à obtenir, très locales et dispersées – rendant les résultats parfois douteux. Il est peut-être possible de représenter tous les paramètres de tous les processus d'un système multicouche à l'aide d'un modèle numérique, mais un tel modèle risquerait d'être très complexe, très théorique, et de rester un simple outil académique.

L'objectif de cette thèse est donc de présenter une méthodologie pratique capable de représenter l'affaissement régional des sols dans un aquifère multicouche surexploité. Une approche multidisciplinaire est proposée afin d'arriver à une meilleure représentation de l'affaissement régional des sols. Des techniques interférométriques de télédétection ainsi que des données de terrain acquises ou déjà existantes sont utilisées pour caler un modèle numérique couplé afin de quantifier l'affaissement. Les travaux réalisés dans le cadre de cette thèse poursuivent ceux de Galloway et al., (1998), Amelung et al., (1999) et Hoffman et al., (2003a) en présentant une méthode pour isoler l'emmagasinement spécifique squelétique (*skeletal specific storage*) des couches individuelles dans un aquifère multicouche. De plus, une meilleure compréhension du bilan d'eau, de la stratigraphie 3D, ainsi que des processus d'affaissement de du terrain à la vallée de Toluca, est entrepris.

Ce chapitre est divisé comme suit : (1) Introduction (2) Mise en contexte (3) Travaux de terrain (4) Évaluation du bilan d'eau (5) Génération d'un modèle géologique 3D (6) Télédétection (7) Modélisation (8) Scenarios pour aider à la gestion de l'aquifère (9) Conclusions et perspectives (10) Les aspects innovateurs de la thèse.

2 MISE EN CONTEXTE DE LA VALLÉE DE TOLUCA

Situation géographique

Le bassin de la Vallée de Toluca a une superficie d'environ 2100 Km^2. Le bassin est adjacent à la vallée de Mexico et la chaîne de montagne Las Cruces forme une frontière naturelle entre les deux bassins (figure 1). Sa position géographique, au centre du pays et à proximité de Mexico, ainsi que le développement rapide des infrastructures, ont permis à la ville de développer une zone industrielle majeure pour le pays. L'étude de la subsidence pour cette thèse a été faite à l'échelle régionale en mettant l'accent sur le corridor industriel. Ce corridor industriel situé près de la ville de Toluca a été en grande partie formé par les industries qui se sont déplacées de la vallée de Mexico à la suite du séisme de 1985.

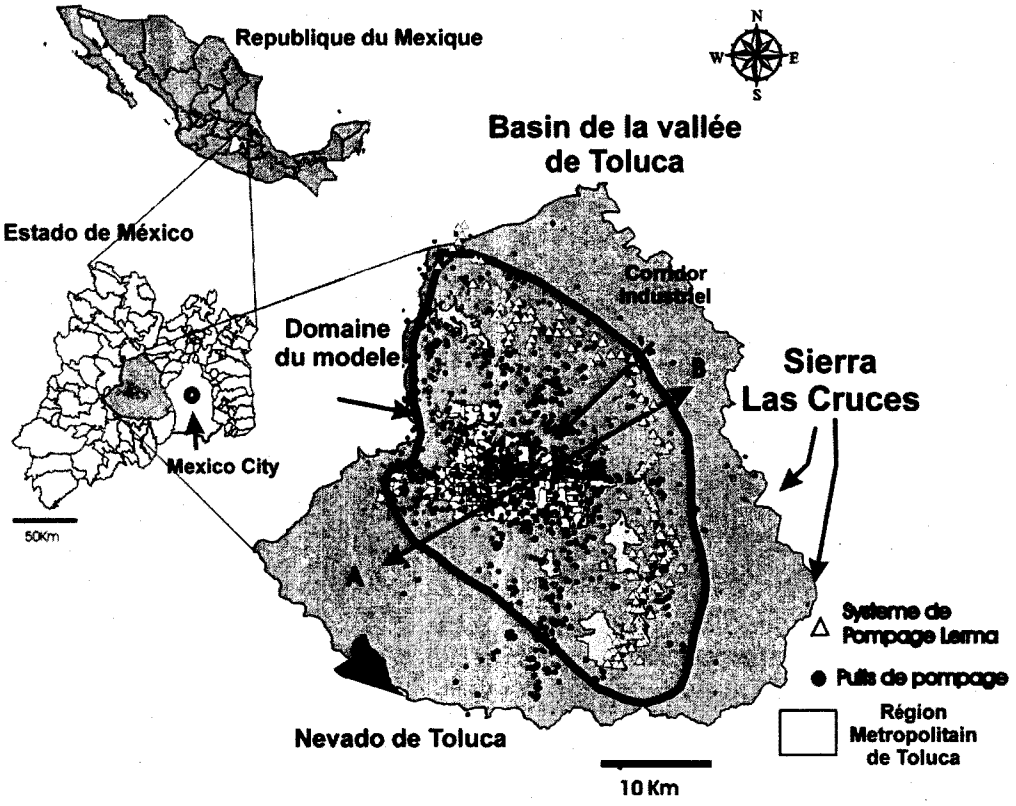


Figure 1 : Position de la vallée de Toluca et la zone d'étude par rapport au Mexique et l'État de Mexico

Population

Selon le recensement de 2005 (INEGI, 2005), la région métropolitaine de Toluca comprend 12 municipalités. En plus d'être la cinquième plus grande zone métropolitaine au Mexique, elle est la plus grande de l'État de Mexico. La population totale de la vallée de Toluca en 2005 se situait autour de 1,7 million de personnes (INEGI, 2005). De 1960 à 2005, la population de la vallée a doublé environ tous les 20 ans (INEGI, 1960-2005).

Climat, réseau hydrique et géologie

La vallée est caractérisée par un climat tempéré avec des hivers secs. La vallée a une température annuelle moyenne de 12-15 °C et reçoit généralement 700 mm de précipitations par année. La température moyenne annuelle, du plus haut point dans la vallée, le Nevado de Toluca, est de -2 a 5 °C et plus de 1200 mm de précipitations (CNA, 2006) (voir Chapitre 2 pour une description plus détaillée du climat).

Étant donné le pompage intensif depuis plusieurs décennies, la rivière Lerma, qui débute aux sources des Lagunes dans le Sud-est du Bassin et sort du bassin dans le Nord-Ouest, a peu de contact hydraulique avec la nappe phréatique. Beaucoup d'industries et de municipalités déversent leurs eaux usées dans celle-ci, ce qui en fait une rivière contaminée agissant plutôt comme un canal qu'une rivière. L'évapotranspiration élevée dans la vallée fait en sorte qu'il y a très peu de tributaires qui se déchargent dans la Lerma.

Le bassin est généralement constitué de deux aquifères, dont la composition minérale varient en fonction de l'origine des matériaux géologiques (voir section 5 ou Chapitre 4 pour une description détaillée de la géologie). L'aquifère inférieur est composé de roches fracturées. L'aquifère supérieur est quant à lui complexe et intercalé d'alluvions et d'argile/silts d'origine lacustre. C'est d'ailleurs ce dernier qui constitue l'objet de nos travaux.

Utilisation de l'eau

Puisque la plupart des plans d'eau de surface dans la vallée sont contaminés, la consommation d'eau potable provient presqu'exclusivement de l'eau souterraine. La demande en eau répond aux besoins de quatre usagés : domestique (52 %), exportation vers la capitale Mexico (38%), industriel (7%), agriculture (3%) (IMTA, 2003) (voir figure 2).

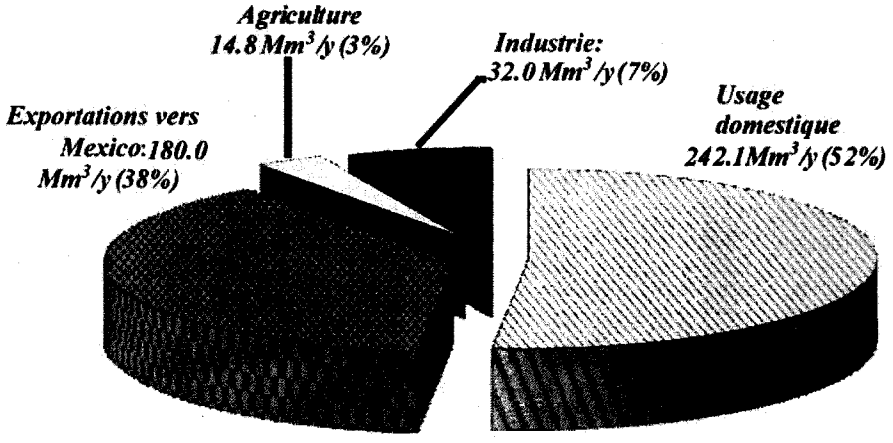


Figure 2: Utilisation de l'eau souterraine dans la vallée de Toluca (valeurs tirées de IMTA (2003) et figure modifié de Calderhead et al. (2009a)

L'extraction excessive de l'eau souterraine dans la vallée de Toluca depuis les 50 dernières années a provoqué une réduction du stockage d'eau, la diminution du niveau phréatique, le changement des directions régionales de l'écoulement souterrain, la diminution et parfois l'extinction des débits des sources dans les régions montagneuses environnantes. Cette réduction du stockage d'eau entraine l'affaissement du terrain dans les milieux argileux, génère multiples fractures et entraîne des phénomènes d'effondrement en surface.

Exportations vers Mexico

Depuis les années 1960, le bassin de Toluca fournit une quantité importante d'eau potable à la ville de Mexico. Une série de 236 puits, nommée le Systema Lerma, fournit actuellement quelque 6.0 m^3s^{-1} d'eau à destination de Mexico, ce qui équivaut à environ 7% des ressources de la vallée de Toluca et 8% de la demande totale d'eau potable pour la ville de Mexico (Legorreta, 1997). La majorité des puits installés ont une profondeur variant entre 200 et 300 m.

3 TRAVAUX DE TERRAIN

Il y a eu plusieurs phases de travaux de terrain entre février 2005 et juillet 2008. La section des travaux de terrain est divisée comme suit : 3.1 Cueillette des données en provenance de la littérature; 3.2 Installation de deux extensomètres; 3.3 Mesures d'affaissement dans les extensomètres; 3.4 Récupération des données de niveau d'eau; et 3.5 Forages pour obtenir des données sur les paramètres géo-mécaniques. D'autres travaux ont été faits dans le contexte d'un suivi à long terme des ressources en eau de la vallée de Toluca, mais ne sont pas utilisés dans cette thèse. Ils sont présentés à l'annexe C.

3.1 Cueillette de données en provenance de la littérature

Une revue des données sur la vallée de Toluca colligées dans différents rapports est entreprise pour maximiser les informations utilisées dans les modèles. Ceci dit, cette phase de terrain a permit d'établir une typologie du fonctionnement de l'aquifère et a

servi à délimiter avec une plus grande précision l'étendue du secteur d'étude. Un inventaire des données météorologiques (CNA, 2006) et géologiques (Lesser y Associados, 1992; Ariel y Consultores, 1996), en plus des journaux de forage pour le Systema Lerma et le système multi-piézomètres a été entrepris. L'obtention des rapports sur le bilan en eau dans la vallée (OEE, 1970; Lesser and Asociados,1992; Ariel and Consultores, 1996; CNA, 2000, GTZ-CNA 2004; INEGI, 1960-2005; voir Calderhead et al., (2009a) pour autres références), a été fait. De plus, les études d'affaissement et de fractures (Figueroa, 1990, 2004; Consultec, 1978; Minor, 2007) dans la zone d'étude ont aussi été utiles pour caler le modèle numérique.

3.2 Installation de deux extensomètres

L'installation d'extensomètres permet de mesurer la compaction du sol avec une précision millimétrique. Deux extensomètres ont été installés, le premier en mai 2006 (Extensomètre-2) et le second en juillet 2006 (Extensomètre-1). La figure 12 montre la position des extensomètres. Des extensomètres se retrouvent à proximité des zones d'affaissement maximal où on retrouve des fractures en surface. Plusieurs fractures sont retrouvées dans les environs du corridor industriel où les niveaux de la nappe diminuent à des rythmes allant jusqu'à 1.4 m par année. Puisque nous n'avions pas en notre possession le logiciel de traitement d'image satellite avant l'installation des extensomètres, nous ne pouvions pas placer les extensomètres dans les zones d'affaissement maximal (environ 15 cm/année). En fait, les extensomètres se retrouvent dans une zone ou il y a de l'affaissement modéré (1 cm/année).

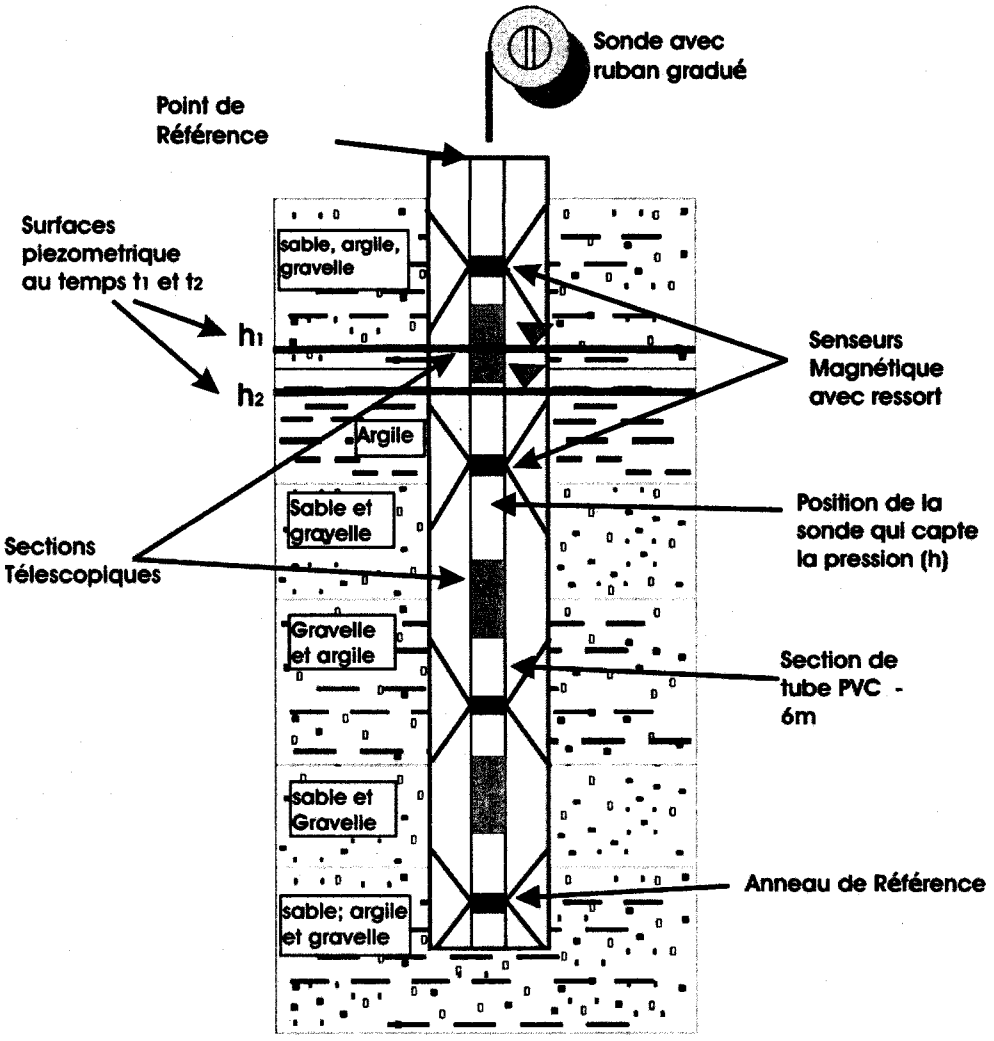


Figure 3: Schéma d'un extensomètre à senseur magnétique. Les variations de surface piézométrique (h1 et h2), ainsi que la position du système d'acquisition de pression (pressure transducer) sont également indiqués. Le dessin n'est pas à l'échelle.

L'installation des extensomètres fut une tâche ardue étant donné les profondeurs des forages. Le matériel acquis pour les extensomètres était conçu pour des profondeurs maximales d'environ 20 m (Roctest, 2009). Plusieurs modifications ont été faites pour obtenir des données à de plus grandes profondeurs (jusqu'à 120 m). Les extensomètres installés dans la vallée de Toluca consistent en un réseau de cibles magnétiques placées à 6 m d'intervalle le long d'un tube en PVC dans un forage (Figure 3). Les sections de tube en PVC de 6 m sont fixées à la paroi du forage au moyen d'un ancrage dont le centre contient un aimant. Les sections de PVC sont connectées l'une à l'autre par des sections télescopiques, permettant un mouvement vertical une fois fixées dans le forage. Une

sonde à commutateur à lames détecte la profondeur des aimants quand elle est descendue dans le tube. Le détecteur est suspendu à un ruban gradué recouvrant le filage d'alimentation électrique. La graduation du ruban sert à déterminer, avec une précision milimétrique, la compaction entre les aimants tout le long du forage. Idéalement les extensomètres se rendraient à la roche-mère, mais étant donné des contraintes budgétaires et la complexité d'installer l'appareil à ces profondeurs, nous nous sommes limités à 120 m (Extensomètre-1) et 80 m (Extensomètre-2).

3.3 Mesures d'affaissement dans les extensomètres

La majorité des lectures dans les extensomètres ont été prises en même temps que le captage d'images satellitaire de la vallée d'ENVISAT et RADARSAT-1 entre décembre 2007 et mai 2008. La Figure 4 montre la distribution des dates de lecture prise dans les extensomètres ainsi que la compaction totale mesurée dans les 107 premiers mètres d'Extensometer-1. Les dates de lecture sont les suivantes: 20-déc-06, 29-mai-07, 25-janv-08, 04-mars-08, 08-avr-08, 24-mai-08, 23-juil-08.

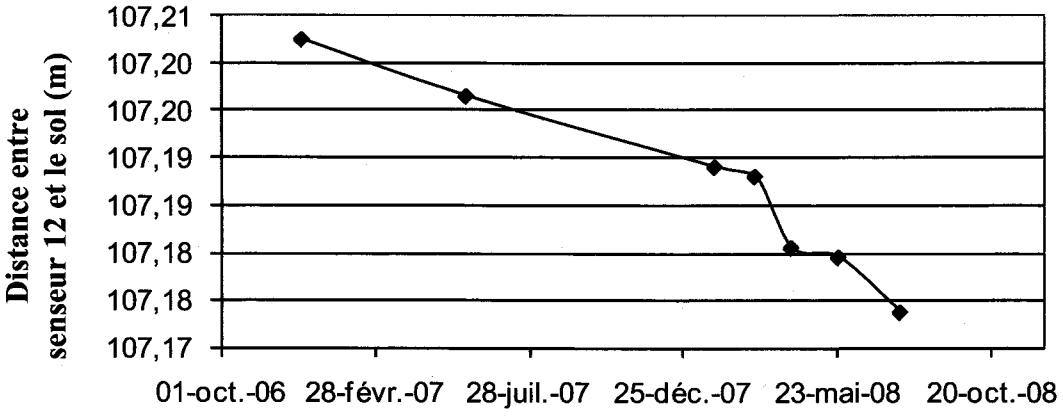


Figure 4 : Distance entre le senseur 12 (profondeur ≈ 107 m) et le sol pour Extensometer-1.

3.4 Récupération des données de niveau d'eau

La collecte de données piézométriques dans les extensomètres a fait partie des campagnes de terrain. Ces niveaux d'eau, ainsi que ceux du système d'acquisition automatique avec une sonde à pression, ont été mesurés tous les 12 heures de juillet 2006 à juillet 2008. Pour complémenter ces lectures, les données des niveaux piézométriques en provenance

du réseau de 52 multi-piézomètres, (CNA, 2008), ont été aussi mises à jour régulièrement.

3.5 Forages pour obtenir des données sur les paramètres géomécaniques

Trois forages ayant une profondeur de 22 mètres ont été réalisés pour déterminer les paramètres géomécaniques tel que pour la porosité, l'indice des vides, la teneur en eau, et le coefficient de compressibilité des argiles. Les forages devaient être localisés dans des milieux où il y a une forte concentration en argile saturée. Voir Annexe D et Figure 13 pour les résultats de ces essais géomécaniques.

4 BILAN EN EAU

L'évaluation du bilan en eau de l'aquifère est un aspect fondamental pour la caractérisation d'un système subissant de l'affaissement. Deux grands paramètres, la recharge et la décharge sont examinés en détail dans cette section.

La croissance urbaine, l'industrialisation et les changements climatiques peuvent entraîner une augmentation du déficit du bilan d'eau. Une méthodologie est proposée pour améliorer le modèle du bilan en eaux souterraines dans le but de quantifier les déficits passé, présent et futur dans la vallée de Toluca, au Mexique.

La recharge est calculée avec une variation spatiale, déterminée à partir de données historiques sur le climat, les prévisions des changements climatiques, ainsi que les multiples paramètres utilisés dans le modèle Hydrologic Evaluation of Landfill Performance (HELP3) (Schroeder et al., 1994). HELP3 est un modèle quasi 2D pour évaluer la recharge d'un système hydrique. Le modèle accepte des données de météo, d'emmagasinement des sols, de fonte de neige, de ruissellement, d'infiltration, d'évapotranspiration, de végétation, de drainage latéral souterrain, de drainage non-saturé vertical et les paramètres de lixiviation.

Pour évaluer l'effet des changements climatiques sur la recharge, l'étude utilise la méthodologie proposée par Jyrkama et Sykes (2007) où seulement les scenarios de changements climatiques régionaux sont simulés. La particularité de cette méthodologie repose sur le fait que l'accent est placé sur le budget global des eaux souterraines et l'impact du changement climatique est considéré comme un facteur parmi plusieurs autres dans le budget.

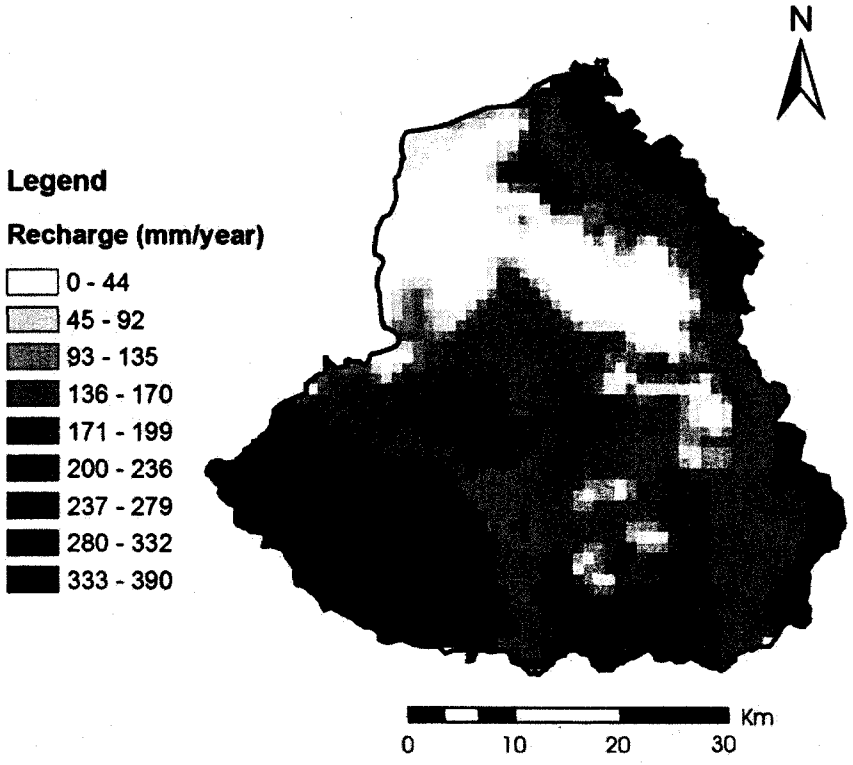


Figure 5: Distribution spatiale de la recharge moyenne dans la vallée de Toluca [mm/année] en utilisant le modèle HELP3 (tirée de Calderhead et al., 2009a).

La vérification du modèle a été fait avec l'aide de modèles d'évapotranspiration (Voir chapitre 2 et Annexe E). La distribution de la recharge est présentée dans la figure 5. La recharge est plus grande dans les régions montagneuses et plus petite dans le centre de la vallée (136-170 mm/an). Dans les zones argileuses au Nord du bassin, il y a peu d'infiltration (0-44 mm/an).

En utilisant les données historiques et les prévisions de recharge et décharge (Calderhead et al., 2009a), le déficit est alors calculé (Tableau 1, Figure 6).

Tableau 1 : Résumé du budget d'eau souterraine entre 1970 et 2050.'-' signifie données non disponibles (tiré de Calderhead et al., 2009a).

				1970	1985	2000	2010	2020	2030	2040	2050
Recharge [Mm^3/year]	Historical Recharge			385.0	373.9	376.2	-	-	-	-	-
	HELP3 Simulations	Average recharge based on 1969-2000 data		376.2	376.2	376.2	376.2	376.2	376.2	376.2	376.2
		Climate Change (based on average recharge and 21 climate models)	average	-	-	376.2	373.0	370.0	367.0	364.0	361.0
			Best case	-	-	376.2	377.8	379.6	381.4	383.2	385.0
	Induced Recharge (R_art)			-	-	1.2	1.5	2.0	5.0	7.5	10.0
Discharge [Mm^3/year]	Spring discharges (Sp)			-55.0	-54.0	-53.0	-52.0	-48.0	-50.0	-48.0	-45.0
	Groundwater flow			-0.048	-0.048	-0.023	-0.024	-0.022	-0.020	-0.015	-0.010
	Pumping	Historical Extraction		-359.9	-413.0	-456.0	-	-	-	-	-
		Expected Extraction (P)	Average	-	-	-	-494.5	-534.8	-571.8	-599.1	-617.9
			Best case	-	-	-	-490.7	-521.0	-543.5	-556.1	-557.7
Deficit [Mm^3/year]	Historical Deficit			-29.9	-93.2	-145.0	-	-	-	-	-
	Expected		Average	-	-	-	-172.0	-210.8	-249.9	-275.6	-292.0
			Best case	-	-	-	-163.4	-187.4	-207.1	-213.4	-207.7

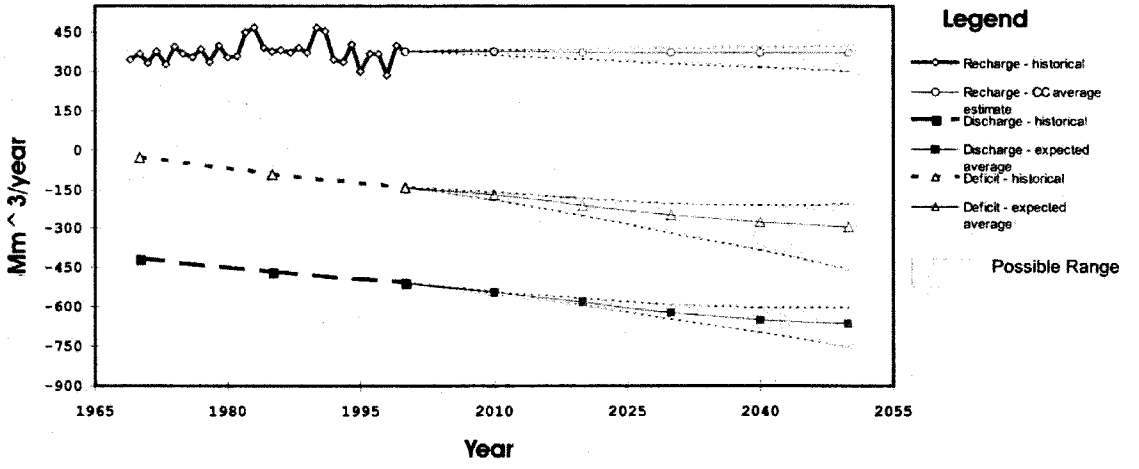


Figure 6: Résumé du budget en eau souterraine entre 1970 et 2050. Entre 1970 et 1999 les données réelles de la recharge sont présentées. Entre 2000 et 2050, la prédiction moyenne incluant les changements climatiques est démontrée. Le déficit est calculé par la somme de la décharge et de la recharge (tirée de Calderhead et al. 2009a).

Les ressources en eau renouvelables sont actuellement exploitées à des taux préoccupants. 38% des ressources en eaux souterraines sont exportés du bassin. Le transfert inter-bassin et la demande locale croissante ont des effets néfastes sur l'approvisionnement en eau souterraine dans la vallée de Toluca. Les volumes actuellement exportés vers la ville de Mexico (6 m^3/s, figure 2), sont supérieurs au déficit

moyen actuel (tableau 1). Ainsi, si demain la Vallée de Toluca devait arrêter tous les transferts d'eau, elle ne serait plus dans une situation déficitaire.

Cette évaluation détaillée des deux composantes les plus importantes du cycle de l'eau (recharge et décharge) montre clairement que la raréfaction de l'eau dans le bassin de Toluca est due principalement au pompage des eaux souterraines (Tableau 1). Les changements climatiques sembleraient jouer un rôle dans l'augmentation du déficit, mais ses effets ne sont pas encore significatifs. L'analyse montre que le pompage actuel des eaux souterraines n'est pas durable. Le déficit actuel est estimé entre 140 et 170 Mm^3/an. À moins de changements drastiques, il est prévu que ce déficit pourrait augmenter jusqu'à 456 Mm^3/an d'ici l'an 2050. En faisant l'hypothèse selon laquelle le bassin était en équilibre en 1962 (figure 6, par extrapolation vers l'arrière), et en intégrant la courbe de déficit moyen de 2008 à 1962, le volume total d'eau enlevé du stockage s'élève à environ 3840 Mm^3. Suite aux résultats de cette étude, ce volume ne peut pas être considéré comme une ressource renouvelable. Le déficit se produisant dans la vallée de Toluca peut être considéré comme un sérieux problème et les projections pour la consommation en eau et les changements climatique renforcent la nécessité pour une gestion responsable de la ressource en eau.

5 GÉOLOGIE

Des roches volcaniques andésitiques fracturées d'âge miocène forment le sous-sol du bassin (figure 7). La roche fracturée forme une cuvette au centre de la vallée, atteignant des profondeurs supérieures à 600 m et affleurant à la surface en bordure de la vallée. La formation volcanique andésitique du Nevado de Toluca est située à l'ouest. La roche fracturée est recouverte par des couches d'argiles lacustres (semi-perméables) et par la formation aquifère Chalma (Ariel et Consultores, 1996), composée d'un mélange de sable, de gravier et d'argile. L'aquifère de la formation de Tarango, mis en place après la formation Chalma, s'étend à partir des flancs de la chaîne de montagne las Cruces à l'est jusqu'au pied du volcan Nevado de Toluca. Cette formation est un mélange hétérogène de matériaux volcaniclastes (Lesser y Asociados, 1992). L'aquifère composé de roches

basaltiques et des flux de cendres de la formation Chichinautzin a été déposé dans la partie orientale de la vallée de Toluca. Dans la partie moyenne supérieure de la vallée, où la plupart du pompage d'eaux souterraines se produit, on retrouve des couches inter-mélangées d'argile lacustre (semi-perméable) et des dépôts d'alluvions (aquifères).

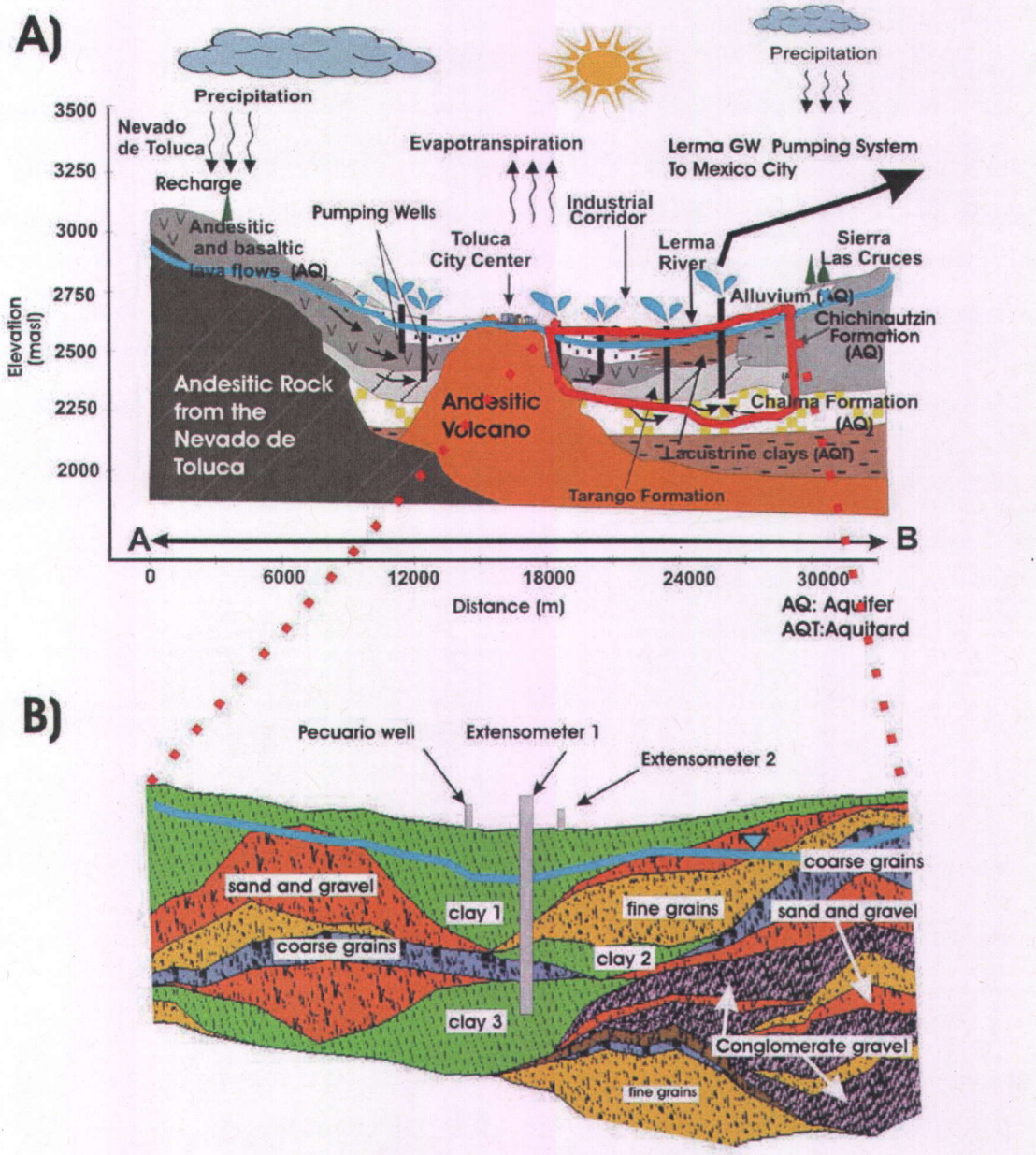


Figure 7: 7A : Modèle conceptuel et géologie de la vallée de Toluca. 7B : Agrandissement de la géologie de la zone d'étude (tirée de Calderhead et al., 2009c).

Pour faire face à la complexité de la stratigraphie de la vallée de Toluca, des journaux de forage sont utilisés pour générer une représentation régionale du modèle géologique 3D.

Un total de 211 journaux de forages (Figure 8A: Lerma 151 puits de pompage, 48 multi-piézomètres, et 12 puits supplémentaires) de la vallée de Toluca ont été utilisés pour créer le modèle géologique 3D. 22 types de matériaux géologiques, allant d'argile et de sable fin jusqu'à un gravier grossier et de la roche volcanique fracturée ont été simplifiés en 10 types de matériaux. En se fiant aux journaux de forage et les sections transversales, le logiciel GMS 6.5 utilise une série d'algorithmes (GMS, 2009) pour l'attribution d'horizons, pour créer des sections transversales entre les forages et, enfin, produire les couches géologiques. Au total, 34 couches géologiques (figure 8B) ont été générées et regroupées par la suite. En effet, l'examen attentif de la stratigraphie de chaque puits combiné avec la comparaison des sections transversales (Ariel Consultores, 1996) a été nécessaire pour obtenir une simplification détaillée de la représentation géologique du bassin.

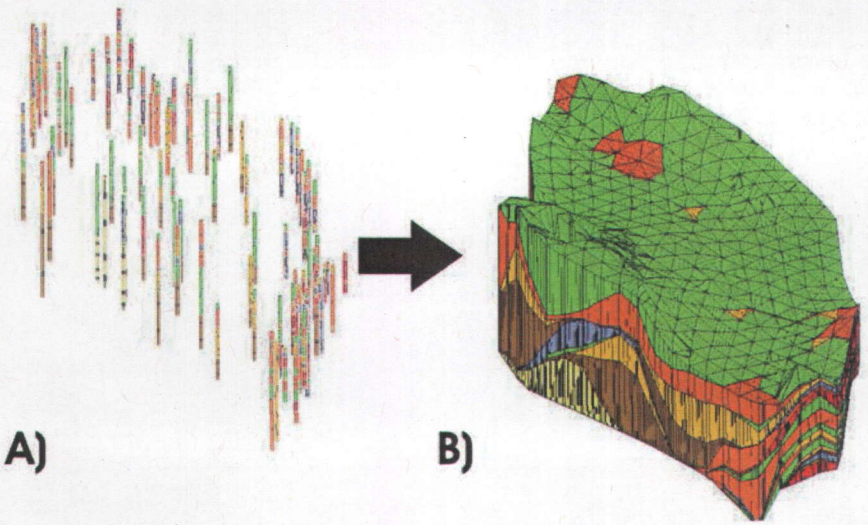


Figure 8: Génération du modèle géologique (8B) à partir de logs de forage (8A).

Puisque la grande majorité de la compaction se manifeste là où se retrouvent les argiles, il est important d'identifier la position ainsi que l'épaisseur des couches d'argile.
En utilisant le modèle géologique présenté dans la figure 8B, il a été possible d'identifier et d'isoler les couches d'argile majeures. La figure 9 présente les deux couches majeures (A et B) ainsi que la somme verticale des épaisseurs d'argile (C).

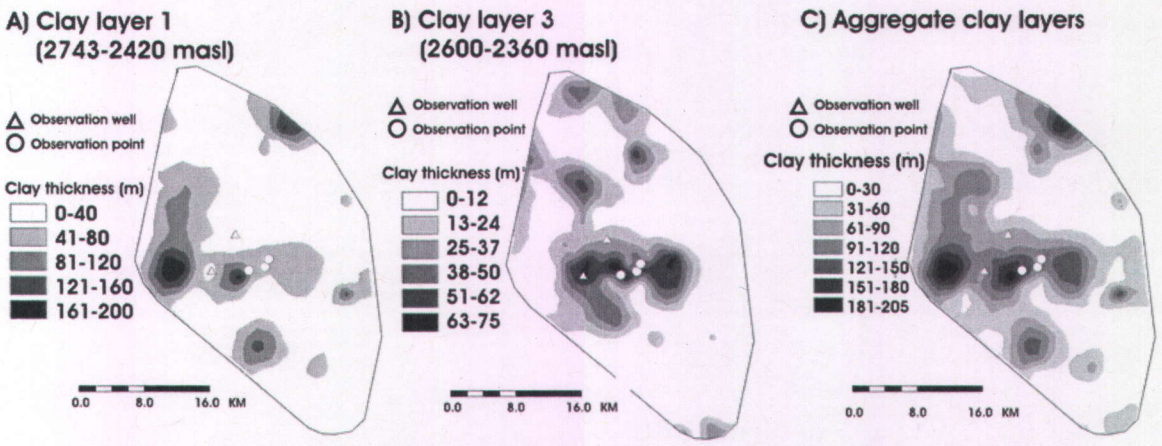


Figure 9: Épaisseurs des couches argileuses majeures (9A-9B) et la somme verticale des épaisseurs des couches argileuses (9C) (tiré de Calderhead et al., 2009c).

6 TÉLÉDÉTECTION

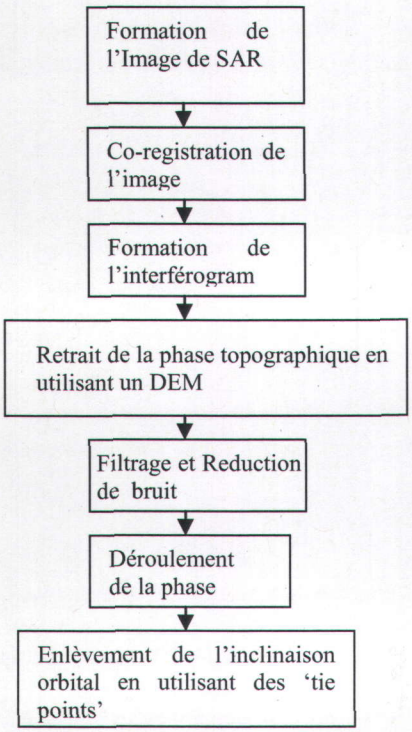
Introduction à InSAR

Les techniques interférométriques ont étés utilisées pour créer des cartes topographiques (e.g. Zebker et Goldstein (1985), Gabriel et al (1989)), pour observer les courants océaniques (Zebker et Goldstein, 1987; Goldstein and Zebker, 1988), mesurer les déplacements de la surface des volcans (Massonnet et al., 1993, 1995) et beaucoup d'autres processus naturels qui ont lieu à la surface de la terre. Galloway et al., (1998) ont été les premiers à utiliser un interférogramme pour caractériser la subsidence, appliqué au cas de la vallée d'Antelope en Californie. Amelung et al., (1999) ont présenté des cartes de subsidence pour mesurer les variations des taux de subsidence selon la saison (été - hiver). Plus tard, Hoffman et al., (2003a) ont utilisé des interférogrammes pour estimer des coefficients d'emmagasinements en 2D.

La technique InSAR (Interferometric Synthetic Aperture Radar) consiste à comparer des images multiples de radar satellitaires acquises avec des points de vue quasiment identiques dans l'espace, mais à des instants différents. Les schémas d'interférence des radars ou "interférogrammes" sont corrigés pour prendre en considération les subtiles différences topographiques et atmosphériques ou barométriques. Les variations sur le terrain se reflètent dans les interférogrammes et procurent ainsi des mesures précises à

quelques millimètres près, sur des superficies pouvant atteindre plusieurs dizaines de kilomètres.

Mentionné brièvement dans Calderhead et al., (2009b), le modèle conceptuel de la méthodologie pour obtenir des images de subsidence est présenté dans la figure 10.



Modifié de Hoffman (2003)

Figure 10. Modèle conceptuel de la méthodologie pour obtenir des images de subsidence par InSAR.

Voir Annexe F pour la théorie de base et les limitations de l'InSAR.

L'utilisation des techniques InSAR dans la Vallée de Toluca

Nous avons obtenu et utilisé des données de l'Agence Spatiale Européenne (ESA) provenant des satellites ERS-1, ERS-2 et ENVISAT, ainsi que de RADARSAT-1 de l'agence spatiale canadienne (ASC). Les images Synthetic Aperture Radar (SAR) sont disponibles sporadiquement pour les années 1996 à 2008 (voir tableau 2).

Tableau 2: Images SAR de la vallée de Toluca acquises entre 1995 et 2008 (tiré de Calderhead et al., 2009b)

Mission	Date	Track	Frame	Pass
ERS-1	12/12/1995	26	3213	descending
ERS-1	28/01/1996	191	369	ascending
ERS-1	07/04/1996	191	369	ascending
ERS-2	21/03/2001	26	3213	descending
ERS-2	17/10/2001	26	3213	descending
ERS-2	15/05/2002	26	3213	descending
ERS-2	28/08/2002	26	3213	descending
ENVISAT ASAR	26/03/2003	2026	3213	ascending
ENVISAT ASAR	09/07/2003	2026	3213	ascending
ENVISAT ASAR	13/08/2003	2026	3213	ascending
ENVISAT ASAR	04/02/2004	2026	3213	ascending
ENVISAT ASAR	14/04/2004	2026	3213	ascending
ENVISAT ASAR	15/12/2004	2026	3213	ascending
ENVISAT ASAR	19/01/2005	2026	3213	ascending
ENVISAT ASAR	08/06/2005	2026	3213	ascending
ENVISAT ASAR	30/11/2005	2026	3213	ascending
ENVISAT ASAR	05/12/2007	2026	3213	ascending
ENVISAT ASAR	13/02/2008	2026	3213	ascending
ENVISAT ASAR	23/04/2008	2026	3213	ascending
ENVISAT ASAR	28/05/2008	2026	3213	ascending
Mission	**Date**	**Abs. Orbit**	**Cycle**	**Pass**
RADARSAT-1 (F4 beam)	05/12/2003	42196	122	ascending
RADARSAT-1 (F4 beam)	29/12/2003	42539	123	ascending
RADARSAT-1 (F4 beam)	10/03/2004	43568	126	ascending
RADARSAT-1 (F4 beam)	01/08/2004	45626	132	ascending
RADARSAT-1 (F4 beam)	29/11/2004	47341	137	ascending
RADARSAT-1 (F4 beam)	23/12/2004	47684	139	ascending
RADARSAT-1 (F4 beam)	14/11/2007	62776	182	ascending
RADARSAT-1 (F4 beam)	25/01/2008	63805	185	ascending
RADARSAT-1 (F4 beam)	13/03/2008	64491	187	ascending
RADARSAT-1 (F4 beam)	24/05/2008	65520	190	ascending

Un total de trois images ERS-1, quatre images ERS-2, 13 images ENVISAT ASAR, ainsi que 10 images RADARSAT-1 ont été obtenues. Toutes les images obtenues entre le 14 novembre 2007 et le 28 mai, 2008 ont été demandées par l'étudiant, c'est-à-dire qu'après une demande formelle, les agences spatiales ont accepté de prendre les images de spécification SAR, *Single-Look-Complex* à ces dates. Toutes les autres images étaient disponibles en archive. À partir de décembre, 2007 tout échantillonnage sur le terrain a été coordonné avec des dates d'acquisition de données de RADARSAT-1 et ENVISAT ASAR.

Tableau 3: Interférogrammes de la Vallée de Toluca avec origine des images (mission) pour faire l'interférogramme, date d'acquisition d'images, ligne de base (baseline) perpendiculaire (b perp.) et ligne de base (baseline) parallèle (b paral.) en mètres, décalage de temps en jours (d_days), ainsi qu'une description de la pertinence de l'interférogramme (tiré de Calderhead et al., 2009b).

Mission	Date 1	Date 2	b perp.	b paral.	d_days	useful
ERS-1	1996-01-28	1996-04-07	26	22	70	yes
ERS-2	2001-03-21	2001-10-17	7121	2723	210	no
ERS-2	2001-10-17	2002-05-15	126	114	210	no
ERS-2	2002-05-15	2002-08-28	516	126	105	no
ENVISAT ASAR	2003-03-26	2003-07-09	869	413	105	no
ENVISAT ASAR	2003-03-26	2003-08-13	858	400	140	no
ENVISAT ASAR	2003-03-26	2004-02-04	74	77	315	yes
ENVISAT ASAR	2003-07-09	2004-02-04	505	126	210	yes
ENVISAT ASAR	2004-02-04	2004-04-14	310	73	70	yes
ENVISAT ASAR	2004-02-04	2004-12-15	64	14	315	yes
ENVISAT ASAR	2004-02-04	2005-01-19	120	46	350	yes
ENVISAT ASAR	2004-04-14	2004-12-15	374	87	245	yes
ENVISAT ASAR	2004-12-15	2005-01-19	56	32	35	yes
ENVISAT ASAR	2004-12-15	2007-12-05	100	74	1085	no
ENVISAT ASAR	2005-01-19	2005-06-08	243	125	140	yes
ENVISAT ASAR	2005-01-19	2005-11-30	94	40	315	yes
ENVISAT ASAR	2005-06-08	2005-11-30	149	85	175	yes
ENVISAT ASAR	2005-11-30	2007-12-05	217	88	735	yes
ENVISAT ASAR	2007-12-05	2008-02-13	29	33	70	yes
ENVISAT ASAR	2007-12-05	2008-04-23	85	86	140	yes
ENVISAT ASAR	2007-12-05	2008-05-28	185	2	175	yes
ENVISAT ASAR	2008-02-13	2008-04-23	172	41	70	yes
ENVISAT ASAR	2008-02-13	2008-05-28	323	108	105	yes
ENVISAT ASAR	2008-04-23	2008-05-28	151	149	35	yes
RADARSAT-1	2003-12-05	2003-12-29	1052	869	24	no
RADARSAT-1	2003-12-05	2004-03-10	592	456	96	yes
RADARSAT-1	2003-12-05	2004-11-29	1291	1074	360	no
RADARSAT-1	2003-12-29	2004-03-10	459	412	72	yes
RADARSAT-1	2003-12-29	2004-08-01	1125	942	216	no
RADARSAT-1	2003-12-29	2004-12-23	841	659	360	yes
RADARSAT-1	2004-03-10	2004-08-01	695	636	144	yes
RADARSAT-1	2004-03-10	2004-11-29	698	617	264	yes
RADARSAT-1	2004-08-01	2004-11-29	1393	1253	120	no
RADARSAT-1	2004-08-01	2004-12-23	312	389	144	yes
RADARSAT-1	2004-11-29	2004-12-23	1081	865	24	no
RADARSAT-1	2004-11-29	2007-11-14	1125	595	625	yes
RADARSAT-1	2004-08-01	2007-11-14	267	310	1200	no
RADARSAT-1	2004-12-23	2007-11-14	44	78	1056	yes
RADARSAT-1	2007-11-14	2008-01-25	521	452	72	yes
RADARSAT-1	2007-11-14	2008-03-13	28	5	120	yes
RADARSAT-1	2007-11-14	2008-05-24	754	654	192	yes
RADARSAT-1	2008-01-25	2008-03-13	492	446	48	yes
RADARSAT-1	2008-01-25	2008-05-24	1239	1015	120	no
RADARSAT-1	2008-03-13	2008-05-24	746	568	72	yes

Le tableau 3 montre les 44 interférogrammes générés par l'étudiant avec le logiciel EarthView InSAR (MDA, 2007). Des 44 interférogrammes, seulement 31 sont considérés comme pertinents, c'est-à-dire qu'il est possible d'obtenir de l'information sur la compaction.

En raison de la décorrélation temporelle et de grandes lignes de base perpendiculaires (perpendicular baselines – Annexe F pour description), les images provenant d'ERS-2 n'étaient pas utilisables pour notre étude. Seulement une paire ERS-1 était utilisable. Les autres paires d'images utilisées dans l'étude proviennent soit d'ENVISAT ASAR ou soit de RADARSAT-1.

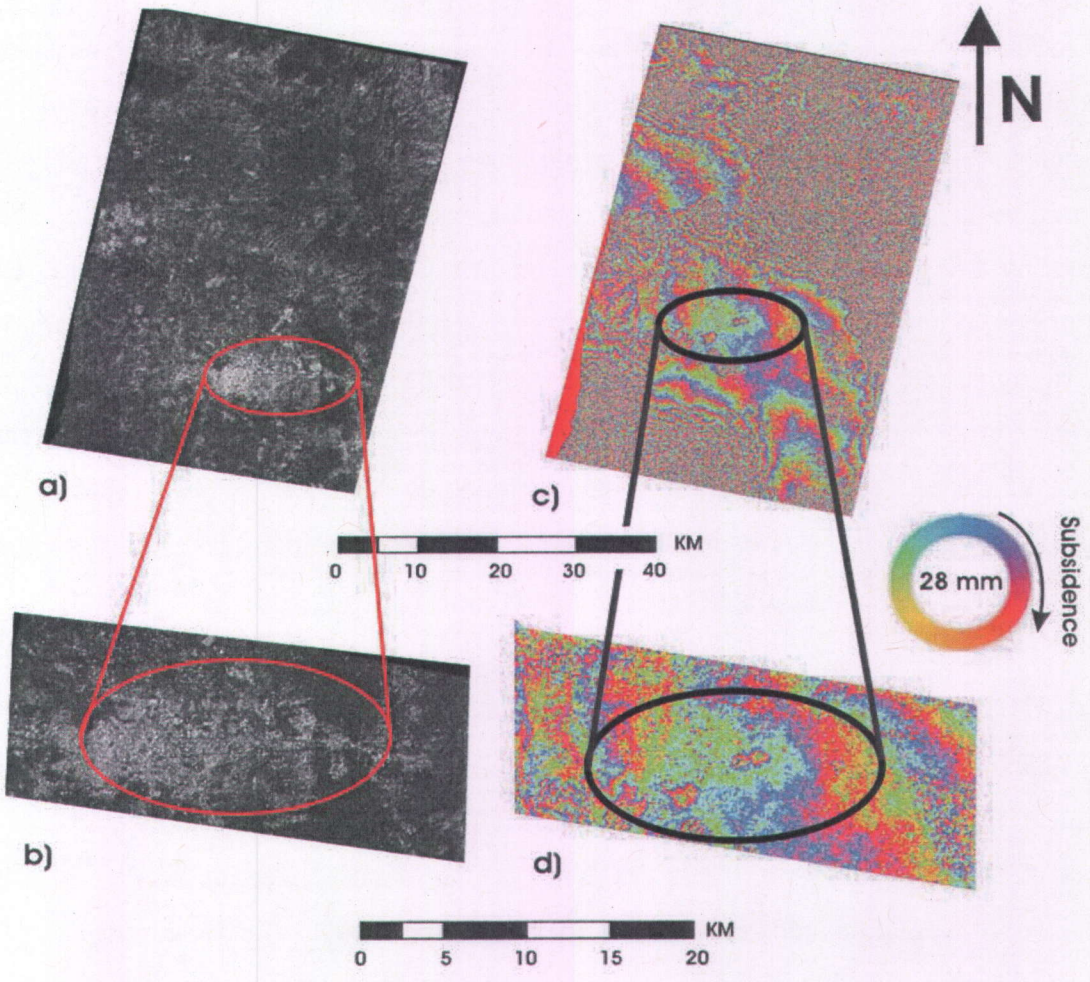


Figure 11 : a) et b) démontrent la cohérence dans la vallée de Toluca pour une paire d'images ENVISAT ASAR acquissent le 5 Décembre 2007 et le 28 Mai, 2008. c) et d) démontrent l'interférogramme de la même paire d'images. b) est un zoom de a) et d) est un zoom de c) (tirée de Calderhead et al., 2009b).

Les figures 11a et 11b montrent la cohérence dans la vallée de Toluca pour une paire d'images ENVISAT ASAR acquisse le 5 décembre 2007 et le 28 mai, 2008. Avec une cohérence élevée, il est plus facile de détecter un mouvement de terrain. La couleur blanche représente une cohérence élevée et les couleurs foncées représentent une faible cohérence. La cohérence est plus élevée dans les zones urbaines et diminue fortement dans les zones végétales et lorsque les images sont acquises pendant la saison de croissance végétative (mai à novembre). De plus, une cohérence élevée est obtenus lorsque les images acquises ont un écart entre les acquisitions de moins d'un an. Dans certain cas il a été possible d'utiliser un écart entre les acquisitions d'image plus long (jusqu'à 3 ans de différence).

Les conditions atmosphériques entraînent des variations dans les interférogrammes. Cependant, les zones d'affaissement ont été observées dans tous les interférogrammes utilisables, donc le signal détecté n'est pas du aux variations atmosphériques. Une zone d'intérêt, où la subsidence est détectée et mesurée, est évidente aux Figures 11c et 11d. Sachant qu'ENVISAT ASAR utilise le radar en bande C (longueur d'onde de 5,6 cm), les estimations préliminaires des mouvements de terrain sont obtenues à partir de l'interférogramme. Une frange complète, rouge-vert-bleue, ou un cycle 2π de phase, représente un déplacement de terrain de $\lambda / 2$ (2,8 cm) quand le sol est plat (souvent le cas dans la Vallée de Toluca), où λ est la longueur d'onde du capteur SAR (voir figure 11). Les relevées de terrain, c'est-à-dire les mesures d'affaissement dans les extensomètres, aident à vérifier les résultats obtenus par cette méthode.

Figures 11c et 11d démontrent l'interférogramme de la même paire d'images (5 décembre 2007 et mai 28, 2008) pour la vallée de Toluca. Les grandes franges de la figure 11c indiquent les zones où la cohérence est suffisante pour détecter les mouvements de terrain. Les pixels épars représentent des zones où l'information ne peut pas être utilisée en raison d'une faible cohérence. Dans la plupart des cas, à l'extérieur des zones urbaines, il est impossible d'obtenir des informations utiles, puisque l'usage des sols est surtout caractérisé par la croissance végétative.

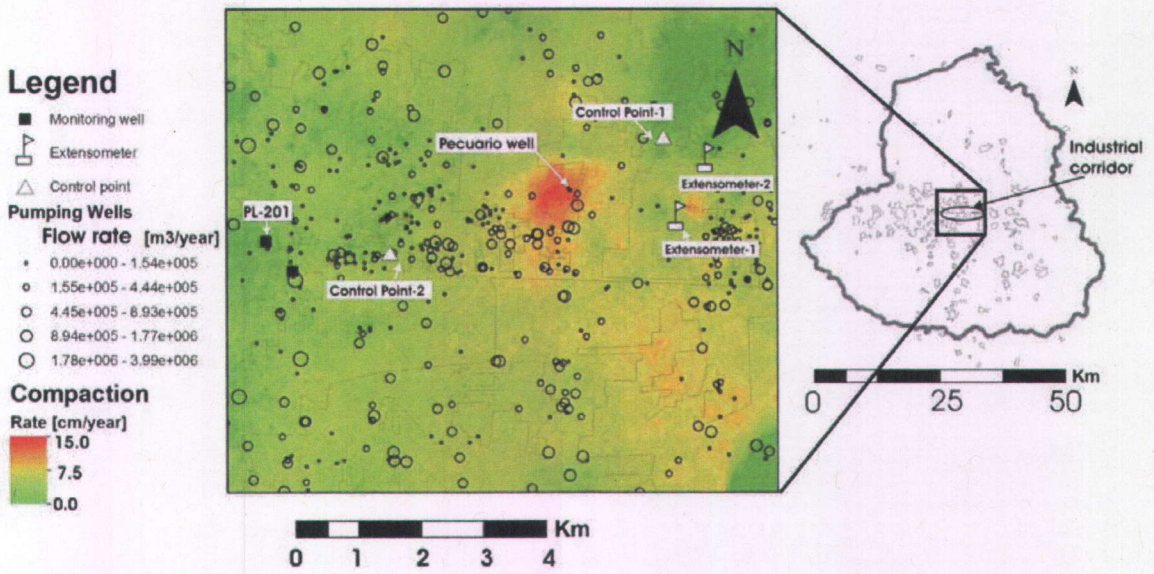


Figure 12: Description de la zone d'intérêt dans la vallée de Toluca; position des extensomètres, points de contrôle, puits d'observation, puits de pompage, et les taux d'affaissement mesurés avec InSAR entre décembre 2007 et mai 2008 (tirée de Calderhead et al., 2009b).

La figure 12 montre un exemple du produit final d'InSAR. On perçoit une carte de déformation du corridor industriel. La région d'affaissement maximal est de couleur rouge. Cette zone est détectée dans tous les interférogrammes mentionnés dans le tableau 3, donc elle n'est pas causée par des perturbations atmosphériques. Dans cette image, le plus haut taux d'affaissement est estimé à 7.2 cm en 175 jours ou 15 cm/an.

7 MODÉLISATION

La théorie de compaction, discutée plus en détail au Chapitre 4 (Calderhead et al., 2009c), se base sur le principe de Terzhagi (1925). Voir Annexe B pour une liste de modeles de compaction. En observant les argiles de la vallée de Toluca (e.g. Figure 13), il est possible de constater qu'elles se déforment tant de façon élastique qu'inélastique.

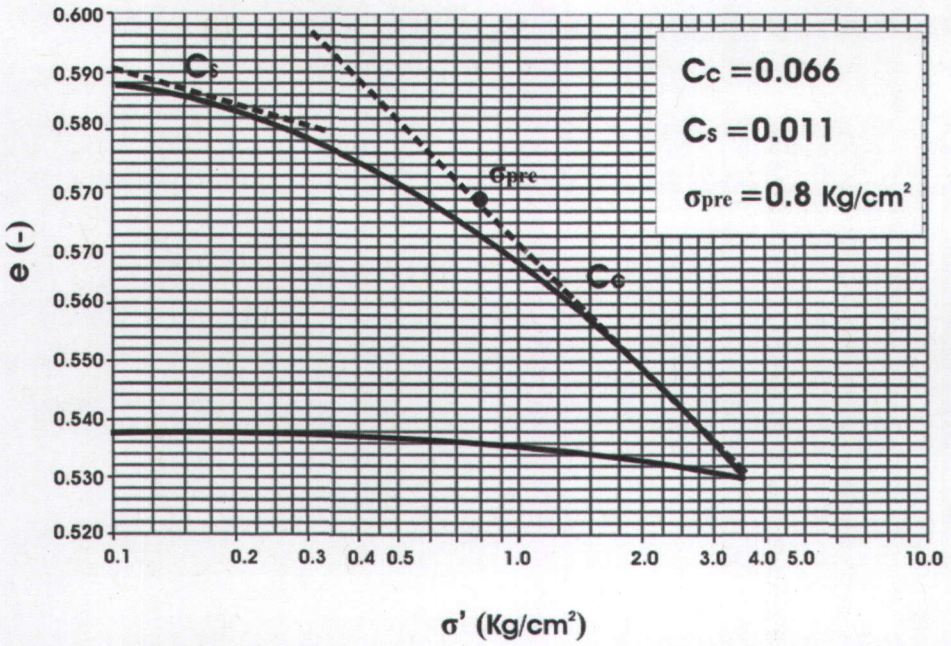


Figure 13: Exemple de résultats de tests de compression d'une argile typique de la Vallée de Toluca (de UAEM, 2008): Indice des vide (e) versus la contrainte effective (σ'), ou $\sigma_{(pre)}$ est la contrainte effective de préconsolidation, C_c est l'indice de compression inélastique et C_s est l'indice de compression élastique (tirée de Calderhead et al., 2009c)

La compressibilité ($\overline{\alpha}$), l'emmagasinement spécifique squelettique élastique (S'_{ske}) et l'emmagasinement spécifique squelettique inélastique (S'_{skv}) peuvent être obtenus de tests de consolidation en utilisant C_c et C_s (Figure 13 et Calderhead et al., 2009c).

Pour tenir compte de la modification significative de l'emmagasinement spécifique squelettique, lorsque la contrainte effective dépasse la contrainte effective de préconsolidation, deux valeurs distinctes sont souvent utilisées. Pour des contraintes supérieures à la contrainte de préconsolidation, S'_{skv} est utilisé, et S'_{ske} est utilisé pour des contraintes inférieur à la contrainte de préconsolidation (figure 13). Dans une certaine mesure, cette approche linéarise la contrainte non-linéaire de la relation de compaction à l'égard de la contrainte de préconsolidation. En observant la figure 13 et autres courbes e - log σ'_{zz} à partir d'essais de consolidation des argiles de la Vallée de Toluca (Minor, 2007), la loi constitutive résultante (représentée par l'équation 8 dans Calderhead et al., 2009c) est une bonne estimation de ces argiles, mais elle n'est qu'une approximation des processus de compaction des sédiments.

De plus, nous constatons qu'il y a des délais de compaction, d'environs 4 mois, avec la baisse du niveau piézométrique (e.g. voir figure 8 du chapitre 2). Étant donné que les délais ne sont pas très grandes par rapport a la longueur des simulations (100 ans), il est supposé qu'en simulant la compaction instantané, les différences avec les simulations et la réalité sont négligeables.

Maintenant que les processus de compactions des argiles de la Vallée de Toluca ont été introduits, l'étape de la modélisation suit et se divise en cinq parties distinctes (1) couplage d'un module de compaction avec le modèle HydroGeoSphere; (2) vérification du nouveau modèle; (3) conception et mise en œuvre du modèle numérique de la vallée de Toluca; (4) calage; et (5) résultats des simulations

7.1 Couplage d'un module de compaction

Une partie importante de cette thèse consiste à intégrer le processus de l'affaissement dû au pompage dans le logiciel de HydroGeoSphere (HGS) (Therrien et al., 2009). HGS est un modèle numérique complet et entièrement intégré décrivant l'écoulement 2D des eaux de surface et l'écoulement souterrain 3D à saturation variable en plus du transport de masse dissout et du transport réactif.

HGS a été amélioré en incorporant un module capable de simuler la déformation instantanée de milieux poro-élastique et poro-inélastique, afin de prendre en considération les phénomènes réversibles et irréversibles. L'accent a été mis sur la déformation inélastique due à la subsidence irréversible des matériaux de l'aquifère qui a lieu dans la Vallée de Toluca. Le module simulant la déformation a été couplé au module d'écoulement HGS pour prendre en considération la compaction instantanée du milieu poreux. La théorie pour représenter le couplage HGS-compaction est présentée au chapitre 4.

La formulation utilisée pour le couplage a été précédemment mise en œuvre dans le modèle en différences-finies, MODFLOW (Leake et Prudic, 1991; Hoffman et al., 2003b, Leake et Galloway, 2007) (Voir chapitre 4). Une différence importante avec les modules

MODFLOW est que le couplage a été fait avec un modèle d'éléments-fini et la méthode de solution implicite utilise l'itération Picard (Calderhead et al., 2009c).

En combinant les termes de compaction à l'équation d'écoulement de HGS, nous obtenons (Voir aussi Chapitre 4):

$$-\nabla \cdot q + \sum \Gamma_{ex} \pm Q = [(1-\gamma^*) * S_s + \gamma * S'_{sk}] \frac{\partial h}{\partial t} \qquad (1)$$

Le couplage ignore les délais de compaction dus à une dissipation lente des charges hydrauliques transitoires dans les argiles et suppose que les charges s'équilibres partout instantanément avec la charge dans l'aquifère environnant. Bien que les délais peuvent être importants dans certaines argiles (par exemple, Mexico), les argiles de la vallée de Toluca ont une réponse de compaction rapide quand il y a une diminution de la charge. (voir figure 19, comparaison de compaction dans l'extensomètre et charge hydraulique dans l'extensomètre).

7.2 Validation du nouveau modèle

Les modules de MODFLOW-SUB et la partie relative à l'écoulement de HGS ont été vérifiés par des solutions analytiques (Hoffmann et al., 2003b; Therrien et al., 2009) et ont été appliqués avec succès à plusieurs études de cas (Galloway and Hoffman, 2007; Therrien et al., 2009). Le nouveau module de compaction dans HGS est ainsi vérifié en le comparant avec MODFLOW-SUB dans la résolution d'un problème. Le scénario (Figure 14) est tiré de Hoffmann et al. (2003b) et décrit dans le Chapitre 4.

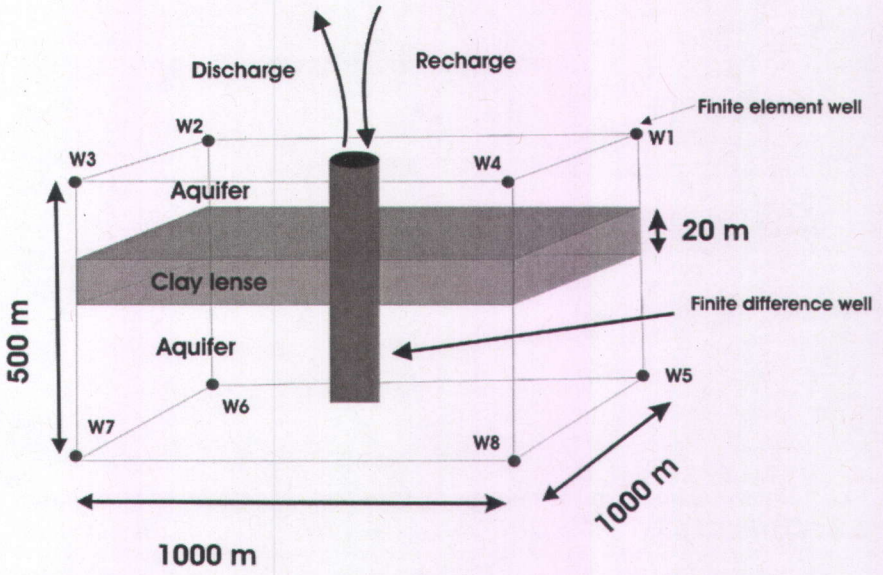


Figure 14: Problème de vérification - Configuration du modèle utilisé pour simuler une variation saisonnière de la contrainte. Les seuls entrants et sortants dans le système sont la recharge ou la décharge par le(s) puits et l'emmagasinement dans l'aquifère et la couche d'argile. Le modèle MODFLOW-SUB en différences-finies utilise un seul puits pour la recharge et la décharge. La méthode d'éléments-finis de HGS utilise les 8 coins du bloc pour les puits (W1-W8), avec le pompage et les débits d'injection, respectivement, divisés par 8 pour chaque puits (tiré de Calderhead et al., 2009c).

La simulation HGS utilise un modèle en éléments-finis et les charges hydrauliques sont donc simulées aux nœuds, et non dans le centre de cellules comme avec MODFLOW. Dans HGS, un élément 3D massif avec 8 nœuds est utilisé. Les taux de pompage sont également répartis entre les 8 nœuds, à l'inverse de MODFLOW où un seul taux est appliqué au centre de la cellule.

Les résultats de la simulation démontrent que les charges hydrauliques calculées à chaque nœud sont égales pour les deux modèles (Figure 15). La compaction totale (subsidence) en HGS (Figure 15) est calculée par la somme verticale de la compaction de chaque nœuds qui ont les mêmes coordonnées x, y.

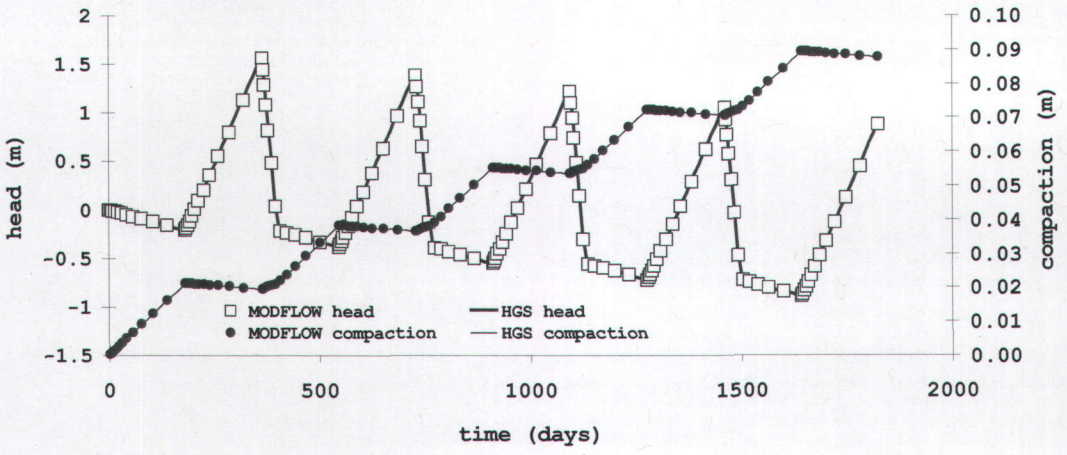


Figure 15: Résultats de vérification démontrant la charge hydraulique et la compaction totale pour les simulations HGS-COMPACTION ET MODFLOW-SUB (tirée de Calderhead et al., 2009c).

Les charges hydrauliques et la compaction totale de la couche calculées dans MODFLOW-SUB et dans HGS-compaction sont présentées à la figure 15. Pour chaque modèle, nous notons que les charges hydrauliques et les valeurs de compaction sont identiques. En utilisant les équations de couplage et les time weighting schemes (implicites) identiques, des résultats identiques ont été obtenus avec les deux modèles.

7.3 Conception et mise en œuvre du modèle numérique dans la Valle de Toluca

Cette section présente la configuration du modèle numérique. Les paramètres qui ont été incorporés dans le modèle régionale sont : les conditions initiales et limites, la recharge, le pompage, la méthode de solution (tableau 4), et le modèle géologique 3D (Figure 16).

Tableau 4: Conception du modèle numérique de la vallée de Toluca (tirée de Calderhead et al., 2009).

SIMULATION SETUP	DESCRIPTION
Boundary Conditions	
Uniform vertical recharge	135 mm/year
Constant head boundary	Nodes at top of layer 1; See Figure 8D for xy location of boundary
Initial conditions	
Hydraulic head	Estimated hydraulic head values from 1950 (based on CNA (2008)
Simulations begin date	January 1st,1950
Total pumping	
1950-1969	312 Mm^3/year
1970-1977	346 Mm^3/year
1978-1993	401 Mm^3/year
1994-2004	456 Mm^3/year
2005-2010	494 Mm^3/year
Solution	
Solution method	Picard Iteration
Absolute convergence criteria	1.0e-4
Maximum iteration	15
Initial timestep	1 day
Maximum timestep	100 days

Pour faire face à la stratigraphie complexe de la vallée de Toluca, une chaîne de traitement utilise des journaux de forage pour générer un maillage 3D utilisable dans HGS (Figure 16). Voir chapitre 4 pour plus de détails.

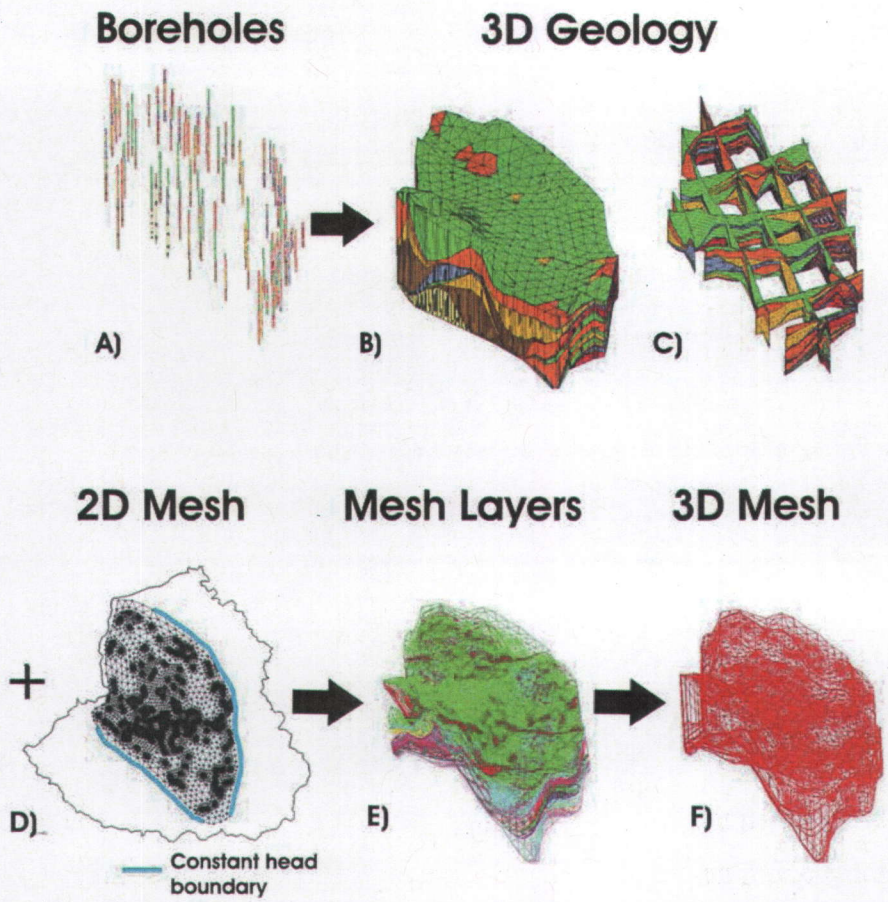


Figure 16: Chaîne de traitement pour l'obtention du modèle en éléments finis 3D. Les journaux de forage (A) sont utilisés pour générer la géologie en 3D (B et C), puis en utilisant les couches géologiques et le maillage 2D (D), la topographie des couches géologiques est extraite (E). Enfin, le maillage 3D (F) est généré (tiré de Calderhead et al., 2009c).

7.4 Calage

Charge hydraulique

Le calage des charges hydrauliques a été effectué en utilisant les charges hydrauliques ou le rabattement mesuré dans les piézomètres à niveaux multiples situés dans la vallée et dans les extensomètres. Les simulations du rabattement (figure 17) suivent, en générale, la charge hydraulique et les valeurs mesurées au PL-201, PL-205, et à Extensometer-1.

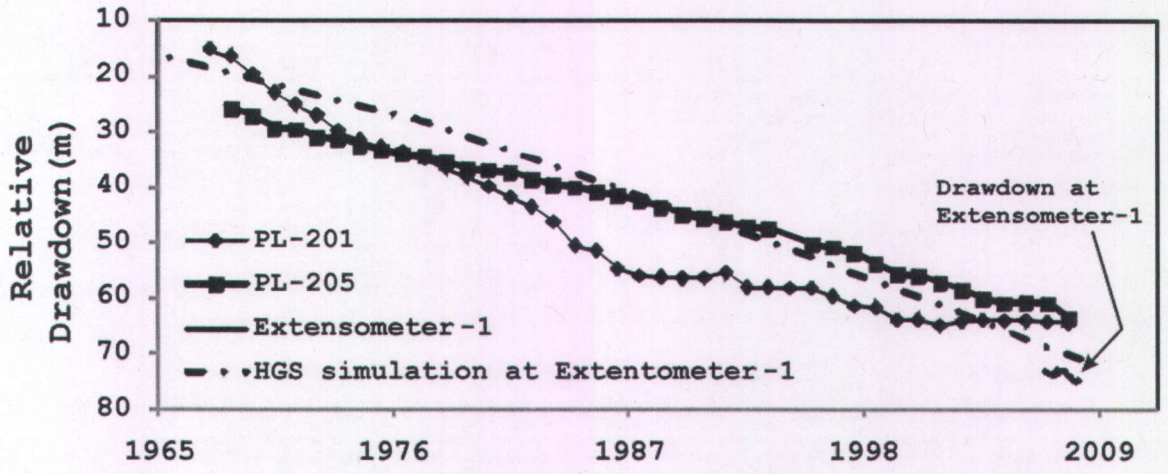


Figure 17: Rabattement relatif mesuré et simulé à l'Extensometre-1 ainsi qu'une comparaison avec les rabattements aux piézomètres multi-niveaux à proximité (PL-201 et PL-205) (tiré de Calderhead et al., 2009c).

Estimer S'_{sk} pour une couche individuelle

En utilisant l`épaisseur des couches argileuses (voir Calderhead et al., 2009c), les interférogrammes (e.g. Figure 18B), les données de pompage (IMTA, 2003) (figure 18A) et les mesures de charge hydraulique, S'_{ki} peut être contraint pour une couche individuelle *i*, appartenant au système de couches N. S'_K représente le coefficient de stockage squelettique du système aquifère des *N* couches en un lieu donné sur le plan xy, et est décrit par:

$$S'_k = \sum_{i=1}^{N} S'_{ki} = \sum_{i=1}^{N} S'_{ski}\, b_i \qquad (2)$$

où b_i est l'épaisseur de la couche *i*. En utilisant les données des journaux de forage, la fraction de matériel compressible (λ_i) peut être estimée pour toutes les couches *N*. En assignant la fraction de matériel compressible pour chaque couche, il est possible d'estimer S'_{sk} pour les couches individuelles d'argile (S'_{ski}). Le chapitre 4 présente la méthode pour assigner les valeurs de S'_{ski} pour chaque couche.

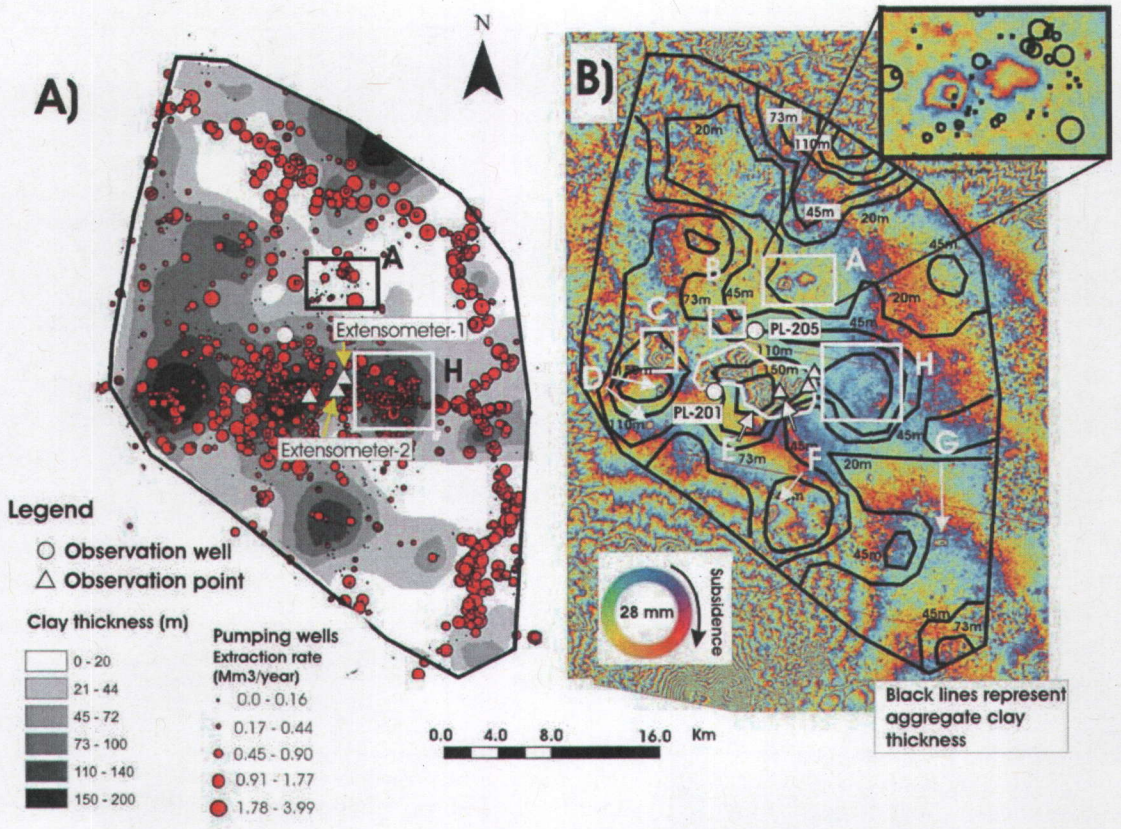


Figure 18: A) Somme verticale des épaisseurs de couches argileuses et position des puits de pompage avec leurs débits respectifs. Les zones blanches-gris-noires représentent la somme verticale des épaisseurs des couches argileuses. B) Interférogramme différentiel de la vallée de Toluca avec un intervalle d'acquisition de 70 jours. Les images ENVISAT ASAR ont été acquises le 5 décembre, 2007 et 13 février, 2008. Un cycle bleu-rouge-jaune représente l'affaissement vers le bas (2.8 cm), et à l'inverse, un cycle bleu-jaune-rouge représente un soulèvement. Les lignes noires représentent la somme verticale des épaisseurs des couches argileuses (à partir de 18A) (tirée de Calderhead et al., 2009c).

Compaction

La figure 19 montre la compaction totale simulée et mesurée à l'Extensometer- 1 par ENVISAT ASAR, RADARSAT-1, les valeurs prélevées sur le terrain à Extensometer-1, et simulé avec HGS. Lors des simulations, le pompage, Ss, S'_{skv}, et S'_{ske} ont été modifié pour obtenir une représentation respectable de la compaction (voir la section sur le calage dans Chapitre 4 et annexe H pour plus de détail).

Les rabattements (WL) simulés et mesurés à l'Extensometer-1 sont aussi montrés. Les simulations de compaction totale suivent relativement bien les résultats InSAR ainsi que les données de terrain.

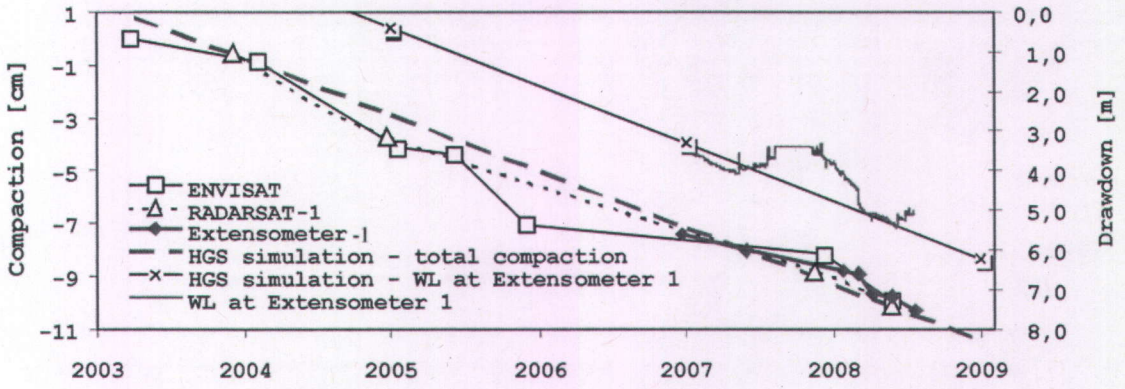


Figure 19: Compaction totale simulée et mesurée à Extensometer-1 par ENVISAT ASAR, RADARSAT-1, Extensometer-1, et les simulations HGS en fonctions du temps. Les rabattement (WL) simulé et mesuré à Extensometer-1 en fonction du temps sont aussi montré (tirée de Calderhead et al 2009c).

7.5 Résultats des simulations de compaction

L'affaissement régional est simulé pour la vallée de Toluca entre 1950 et 2010. La compaction totale pour les années 1952, 1963, 1978, 1991, 2003, et 2009 est présentée à la figure 20. On note qu'il y a peu d'affaissement avant 1978 et qu'à partir de cette date l'affaissement est surtout situé dans le centre de la vallée, là où il y a un pompage important et où les couches d'argiles sont épaisses. En 2009, un affaissement totale maximal de près de 2 mètres est simulé. Le rabattement de la charge hydraulique est présenté dans la section suivante.

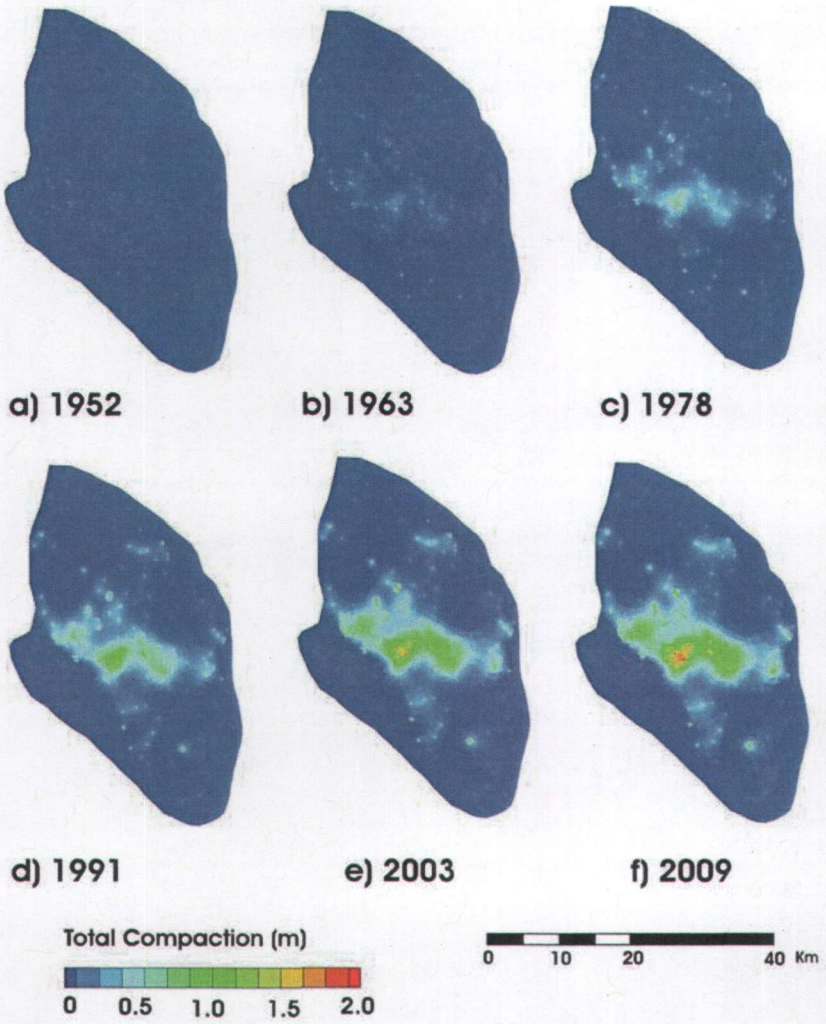


Figure 20: Évolution de l'affaissement régional dans la vallée de Toluca de 1960 à 2009 simulé avec HGS-Compaction (tirée de Calderhead et al., 2009c).

En comparant les simulations avec les resultats InSAR (figure 21), il est possible de constater qu'ils ne sont pas identiques. Par contre, les résultats sont acceptables et les simulations ainsi que les résultats InSAR reproduisent un affaissement semblable.

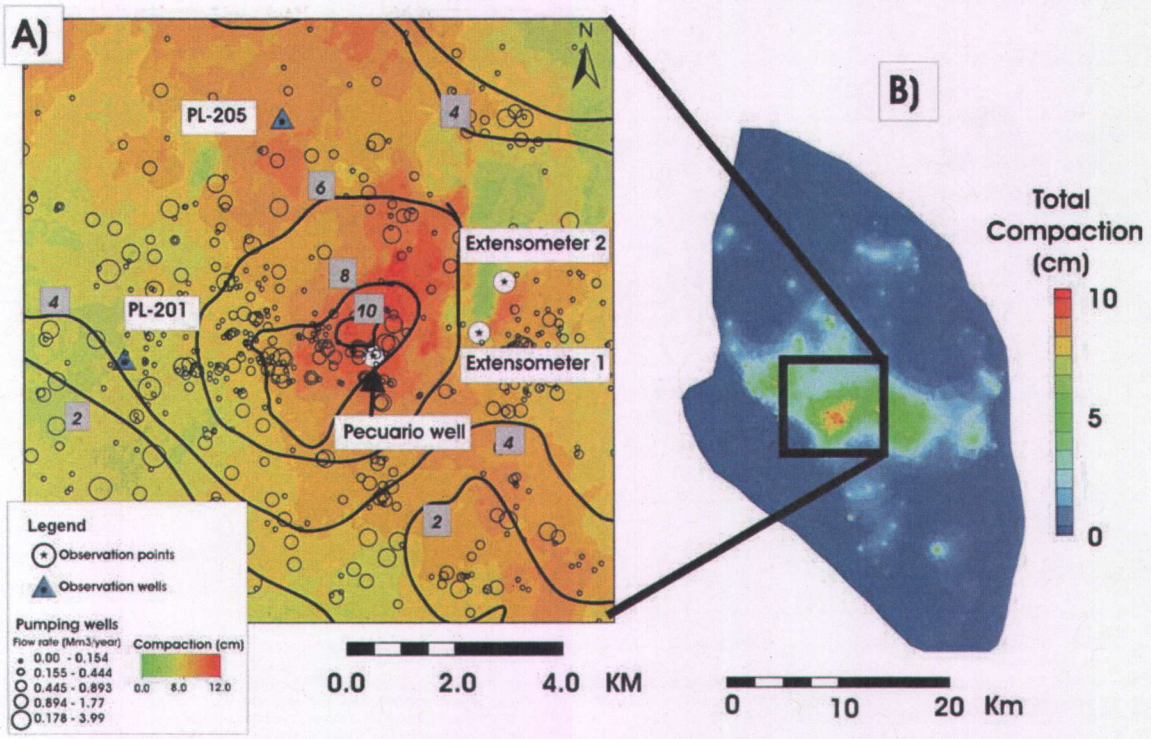


Figure 21: A) Simulation HGS-compaction (lignes solides noires) superposée à la carte de subsidence D-InSAR (remplissage en couleur) dans les 175 jours entre le 5 décembre 2007 et le 28 mai, 2008. L'emplacement des puits de pompage avec les taux de pompage est également indiqué. B) L'emplacement de la zone de compaction ainsi que la compaction régionale. (tirée de Calderhead et al., 2009c)

8 GESTION DE L'AQUIFÈRE

Huit scenarios avec des combinaisons différentes de taux de pompage, taux de recharge, et localité de pompage sont présentés afin d'aider à comprendre les possibilités d'affaissements futurs. Les scénarios 1-3 (Tableau 5) examinent les scenarios de recharge et de pompage dans le pire des cas (Scenario 1), le meilleur des cas (scenario 2), et les tendances moyennes attendues (scenario 3) (basés sur Calderhead et al., 2009a; et le IPCC (2007)). Les exportations vers Mexico augmentent (8 m^3/s) dans le pire des cas, diminue (3 m^3/s) dans le meilleur des cas, et reste constant (6 m^3/s) pour le scénario moyen. Un scénario probable est que le pompage vers Mexico diminue. Ainsi les scénarios 4 et 5 voient les exportations vers Mexico diminuer à 0 m^3/s et 3 m^3/s respectivement, tout en gardant des valeurs moyennes pour tous les autres paramètres. Le scénario 6 examine la possibilité de diminuer le pompage à Toluca (-25%) et Mexico (-

50%) à un taux plus durable. Les scénarios 7 et 8 utilisent le modèle de l'épaisseur d'argile (Calderhead et al., 2009c) pour déplacer les puits de pompage des zones à forte teneur en argile vers des zones à plus faible teneur en argile. Le scénario 7 utilise le pompage moyen attendu et le scénario 8 diminue les taux de pompage (aux valeurs du scénario 6). En diminuant le pompage pour l'usage local, les scénarios 6 et 8 impliquent une importation de l'eau à partir des bassins environnants.

Tableau 5: Scenarios de pompage 2010-2050 (tiré de Calderhead et al., 2009d).

Scenario	Lerma pumping (to Mexico City)	Toluca Pumping	Recharge	Description
1	33% increase	worst case	worst case	Worst case expected with 33% increased Lerma pumping
2	50% decrease	best case	best case	Best case expected with 50% decrease in Lerma
3	constant at 6m3/s	average	average case	Average case with Lerma pumping constant at 6m3/s
4	Stop Lerma pumping (0m3/s)	average	average case	Average case with stopping Lerma pumping
5	50% decrease	average	average case	Average case with a 50% decrease in Lerma pumping
6	50% decrease	decrease by 25%	average case	Decrease Lerma pumping by 50% and decrease Toluca Basin pumping by 25%
7	constant at 6m3/s	average	average case	Move pumping centres to locations with less clay (see figure 4)
8	50% decrease	decrease by 25%	average case	Move pumping centres to locations with less clay (see figure 4) and decrease Toluca Basin pumping by 25% and Lerma Pumping by 50%

La figure 22 présente les simulations de la distribution du rabattement de la charge hydraulique depuis 1950, pour le scénario 3 (tableau 5) entre 1962 et 2050. Le rabattement régional commence vers 1962 et augmente au cours des années à cause de l'augmentation du déficit en eaux souterraines. En 1990, il ya déjà un rabattement marqué de plus de 40 mètres dans le centre de la vallée. Ceci progresse de manière significative au cours des 60 années qui suivent, en augmentant jusqu'à plus de 120 m dans le corridor industriel en 2050.

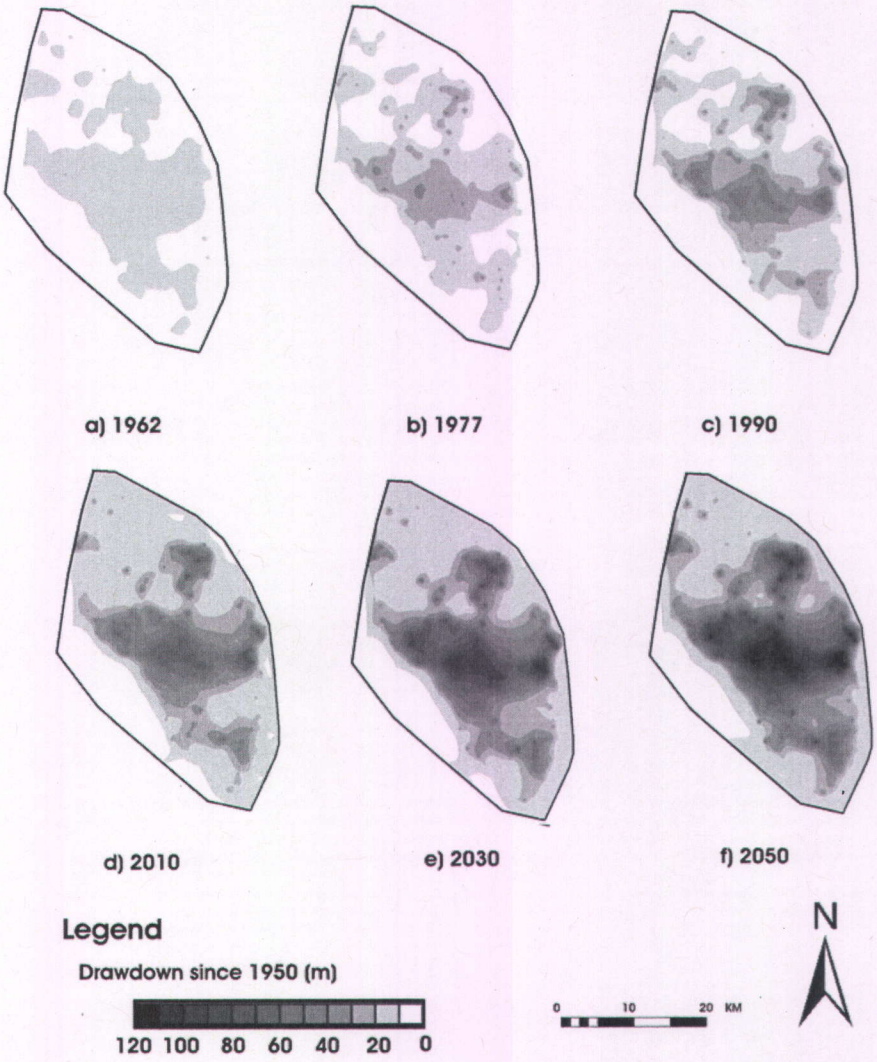


Figure 22: Rabattement de la charge hydraulique simulé depuis 1950 et présenté pour les années a)1962, b)1977, c)1990, d) 2010, e)2030, et f)2050 (tirée de Calderhead et al., 2009d).

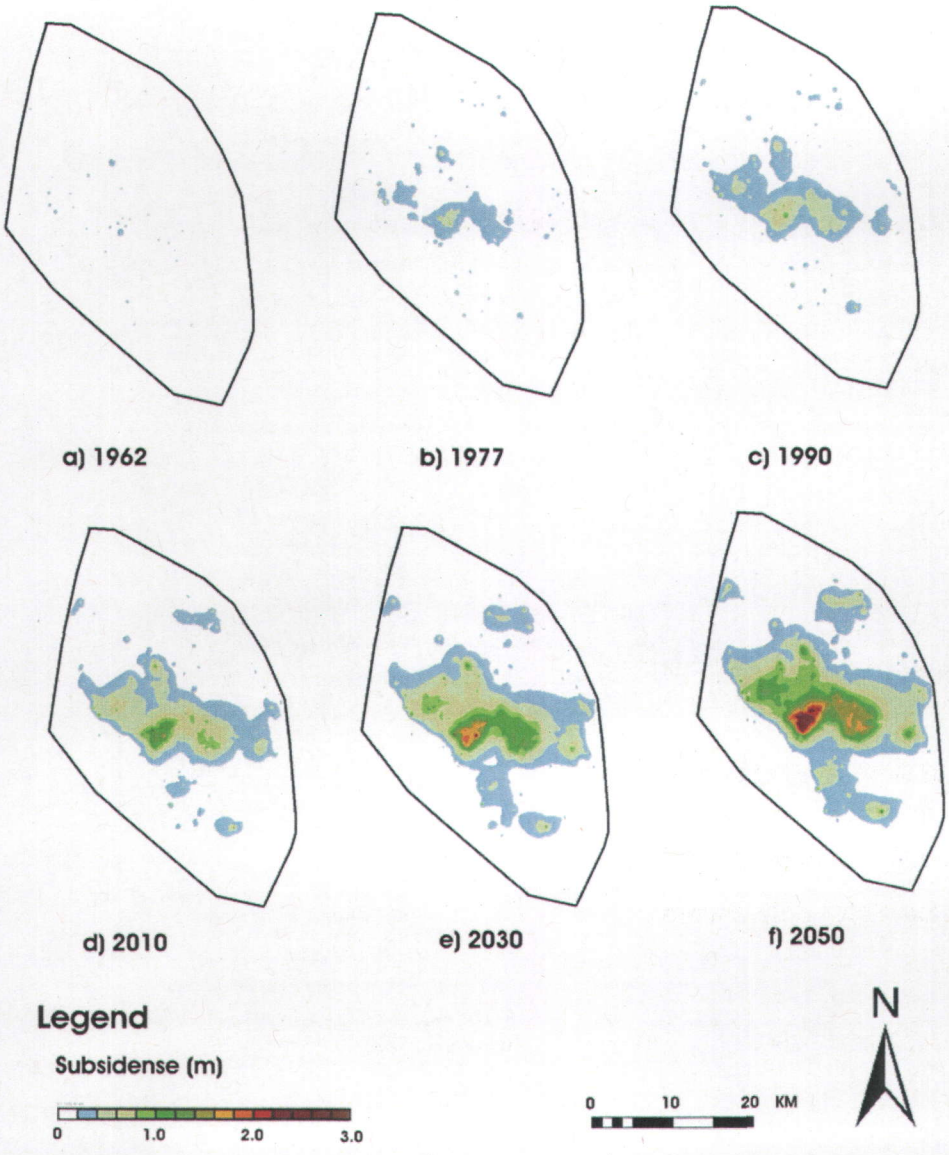


Figure 23: Distribution de la subsidence totale entre 1962 et 2050 (scénario 3) (tirée de Calderhead et al., 2009d).

La Figure 23 montre la progression de l'affaissement total dans la vallée de Toluca. Les résultats de 1962 à 2050 sont basés sur le scénario moyen prévu (scénario 3). Les simulations débutent en 1950 et en 1962 la subsidence totale est locale et négligeable (<0,4 m). Les affaissements sont progressivement plus importants à partir de cette date et parviennent à un affaissement total maximum de 3,8 m en 2050. La zone d'affaissement

maximale est située dans le corridor industriel (figure 1) où il y a des taux de pompage élevés, un rabattement élevé, et où il y a d'épaisses couches argileuses compressibles.

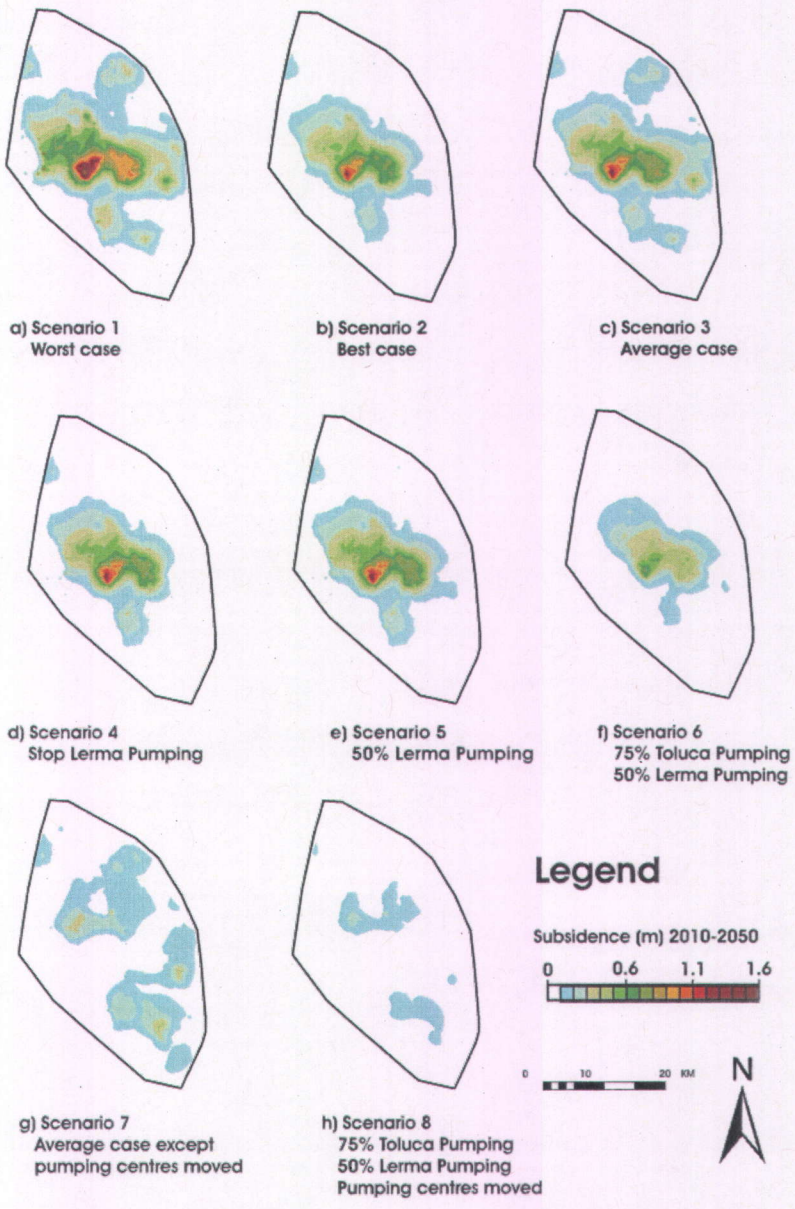


Figure 24: Résultats des simulations pour les scenarios 1-8 (tirée de Calderhead et al., 2009d).

La figure 24 présente les résultats de compaction total entre 2010 et 2050 pour les huit scénarios. Les scénarios 1 à 3 présentent respectivement les effets du pire, du meilleur, et du moyen scénario, en ce qui concerne les changements climatique et les paramètres de pompage. Calderhead et al. (2009a) a démontré que les changements climatiques ne sont

pas le facteur le plus important dans le bilan d'eau et donc le pompage excessif sera responsable de la grande majorité des effets de la subsidence. La subsidence totale maximum atteint 2,2 m pour le pire des cas (scénario 1), 1,4 m pour le meilleur scénario (scénario 2), et 1,6 m pour le scénario présentant les tendances moyennes attendues (scénario 3). En comparant ces scénarios, l'étendue spatiale de la zone affecté est similaire et les différences maximale entre le pire et le meilleur scenario est de 0,8 m pour la période de 40 ans.

Il n'y a que des différences subtiles entre complètement arrêter les exportations (scénario 4) et les réduire de la moitié (scénario 5). Toutefois, il existe des différences significatives entre les exportations constantes (scénario 3) et la réduction des exportations de moitié (scénario 5).

Le changement le plus marqué dans la subsidence se produit lorsque les centres de pompage sont déplacés (scénarios 7 et 8) à des endroits où il n'y a pas d'argile. La compaction totale peut être considérablement réduite, simplement en déplaçant les centres de pompage à différents endroits dans la vallée. Les résultats les plus souhaitables (scénario 8) montrent un affaissement maximal de <0,3 m en 2050. Ailleurs il n'y a que de l'affaissement limité dans toute la vallée.

9 CONCLUSIONS ET PERSPECTIVES

Bilan en eau

En ce qui concerne le bilan en eau, cette étude des deux composantes les plus importantes du cycle de l'eau (la recharge et le décharge) montre clairement que la diminution de la disponibilité de l'eau dans le bassin de Toluca est principalement due à des effets anthropiques et que le taux de pompage actuelle n'est pas soutenable. De plus, les estimations de changement climatique doivent être prises en considération car elles seront potentiellement un facteur important sur le déficit budgétaire des eaux souterraines dans l'avenir, surtout dans les régions vulnérable aux sécheresses.

InSAR

En comparant les résultats D-InSAR au données de compaction des extensomètres, il est possible de constater qu'il existe une corrélation directe. D'après les résultats, l'affaissement régional est bien quantifié par la méthode InSAR. En contrastant les images des capteurs ENVISAT ASAR et RADARSAT-1, il a été constaté que les lignes de bases (*baselines)* courtes (< 500 m) et des acquisitions d'images à intervalle de temps petite (< 1 an) conduisent à des résultats plus précis et mieux corrélées. Les argiles dans le couloir industriel se compactent d'une façon relativement linéaire, où les différents taux de compaction sont fonctions des propriétés géologiques et du taux de pompage. Les taux de subsidence maximale actuelle sont estimés à 15 cm/an à certains endroits. L'affaissement total maximal d'un point situé dans la vallée entre novembre 2003 et mai 2008 est d'environ 40 cm.

Modélisation

L'interférométrie radar, le modèle géologique 3D, les données de terrain acquises et existantes ont permis à contraindre le modèle numérique écoulement-compaction. Les charges hydrauliques, le rabattement, et l'affaissement régional et local sont observées. Les résultats D-InSAR, les extensomètres, et les simulations numériques de la subsidence coïncident relativement bien. Il est constaté que la partie supérieure de l'aquifère est la partie la plus compressible. Des simulations montrent que, depuis la subsidence régionale a débuté dans les années 1960, elle a atteint 2 m dans le couloir industriel, là où le pompage est excessif et ou les couches d'argile sont épaisses.

Gestion de l'aquifère

Concernant les scenarios, complètement arrêter les exportations vers la ville de Mexico n'est pas le facteur le plus important pour le contrôle de la subsidence, car le système de pompage se situe principalement dans les régions à faible teneur en argile. Toutefois, diminuer les exportations de 50% et déplacer les centres de pompage à des endroits avec une faible teneur en argile, engendre un effet positif sur le bilan global de l'eau et la subsidence. Une grande partie des affaissements aurait pu être évitée s'il y avait eu une politique en place pour limiter le pompage dans les zones compressibles.

10 LES ASPECTS INNOVATEURS DE LA THÈSE.

Cette partie récapitule les contributions significatives de cette thèse à l'avancement des connaissances dans le domaine de l'hydrogéologie, l'affaissement des sols, et la télédétection.

Plus spécifiquement, les contributions scientifiques sont les suivantes :

- Une amélioration de la compréhension du bilan en eau souterraine (recharge et décharge) pour la vallée de Toluca avec une méthodologie distincte (Chapitre 2)
- Des inclusions de changements climatiques dans les scénarios de comportement de recharge pour la vallée de Toluca (chapitre 2 et 5)
- Une amélioration du modèle géologique 3D, ainsi que la délimitation des couches compressibles pour la vallée de Toluca (chapitre 4)
- L'obtention d'images SAR pour la vallée de Toluca (Chapitre 3)
- L'utilisation de l'InSAR pour quantifier la compaction régionale dans la vallée de Toluca (Chapitre 3, 4)
- Les interférogrammes avec des images provenant de deux satellites différents (RADARSAT-1 et ENVISAT ASAR) sont comparés (Chapitre 3)
- Des méthodes de terrain novatrices pour l'installation d'extensomètre ont été entreprises (Chapitre 1)
- L'installation du réseau de suivi de niveau d'eau souterraine la vallée de Toluca (Chapitre 1)
- L'amélioration du modèle numérique HydroGeoSphere avec un module de compaction (Chapitre 4)
- L'utilisation d'InSAR, un modèle géologique 3D, et des données de pompage pour contraindre les paramètres de compressibilité (S'_{sk}) (Chapitre 4)
- Des scenarios de pompage interbassin (présenté dans le Chapitre 5) pour la gestion de l'eau du bassin pouvant servir d'exemple pour tout autres bassin présentant cette problématique de subsidence et de surexploitation de l'aquifère.

Références

Amelung, F., Galloway, D. L., Bell, J.W., Zebker, H. A., & Laczniak, R. J. (1999). Sensing the ups and downs of Las Vegas: InSAR reveals structural control of land subsidence and aquifer-system deformation. Geology, 27, 483–486.

Ariel and Consultores, 1996. Hydrodynamic modeling study and design optimization of the monitoring well networks for the aquifers of Caldera, San Luis Potosi and Toluca (Part 3: Aquifer of Toluca) Estudio de Simulacion Hidrodinamica y Diseno Optimo de las Redes de Observacion de los acuiferos de Calera, San Luis Potosi y Toluca (Tomo 3: Acuifero de Toluca). CNA (Comisión Nacional del Agua) México, DF, Unitecnia pp. 308.

Biot, M.A. (1941) General theory of three dimensional consolidation. Journal of Applied physics. 12:155-164.

Calderhead A. I., Martel, R. Rivera, A., Garfias, J., Therrien, R., An increasing groundwater budget deficit induced by urbanization, industrialization, and climate change in the Toluca Valley, Mexico. Hydrological processes. (to submit in October 2009a).

Calderhead, A. I., Martel, R., Allasset, P-J., Rivera, A., Garfias, J, Land subsidence induced by groundwater pumping, monitored by C-band D-InSAR and field data in the Toluca Valley, Mexico. Canadian journal of remote sensing (accepted 2009b).

Calderhead A. I., Martel, R. Rivera, A., Garfias, J., Therrien, R., Simulating pumping-induced regional land subsidence in a complex aquifer system. Advances in water resources (to submit in October 2009c).

Calderhead A. I., Martel, A., Garfias, J., R. Rivera, Therrien, R., Groundwater pumping scenarios for minimizing land subsidence in the Toluca Valley, Mexico: tools for policy design. Water Resources Management (to submit in October 2009d)

CNA, 2000. Determinacion de la disponibilidad de agua en el acuifero Valle de Toluca. CNA (Comisión Nacional del Agua) México, DF, Unitecnia: 26.

CNA, 2006. Datos climatológico, Servicio Meteorológico Nacional, Comisión Nacional del Agua.

CNA 2007. Base Aquiferos Nacional y Regional. Comisión Nacional del Agua

CNA 2008. Zonas de Reserva de Agua Potable para la ciudad de Toluca. Gerencia de Agua Subterania, Comision Nacional del Agua, Subdirection Tecnica.

GTZ-CNA, 2004. Modelo de Simulación Hidrodinámica del Acuífero del Valle de Toluca, Estado de México. Deutsche Gesellschaft fur Technische Zusammenarbeit - Comisión National del Agua.

Consultec (1978). Study of the behavior of fractures in the upper Lerma river basin reports I-III . Estudio del compotamiento de grietas en el valle del Alto Rio Lerma. Informes I-III.

DGCOH, 1992. Regional hydrogeologic study of the Valleys of Toluca and Ixtlahuaca: Part I. Estudio Hidrogeologico Regional de los Valles de Toluca e Ixtlahuaca: Tomo I: 214.

Ferronato, M., Gambolati, G., Teatini, P., Baù, D. Stochastic poromechanical modeling of anthropogenic land subsidence (2006) International Journal of Solids and Structures, 43 (11-12), pp. 3324-3336.

Figueroa Vega, G. E., (1990) Estudio sobre el comportamiento reciente del acuifero de la ciudad de Toluca y su relacion con el problema de agrietamientos de la zona poniente de la misma. CEAS, The state of Mexico, May 1990.

Figueroa Vega, G. E, (2004) El agrietamiento de la ciudad de Toluca, Consejo consultivo de Agua, December 2004.

Gabriel, A.K., Goldstein, R.M., Zebker, H.A. Mapping small elevation changes over large areas: differential radar interferometry (1989) Journal of Geophysical Research, 94 (B7), pp. 9183-9191.

Galloway, D.L., Hudnut, K.W., Ingebritsen, S.E., Phillips, S.P., Peltzer, G., Rogez, F., & Rosen, P.A. (1998). Detection of aquifer system compaction and land subsidence using interferometric synthetic aperture radar, Antelope Valley, Mojave Desert, California. Water Resources Research, 34, 2573-2585

Galloway, D.L., Hoffmann, J. The application of satellite differential SAR interferometry-derived ground displacements in hydrogeology (2007) Hydrogeology Journal, 15 (1), pp. 133-154.

Gambolati, G., 1972. A three-dimensional model to compute land subsidence. Bullet. Int. Ass. Hydrolog. Sci. 17 (1972), pp. 219–226.

GMS, 2009. GMS 6.5 User guide, GMS - Salt lake City, Utah.

Goldstein, R.M., Zebker, H.A. Interferometric radar measurement of ocean surface currents (1988) Nature, 328 (6132), pp. 707-709.

GTZ-CNA, 2004. Modelo de Simulación Hidrodinámica del Acuífero del Valle de Toluca, Estado de México. Deutsche Gesellschaft fur Technische Zusammenarbeit - Comisión National del Agua.

Harbaugh, A.W., Banta, E.R., Hill, M.C., and McDonald, M.G., 2000, MODFLOW-2000, the U.S. Geological Survey modular ground-water model—User guide to modularization concepts and the ground-water flow process: U.S. Geological Survey Open-File Report 00-0092, 121 p.

Hawksworth, J., 2006. The World in 2050: How big will the emerging market economies get and how can the OECD compete?, Pricewaterhouse Coopers, London.

Helm, D. C., 1975. One-dimensional simulation of aquifer system compaction near Pixley, California, 1, Constant parameters, Water Resour. Res., 11, 465–478,

Hoffmann, J., Galloway, D. and Howard, A. J., 2003a. Inverse Modeling of Interbed Storage Parameters Using Land Subsidence Observations, Antelope Valley, California. Water Resource Research, Vol. 39, No.2, 1231.

Hoffmann, J., Leake, S.A., Galloway, D.L., and Wilson, A.M, 2003b, MODFLOW-2000 ground-water model—User guide to the Subsidence and Aquifer-System Compaction (SUB) Package: U.S. Geological Survey Open-File Report 03–233, 46 p.

IMTA, 2003. Censo del utilización del agua en el valle de Toluca. Instituto Mexicano de Tecnologia del Agua.

INEGI, 1960. Censo general de población y vivienda 1960. Instituto Nacional de Estadística, Geografía e Informática.

INEGI, 1970. Censo general de población y vivienda 1970. Instituto Nacional de Estadística, Geografía e Informática.

INEGI, 1980. Censo general de población y vivienda 1980. Instituto Nacional de Estadística, Geografía e Informática.

INEGI, 1990. Censo general de población y vivienda 1990. Instituto Nacional de Estadística, Geografía e Informática.

INEGI, 2000. Censo general de población y vivienda 2000. Instituto Nacional de

Estadística, Geografía e Informática.

INEGI, 2001. Instituto Nacional de Estadística, Geografía e Informática, Sinthesis of geographic information for the state of Mexico. Síntesis de información Geográfica del Estado de Mexico

INEGI, 2005. Censo general de población y vivienda 2005. Instituto Nacional de Estadística, Geografía e Informática.

IPCC, 2007. Climate Change 2007: The Physical Science Basis. Contribution of Working Group I to the Fourth Assessment Report of the Intergovernmental Panel on Climate Change [Solomon, S., D. Qin, M. Manning (eds.)].

Jyrkama, M.I., Sykes, J.F. 2007. The impact of climate change on spatially varying groundwater recharge in the grand river watershed (Ontario). Journal of Hydrology, 338, 237–250

Leake, S.A., and Prudic, D.E., 1991, Documentation of a computer program to simulate aquifer-system compaction using the modular finite-difference ground-water flow model: U.S. Geological Survey Techniques of Water-Resources Investigations, book 6, chap. A2, 68 p.

Leake, S.A., and Galloway, D.L., 2007, MODFLOW ground-water model—User guide to the Subsidence and Aquifer-System Compaction Package (SUB-WT) for water-table aquifers: U.S. Geological Survey, Techniques and Methods 6–A23, 42 p.

Legorrreta, J., 1997. Rainfall, the key to the future of the Valley of Mexico. La Jornada Ecologica, 5(58): 1-12.

Lesser y Asociados, S.A., 1992. Diagnostic study of the aquifer of the Valley of Toluca to implement a program for the extraction of groundwater. Estudio para el Diagnostico del acuífero del Valle de Toluca, para implementar la reglamentación de la extracción del agua subterránea.

Li CJ, Tang XM, Ma TH (2006) Land subsidence caused by groundwater exploitation in the Hangzhou-Jiaxing-Huzhou. Plain, China. Hydrogeol J 14:1652–1665

Massonnet, D., Rossi, M., Carmona, C., Adragna, F., Peltzer, G., Feigl, K., & Rabaute, T. (1993). The displacement field of the Landers earthquake mapped by radar interferometry. Nature, 364, 138-142

Massonet, D., Briole, P., & Arnaud, A. (1995). Deflation of Mount Etna monitored by

spaceborne radar interferometry. Nature, 375, 567–570.

MDA, 2007. EV-InSAR Users Guide, Version 4.0. MDA Geospatial Services, Nepean, Ontario. Canada.

Metropoli, 2008. Pierde Edomex batalla legal sobre acuíferos. In: Metropoli (Editor). Metropoli, Mexico, Mexico, last accessed June 4th 2008. http://www.metropoli.org.mx/modules.php?name=News&file=article&sid=3439

Minor Villar, A-M. 2007. Determinación del esfuerzo de corte de los distintos tipos de arcilla del Valle de Toluca bajo diferentes condiciones de humedad. Masters Thesis, UAEM, March 2007.

OEE, 1970. Los acuíferos del alto Lerma pub. No. 7, . report for Oficina de estudios especiales (OEE) de la CHCVM-SRH

Ortega, A., Cherry, J.A. and Rudolph, D.L. 1993. Large Scale Aquitard Consolidation Near Mexico City. Groundwater, vol. 31:5, p. 708-717.

Ortega, A., Rudolph, D.L. and Cherry, J.A. 1999. Analysis of Long-term land Subsidence near Mexico City: Field Investigations and Predictive Modeling. Water Resources Research, vol. 35:11, p. 3327-3341.

Rivera, A., E. Ledoux and G. de Marsily, 1991. Nonlinear modeling of groundwater flow and total subsidence of the Mexico City aquifer-aquitard system. FISOLS (IV Inter. Symposium on Land Subsidence); 12-17 May 1991 Houston Texas, USA. IAHS Publication no. 20; pp 45-58.

Roctest (2009) R-4 magnetic reed switch probe extensometer system, Roctest http://www.roctest.com/modules/AxialRealisation/img_repository/files/documents/R4-E5013D-W.pdf

Rudolph, D.L., Frind, E.O. Hydraulic response of highly compressible aquitards during consolidation (1991) Water Resources Research, 27 (1), pp. 17-30.

Rudolph, D.L., Sultan, R., Garfias, J. and McLaren, R.G., 2006. Significance of enhanced infiltration due to groundwater extraction on the disappearance of a headwater lagoon system: Toluca Basin, Mexico. Hydrogeology Journal, 14(1-2): 115-130.

Schroeder, P.R. Dozier, T.S., Zappi, P. A., McEnroe, B. M., Sjostrom, J.W., Peyton, R. L., (1994). The Hydrologic Evaluation of Landfill Performance (HELP3) Model: Engineering Documentation for Version 3, Environmental Protection Agency Office of

Research and Development, Washington, DC.

Shearer TR (1998) A numerical model to calculate land subsidence applied at Hangu in China. Eng Geol 49:85–93

Teatini, P., Ferronato, M., Gambolati, G., Bertoni, W., Gonella, M. A century of land subsidence in Ravenna, Italy (2005) Environmental Geology, 47 (6), pp. 831-846.

Terzaghi, K. (1925). Earthworks mechanics based on soil physics. Erdbaumechanik auf bodenphysikalisher Grundlage, Franz Deuticke, Vienna.

Therrien, R., .G. McLaren, E.A. Sudicky, S.M. Panday (2009) User Guide: HydroGeoSphere - A Three-dimensional Numerical Model Describing Fully-integrated Subsurface and Surface Flow and Solute Transport. University of Waterloo.

UAEM, 2007. Compilation of clay compressibilities of the Toluca Valley, Mexico.

UAEM, 2008. Universidad Autonoma del Estado de Mexico, Faculdad de Ingeneria, Laboratorio de Materiales. Report on consolidation and linear contraction tests- August, 2007

UNEP. 2008. Mexico's Annual population Growth Rate. United Nations Environment Programme data, http://www.unep.org/.

Zebker, Howard A., Goldstein, Richard M. TOPOGRAPHIC MAPPING FROM INTERFEROMETRIC SYNTHETIC APERTURE RADAR OBSERVATIONS. (1985) Digest - International Geoscience and Remote Sensing Symposium (IGARSS), pp. 113-117.

Zebker, Howard A., Goldstein, Richard M. INTERFEROMETRIC SYNTHETIC APERTURE RADAR OBSERVATIONS OF OCEAN WAVES (1987) Digest - International Geoscience and Remote Sensing Symposium (IGARSS), p. 783.

Liste des Tableaux

Tableau 1 : Résumé du budget d'eau souterraine entre 1970 et 2050.'-' signifie données non disponibles (tiré de Calderhead et al., 2009a). 15

Tableau 2: Images SAR de la vallée de Toluca acquises entre 1995 et 2008 (tiré de Calderhead et al., 2009b)..... 21

Tableau 3: Interférogrammes de la Vallée de Toluca avec origine des images (mission) pour faire l'interférogramme, date d'acquisition d'images, ligne de base (baseline) perpendiculaire (b perp.) et ligne de base (baseline) parallèle (b paral.) en mètres, décalage de temps en jours (d_days), ainsi qu'une description de la pertinence de l'interférogramme (tiré de Calderhead et al., 2009b)..... 22

Tableau 4: Conception du modèle numérique de la vallée de Toluca. 31

Tableau 5: Scenarios de pompage 2010-2050 (tiré de Calderhead et al., 2009d)..... 38

Liste des figures

Figure 1 : Position de la vallée de Toluca et la zone d'étude par rapport au Mexique et l'État de Mexico 7

Figure 2: Utilisation de l'eau souterraine dans la vallée de Toluca (valeurs tirées de IMTA (2003) et figure modifié de Calderhead et al. (2009a) 8

Figure 3: Schéma d'un extensomètre à senseur magnétique. Les variations de surface piézométrique (h1 et h2), ainsi que la position du système d'acquisition de pression (pressure transducer) sont également indiqués. Le dessin n'est pas à l'échelle. 11

Figure 4 : Distance entre le senseur 12 (profondeur ≈ 107 m) et le sol pour Extensometer-1 12

Figure 5: Distribution spatiale de la recharge moyenne dans la vallée de Toluca [mm/année] en utilisant le modèle HELP3 (tirée de Calderhead et al., 2009a). 14

Figure 6: Résumé du budget en eau souterraine entre 1970 et 2050. Entre 1970 et 1999 les données réelles de la recharge sont présentées. Entre 2000 et 2050, la prédiction moyenne incluant les changements climatiques est démontrée. Le déficit est calculé par la somme de la décharge et de la recharge (tirée de Calderhead et al. 2009a). 15

Figure 7: 7A : Modèle conceptuel et géologie de la vallée de Toluca. 7B : Agrandissement de la géologie de la zone d'étude (tirée de Calderhead et al., 2009c). 17

Figure 8: Génération du modèle géologique (8B) à partir de logs de forage (8A). 18

Figure 9: Épaisseurs des couches argileuses majeures (9A-9B) et la somme verticale des épaisseurs des couches argileuses (6E) (tiré de Calderhead et al., 2009c) 19

Figure 10. Modèle conceptuel de la méthodologie pour obtenir des images de subsidence par InSAR. 20

Figure 11 : a) et b) démontrent la cohérence dans la vallée de Toluca pour une paire d'images ENVISAT ASAR acquissent le 5 Décembre 2007 et le 28 Mai, 2008. c) et d) démontrent l'interférogramme de la même paire d'images. b) est un zoom de a) et d) est un zoom de c) (tirée de Calderhead et al., 2009b). 23

Figure 12: Description de la zone d'intérêt dans la vallée de Toluca; position des extensomètres, points de contrôle, puits d'observation, puits de pompage, et les taux d'affaissement mesurés avec InSAR entre décembre 2007 et mai 2008 (tirée de Calderhead et al., 2009b). 25

Figure 13: Exemple de résultats de tests de compression d'une argile typique de la Vallee de Toluca (de UAEM, 2008): Indice des vide (e) versus la contrainte effective (σ'), ou $\sigma'(pre)$ est la contrainte effective de préconsolidation, Cc est l'indice de compression élastique et Cs est l'indice de compression inélastique (tirée de Calderhead et al., 2009c) 26

Figure 14: Problème de vérification - Configuration du modèle utilisé pour simuler une variation saisonnière de la contrainte. Les seuls entrants et sortants dans le système sont la recharge ou la décharge par le(s) puits et l'emmagasinement dans l'aquifère et la couche d'argile. Le modèle MODFLOW-SUB en différences-finies utilise un seul puits pour la recharge et la décharge. La méthode d'éléments-finis de HGS utilise les 8 coins du bloc pour les puits (W1-W8), avec le pompage et les débits d'injection, respectivement, divisés par 8 pour chaque puits (tiré de Calderhead et al., 2009c). 29

Figure 15: Résultats de vérification démontrant la charge hydraulique et la compaction totale pour les simulations HGS-COMPACTION ET MODFLOW-SUB (tirée de Calderhead et al., 2009c). 30

Figure 16: Chaîne de traitement pour l'obtention du modèle en éléments finis 3D. Les journaux de forage (A) sont utilisés pour générer la géologie en 3D (B et C), puis en utilisant les couches géologiques et le maillage 2D (D), la topographie des couches géologiques est extraite (E). Enfin, le maillage 3D (F) est généré (tiré de Calderhead et al., 2009c). 32

Figure 17: Rabattement relatif mesuré et simulé à l'Extensometre-1 ainsi qu'une comparaison avec les rabattements aux piézomètres multi-niveaux à proximité (PL-201 et PL-205) (tiré de Calderhead et al., 2009c). 33

Figure 18: A) Somme verticale des épaisseurs de couches argileuses et position des puits de pompage avec leurs débits respectifs. Les zones blanches-gris-noires représentent la somme verticale des épaisseurs des couches argileuses. B) Interférogramme différentiel de la vallée de Toluca avec un intervalle d'acquisition de 70 jours. Les images ENVISAT ASAR ont été acquises le 5 décembre, 2007 et 13 février, 2008. Un cycle bleu-rouge-jaune représente l'affaissement vers le bas (2.8 cm), et à l'inverse, un cycle bleu-jaune-rouge

représente un soulèvement. Les lignes noires représentent la somme verticale des épaisseurs des couches argileuses (à partir de 18A) (tirée de Calderhead et al., 2009c). 34

Figure 19: Compaction totale simulée et mesurée à Extensometer-1 par ENVISAT ASAR, RADARSAT-1, Extensometer-1, et les simulations HGS en fonctions du temps. Les rabattement (WL) simulé et mesuré à Extensometer-1 en fonction du temps sont aussi montré (tirée de Calderhead et al 2009c 35

Figure 20: Évolution de l'affaissement régional dans la vallée de Toluca de 1960 à 2009 simulé avec HGS-Compaction (tirée de Calderhead et al., 2009c)..... 36

Figure 21: A) Simulation HGS-compaction (lignes solides noires) superposée à la carte de subsidence D-InSAR (remplissage en couleur) dans les 175 jours entre le 5 décembre 2007 et le 28 mai, 2008. L'emplacement des puits de pompage avec les taux de pompage est également indiqué. B) L'emplacement de la zone de compaction ainsi que la compaction régionale. (tirée de Calderhead et al., 2009c)..... 37

Figure 22: Rabattement simulé depuis 1950 et présenté pour les années a)1962, b)1977, c)1990, d) 2010, e)2030, et f)2050 (tirée de Calderhead et al., 2009d). 39

Figure 23: Distribution de la subsidence totale entre 1962 et 2050 (scénario 3) (tirée de Calderhead et al., 2009d)..... 40

Figure 24: Résultats des simulations pour les scenarios 1-8 (tirée de Calderhead et al., 2009d)..... 41

Partie 2

Chapitre 2:

An increasing groundwater budget deficit induced by urbanization, industrialization, and climate change in the Toluca Valley, Mexico

Résumé

La croissance urbaine, l'industrialisation et les changements climatiques peuvent entraîner un pompage supérieur à la recharge des eaux souterraines. Une méthodologie est proposée pour améliorer le modèle du bilan des eaux souterraines dans le but de déterminer la disponibilité de l'eau et de déficit passé, présent et futur. La méthodologie a des applications à des régions de plus en plus urbanisé, industrialisé et avec les tendances de sécheresse, dont la vallée de Toluca, au Mexique. Cette étude comprend l`étude de la recharge variable dans l`espace déterminée à partir de données historiques sur le climat, les prévisions de changement climatique, et les multiples paramètres utilisés dans le modèle HELP3. D`après HELP3, la recharge moyenne du bassin Toluca au cours des 35 dernières années est estimé à 376 millions de mètres cubes par an (Mm^3/an). En examinant les prévisions de changement climatique, d'ici 2050, le scénario moyen projette que la recharge diminuera de 15 Mm^3/an, et dans le pire des cas, jusqu'à une baisse maximal de 88 Mm^3/an. Le pompage des eaux souterraines a augmenté régulièrement depuis 1970 et est actuellement estimé à 484 Mm^3/an. Le déficit actuel est estimé à plus de 150 Mm^3/an avec la projection moyenne à plus de 292 Mm^3/an en 2050. L'utilité du modèle HELP3 est démontré, mais il est important de ne pas compter uniquement sur ce modèle pour déterminer la recharge et que la vérification des résultats avec d'autres modèles d'évapotranspiration et de ruissellement est nécessaire. Cette étude de deux des composantes les plus importantes du cycle de l'eau (la recharge et la décharge) montre clairement que la diminution de la disponibilité de l'eau dans le bassin de Toluca est principalement due aux effets anthropiques et que le taux de pompage ne sont pas durables.

An increasing groundwater budget deficit induced by urbanization, industrialization, and climate change in the Toluca Valley, Mexico

A I Calderhead[1], R Martel[1], A Rivera[2], J Garfias[3] and R Therrien[4]

[1] Institut national de la recherche scientifique - Centre Eau, Terre & Environnement, 490 de la Couronne, Quebec, QC G1K 9A9, Canada

[2]Geological Survey of Canada, Natural Resources Canada, 490 de la Couronne, Quebec, QC G1K 9A9, Canada

[3]Universidad Autónoma del Estado de México, Facultad de Ingeniería (CIRA), Cerro de Coatepec, s/n, C.U., Toluca, MEX 50130, México

[4]Département de géologie et de génie géologique, Université Laval, Québec, QC G1K 7P4, Canada

Keywords: recharge, discharge, groundwater budget, HELP3, climate change, Toluca, Mexico

Abstract

Urban growth, industrialization, and climate change can often result in groundwater pumping exceeding recharge. A methodology is proposed to improve the groundwater budget model by determining past, present, and future recharge and dischage. The model is applied to an increasingly urbanized and industrialized region with drying tendencies: the Toluca Valley, Mexico. This study includes spatially-variable recharge determined from historical climate data, climate change predictions, and the multiple parameters used in the Hydrologic Evaluation of Landfill Performance (HELP3) model. The change to the virgin recharge and discharge rates from pumping is also considered. Using HELP3, the average recharge for the Toluca basin in the past 35 years is estimated at 376 million cubic meters per year (Mm^3/year). When considering climate change predictions, by 2050 the average scenario projects recharge to decrease by 15 Mm^3/year, and in a worst case scenario up to a maximum decrease of 88 Mm^3/year. Groundwater pumping has increased steadily since 1970 and is presently estimated at 484 Mm^3/year. Current deficit estimates are over 150 Mm^3/year with average projections increasing to over 292

Mm^3/year by 2050. This study of two of the most important components of the water cycle (recharge and discharge) clearly shows that the decreasing water availability in the Toluca basin is due mainly to anthropogenic effects and that the current pumping rates are not sustainable. Climate change estimates should also be considered as they are potentially an important factor on the groundwater budget deficit in the future, especially in regions with high drying tendencies.

1 INTRODUCTION

Several major cities in the world are growing at a rate that creates mounting pressures on water resources. Over the past 50 years, several studies in the south western United States and central and northern Mexico have documented the deterioration of water quality and resources. Climate change patterns in this general region show that precipitation will likely decrease and temperature will increase (IPCC, 2007). It is now important, more than ever, in areas with increasing population, intensive industry and agriculture, and increasing drying tendencies, to properly quantify the water budget of groundwater basins in order to enable decision makers to act according to the findings.

The increased groundwater extraction from the aquifer system has caused a reversal in the direction of vertical hydraulic gradients, the disappearance of artesian springs and wetlands and land subsidence within the basin. The groundwater budget in the Toluca Valley has been evaluated by OEE (1970); Lesser and Asociados (1992); Ariel and Consultores (1996); CNA (2002) and GTZ-CNA (2004). These studies, however, lack a detailed analysis of recharge and present, in most cases, an incomplete survey of the pumping. To evaluate recharge, the above studies did not take into account several parameters and in several cases results were averaged over large territories. Jyrkama et al., (2002), Allen et al. (2004), Scibek and Allen (2006), and Jyrkama and Sykes (2007) use the spatially variable HELP approach for quantifying recharge with an emphasis placed on the effects of climate change in northern climates. In terms of recharge and climate change, this study follows the Jyrkama and Sykes (2007) approach where only general climate change scenarios are simulated. The difference in this study from other

climate change and groundwater studies is that the emphasis is placed on the overall groundwater budget with the impact of climate change considered as one of several factors in the budget.

The objective of this work is to improve the groundwater budget model in order to determine the past, current, and future deficit and water availability of the temperate-with-dry-winters climate of the Toluca Valley Basin. Using both observed climate data and climate change scenarios, this work applies a spatially variable version of the Hydrologic Evaluation of Landfill Performance (HELP/HELP3) model (Schroeder et al., 1994) over a watershed to obtain current and future recharge distributions; additionally, in using past and future discharges from the basin based on observed pumping, water levels, and consumption predictions of the basin. The deficit is then obtained and the findings can be used to manage the resources in a sustainable way.

2 THE TOLUCA VALLEY

The Toluca Valley basin (figures 1 and 2) covers an area of approximately 2100 Km^2. The basin is adjacent to the Mexico City Valley, with the Sierra Las Cruces forming a natural border between the two basins. The Toluca Valley's geographic position in the center of the country and proximity to Mexico City, as well as its rapidly developing infrastructure, have allowed the city to grow into a major industrial zone for the country.

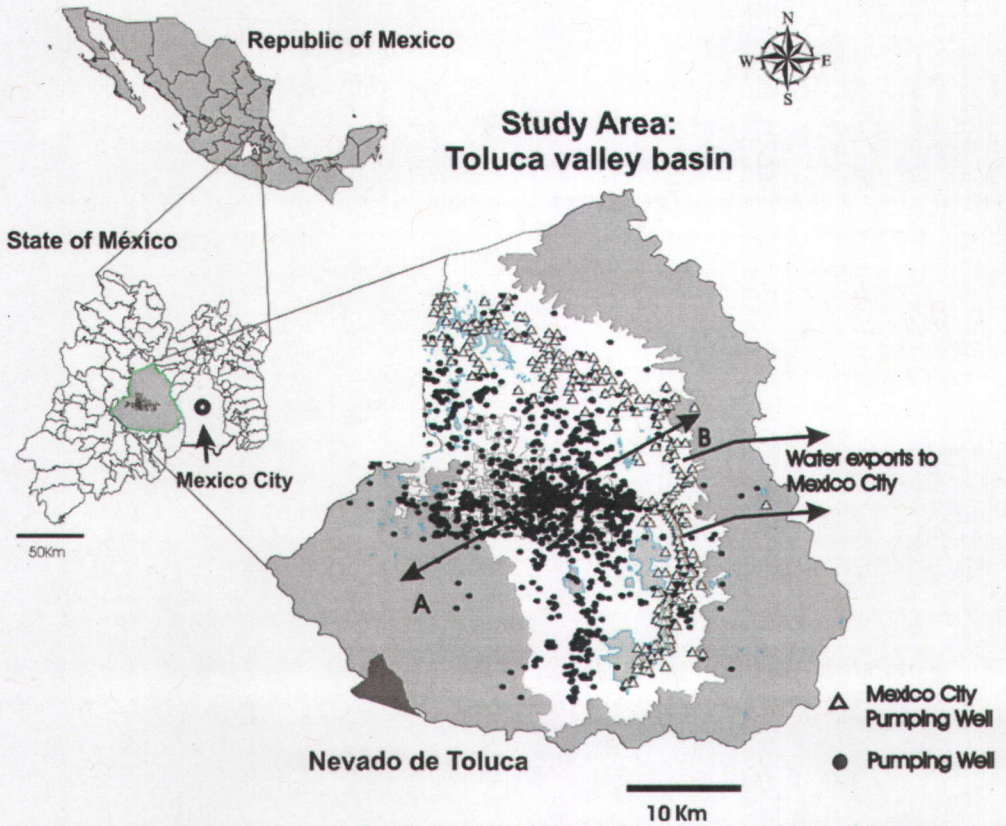


Figure 1: Location map of the Toluca Valley within the Republic of Mexico and the State of Mexico. Over 935 pumping wells are in operation in the Valley, including the 230 pumping well system, located along the Lerma river on the eastern edge of the valley, and pumping water to Mexico City.

According to the 2005 census (INEGI, 2005), the metropolitan area of Toluca, including 12 neighbouring municipalities, is the fifth most populous metropolitan area in Mexico and the largest within the State of México. The total population of the Toluca Valley in 2005 was just over 1.7 million people (INEGI, 2005). From 1960 to 2005, the population

of the valley has doubled every 20 years (INEGI, 1960-2005). Based on United Nation projections for Mexico (UNEP, 2008), the population of the valley will reach a plateau of 2.2 million people in 2050.

The conceptual model of the Toluca Valley basin, including general water cycling, groundwater pumping and the major geological features found within the basin, is shown in figure 2. Historically, for wells located near the ancient lakes on the eastern basin floor of the Toluca Basin, groundwater levels were either near surface or emerged above the land surface (Lesser and Asociados, 1992). Currently, there is a significant decrease in the water level within the basin primarily due to groundwater pumping, and the loss is increasing with time. There are presently more than 935 pumping wells in the Toluca Valley. Increasing local demand for water and climatic drying tendencies also add to the stresses on the aquifer.

Inter-basin water transfer in the Toluca Valley occurs in the form of water being exported from the basin. The Lerma system wells are a groundwater pumping system operated by Mexico City and consisting of 396 pumping wells located along the upper section of the Lerma River (Figure 1). The system has been in operation since the late 1960's and captures a large portion of the recharge water entering from the Sierra Las Cruces, which is then exported to Mexico City at a rate approximately equal to 6.0 m^3/s.

Consolidated, volcanic andesitic rocks from the Miocene age form the basement material in the basin (Figure 2). The fractured rock forms a bowl in the centre of the valley, reaching depths greater than 600 m and cropping out to the surface at the edges of the valley. The andesitic volcano formation of the Nevado de Toluca core is located to the west. The fractured rock is overlain by layers of pure lacustrine clays (aquitard) and by the Chalma formation aquifer, composed of a mixture of sand, gravel and clay. The Tarango formation aquifer, deposited after the Chalma formation, extends from the flanks of the Sierra las Cruces mountains in the east across the basin floor to the foot of the Nevado of Toluca volcano. This formation is a heterogeneous mixture of volcaniclasitc materials (Lesser and Asociados, 1992). The basaltic and ash-flows aquifer of the

Chichinautzin formation were deposited in the eastern portion of the Toluca Valley. In the upper middle portion of the valley, where most of the groundwater pumping occurs, complex interlayering of lacustrine clay (aquitard) and alluvium deposits (aquifer) is found. Also included in figure 2 are the HELP3 layers, which will be examined further in section 3.1.

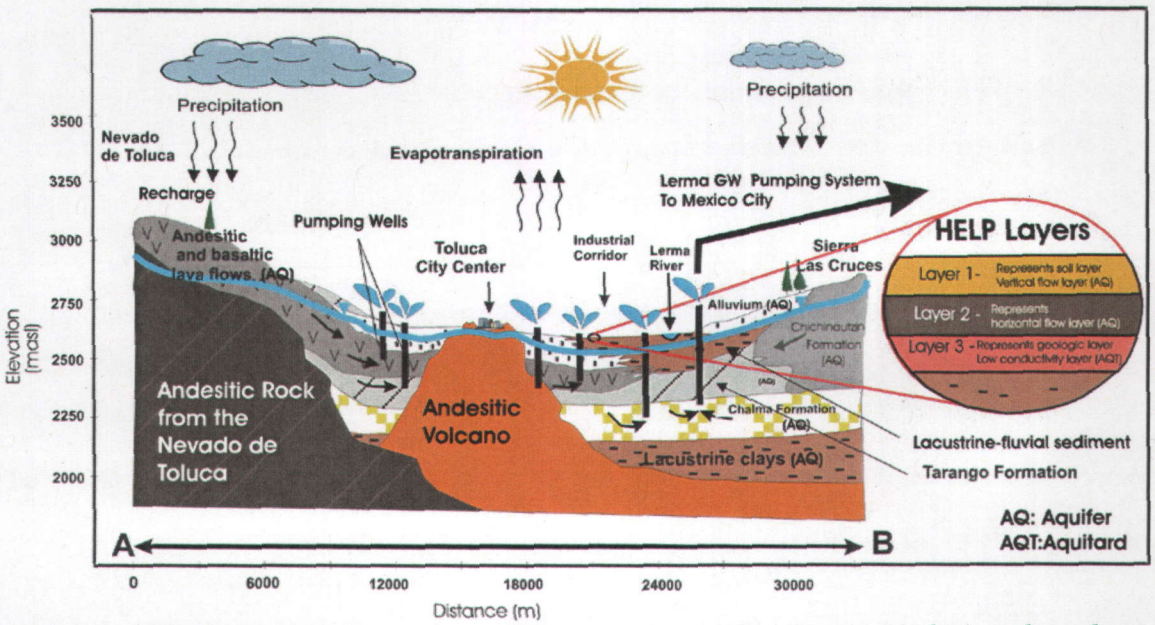


Figure 2: 2D view of the conceptual model for the Toluca Valley Basin including geologic layers and HELP3 layers. Cross section A-B is located on figure 1. Modified from Ariel and Consultores (1996) and Rudolph et al., (2006).

3 METHODOLOGY

The basic water budget equation can be written as:

$$R = D + P +/- \partial V/\partial t = 0, \qquad (1)$$

where R is groundwater recharge defined with units [L^3/T] (for purposes of this work, the units are assigned Mm^3/year or millions of cubic meters per year), generally assumed to come from precipitation and be unaffected by pumping, D is groundwater discharge [Mm^3/year] or water that is not captured by pumping such as discharge to streams and lakes, evaporation, evapotranspiration, and P is the net rate of extraction from pumping

wells [Mm^3/year]. $\partial V/\partial t$ is the rate of removal of water from storage [Mm^3/year]. The sign of $\partial V/\partial t$ is negative if there is a deficit and positive if there is a surplus.

Theis (1940), Bredehoeft (2002), Sophocleous et al. (2004), and Devlin and Sophocleous (2006), argue that this frequently used equation usually excludes the impact of pumping on recharge and discharge. Bredehoeft (2002) modified equation 1 to consider both discharge and recharge as a function of pumping:

$$(R_0 + \Delta R_0) - (D_0 + \Delta D_0) - P + /- \frac{\partial V}{\partial t} = 0 \qquad (2)$$

where R_0 is the virgin recharge rate prior to pumping (same as R in equation 1) [Mm^3/year], ΔR_0 is the change to the virgin recharge rate due to pumping [Mm^3/year], D_0 is the natural or virgin discharge rate [Mm^3/year], ΔD_0 is the change to the virgin discharge rate due to pumping (Mm^3/year). ΔD_0 can be defined as the sum of the yearly change to the discharge rate due to pumping ΔD_{yi} [Mm^3/year] - since pumping began, by the following relation:

$$\Delta D_0 = \sum_{i}^{n} \Delta D_{yi} \qquad (3)$$

where i is the year 1,2,3,...n, since pumping began.

Each parameter of equation 2 is examined for the case of the Toluca Valley. Additionally, equation 2 is modified to represent the virgin natural recharge (R_0) as a function of the parameters used in HELP3. HELP3 is a quasi 2-D hydrologic model which was originally used for calculating the water budget at landfill sites. HELP3 considers climatic and geologic data and it simulates snow melt, runoff, infiltration, evapotranspiration, plant growth, soil humidity, subsurface runoff, and unsaturated flow (Schroeder et al. 1994). The HELP/HELP3 model has been extensively tested and used to evaluate infiltration (Fleenor and King, 1995; Woyshner and Yanful, 1995; Benson and Pliska, 1996; Khire et al., 1997; Chammas et al., 1999; Berger, 2000; Gogolev, 2002; Risser et al., 2005, and Croteau, 2006).

With the objective of combining equation 2 with the parameters used in HELP3, and considering the hydrologic behaviour of the Toluca Valley, the water budget for the Toluca Valley is described by equation 4:

$$\left(R_0 \begin{pmatrix} R_P, R_T, R_{RL}, R_{RAD}, R_{LAT}, R_{GS}, \\ R_{WS}, R_{LAI}, R_{ED}, R_{SCS}, R_b, R_\theta, \\ R_{WP}, R_{FC}, R_{KSAT}, R_{DD}, R_{SL} \end{pmatrix} + R_{ART} + \Delta R_0 \right) - GW_{flow} - Sp - P + / - \frac{\partial V}{\partial t} = 0 \qquad (4)$$

where the parameters used in HELP3 to compute R_0 are described in table 1.

Since HELP3 considers evaporation, evapotranspiration and runoff, and considering that there is limited interaction between surface water and groundwater in the Toluca Valley (Lesser and Asociados, 1992), discharges from equation 4 are assumed to come from natural groundwater flow (GW_{flow} [Mm^3/year]), spring discharge (Sp [Mm^3/year]), and pumping (P) [Mm^3/year]. GW_{flow} and Sp both decrease with increasing groundwater pumping and consider ΔD_0. Artificial recharge (R_{ART}) [Mm^3/year] is added to equation 4 to account for induced recharge from infiltration wells. Artificial recharge in the Toluca Valley comes in the form of precipitation captured from roofs and infiltrated into the aquifer.

Schroeder et al. (1994) gives a more detailed description on how recharge (R_0) is computed in terms of the various parameters of the HELP3 model. To date, the water budget model presented is the only one available in the literature that uses the Bredehoeft (2002) approach, which takes into account the change to the virgin recharge and discharge rates due to pumping, combined with spatially-variable recharge and climate change computed with HELP3.

The Logical Model (figure 3) describes how the various data are used and processed to obtain the groundwater budget. A description on how Q_{on} (total recharge) [Mm^3/year] and Q_{off} (total discharge) [Mm^3/year] are obtained is given in sections 3.1 and 3.2 respectively.

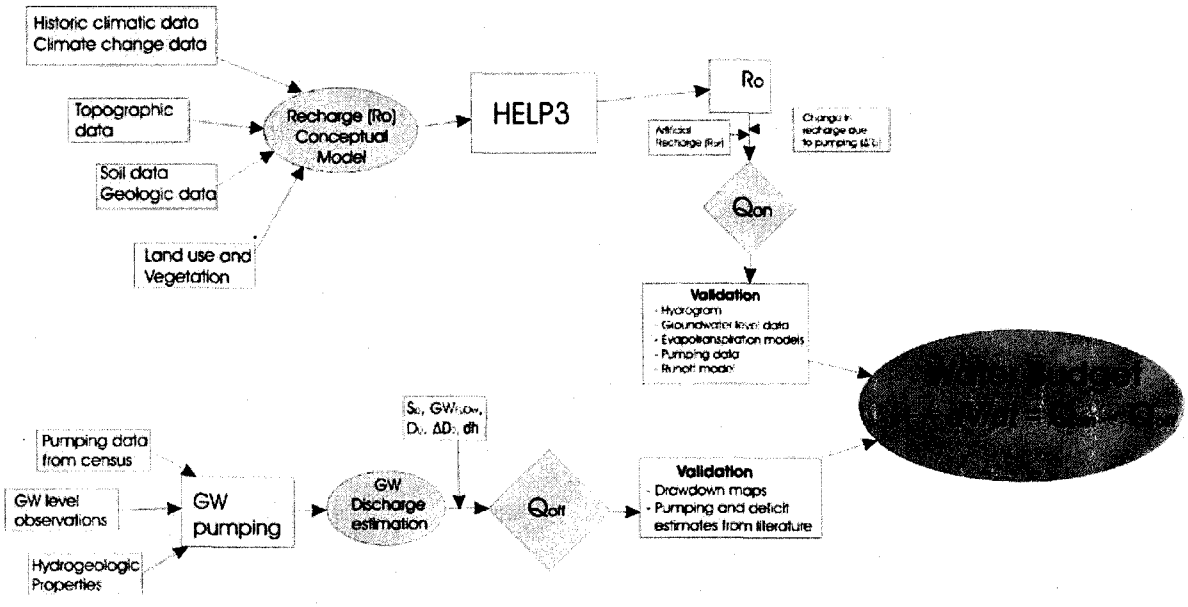


Figure 3: Logical Model for determining the groundwater budget at a given time where Q_{on} and Q_{off} are respectively total recharge and total discharge (including pumping) from the basin and $\partial V/\partial t$ is the change in storage.

The overall approach of this study is to use all available data to simulate the groundwater budget of the Toluca Valley. HELP3 simulations enable a spatially variable representation of historical and predicted (with average, best, and worst case scenarios) recharge using daily data input values to obtain yearly recharge estimates. Historical and predicted yearly discharge from the aquifer (with average, best, and worst case scenarios) are calculated as a function of extraction from pumping wells, the groundwater flow off the basin, the change to the virgin discharge rate, and spring discharge. Total discharge and recharge are summed with the objective of quantifying historical and projected groundwater deficit.

3.1 Total Recharge (Q_{on})

The total recharge (Q_{on}) is a function of the virgin recharge rate R_0, artificial recharge (R_{ART}), and the change in recharge due to pumping ΔR_0. To summarize the process for obtaining the recharge, from figure 3, recharge (R_0) is estimated by using climatic, topographic, soil, geologic, land use, and vegetation data obtained from various sources (table 1). The conceptual model is formed and the data is discretized into 1 km^2 cells. The

recharge data is then processed with the HELP3 model to obtain values for recharge. The sum of recharge for all cells gives the total recharge. Artificial recharge (R_{art}) and change in recharge (ΔR_0) values are added to R_0 to obtain the total recharge (Q_{on}). Below the methodology in obtaining R_0 is described.

Table 1 Description of HELP3 parameters and source of data.

Parameter	Name	Units	Source of data
R_P	Precipitation	[m^3/d]	Weather stations (15062, 15229, 15293, 15056) (CNA, 2006). Climate change data based on CNA (2006) and IPCC(2007).
R_T	Temperature	[°C]	Weather stations (15062, 15229, 15293, 15056) (CNA, 2006). Climate change data based on CNA (2006) and IPCC(2007).
R_{rad}	Solar Radiation	[MJ/m^2]	Stochastically simulated as a function of temperature, precipitation, and latitude (Schroeder et al., 1994)
R_{RL}	Quarterly relative humidity	%	From Schroeder et al., 1994.
R_{Lat}	Latitude	[° lat]	Longitude and latitude map
R_{GS}	Growing season	[days]	Weather stations (15062, 15229, 15293, 15056) (CNA, 2006)
R_{LAI}	Leaf area index	[-]	Vegetation cover map (SICHEM 1999) and empirically derived table (Scurlock et al. 2001)
R_{ED}	Evaporative depth	[m]	Vegetation comer map (SICHEM 1999)
R_{SCS}	Soil Conservation Service curve number	[-]	Pedology map (SICHEM 1999) and Land use map (IMTA 2003) and empirical tables from Purdue (2008)
R_b	Layer thickness	[m]	Pedology, geology maps (SICHEM 1999) and borehole data
R_θ	Porosity	[-]	Pedology and geology maps (SICHEM 1999) and descriptions based on Machorro (1978), INEGI (2001)
R_{WP}	Wilting point	[-]	Pedology, geology and vegetation cover maps (SICHEM 1999) and descriptive tables (Schroeder et al., 1994)
R_{FC}	Field capacity	[-]	Pedology, geology and vegetation cover maps (SICHEM 1999) and descriptive tables (Schroeder et al., 1994)
R_{Ksat}	Saturated hydraulic conductivity	[m/s]	Pedology and geology maps (SICHEM 1999) and descriptions based on Machorro (1978), INEGI (2001)
R_{DD}	Distance from drain	[m]	Based on Croteau (2006)
R_{SL}	Slope	[-]	DEM (NASA, 2008)

Recharge Domain for HELP3

The spatial extent in the X-Y plane is based on the basin limits. The Toluca Valley basin was discretized into a square grid with nodes placed 1000 m apart. There are a total of 2117 nodes each representing 1 km^2. The resolution of the available data did not warrant a much larger number of nodes. Infiltration over several years was calculated for each node and the sum of all infiltration values is considered to be the recharge to the aquifers in the basin (R_0). Further in this section artificial recharge (R_{ART}) and the effects of pumping on recharge (ΔR_0) are considered.

When determining parameters at each node, values were, in most cases, obtained from available GIS maps. The maps include pedology, geology (see appendix G), land use, vegetative cover, and a digital elevation model. For the mapped parameters, values were extracted from the maps at each of the 2117 nodes using routines available in ArcGIS 9.2 and the desired parameter was either used directly or empirically derived. For example, the extracted slope value was obtained directly from the DEM and the vegetative cover map was used to determine the Leaf Area Index (*LAI*) based on empirical tables describing *LAI* as a function of vegetation type.

HELP3 uses 3 types of layers. A 'type 1' layer is characterized by vertical flow and it is where all the evapotranspiration occurs. A 'type 2' layer is a lateral drainage layer and a 'type 3' layer is a low permeability layer acting as a barrier. A 'type 2' layer is always found immediately above a 'type 3' layer and its hydraulic conductivity is generally higher than a type 3 layer.

A topographic map, a soil map, a geologic map, and borehole data were used to construct the recharge domain. The 3D geological setting is highly variable in the Toluca Valley. For simplification purposes, the HELP3 recharge domain is divided evenly into 3 layers, throughout the basin, having each a thickness of 1.5 m (figure 2), for a total thickness of 4.5 metres starting at the land surface. This assumption is made because of the complexity of the geology and because 3 layers totalling 4.5 metres is sufficient for

representing the influx if the permeability's are sufficiently well defined. K_{sat} is the dominant parameter controlling infiltration and over long periods, larger layer thicknesses will not affect total infiltration. Layer 3's K_{sat} was assigned as a function of the lowest K_{sat} in the unsaturated zone below each node, which varies between 10^{-6} to 10^{-8} m/s. In the valley, the impermeable layer is often in the form of a clay barrier, and in the higher altitudes the low permeability layers are in the form of consolidated rocks (SICHEM, 1999). Another assumption is that even though the water level decreases, all percolation below 4.5 metres is recharge. The first layer of the model is assigned a type 1 and the properties are based on soil maps and their descriptions (Machorro 1978; INEGI, 2001; SICHEM, 1999). Layer 2 is assigned a 'type 2' and Layer 3 is assigned a 'type 3'. For all nodes in Layer 2, it is assumed that the physical properties were identical to Layer 3, which is based on the geologic map, excluding hydraulic conductivity which was set to 1-2 orders of magnitude higher than Layer 3's.

Historical Climate data approach used with HELP3

The spatially-variable version of HELP3 normally uses only one climate station. However, due to the large variability in climatic conditions of the Toluca Valley, four climatic regions for the model are considered. The four regions are primarily dependant on altitude and are as follows: High Nevado, Middle Nevado & High Sierra, Lower Nevado & Lower Sierra, and Vallley (table 2). The climate conditions described in table 2 are based on available data from weather stations. Occasionally daily data was not available from the data set and missing values were interpolated. The total annual rainfall varies from averages of 1,250 mm in the highest areas to 700 mm in the valley (figure 4). A large portion (85%) of the rainfall occurs between May and October. In the valley, the average annual temperature ranges from 11 to 16 °C, with May being the warmest month and January the coldest. The Nevado de Toluca's annual mean temperature ranges from -2 to 5 °C. Figure 4 shows the variability in annual precipitation at two weather stations. For all parameters, daily values are input into the model and yearly output are used for the analysis. Meteorological data is extrapolated over missing periods.

Table 2: Climate data for 4 climatic regions of the Toluca Valley based on CNA (2006)

Location and data span	Weather station #	Altitude (masl)	Reading	Precipitation (mm)	Year	Growing season	Wind Speed (km/h)
Higher Nevado 1969-1986	15062	3800 - 4690	max	1626	1969	May 1 - June 10	
			min	909	1983		
			average	1249	-		16.2
Mid Nevado & High Sierra 1978-1986	15229	3100 - 3799	max	1489	1984	Feb 7 – Dec 21st	
			min	786	1982		
			average	993	-		14
Lower Nevado & Lower Sierra 1994-2001	15293	2700 - 3099	max	1234	1995	Year round	
			min	685	1994		
			average	1010	-		12
Valley 1978-1991	15056	2500 - 2699	max	888	1978	Year round	
			min	563	1990		
			average	793	-		11

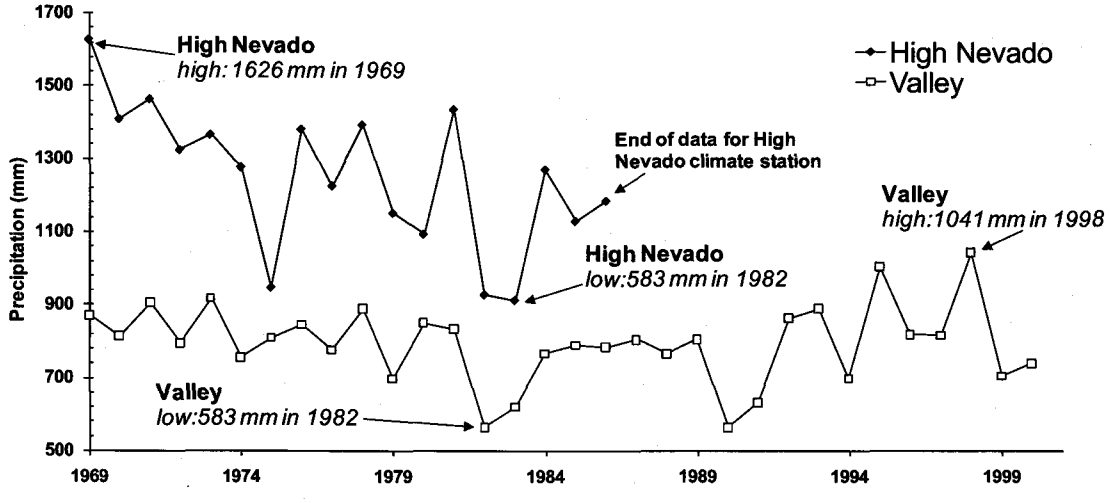


Figure 4: Yearly precipitations at the Valley and High Nevado weather stations 1969 -2000 (after CNA, 2006).

Climate change

Estimating the change in climate variables in the future with a reasonable level of confidence is very difficult and involves large uncertainty. If one is to downscale the predicted results from a Global Climate Model (GCM) to the scale of a basin, additional error and uncertainty is added to the analysis. Following the approach used by Jyrkama

and Sykes (2007), the objective of this climate change analysis is not to determine with any degree of confidence what will specifically happen in the future as a result of climate change in the Toluca Basin. Based on historical climate data and generally accepted climate change predictions, recharge patterns are simulated and observed.

The generally accepted climate change predictions are based on the International Panel on Climate Change's (IPCC) 4th report. Regional averages of temperature and precipitation projections from a set of 21 GCMs form the multi-model data set (MMD) for the A1B scenario (The A1B scenario provides a good mid-line scenario for carbon dioxide output and economic growth). The mean temperature and precipitation responses are first averaged for each model over all available realisations of the 1980 to 1999 period from the 20th Century Climate in Coupled Models (20C3M) simulations and the 2080 to 2099 period of A1B (IPCC, 2007).

From the 21 models, the IPCC reported the following general predictions in the general area of the Toluca Valley over the next 100 years (IPCC, 2007):

1. Precipitation is projected to decrease with an average change over 100 years of -9% for all models, with models predictions ranging between an increase of +9% and a decrease of -48%.

2. Temperature is projected to increase with an average change over 100 years of 3.2°C for all models, with a minimum increase of 1.8°C and a maximum increase of 5°C.

3. Incoming solar radiation will likely decrease due to increases in greenhouse gases.

4. Mexico, and to a greater degree Northern Mexico, are among the zones worldwide with the highest drying tendencies over land in the 21st century.

Based on the predictions above, the climate change scenarios shown in Table 3 are examined. For these scenarios, simulations are run from 2000 until 2050. Yearly values are used and assumed to increase or decrease linearly from 2000 to 2100, which is the period covered by the climate models. For example, in the case of average precipitation

for scenario 2, the total decrease in 2050 would be half of -9%, or -4.5%. Greenhouse gases are expected to increase and reduce solar radiation, however, upon running several simulations and varying solar radiation by large proportions, very negligible differences were noticed in the output, thus varying solar radiation is not considered in the scenarios.

Table 3: Climate change scenarios. Scenario 1 is the base case and scenarios 2-4 are run from 2000 to 2050.

Scenario	Description
1	Base case : Average of available historical daily temperature, precipitation, and simulated solar radiation from 1969 to 2000
2	Model average : Precipitation decreases by -9 %, Temperature increases by 3.2°C
3	Worst case : Precipitation decreases by -48%, Temperature increases by 5.0°C
4	Best case : Precipitation increases by +9%, Temperature increases by 1.8°C

Calibration of the HELP3 Model

River discharges could not be used to calibrate the HELP3 recharge model because the Toluca valley is a wide basin in a temperate climate with dry winters, where evapotranspiration is the dominant parameter and because there is very little interaction between the river and the aquifer. The Toluca valley is on the border between a semi-arid climate and a temperate climate (Mcnight & Hess, 2000). HELP3 can have difficulty in estimating water balances in arid climates where upward fluxes can be high (Jyrkama and Sykes, 2007). Using HELP3 for this type of climate and basin did not yield good results for the evapotranspiration and runoff calculations; however the recharge values are in line with other recharge estimates. Runoff values were high and evapotranspiration values were low; thus it was found that most of the HELP3 calculated runoff probably evaporated into the atmosphere. To better understand the recharge, evapotranspiration and runoff was examined more closely. Evapotranspiration was calculated at 39 weather stations in the valley with the Thornthwaite, Hargreaves, Hannon, and Turc methods. The results from these calculations were used to better calibrate the HELP3 model. It was found that by considering the runoff as evapotranspiration, the results were acceptable. In this temperate climate with dry winters, it was found that it is important to not rely solely on the HELP3 model for determining recharge. The advantage of the HELP3 model over

the other models is that it considers soil properties, vegetation, and land use and the spatially-variable version of HELP3 is very useful in determining the spatial distribution of the recharge. Additionally, general climate change data is easily integrated into the model.

R_{ART} and ΔR_0

From *equation 4,* the artificial recharge (R_{ART}) is not accounted for in HELP3. Current estimates of artificial recharge were obtained from CNA (2002) and are shown in table 5. In addition to new bylaws requiring industrial buildings to capture and inject water from precipitation into the upper aquifers. Carillo-Rivera (2008), J. J. and Gaskin (2008) mention that artificial recharge from treated water sewage is another potential source for recharge in Mexico City. It is expected that Toluca can capitalize on this technology in the coming years; thus in the projections, artificial recharge is expected to increase.

Due to the difficulty in obtaining data representative of the change to the virgin recharge rate due to pumping (ΔR_0), some assumptions are made. Adjacent basin aquifers, such as the Mexico City aquifers are also depleting due to growing populations and excessive groundwater pumping (Ortega and Farvolden, 1989; Rivera et al., 1991; Carrera-Hernandez and Gaskin, 2008). If the adjacent aquifers are depleting at a similar rate to the Toluca basin, then there is a smaller influence from ΔR_0. Additionally, precipitation is considered the dominant recharge variable, thus ΔR_0 is considered negligible and assigned a value of 0; however the value is most likely higher.

3.2 Discharge (Q_{off}):

From figure 3, the groundwater discharge conceptual model is obtained by using all the groundwater pumping data from census information (IMTA, 2003, CNA, 2003), quarterly groundwater level observations from CNA (2008), and hydrogeologic properties (Ariel and Consultores, 1996; GTZ-CNA, 2004) from 1970 to 2008. The discharge value (Q_{off}) is verified by measuring the change in storage data obtained from differences in piezometric surfaces based on CNA (2008), and yearly deficit estimates

(CNA, 2007). Given the recharge values, the difference in peizometric surfaces gives us the clearest estimate of the change in groundwater storage and therefore the discharge.

Excessive groundwater pumping in the Toluca Valley has lowered the water table to a point where the river system has little contact with the groundwater system (Lesser and Asociados, 1992). HELP3 measures the net infiltration to the aquifer and, since there is very little interaction between the aquifer and the river, and semi arid climate leads to high evapotranspiration rates, it can be assumed that river and stream discharges are accounted for in the HELP3 model. HELP3 does not consider spring discharges (*Sp*), it includes Sp as recharge entering the aquifer, however, this water later comes to the surface and discharges; therefore this parameter will be accounted for in the discharge model. HELP3 does not consider pumping therefore historical and predicted discharge from the aquifer is measured as a function of extraction from pumping wells (*P*), the groundwater flow off the basin (GW_{flow}), and spring discharge (*Sp*).

Groundwater extraction from pumping wells (P):

Industrial (7%) and agricultural (3%) uses account for a relatively small percentage of the total volume compared to the domestic (52%) use and volume exported to Mexico City (38% or 6.0 m^3/s) (figure 5)).

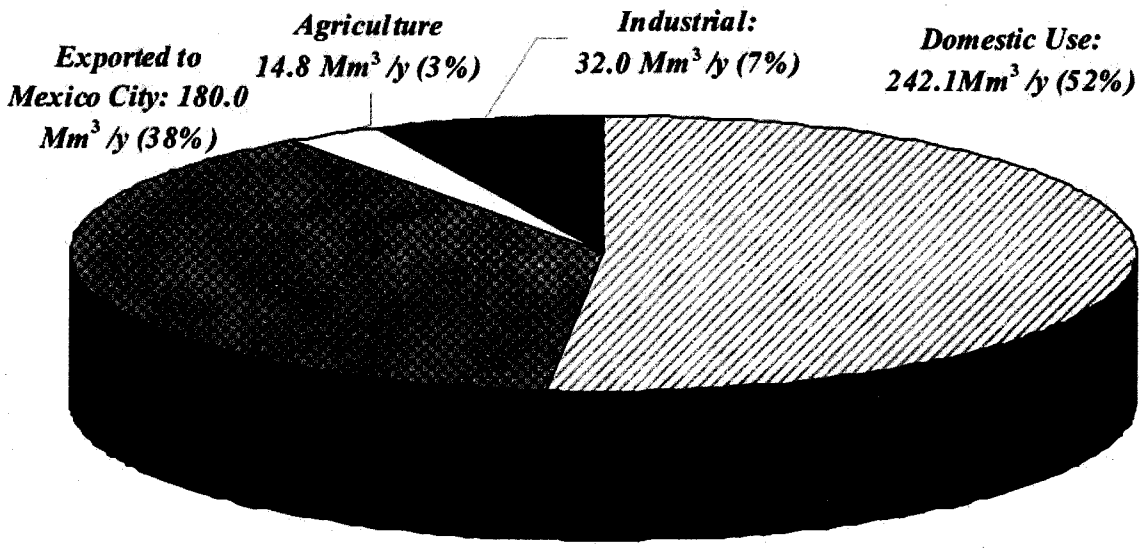


Figure 5: Groundwater use in the Toluca Valley based on IMTA (2003)

In making projections for future consumption, several assumptions are made. Projections on domestic use of groundwater are based on the population growth (INEGI 1960-2005) and UN projections of population growth for Mexico (UNEP, 2008). Given the total pumping volumes in 2010, the projected volumes are assigned values proportional to their population. Over a 40 year period (2010-2050) projected annual growth rates gradually decrease by 1.36 (1.34 to -0.2) for the average case (UNEP, 2008), 0.34 (1.34 to 1.0) for the worst case, and 1.64 (1.34 to -0.5) for the best case.

Projected industrial use of water is based on Mexico's projected Gross Domestic Product (GDP) (Hawksworth, 2006) – assuming a constant percentage of industrial pumping (Figure 5). Worst case and best case scenarios respectively add and subtract 8% of expected industrial use water volumes.

Exports to Mexico City have not significantly increased in the last 10 years (Legoretta, 1997; CNA, 2007), therefore a constant export volume is assumed for all projections. It is believed that legal action between the State of Mexico and Mexico City (Metropoli, 2008) will deter additional inter-basin transfer because the state of Mexico will be more protective of its water resources. This reinforces the assumption that the exported volume will not increase, or perhaps even decrease.

Between 1989 and 1999, agriculture using irrigation fluctuated around 153 000 ha with no significant increase or decrease (INEGI 2001); therefore it is assumed that agricultural use of water remains constant for all scenarios.

Groundwater flow (GW_{flow})

Based on topography, the only region with natural groundwater discharge (GW_{flow}) is at the north-west corner of the basin, at the location where the Lerma river exits the Toluca basin and enters the Ixtlahuaca basin. Darcy's law (equation 5) is applied to determine differences in the groundwater flux (q) [L/T] discharged from the basin

$$q = -K\frac{\partial h}{\partial x}, \qquad (5)$$

where K is the hydraulic conductivity and $\frac{\partial h}{\partial x}$ represents the hydraulic gradient. The flux is then multiplied by the discharge area (A) to obtain the discharge flux (Q) [Mm^3/year] (equation 6)

$$Q = q \cdot A \qquad (6)$$

Monitoring well data is used to obtain hydraulic gradients (*dh/dx*) from equipotential lines (see figure 7 of results).

3.3 Change-of-storage $(-\frac{\partial V}{\partial t})$

The groundwater deficit in the Toluca Valley has been evaluated by OEE (1970); Lesser and Asociados (1992); Ariel and Consultores (1996); CNA (2002) and GTZ-CNA (2004). To evaluate recharge, the above studies did not take into account climate change, soil, vegetation, and land use properties and in several cases results were averaged over large territories. The OEE (1970) study averaged the recharge over the entire basin; According to the IMTA (2003) study, Lesser and Asociados (1992) and Ariel and Consultores (1996) underestimated the amount of pumping wells in the valley. Only the latest budget study, GTZ-CNA (2004), considered the more complete water use census, IMTA (2003).

In the Toluca Valley Q_{off} is greater than Q_{on} therefore the difference between Q_{on} and Q_{off} is the rate of removal of water from storage $(-\partial V/\partial t)$ or "deficit" [Mm^3/year] (equation 7). This deficit leads to other issues on water availability that will be addressed in the discussion.

$$Q_{on} - Q_{off} = -\frac{\partial V}{\partial t} \qquad (7)$$

Two approaches for obtaining the deficit are implemented. The first relies upon subtracting the calculated discharge from the recharge (equation 7) using sections 3.1 and 3.2. The second approach involves calculating the volume of water that has been

removed from storage through means of subtracting one drawdown map from another. The second method is described below.

For the Toluca Valley case, observed hydraulic head data, surveyed by the Gerencia de Agua Subterránea, Comisión Nacional del Agua (CNA, 2008) is used to create piezometric surface maps. For recent deficit estimates, the data from February 2006 and 2008 are used to create the maps. Spatial variability is taken into consideration by using 1209 nodes spaced in rows 1 km apart in the center of the valley. ArcGIS 9.2 is used to a) interpolate well data from both dates using the spline method b) obtain drawdown then interpolate the drawdown values and c) extract drawdown values at each of the 1209 nodes (see Figure 9 in results section for locations). Due to a lack of hydraulic head data in the mountainous regions, only nodes in the center of the valley are included in the calculation of the deficit between 2006 and 2008. It is also assumed that the drawdown in the mountainous regions does not represent a large volume. The drawdown map is converted into a yearly quantity of water removed from the basin. Based on field data it is assumed that the average porosity is 0.30 (Ariel Consultores, 1996).

4 RESULTS

4.1 Recharge simulations

A problem in calibrating the HELP3 model was that some parameters were very sensitive to minor fluctuations in values. Although many of the parameters were adjusted, the hydraulic conductivity (R_{Ksat}) was most used to calibrate the model. R_{Ksat} was especially sensitive and slight changes would affect the overall R_0 result. As mentioned in section 3.1, another problem encountered with the HELP3 model is that since the Toluca Valley is a wide basin with a small drainage channel (Lerma river), the evapotranspiration values calculated by HELP3 were low and the runoff values were high. To compensate for the high values, it was assumed that the excess runoff calculated by HELP3 actually evaporated. This approach led to reasonable results, possibly because HELP3 is more accurate in temperate climates.

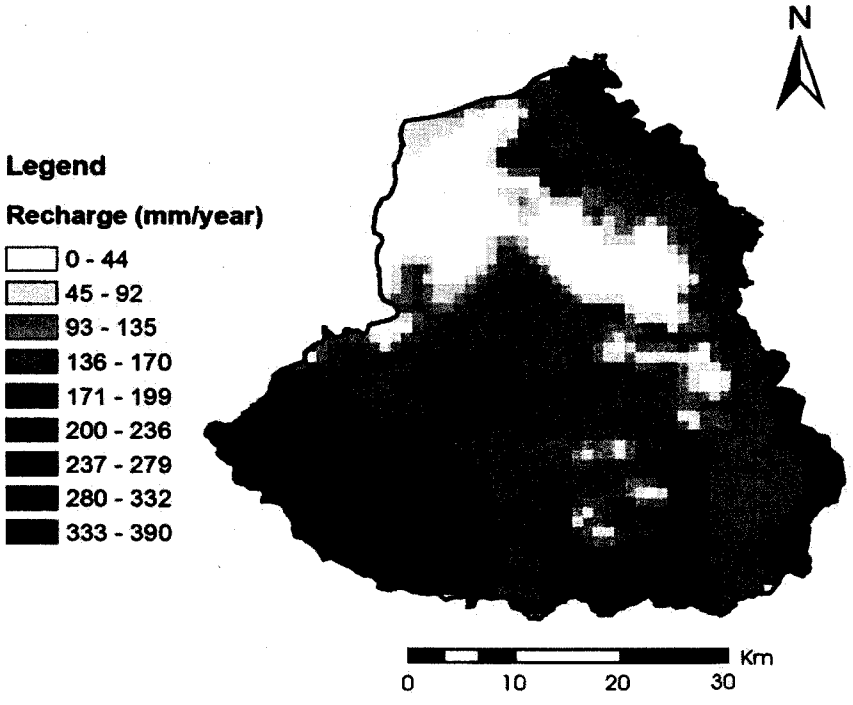


Figure 6: Spatially variable distribution of average recharge (R_0) in the Toluca Valley [mm/year] based on the HELP3 model.

Figure 6 shows the distribution of the average simulation (climate data from 1969-2000) where the total recharge (sum of recharge for all 2117 nodes) is 376.2 Mm^3/year. For the historic data, two more scenarios were examined: a year with high values of precipitation and a year with low values of precipitation. The choice of the precipitation value was based on observing the entire data set and selecting the respective years according to the amount of precipitation (figure 5). Since there were four different climatic regions with varying data ranges, the wettest, driest and average precipitation years were selected for each of the four climate regions. Based on maximum and minimum precipitation, average high and low values were 466 Mm^3/year and 298 Mm^3/year, respectively. Other average recharge estimates from the literature vary between 256 Mm^3/year (Ariel and Consultores, 1996), using groundwater levels to infer recharge, and 430 Mm^3/year (CNA-GTZ 2004), using the method of a uniform coefficient of vertical infiltration. Pumping can interfere in the interpretation of recharge when using water levels and compared to the HELP3 method, and uniform infiltration coefficients are a simplistic approach to a complex problem.

Comparing climate change results (table 5), it is seen that with the average climate change scenario, the average recharge in 2050 decreases 15.2 Mm^3/year or -4% from an average scenario without climate change. In the worst case scenario, the average recharge decreases by 88.2 Mm^3/year or -23.4% and in the best case scenario the recharge increases by 8.8 Mm^3/year or +2.3%.

As would be expected from Figure 6, recharge is highest in the mountains. The low permeability soils in the north central part of the basin is the main reason for the low infiltration rates. Higher recharges in the south are mostly attributed to the soil and geologic context. Where the City is located, in the centre of the basin, higher recharge rates are the result of very little vegetation - shorter evaporative depth, the SCS curve number, and wilting point.

The 240-340 mm of recharge in the sierra Las Cruces is on the lower end of estimates by Ortega and Farvolden (1989), who estimate that recharge in these areas is in the 30-50% range of total precipitation.

It should finally be noted that the approximately $6m^3$/s pumping rate exported to Mexico City using the Lerma System represents 61% of the recharge from the Las Cruces mountain chain.

4.2 Discharge results

Results for the discharge parameters (GW_{flow}, ΔD_0, ΔD_{yi}, S_p, P) are presented below.

Natural groundwater flow (GW_{flow}), Change in Virgin Discharge Rate due to Pumping (ΔD_0), and yearly Change in Virgin Discharge Rate due to Pumping (ΔD_{yi}):

The piezometric surfaces of 1970 and 2004 are compared. The saturated hydraulic conductivity was obtained using a borehole log (PL-226) and pumping tests in the valley. Based on the boreholes, an impermeable layer is found below an elevation of 2413 m.

The hydraulic gradient is used to determine the lateral extent of the discharge area (A), and the vertical extent of the area (A) is obtained from the average saturated thickness exiting the basin in 1970: 146 m, and 2004: 122 m. Hydraulic conductivity is estimated at 5.0×10^{-7} for a sand/clay and gravel/clay aquifer.

The results from this section can be used to obtain values for the yearly change to the discharge rate due to pumping (ΔD_{yi}) for 1970 and 2004 and estimate the decrease in GW_{flow} over time.

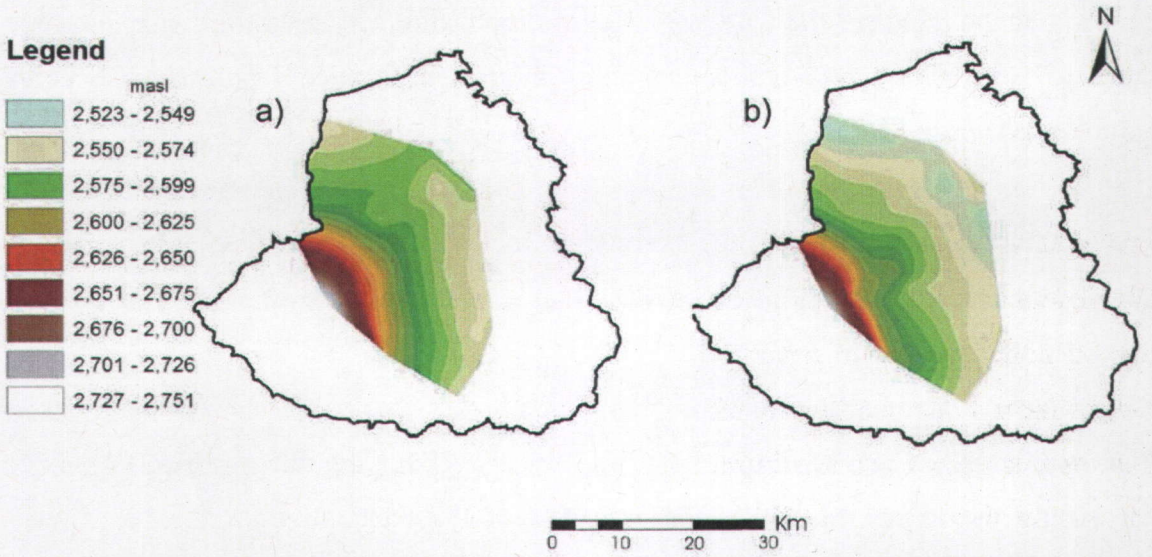


Figure 7: Piezometric surface of the Toluca Valley used to quantify discharge from the basin; a) February 1970 and b) February 2004.

Table 4: Natural groundwater flow (GW_{flow}) exiting the basin: estimates for February 1970 and 2004

Parameter	Units	1970	2004
dh/dx_i	-	-2,54E-03	-1,49E-03
K	Mm/year*	1,58E-05	1,58E-05
q	Mm/year*	4,01E-08	2,36E-08
A	Mm^2**	1,17E+00	1,02E+00
Q	**Mm^3/year**	**-4,67E-02**	**-2,41E-02**

*Mm/year represents millions of meters per year
**Mm^2 represents millions of square metres

From the piezometric head data and using equation 3, it is possible to calculate the average yearly change in discharge rate due to pumping between two years:

$$\Delta D_{y_ave} = \frac{\Delta D_{y1} - \Delta D_{y2}}{y2 - y1} \qquad (8)$$

Although pumping has increased in a non-linear fashion, ΔD_{y_ave} is useful at estimating ΔD (equations 2-4). The calculated discharge in 2004 is approximately half of that in 1970 (table 4): ΔD_{y2004} - ΔD_{y1970} = 0.023 Mm^3/year. Therefore, over 34 years, ΔD_{y_ave} = 673 m^3/year. Assuming that a close-to virgin discharge rate last occurred in the mid 1950's, it is estimated that ΔD_0 is well under 0.04Mm^3/year. Although an exact virgin discharge rate is not provided above, the general tendency for ΔD_0 is observed. GW_{flow}, ΔD_{y_ave}, and ΔD_0, are several orders of magnitude smaller than the other discharge parameters thus they are considered negligible. From figure 7, in 1970 the general groundwater flow was from the Nevado and the Sierra towards the center of the valley, with groundwater exiting at the North-West corner of the basin. Increased pumping of deep wells throughout the basin has altered groundwater flow directions, forming a depression cone in the metropolitan area of the valley and a net decrease in groundwater flow (GW_{flow}) exiting the basin is observed between 1970 to 2004. The decreasing GW_{flow} pattern is expected to continue into the future until GW_{flow} tends to 0 or negative values. Negative values would imply flow from adjacent basins is entering the Toluca Basin.

Spring discharge (Sp)

The DGCOH (1992) and others suggest that spring discharges (*Sp*) have been steadily decreasing with time. CNA (2005) estimates that spring discharges account for a total of 54 Mm^3/year. To compensate for the decreasing piezometric surface it is assumed that the value was as high as 65 Mm^3/year in 1970 and will decrease to 45 Mm^3/year in 2050 (table 5). Future studies on discharges and water budget should include field work examining the spring discharges with the objective of better quantifying the decrease in spring discharges.

Groundwater pumping (P):

Obtaining a representative estimate of all pumping in the Toluca Valley is challenging. A reliable census requires an accurate depiction of the real pumping occurring in the valley. Based on the most recent data (IMTA, 2003; CNA-GTZ, 2004), in 2002 an estimated 933 wells withdrew a total 462 Mm^3/year (table 5 and Figure 8). Observed and projected pumping rates are shown in figure 8. In terms of projections, the best case and worst case scenario are shown as low and high respectively.

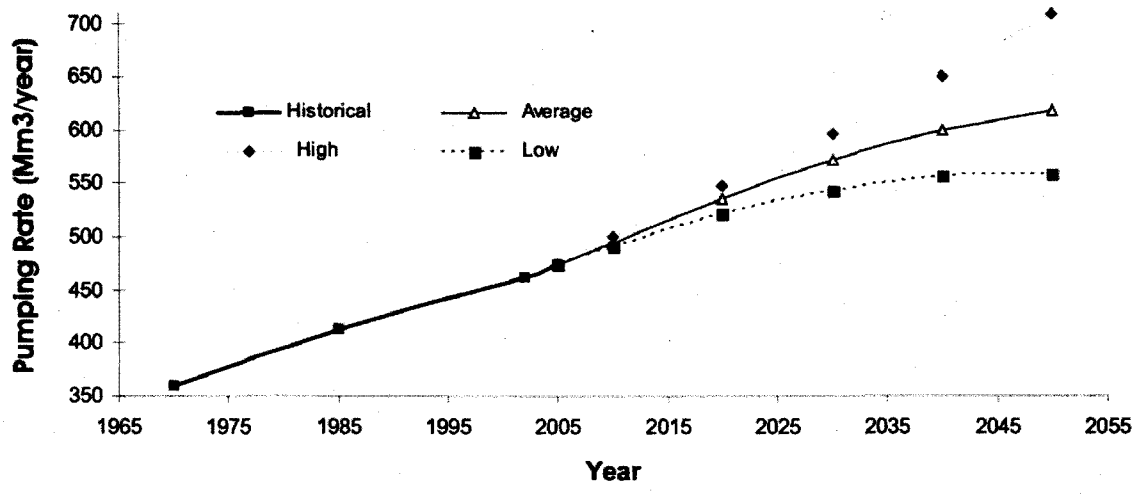


Figure 8: Observed and expected groundwater extraction from pumping wells - 1970 to 2050.

4.3 Deficit

Using the average historical values (1970-2000) obtained for recharge in section 4.1 and the pumping estimates based on the IMTA (2003), the extrapolated total deficit for 2010 is 172 Mm^3/year (table 5, figure 10). The minimum, average, and maximum pumping projections are shown in table 5 and figure 10.

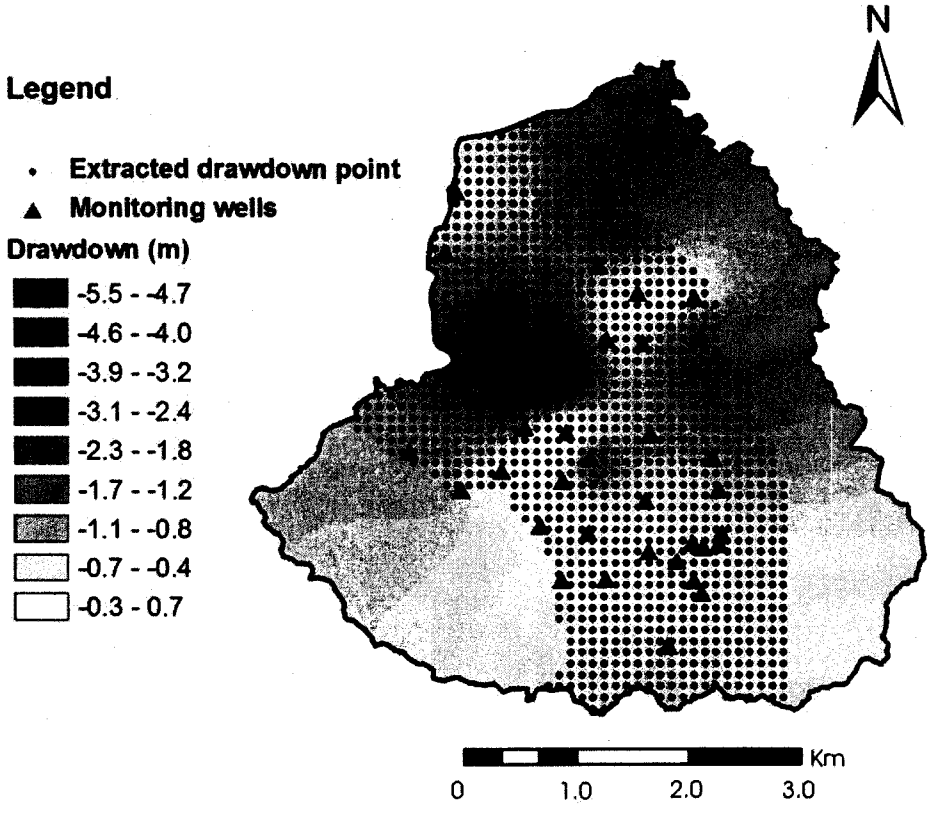


Figure 9: Difference in hydraulic heads between February 2006 and 2008. Measurements were taken in the lower aquifer at 150 m depth. Locations of extracted drawdown points and multilevel monitoring wells are indicated on the map.

Based on the drawdown map method (Figure 9), the total difference in volume of water between February 2006 and February 2008 is 282 Mm^3. Therefore the average yearly deficit is 141 Mm^3. Using the same method from 1970 to 2004 there is a difference of 2664 Mm^3; this works out to an average loss of 78 Mm^3/year. Although little information is available on the methods used for calculating the deficit, the Comisión Nacional del Agua's most recent deficit estimate for 2007 is 139 Mm^3/year. This estimate is low due, possibly, to unregistered pumping wells. Comparing the drawdown map method to the projections based on IMTA (2003), one notices that there is a discrepancy of 26 Mm^3/year. It can be argued that the value of 141 Mm^3/year is too low because it does not take into account the entire basin. For that reason, the true deficit could be higher.

Table 5 and figure 10 summarize the values obtained for the recharge, the discharge, and the deficit for the Toluca Valley. Historical data dating back to 1970 is used and

projections start from the year 2000 when the calculated deficit is 145 Mm^3/year. It is acknowledged that there is error in the historical estimates; however it is assumed this error is minor and therefore uncertainty is limited to the projections. Recharge values, including induced recharge (R_{art}), from 1969 to 2000 are actual recharge values; the overall yearly average for that time period is estimated at 376.2 Mm^3/year. Recharge projections are based on the average value mentioned above and Climate Change (*CC*) average variations (IPCC, 2007), and not yearly minimum and maximum recharge. The discharge projections account for the best case and worst case scenarios discussed in 3.2. The projected deficit is the sum of the recharge and discharge for each scenario. By background extrapolating the deficit curve, one can notice that the last year without deficit occurred around the year 1962. The average estimate shows a deficit of 165 Mm^3/year in 2007 and, in a worst case scenario, reaching a yearly deficit of up to 456 Mm^3/year by 2050.

Table 5 : Summary of the observed and expected groundwater budget from 1970 to 2050.'-' implies data is not relevant. In the deficit section, average, worst case, and best case scenarios are summed respectively with the corresponding case and additional parameters (R_{art}, GW_{flow}, S_p) are included in the calculation. Climate change simulations are based on average recharge and 21 climate models (IPCC, 2007).

				1970	1985	2000	2010	2020	2030	2040	2050
Recharge [Mm^3/year]	Historical Recharge			385,0	373,9	376,2	-	-	-	-	-
	HELP3	Climate Change	average	-	-	376,2	373,0	370,0	367,0	364,0	361,0
			Best case								
			Worst case								
	Induced Recharge (R_art)			-	-	1,2	1,5	2,0	5,0	7,5	10,0
Discharge [Mm^3/year]	Spring discharges (Sp)			55,0	54,0	53,0	52,0	48,0	50,0	48,0	45,0
	Groundwater flow			0,048	0,048	0,023	0,024	0,022	0,020	0,015	0,010
	Pumping	Historical Extraction		359,9	413,0	456,0	-	-	-	-	-
		Expected Extraction (P)	Average	-	-	-	494,5	534,8	571,8	599,1	617,9
			Best case								
			Worst case								
Deficit [Mm^3/year]	Historical Deficit			29,9	93,2	145,0	-	-	-	-	-
	Expected		Average	-	-	-	172,0	210,8	249,9	275,6	292,0
			Best case								
			Worst case								

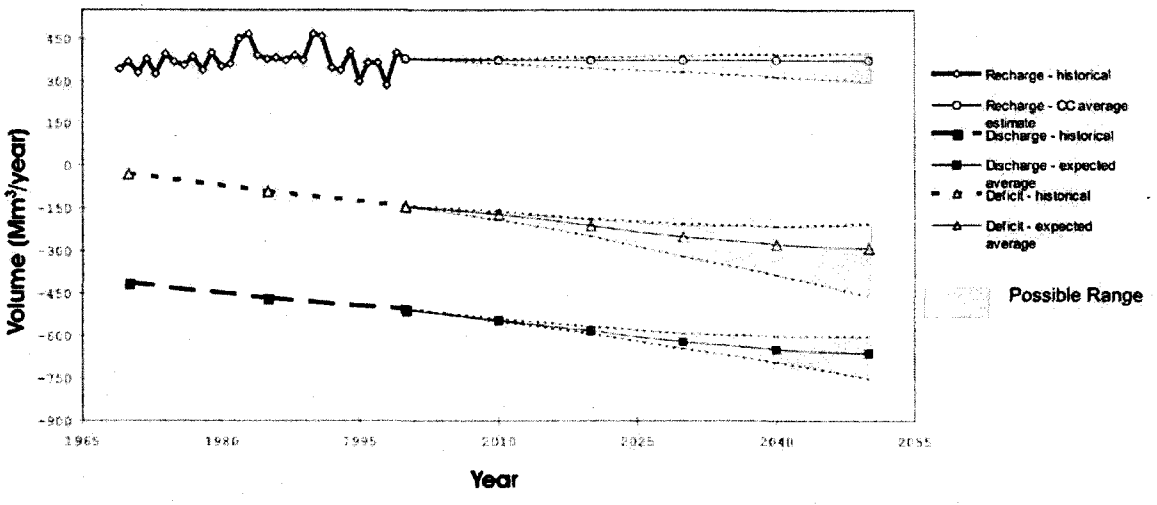


Figure 10: Observed and expected groundwater recharge, pumping, and deficit from 1970 to 2050. Recharge values include induced recharge (R_{art}). From 1969 to 1999 actual recharge values are shown; the average for that time period is estimated at 376.2 Mm^3/year. Recharge from 2000 to 2050 is based on the average value mentioned above and Climate Change (CC) average variations (IPCC, 2007). Historical discharge is based on the literature and groundwater levels and future discharge is based on the projections discussed in section 3.2. The deficit is the sum of the recharge and the discharge.

In both cases of ΔR_0 and ΔD_0, the estimated values do not represent a significant volume compared to the overall recharge and pumping occurring in the basin. The estimates clearly show that the deficit gets worse with time until tapering off due to a decrease in population growth. The consequences of this deficit are already quite apparent in the Toluca Valley: disappearing wetlands, land subsidence due to clay compaction, changes in flow patterns, wells drying up and the need to drill deeper for water.

5 DISCUSSION AND CONCLUSION

Urbanization, intensive industrial practices, and climate change are expected to play an important role on the groundwater budget of many urban centers of central and northern Mexico and the south-western United States in the coming years. Worldwide, several areas are expected to experience drying tendencies over the next century; these areas, where urban centers are found, include south-western Australia, the Western Cape Provinces of South Africa, the southern Andes, the Mediterranean and Mexico (IPCC, 2007). Applying the methodology from this study to these areas where water resources

are threatened, would be of use not only in determining recharge variations, but also the expected deficit. This work has provided valuable insight into the groundwater budget of the Toluca Valley basin. It is important to consider the most complete set of parameters possible when quantifying the present and future groundwater budgets. Applying the spatially variable HELP3 model over the entire watershed with observed climate data and general climate change predictions is useful in observing the distribution and differences in recharge throughout the basin. It was found that, in the case of the temperate-with-dry-winters climate of the Toluca Valley, it is important to not rely solely on the HELP3 model for determining the recharge value and that verifying the results with river discharges or other evapotranspiration and runoff models is necessary. The advantage of the HELP3 model over the other models is the relative distribution of recharge over the entire basin, and it also considers a range of climate parameters, soil properties, vegetation, land use, and general climate change scenarios are easily implemented. Upper and lower estimates based on past precipitation allow us to set limits on annual recharge. Climate change scenarios provide insight into possible future average recharge rates. Concerning discharge, a reliable water-use census and accurate groundwater level data are important in obtaining accurate discharge estimates.

Average estimates show pumping will stabilize around 2050, however following the ICPP (2007) report, the deficit will continue to increase due to climate change (figure 10). The decreasing deficit rate does not imply that the resources will not be exhausted. In this study the term "water availability" is used as a relative term to indicate the presence of a *renewable* water resource; that is, the yearly surface water runoff and groundwater recharge; whereas groundwater stored in the aquifer is considered a *non-renewable* resource. The renewable part of the groundwater system can be considered as a yearly *flux*, while the groundwater stored in the aquifer can be considered a *pool*. If one extracts a *net annual volume* of the fluxes for groundwater (recharges minus discharges), then the system is said to be in hydrodynamic equilibrium and it is considered to be sustainable. However when a *deficit* in the water budget is created and maintained for long time, the water extraction in the system is said to be unsustainable. Depending on the circumstances, the total water availability may also be considered as the sum of the

fluxes and the pools, the renewable and non-renewable resource. But that is a management decision based on several factors and its discussion is beyond the scope of this study.

With respect to changes in recharge and discharge due to pumping, it has been shown that pumping has an effect on natural groundwater flow (GW_{flow}) and an average value has been found for the yearly change in discharge ΔD_y (673 m^3/year) between 1970 and 2004. GW_{flow}, ΔD_y, and therefore ΔD, are several orders of magnitude smaller than the other discharge parameters thus they are considered negligible. As discussed in section 4.1, it is estimated that ΔR_0 is also negligible. If more infiltration wells are built and new technologies allow, the artificial recharge (R_{ART}) could become an important parameter in setting off part of the deficit. A more thorough study of the spring discharges would be useful to properly define the natural discharge from the aquifer. Another source of potential artificial recharge not considered in this study is leaking pipes and sewage systems in the city of Toluca. It is estimated that this form of recharge accounts for 9.5 m^3/s for Mexico City with a population of 15 million (Birkle et al., 1998). Since Toluca's population is approximately 1/8 the size of Mexico, one could expect a loss in the order of 1m^3/s. These values were not included in the budget calculation however they could be considered for future budget estimates.

Although the Toluca Valley's non-renewable water resources are being exploited at worrying rates, still 38% of the groundwater resources are exported out of the basin. Inter-basin water transfer and growing local demand is having detrimental effects on the groundwater supply of the Toluca Valley. Comparing the volume currently exported to Mexico City (6 m^3/s, figure 5), it is less than the current average deficit shown in table 5. Thus, if tomorrow the Toluca Valley stopped all water transfers, they would no longer be in a deficit situation. It is of interest that the approximately 6m^3/s pumping rate exported to Mexico City using the Lerma System represents 61% of the recharge from the Las Cruces mountain chain.

This detailed assessment of two of the most important components of the water cycle (recharge and discharge) clearly shows that the decreasing water availability in the Toluca basin is due mostly to groundwater pumping (Figure10). To a lesser degree, climate change may play a role in the increasing deficit. The analysis shows that the current groundwater pumping is not sustainable. The current deficit is estimated to be between 140 and 170 Mm^3/year. Unless there are drastic changes, it is anticipated that this deficit could increase up to, 456 Mm^3/year by the year 2050. Assuming that the last time the groundwater budget was at equilibrium was the year 1962 (figure 10 by backwards extrapolating), integrating the average deficit curve from 2008 to 1962, the total volume of water removed from storage is circa 3840 Mm^3. Following the results of this study, this volume can not be considered as a renewable resource. The current deficit occurring in the Toluca Valley can be considered problematic and projections based on expected water consumption and climate change reinforce the need for management of the water resources to be addressed.

6 ACKNOWLEDGEMENTS

The authors wish to thank Miroslav Nastev for valuable contributions to the recharge model. We are also thankful to Sergio Murillo and the Comision Nacional del Agua for their logistical support on the field. We are grateful to the Ministère des Relations Internationales, CONACyT, the Autonomous University of the State of México (UAEM), NSERC (a discovery grant held by Richard Martel), AUCC/IDRC, and the Ministère d'Éducation du Québec for their financial support.

References

Allen, D.M., Mackie, D.C., Wei, M., 2004. Groundwater and climate change: a sensitivity analysis for the Grand Forks aquifer, southern British Columbia, Canada. Hydrogeology Journal 12, 270–290.

Ariel Consultores, 1996. Hydrodynamic modeling study and design optimization of the monitoring well networks for the aquifers of Caldera, San Luis Potosi and Toluca (Part 3: Aquifer of Toluca) Estudio de Simulacion Hidrodinamica y Diseno Optimo de las Redes de Observacion de los acuiferos de Calera, San Luis Potosi y Toluca (Tomo 3: Acuifero de Toluca). CNA (Comisión Nacional del Agua) México, DF, Unitecnia pp. 308.

Benson, C.H., Pliska, R.J., 1996. Final covers: HELP needs help from the field. Waste Age 27 (3), 89–98.

Berger, K., 2000. Validation of the hydrologic evaluation of landfill performance (HELP) model for simulating the water balance of cover systems. Environmental Geology 39 (11), 1261–1274.

Birkle, P., V. Torres Rodríguez, E. González Partida, 1998. The water balance for the Basin of the Valley of Mexico and implications for future water consumption Hydrogeology Journal, 6:500–517

Bredehoeft, J.D., 2002. The water budget myth revisited: Why hydrogeologists model. Ground Water, 40 (4): 340-345.

Carrera-Hernandez, J.J. and Gaskin, S.J., 2008. Spatio-temporal analysis of potential aquifer recharge: Application to the Basin of Mexico. Journal of Hydrology, 353(3-4): 228-246.

Carrillo-Rivera, J.J., Cardona, A., Huizar-Alvarez, R. and Graniel, E., 2008. Response of the interaction between groundwater and other components of the environment in Mexico. Environmental Geology, 55 (2): 303-319.

Chammas, G.A., Geddis, M., McCaulou, D.R., 1999.A comparison of two models for simulating the water balance of soil covers under semi-arid conditions. In: Proceedings of the National Meeting of the American Society for Surface Mining and Reclamation, 2, pp. 688–695.

CNA, 2000. Determinacion de la disponibilidad de agua en el acuifero Valle de Toluca. CNA (Comisión Nacional del Agua) México, DF, Unitecnia: 26.

CNA, 2006. Datos climatológico, Servicio Meteorológico Nacional, Comisión Nacional del Agua.

CNA 2007. Base Aquiferos Nacional y Regional. Comisión Nacional del Agua

CNA 2008. Zonas de Reserva de Agua Potable para la ciudad de Toluca. Gerencia de Agua Subterania, Comision Nacional del Agua, Subdirection Tecnica.

Croteau, A., 2006. Détermination de la distribution spatiale et temporelle de la recharge à l'aquifère régional transfrontalier du bassin versant de la rivière Châteauguay, Québec et États-unis., Masters Thesis, Centre Eau Terre Environnement, Institut national de la recherche scientifique. Quebec, Canada

Devlin, J.F. and Sophocleous, M., 2006. The persistence of the water budget myth and its relationship to sustainability. Hydrogeology Journal, 13(4): 549-554.

DGCOH, 1992. Regional hydrogeologic study of the Valleys of Toluca and Ixtlahuaca: Part I. Estudio Hidrogeologico Regional de los Valles de Toluca e Ixtlahuaca: Tomo I: 214.

Fleenor, W.E., King, I.P., 1995. Identifying limitations on use of the HELP model. In: Dunn R.J., Singh, U.P. (Eds.), Landfill Closures. Environmental Protection and Land Recovery. ASCE, Geotechnical Special Publication 53, pp. 121–138.

Gogolev, M.I., 2002. Assessing groundwater recharge with two unsaturated zone modeling technologies. Environmental Geology 42, 248–258.

GTZ-CNA, 2004. Modelo de Simulación Hidrodinámica del Acuífero del Valle de Toluca, Estado de México. Deutsche Gesellschaft fur Technische Zusammenarbeit - Comisión National del Agua.

Hawksworth, J., 2006. The World in 2050: How big will the emerging market economies get and how can the OECD compete?, Pricewaterhouse Coopers, London.

IMTA, 2003. Censo del utilización del agua en el valle de Toluca. Instituto Mexicano de Tecnologia del Agua.

INEGI, 1960. Censo general de población y vivienda 1960. Instituto Nacional de Estadística, Geografía e Informática.

INEGI, 1970. Censo general de población y vivienda 1970. Instituto Nacional de

Estadística, Geografía e Informática.

INEGI, 1980. Censo general de población y vivienda 1980. Instituto Nacional de Estadística, Geografía e Informática.

INEGI, 1990. Censo general de población y vivienda 1990. Instituto Nacional de Estadística, Geografía e Informática.

INEGI, 2000. Censo general de población y vivienda 2000. Instituto Nacional de Estadística, Geografía e Informática.

INEGI, 2001. Instituto Nacional de Estadística, Geografía e Informática, Sinthesis of geographic information for the state of Mexico. Síntesis de información Geográfica del Estado de Mexico

INEGI, 2005. Censo general de población y vivienda 2005. Instituto Nacional de Estadística, Geografía e Informática.

IPCC, 2007. Climate Change 2007: The Physical Science Basis. Contribution of Working Group I to the Fourth Assessment Report of the Intergovernmental Panel on Climate Change [Solomon, S., D. Qin, M. Manning (eds.)].

Jyrkama, M.I., Sykes, J.F., Normani, S.D., 2002. Recharge estimation for transient ground water modeling. Ground Water 40 (6), 638–648.

Jyrkama, M.I., Sykes, J.F. 2007. The impact of climate change on spatially varying groundwater recharge in the grand river watershed (Ontario). Journal of Hydrology, 338, 237–250

Khire, M.V., Benson, C.H., Bosscher, P.J., 1997. Water balance modeling of earthen final covers. Journal of Geotechnical and Geoenvironmental Engineering 123, 744–754.

Legorrreta, J., 1997. Rainfall, the key to the future of the Valley of Mexico. La Jornada Ecologica, 5(58): 1-12.

Lesser and Asociados, S.A., 1992. Diagnostic study of the aquifer of the Valley of Toluca to implement a program for the extraction of groundwater. Estudio para el Diagnostico del acuífero del Valle de Toluca, para implementar la reglamentación de la extracción del agua subterránea.

Machorro, C.S., 1978. Unidades del suelo: Interpretadas para su uso en ingeniería civil y aprovechadas por el campesino en usos agropecuarios. Manual CECSA, Mexico.

McKnight, T. L., Hess, D. 2000. Climate Zones and Types: The Köppen System, Physical Geography: A Landscape Appreciation. Upper Saddle River, NJ: Prentice Hall, pp. 226-229.

Metropoli, 2008. Pierde Edomex batalla legal sobre acuíferos. In: Metropoli (Editor). Metropoli, Mexico, Mexico, last accessed June 4th 2008. http://www.metropoli.org.mx/modules.php?name=News&file=article&sid=3439

NASA, 2008. National Aeronautics and Space Administration. Jet Propulsion Laboratory of the California Institute of Technology. The Shuttle Radar Topographic Mission http://www2.jpl.nasa.gov/srtm/index.html

OEE, 1970. Los acuíferos del alto Lerma pub. No. 7, . report for Oficina de estudios especiales (OEE) de la CHCVM-SRH

Ortega G, A. and Farvolden, R.N., 1989. Computer analysis of regional groundwater flow and boundary conditions in the Basin of Mexico. Journal of Hydrology, 110(3-4): 271-294.

Purdue, 2008. SCS Curve Number Method, West Lafayette, Indiana, last accessed June 4th 2008. http://www.ecn.purdue.edu/runoff/documentation/scs.htm

Richardson, C.W., 1981. Stochastic simulation of daily precipitation, temperature, and solar radiation. Water Resources Research, 17(1): 182-190.

Risser, D.W., Gburek, W.J., Folmar, G.J., 2005. Comparison of methods for estimating ground-water recharge and base flow at a small watershed underlain by fractured bedrock in the Eastern United States. US Geological Survey Scientific Investigations Report 2005-5038.

Rivera, A., E. Ledoux and G. de Marsily, 1991. Nonlinear modeling of groundwater flow and total subsidence of the Mexico City aquifer-aquitard system. FISOLS (IV Inter. Symposium on Land Subsidence); 12-17 May 1991 Houston Texas, USA. IAHS Publication no. 20; pp 45-58.

Rudolph, D.L., Sultan, R., Garfias, J. and McLaren, R.G., 2006. Significance of enhanced infiltration due to groundwater extraction on the disappearance of a headwater lagoon system: Toluca Basin, Mexico. Hydrogeology Journal, 14(1-2): 115-130.

Scibek, J., Allen, D.M., 2006. Comparing modelled responses of two high-permeability unconfined aquifers to predicted climate change. Global and Planetary Change 50, 50–

62.

Schroeder, P.R. Dozier, T.S., Zappi, P. A., McEnroe, B. M., Sjostrom, J.W., Peyton, R. L., 1994. The Hydrologic Evaluation of Landfill Performance (HELP3) Model: Engineering Documentation for Version 3, Environmental Protection Agency Office of Research and Development, Washington, DC.

Scurlock, J.M.O., Asner, G.P. and Gower, S.T., 2001. Worldwide Historical Estimates of Leaf Area Index, 1932–2000. Oak ridge National Laboratory - Report for Department of Energy (USA), ORNL/TM-2001/268.

SICHEM, 1999. Sistema de Information para las cuencas hidrologicas del estado de Mexico. Centro Interamericano de Recursos del Agua UAEM.

Sophocleous, M., Devlin, J.F. and Bredehoeft, J.D., 2004. "The water budget myth revisited: Why Hydrogeologists Model," by John D. Bredehoeft, July-August 2002 issue, v. 40, no. 4: 340-345. Ground Water, 42(4): 618-619.

Theis, C.V., 1940. The source of water derived from wells: Essential factors controlling the response of an aquifer to development. Civil Engineering, 10(5): 277-280.

UNEP, 2008. Mexico's Annual population Growth Rate. United Nations Environment Programme data, http://www.unep.org/

Woyshner, M.R., Yanful, E.K., 1995. Modelling and field measurements of water percolation through an experimental soil cover on mine tailings. Canadian Geotechnical Journal 32, 601–609.

List of tables

Table 1 Description of HELP3 parameters and source of data..... 73

Table 2: Climate data for 4 climatic regions of the Toluca Valley based on CNA (2006) 76

Table 3: Climate change scenarios. Scenario 1 is the base case and scenarios 2-4 are run from 2000 to 2050. 78

Table 4: Natural groundwater flow (GWflow) exiting the basin: estimates for February 1970 and 2004 86

Table 5 : Summary of the observed and expected groundwater budget from 1970 to 2050.'-' implies data is not relevant. In the deficit section, average, worst case, and best case scenarios are summed respectively with the corresponding case and additional parameters (Rart, GWflow, Sp) are included in the calculation. Climate change simulations are based on average recharge and 21 climate models (IPCC, 2007)..... 90

List of figures

Figure 1: Location map of the Toluca Valley within the Republic of Mexico and the State of Mexico. Over 935 pumping wells are in operation in the Valley, including the 230 pumping well system, located along the Lerma river on the eastern edge of the valley, and pumping water to Mexico City. 66

Figure 2: 2D view of the conceptual model for the Toluca Valley Basin including geologic layers and HELP3 layers. Cross section A-B is located on figure 1. Modified from Ariel and Consultores (1996) and Rudolph et al., (2006)..... 68

Figure 3: Logical Model for determining the groundwater budget at a given time where Qon and Qoff are respectively total recharge and total discharge (including pumping) from the basin and $\partial V/\partial t$ is the change in storage. 71

Figure 4: Yearly precipitations at the Valley and High Nevado weather stations 1969 - 2000 (after CNA, 2006)..... 76

Figure 6: Spatially variable distribution of average recharge (R0) in the Toluca Valley [mm/year] based on the HELP3 model. 84

Figure 7: Piezometric surface of the Toluca Valley used to quantify discharge from the basin; a) February 1970 and b) February 2004. 86

Figure 8: Observed and expected groundwater extraction from pumping wells - 1970 to 2050. 88

Figure 9: Difference in hydraulic heads between February 2006 and 2008. Measurements were taken in the lower aquifer at 150 m depth. Locations of extracted drawdown points and multilevel monitoring wells are indicated on the map.. 89

Figure 10: Observed and expected groundwater recharge, pumping, and deficit from 1970 to 2050. Recharge values include induced recharge (Rart). From 1969 to 1999 actual recharge values are shown; the average for that time period is estimated at 376.2 Mm3/year. Recharge from 2000 to 2050 is based on the average value mentioned above and Climate Change (CC) average variations (IPCC, 2007). Historical discharge is based on the literature and groundwater levels and future discharge is based on the projections discussed in section 3.2. The deficit is the sum of the recharge and the discharge..... 91

Chapitre 3: Land subsidence induced by groundwater pumping, monitored by C-band D-InSAR and field data in the Toluca Valley, Mexico

Résumé

Le pompage excessif de l'eau souterraine dans les aquifères compressible conduit à la subsidence, et peut potentiellement causer des dommages importants aux bâtiments et aux infrastructures. Differential Synthetic Aperture Radar Interferometry (D-InSAR) est une technique utilisée pour détecter la déformation de surface avec une precision de moins d'un centimètre. L'objectif de ce travail est de présenter une approche qui utilise D-InSAR et les données de terrain pour quantifier la subsidence induit par le pompage des eaux souterraines, avec un focus de la vallée de Toluca, au Mexique. De plus, les résultats des différents capteurs D-InSAR sont comparés et contrastées. La région d'intérêt a été portée sur le couloir industriel de la vallée de Toluca, au Mexique. Les images SAR (synthetic aperture radar) étaient disponibles entre décembre 1995 et mai 2008. Un total de 30 images SAR d'ERS-1, ERS-2, ENVISAT ASAR et RADARSAT-1 en bande C ont été acquises et traités. Quarante quatre paires D-InSAR ont été traitées dont 31 interférogrammes et cartes de subsidence sont utilisables. La vérification des résultats a été fait à partir de deux systèmes d'extensomètre. De plus, les niveaux des eaux souterraines ont été utilisés pour indiqué la localisation potentiel de la subsidence. La vallée de Toluca, avec un climat semi-aride-tempéré, une concentration urbaine importante, et une subsidence lente, sont des conditions très appropriés pour l'application de la technique D-InSAR. Pour tous les paires d'images D-InSAR, de grandes lignes de base (base lines), les effets atmosphériques, décorrélation temporelle, et la couverture végétale ont été les facteurs limitant l'obtention d'un maximum d'interférogrammes utilisables. En comparant les résultats D-InSAR avec les extensomètres, nous remarquons qu'il existe une corrélation directe. En contrastant les images des capteurs ENVISAT ASAR et RADARSAT-1, il a été constaté que les lignes de bases (*baselines)* courtes (< 500 m) et des acquisitions d'images à intervalle de temps petite (< 1 an) conduisent à des résultats plus précis et mieux corrélées. Les argiles dans le couloir industriel se compactent d'une façon relativement linéaire, où les différents taux de compaction sont fonctions des propriétés géologiques et du taux de pompage. Il y a environs 4 mois de délais entre la baisse du niveau piezométrique et la compaction. Les taux de subsidence maximale actuelle sont estimés à 15 cm/an à certains endroits. L'affaissement total

maximal d'un point situé dans la vallée entre novembre 2003 et mai 2008 est d'environ 40 cm. Il est estimé que le montant total maximum de subsidence depuis 1962 est de plus de 2,0 mètres.

Land subsidence induced by groundwater pumping, monitored by C-band D-InSAR and field data in the Toluca Valley, Mexico

Calderhead, A I (aicalderhead@gmail.com), Institut national de la recherche scientifique - Centre Eau, Terre & Environnement, 490 de la Couronne, Quebec, QC G1K 9A9, Canada

Martel, R (richard.martel@ete.inrs.ca), Institut national de la recherche scientifique - Centre Eau, Terre & Environnement, 490 de la Couronne, Quebec, QC G1K 9A9, Canada

Alasset, P-J (Pierre-Jean.Alasset@NRCan-RNCan.gc.ca) Canada Centre for Remote Sensing, Natural Resources Canada, 588 Booth Street, Ottawa ON K1A 0Y7, Canada

Rivera, A (arivera@nrcan.gc.ca), Geological Survey of Canada, Natural Resources Canada, 490 de la Couronne, Quebec, QC G1K 9A9, Canada

Garfias, J (jgarfiass@uaemex.mx), Universidad Autónoma del Estado de Mexico, Facultad de Ingeniería (CIRA), Cerro de Coatepec, s/n, C.U., Toluca, MEX CP 50130, Mexico

Abstract

Excessive groundwater pumping from compressible aquifers leads to land subsidence potentially causing significant damage to buildings and infrastructure. Differential Synthetic Aperture Radar Interferometry (D-InSAR) is a powerful technique used for detecting surface deformation with sub-centimetre accuracy. The objective of this work is to present an approach using C-band D-InSAR field data for quantifying land subsidence induced by groundwater pumping with a focus of the Toluca Valley, Mexico. Additionally, D-InSAR results from different sensors are compared and contrasted. The region of interest was focused on the industrial corridor of the Toluca Valley, Mexico. Image data were available from December 1995 until May 2008. A total of 30 SAR images from ERS-1, ERS-2, ENVISAT ASAR and RADARSAT-1 C-band sensors were used. Forty four D-InSAR pairs were generated with 31 usable interferograms and subsidence maps. Verifying the InSAR results involved installing and taking measurements from two extensometer systems. Additionally, groundwater levels are used as an indication for locating where subsidence could occur. For all D-InSAR image pairs, large baselines, atmospheric effects, temporal decorrelation, and vegetative cover were the limiting factors in obtaining a maximum number of usable interferograms. Comparing D-InSAR results with the extensometers, we notice that there is a direct correlation.

When contrasting the ENVISAT ASAR and RADARSAT-1 sensors, it was found that shorter baselines and shorter time separation between image acquisitions led to more accurate results and better correlation in terms of the spatial distribution and magnitude of the subsidence. The clays in the industrial corridor compact in a relatively linear fashion where varying compaction rates are a function of drawdown and geologic properties. The geological setting and the drawdown had varying effects on the rate of subsidence where, in 3 different locations, 1.0 m of drawdown lead to between 1 and 8 cm of compaction. The data shows that there is approximately a 4 month delay between a decrease in hydraulic head and compaction. Current subsidence rates are estimated at up to 15 cm/year in certain locations. The total maximum subsidence for a point location in the valley between November 2003 and May 2008 is approximately 40 cm. It is estimated that the maximum total subsidence since 1962 is over 2.0 metres.

1 INTRODUCTION

In many urban settings, excessive groundwater pumping from aquifers composed of compressible clays leads to land subsidence, potentially causing significant damage to buildings and infrastructure. Before Differential Synthetic Aperture Radar Interferometry (D-InSAR), subsidence studies were limited to field observations and numerical modelling of the process. Recent studies of land subsidence have focussed on using D-InSAR as a tool to quantify the regional extent of subsidence.

Synthetic Aperture Radar (SAR) antennae are a type of active microwave radar antenna sending and receiving signals to and from objects on Earth. They are designed to take advantage of a satellite's movement by creating a "synthetic" aperture or opening (JPL, 2008). Most SAR applications make use of the amplitude of the return signal, and ignore the phase data; however, interferometry uses the phase of the reflected radiation. SAR Interferometry (InSAR) is based on the difference between the phase from two processed SAR complex images acquired from 2 different positions (2 antennae on the same plane) or from 2 different times (a single antenna acquiring images at two separate times). The resulting image obtained from the difference of phase between the SAR images is called

the interferogram. Ground movement can be extracted from the shift in phase; however, the measured phase is also composed of other noise from imaging geometry, instrument characteristics, and temporal changes on the land surface and the atmosphere. Differential InSAR (D-InSAR) removes the topography component of the measured phase by using a Digital Elevation Model (DEM). This powerful technique is used for detecting surface deformation on the sub-centimetre scale (Franceschetti and Lanari, 1999).

In the 80's and early 90's SAR data were collected by aircraft overflying specific terrain, however, since the mid 1990's satellite data have been more frequently used. The InSAR technique has been used to study surface displacement due to earthquakes (Massonet et al., 1993; Peltzer & Rosen, 1995; Stramondo et al., 1999), volcanic eruptions (Massonet et al., 1995; Salvi et al., 2004) groundwater extraction (Galloway et al., 1998; Amelung et al., 1999; Hoffmann 2001); landslides (Colesanti & Wasowski, 2006; Hilley et al., 2004; Peyret, 2008) glacier movement (Winebrenner et al., 1997; Rignot et al., 2001; Fatland & Lingle, 2002; Li et al., 2008), water levels in wetlands (Wdowinski et al., 2008; Lu & Kwoun, 2008), and other surface movement processes. Research in these areas has shown surface movement measurements with sub-centimetre accuracy.

Although subsidence due to groundwater pumping and other types of land movement is a common occurrence in Mexico, land movement has only been measured by D-InSAR on a few occasions. Documented cases show land movement from volcanic activity (Carnec & Fabriol, 1999; Farina et al., 2007; Pinel et al., 2008), land subsidence in Mexico City (Strozzi & Wegmüller, 1999; Cabral et al., 2003; Lopez-Quiroz et al., 2007), and earthquakes (Sarychikhina et al., 2007).

Considering the availability of many images from RADARSAT-1 and ENVISAT-ASAR, PS-InSAR or CTM-InSAR would have been the preferred method for determining total compaction over D-InSAR because more confidence is given to results. However, due to restrictions in obtaining capable software, and due to ease of use, D-InSAR was the preferred method for measuring compaction.

The objective of this work is to present a multi-disciplinary approach for monitoring land subsidence induced by groundwater pumping by combining C-band D-InSAR results and field data in the Toluca Valley, Mexico. Additionally, D-InSAR results from different sensors are compared and contrasted.

The Toluca Valley's semi-arid to temperate climate, high concentration of urban backscattering from objects such as buildings and other cement structures, along with the slow deformation of land due to groundwater pumping in a compressible aquifer are very suitable conditions for applying the D-InSAR technique. Results from two C-band sensors (5.6 cm wavelength), ENVISAT ASAR (resolution of ~30m) and RADARSAT-1 in fine beam mode (resolution of ~8 m), using data from December, 2003 to May, 2008, are compared and contrasted with extensometer readings and groundwater levels for the same time period. Variations in subsidence patterns are observed and differences between sensors are examined.

2 STUDY AREA

The Toluca Valley basin (Figures 1 and 2) covers an area of approximately 2100 km^2 in the centre of Mexico. The basin is adjacent to the Mexico City Valley, with the Sierra Las Cruces forming a natural border between the two basins. The Toluca Valley's geographic position in the centre of the country, proximity to Mexico City, as well as its rapidly developing infrastructure, have allowed the city to grow into a major industrial zone for the country. The industrial corridor located to the East of downtown Toluca has a high concentration of pumping wells, compressible clay content, and is the area where most of the subsidence occurs.

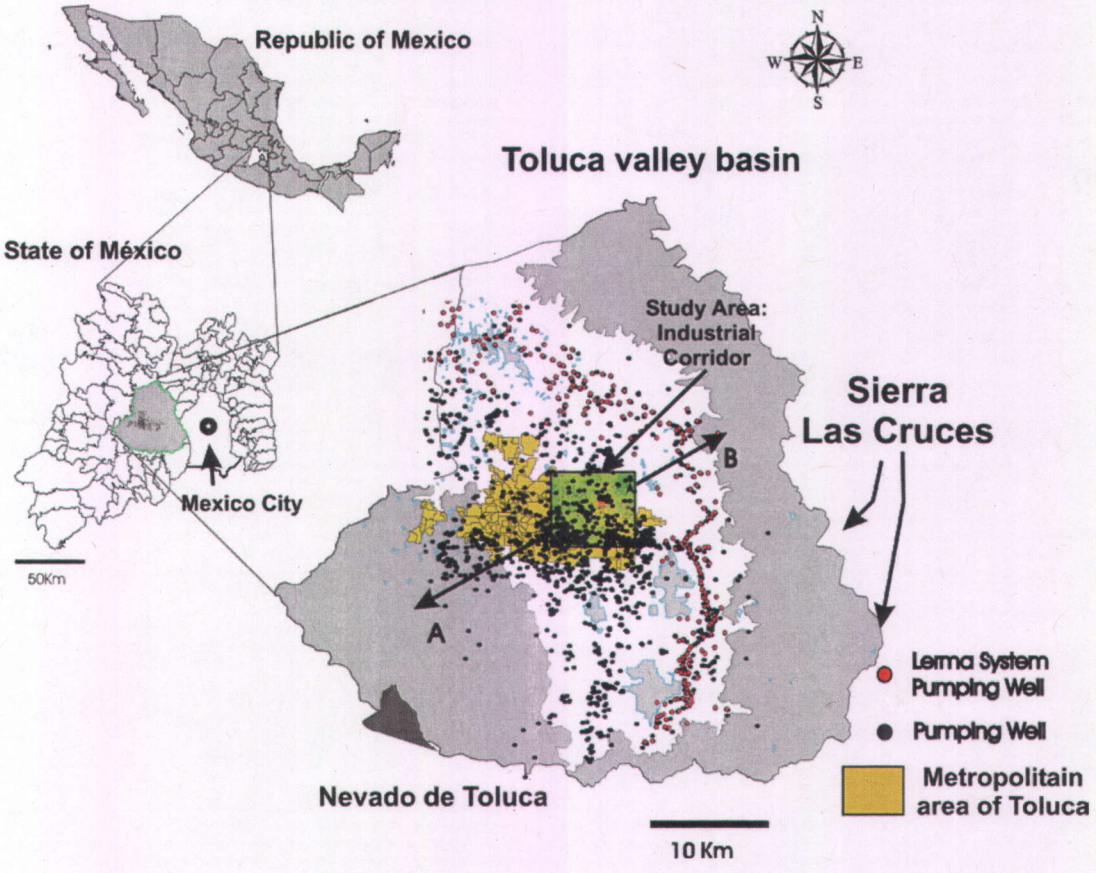


Figure 1: Location map of the Toluca Valley and the industrial corridor within the Republic of Mexico and the State of Mexico. Cross section A-B is shown is Figure 2. A deformation map is in the centre of the valley (Modified from Calderhead et al., 2009).

GEOLOGICAL SETTING

The Toluca Valley is located in what is known as the Faja Volcanica Transmexicana (Ariel and Consultores, 1996). This region was a tectonically active zone in the Upper to Mid-Tertiary period forming a series of Northwest-Southeast trending fault systems throughout much of southern Mexico. The two main features defining the basin are the Nevado de Toluca volcano to the South-West, and the Sierra Las Cruces mountain chain to the East.

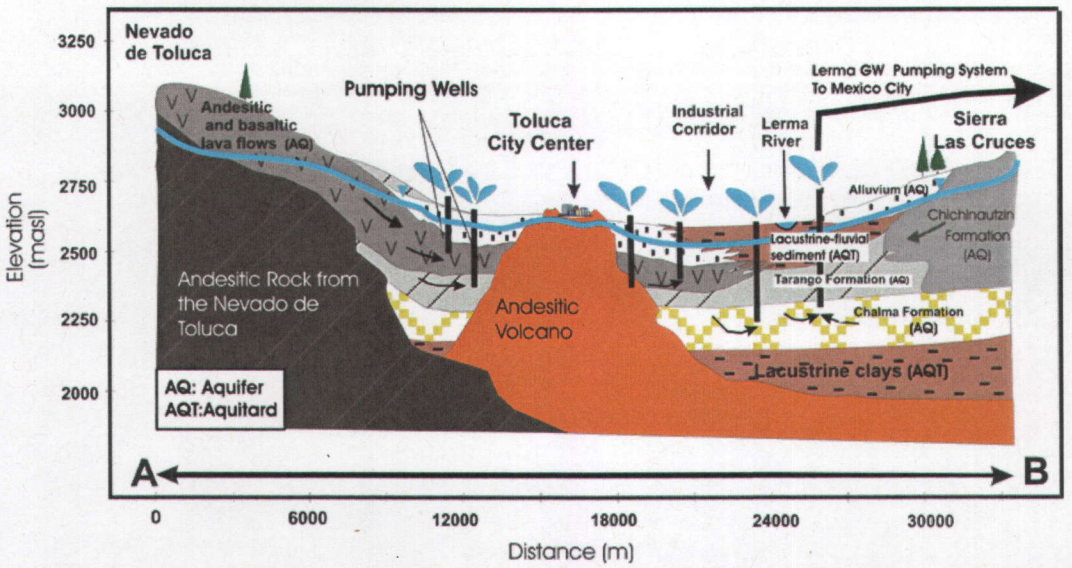


Figure 2: 2D view of the conceptual model for the Toluca Valley Basin. Cross section A-B is located on Figure 1. (Modified from Calderhead et al., 2009)

Volcanic andesitic rock from a buried volcano in the centre of the valley (Miocene age) forms the basement in the basin. The bedrock forms a bowl in the centre of the valley, reaching depths greater than 600 m and cropping out to the surface at the edges of the valley. The andesitic volcano formation of the Nevado de Toluca core is located to the West. The bedrock is overlain by a confining layer of pure lacustrine clays and by the Chalma formation aquifer, composed of a mixture of sand, gravel and clay. The Tarango formation aquifer, deposited after the Chalma formation, extends from the flanks of the Sierra Las Cruces Mountains in the East across the basin floor to the foot of the Nevado of Toluca volcano. This formation is a heterogeneous mixture of volcaniclasitc materials (Lesser and Asociados, 1992). The basaltic and ash flows of the Chichinautzin formation were deposited in the eastern portion of the Toluca Valley and act as an aquifer. In the upper middle portion of the valley, where most of the groundwater pumping occurs, complex interlayering of lacustrine clay (aquitard) and alluvium deposits (aquifer) are found. The sequence of layers is shown schematically in Figure 2. The industrial corridor, adjacent to the Lerma River (Figure 2), is located on what used to be a flood plain. Occasionally, during heavy rainfall parts of the industrial corridor become a flood plain.

GROUNDWATER RESOURCES

Historically, in the Toluca Valley, groundwater levels were either at depths close to the surface or emerged above the land surface in artesian conditions (Lesser and Asociados, 1992). Currently, there is a significant decrease in the water level within the basin primarily due to groundwater pumping, and the decrease is increasing with time (Calderhead et al., 2009). There are more than 935 pumping wells in the Toluca Valley (IMTA, 2003). Groundwater exports occur in the form of the Lerma system wells, a groundwater pumping system operated by Mexico City and consisting of 396 pumping wells located along the upper section of the Lerma River (Figure 1). The system has been in operation since the late 1960's and captures a large portion of the recharge water entering from the Sierra Las Cruces, which is then exported to Mexico City at approximately 6.0 m^3/s (Calderhead et al., 2009). Increasing local demand for water has also added to stresses on the aquifer system.

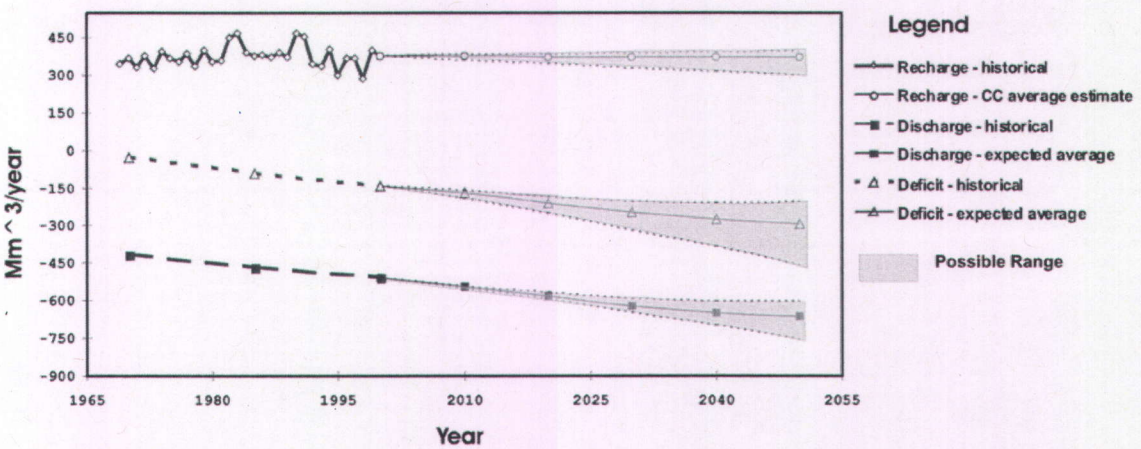


Figure 3: Observed and expected groundwater recharge, pumping, and deficit from 1970 to 2050. From 1970 to 1999 actual recharge values are shown. From 2000 to 2050 average expected recharge including climate change is shown. Recharge, discharge and deficit projections are based on Calderhead et al. (2009). The deficit is the sum of the recharge and the discharge. Modified from Calderhead et al. (2009)

An increasing groundwater deficit occurring in the Toluca Valley is shown in Figure 3. The growing demand for groundwater (CNA, 2008; Calderhead et al. 2009) and the expected drying tendencies of the region (ICCP, 2007) lead to an increasing deficit. By bacwwards extrapolating, it is seen that the deficit begins in the early 1960's and is continually increasing. The stresses imposed on the aquifers have caused significant

changes on the water flow patterns, a reversal in the direction of vertical hydraulic gradients, the disappearance of artesian springs and wetlands, and the formation of fractures and regional land subsidence.

3 METHODS AND MATERIALS

3.1 Brief description of D-InSAR

Interferometry uses the phase of reflected radiation. The phase of the return wave depends on the distance to the ground, since the path length to the ground and back will consist in a number of whole wavelengths plus some fraction of a wavelength. The total distance to the satellite (i.e. the number of whole wavelengths) is not known, but the extra fraction of a wavelength can be measured extremely accurately. D-InSAR uses two SAR images of the same area taken from slightly different positions at two different times, measures the difference in phase between 2 scene images (master and slave images) in a co-registered pixel by pixel basis and removes the topographic phase component using a DEM, producing an image known as a differential interferogram. This is measured in radians of phase difference and, due to the cyclic nature of phase, is recorded as repeating fringes which each represent a full 2π cycle (half of satellite wavelength, i.e. 2.8 cm 2.8 cm of line of sight displacement in the C-band case).

In practice, the phase is also affected by several other factors, which together make the raw phase return in any one SAR image essentially arbitrary, with no correlation from pixel to pixel. To get any useful information from the phase, some of these effects must be isolated and removed. The phase difference of an InSAR data pair ($\Delta\phi$) separated by a spatial and temporal baseline can be described as follows (Massonnet & Feigl, 1998; Mora et al., 2003; Rocca et al., 1997; Chatterjee et al., 2006):

$$\Delta\phi = \delta\phi_{flat} + \delta\phi_{top} + \delta\phi_{disp} + \delta\phi_{atm} + \delta\phi_{noise} \pm n \times 2\pi \qquad (1)$$

$$\Delta\phi = \frac{4\pi \cdot B_{\perp} \cdot r}{\lambda \cdot \rho \cdot tg\theta} + \frac{4\pi \cdot B_{\perp} \cdot h}{\lambda \cdot \rho \cdot \sin\theta} + \frac{4\pi \cdot \delta\rho}{\lambda} + \delta\phi_{atm} + \delta\phi_{noise} \pm n \cdot 2\pi \qquad (2)$$

where, $\delta\phi_{flat}$, $\delta\phi_{top}$, $\delta\phi_{disp}$, $\delta\phi_{atm}$, and $\delta\phi_{noise}$ represent phase difference from the spatial baseline of the data pair assuming a flat Earth, topographic unevenness of the terrain, ground displacement along the radar line-of-sight, atmospheric disturbance resulting from spatio-temporal variation in the atmosphere, and random noise resulting from radar instrument and temporal decorrelation between two images of the pair respectively. In the term, $n \cdot 2\pi$, n is a discrete number, including 0 and represents the number of phase cycles in the wrapped phase difference ($\Delta\phi$). λ, θ, ρ, $B_{\perp}$, r, h and $\delta\rho$ are radar wavelength, look angle, slant range distance of the master image, perpendicular baseline component of the data pair, slant range difference of the data pair due to orbital separation, topographic height of the given point and ground displacement parallel to radar line of sight (LOS) respectively. (See limitations of D-InSAR in Annexe-F)

3.2 Image data and processing

Image Data for the Toluca Valley

The images processed to obtain deformation maps are C-Band single look complex (SLC) SAR images over the Toluca Valley and its industrial corridor. SLC SAR data originating from ERS-1, ERS-2, ENVISAT ASAR, and RADARSAT-1 were acquired (Table 2). In addition to the SLC SAR data, to remove the topographic phase from the interferogram we used a 90 meters DEM from the Shuttle Radar Topography Mission (SRTM version 2, Farr T.G. et al., 2007) of the Toluca Valley. A more precise DEM was not available for the region. Spatial resolution for the ERS-1, ERS-2 and ENVISAT ASAR data is 30 metres while the spatial resolution for RADARSAT-1 in Fine beam mode is 8 metres.

Table 1: Acquired images between 1995 and 2008

Mission	Date	Track	Frame	Pass
ERS-1	12/12/1995	26	3213	descending
ERS-1	28/01/1996	191	369	ascending
ERS-1	07/04/1996	191	369	ascending
ERS-2	21/03/2001	26	3213	descending
ERS-2	17/10/2001	26	3213	descending
ERS-2	15/05/2002	26	3213	descending
ERS-2	28/08/2002	26	3213	descending
ENVISAT ASAR	26/03/2003	2026	3213	ascending
ENVISAT ASAR	09/07/2003	2026	3213	ascending
ENVISAT ASAR	13/08/2003	2026	3213	ascending
ENVISAT ASAR	04/02/2004	2026	3213	ascending
ENVISAT ASAR	14/04/2004	2026	3213	ascending
ENVISAT ASAR	15/12/2004	2026	3213	ascending
ENVISAT ASAR	19/01/2005	2026	3213	ascending
ENVISAT ASAR	08/06/2005	2026	3213	ascending
ENVISAT ASAR	30/11/2005	2026	3213	ascending
ENVISAT ASAR	05/12/2007	2026	3213	ascending
ENVISAT ASAR	13/02/2008	2026	3213	ascending
ENVISAT ASAR	23/04/2008	2026	3213	ascending
ENVISAT ASAR	28/05/2008	2026	3213	ascending
Mission	**Date**	**Abs. Orbit**	**Cycle**	**Pass**
RADARSAT-1 (F4 beam)	05/12/2003	42196	122	ascending
RADARSAT-1 (F4 beam)	29/12/2003	42539	123	ascending
RADARSAT-1 (F4 beam)	10/03/2004	43568	126	ascending
RADARSAT-1 (F4 beam)	01/08/2004	45626	132	ascending
RADARSAT-1 (F4 beam)	29/11/2004	47341	137	ascending
RADARSAT-1 (F4 beam)	23/12/2004	47684	139	ascending
RADARSAT-1 (F4 beam)	14/11/2007	62776	182	ascending
RADARSAT-1 (F4 beam)	25/01/2008	63805	185	ascending
RADARSAT-1 (F4 beam)	13/03/2008	64491	187	ascending
RADARSAT-1 (F4 beam)	24/05/2008	65520	190	ascending

D-InSAR processing and selected parameters

The software used to process the SLC radar images is EV-InSAR 4.0 ® by MacDonald, Dettwiler and Associates Ltd. (MDA). The major steps executed by the software are briefly described in figure 10 of Chapter 1.

3.3 Field data acquisition

Hydraulic head change and geo-mechanical properties have a direct consequence on the amount of subsidence (Terzaghi, 1925). The working hypothesis is therefore based on Terzaghi's 1D compaction principle where a drop in hydraulic head produces compaction. Numerical modelling is often used for representing subsidence processes however the scope of this study is limited to monitoring subsidence through D-InSAR

and the use of field data. The following section describes the two types of field data obtained from the Toluca valley: groundwater levels and extensometer readings.

Water levels

Two sources of hydraulic head data are used in this study. The first source involves the long-term monitoring of water levels in the basin by a multi-level piezometer (CNA, 2008) where multilevel data is available from 1969 to present. The multi-piezometer data of PL-201 at a depth of 79 m is used because it has reliable data and it is one of the closest monitoring wells to the region of interest. The other data set comes from a pressure transducer installed at the Extensometer-1 well (Figure 4). The water level at Extensometer-1 is measured every 12 hours and data is available from December 2006 to July 2008. Some data is missing between August and November 2007. The water levels in this study are used only as an indication of the compaction that is to be expected.

Extensometer measurements

Historical geodetic information and accurate field subsidence measurements were not available for the Toluca valley. The objective of installing the extensometers was to obtain accurate field measurements at point locations.

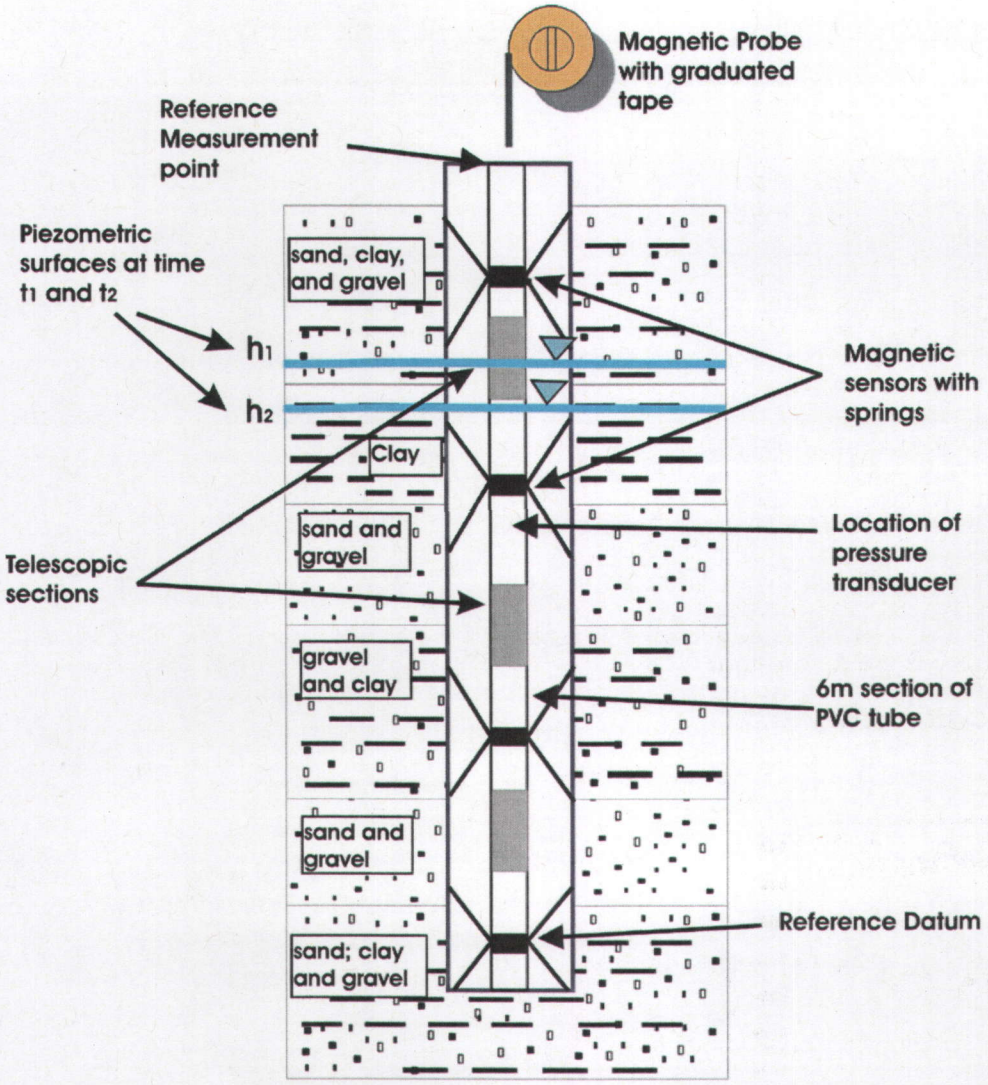


Figure 4: Schematic drawing of the magnetic probe extensometer. Piezometric surface variations with time and location of pressure transducer are also represented. Drawing is not to scale.

Two R-4 magnetic reed switch probe extensometer systems by Roctest® (Roctest, 2009) were installed in the Industrial Corridor (Figure 6). Boreholes with a 15 cm diameter were bored by a rotary drill and reach 115 and 78 meters depth respectively for Extensometer-1 and Exsensometer-2. The extensometers (Figure 4) consist of magnetic targets, surrounding the centre of a 7 cm radius, 6 m long PVC pipe; the 6 m sections of PVC pipe are separated by telescopic joints. The spring anchors attached to the PVC pipe and joined by telescopic joints are lowered to the bottom of the borehole then released

with an external draw wire. Any compaction or swelling below the bottom anchor is not measured by the extensometer.

Once the extensometer is installed, a magnetic probe, lowered down the access pipe, detects the position of the magnet anchors. The probe is suspended by a single graduated tape that incorporates the electrical leads. The tape graduation is used to determine the deformation between magnetic anchor points along the pipe's axis. For this study, reading frequencies from the extensometers varied from 1 to 6 months and spanned two years beginning in July of 2006 and ending in July of 2008.

Extensometer-2 is located North-East of Extensometer-1 (Figure 6). The location was chosen due to noticeable subsidence affecting structures. To insure all compaction is measured, it would have been preferable to have the bottom of the extensometer reach bedrock. It is however estimated, by observing adjacent borehole logs, that the bedrock is probably located well below 300 meters depth. Thus, the cost and technical difficulty prohibited reaching the bedrock. It is estimated that most of the compaction due to pumping occurs in the upper 100 meters of the groundwater flow system, where the pores lose saturation, compressible materials are newer, and clay content is high.

4 RESULTS

D-InSAR image pairs are presented in Table 3. The perpendicular baseline, parallel baseline, time difference, usefulness, and figure number are also indicated. The highest quality interferograms over the city of Toluca originated from D-InSAR pairs with baselines under 600 m, a maximum time difference in pair acquisition of one year, and images acquired during the dry season (early November to late April). Typical of C-Band InSAR, the coherence is best in and around urban centres where little vegetation is found. These areas have a large density of man-made reflectors such as buildings, parking lots, cement structures and comparatively little vegetative disturbance. The dry season corresponds to the period with the least amount of vegetation growth and thus the least amount of temporal decorrelation.

Table 2: InSAR pair acquisition dates, perpendicular baseline (b perp.) and parallel baseline (b paral.) in metres, and time difference in days (d_days) are listed. Also listed are the figure numbers where results from subsidence maps are presented in this study.

Mission	Date 1	Date 2	b perp.	b paral.	d_days	useful	Figures
ERS-1	28/01/1996	07/04/1996	26	22	70	yes	9
ERS-2	21/03/2001	17/10/2001	7121	2723	210	no	-
ERS-2	17/10/2001	15/05/2002	126	114	210	no	-
ERS-2	15/05/2002	28/08/2002	516	126	105	no	-
ENVISAT ASAR	26/03/2003	09/07/2003	869	413	105	no	-
ENVISAT ASAR	26/03/2003	13/08/2003	858	400	140	no	-
ENVISAT ASAR	26/03/2003	04/02/2004	74	77	315	yes	7,8,9,10,11a
ENVISAT ASAR	09/07/2003	04/02/2004	505	126	210	yes	-
ENVISAT ASAR	04/02/2004	14/04/2004	310	73	70	yes	-
ENVISAT ASAR	04/02/2004	15/12/2004	64	14	315	yes	-
ENVISAT ASAR	04/02/2004	19/01/2005	120	46	350	yes	7,8,9,10,11b
ENVISAT ASAR	14/04/2004	15/12/2004	374	87	245	yes	-
ENVISAT ASAR	15/12/2004	19/01/2005	56	32	35	yes	-
ENVISAT ASAR	15/12/2004	05/12/2007	100	74	1085	no	-
ENVISAT ASAR	19/01/2005	08/06/2005	243	125	140	yes	7,8,9,10,11c
ENVISAT ASAR	19/01/2005	30/11/2005	94	40	315	yes	-
ENVISAT ASAR	08/06/2005	30/11/2005	149	85	175	yes	7,8,9,10,11d
ENVISAT ASAR	30/11/2005	05/12/2007	217	88	735	yes	7,8,9,10,11e
ENVISAT ASAR	05/12/2007	13/02/2008	29	33	70	yes	-
ENVISAT ASAR	05/12/2007	23/04/2008	85	86	140	yes	-
ENVISAT ASAR	05/12/2007	28/05/2008	185	2	175	yes	5,6,7,8.9,1011f,12
ENVISAT ASAR	13/02/2008	23/04/2008	172	41	70	yes	-
ENVISAT ASAR	13/02/2008	28/05/2008	323	108	105	yes	-
ENVISAT ASAR	23/04/2008	28/05/2008	151	149	35	yes	-
RADARSAT-1	05/12/2003	29/12/2003	1052	869	24	no	-
RADARSAT-1	05/12/2003	10/03/2004	592	456	96	yes	-
RADARSAT-1	05/12/2003	29/11/2004	1291	1074	360	no	7,8,9,10
RADARSAT-1	29/12/2003	10/03/2004	459	412	72	yes	-
RADARSAT-1	29/12/2003	01/08/2004	1125	942	216	no	-
RADARSAT-1	29/12/2003	23/12/2004	841	659	360	yes	-
RADARSAT-1	10/03/2004	01/08/2004	695	636	144	yes	-
RADARSAT-1	10/03/2004	29/11/2004	698	617	264	yes	-
RADARSAT-1	01/08/2004	29/11/2004	1393	1253	120	no	-
RADARSAT-1	01/08/2004	23/12/2004	312	389	144	yes	-
RADARSAT-1	29/11/2004	23/12/2004	1081	865	24	no	-
RADARSAT-1	29/11/2004	14/11/2007	1125	595	625	yes	7,8,9,10
RADARSAT-1	01/08/2004	14/11/2007	267	310	1200	no	-
RADARSAT-1	23/12/2004	14/11/2007	44	78	1056	yes	-
RADARSAT-1	14/11/2007	25/01/2008	521	452	72	yes	-
RADARSAT-1	14/11/2007	13/03/2008	28	5	120	yes	-
RADARSAT-1	14/11/2007	24/05/2008	754	654	192	yes	7,8,9,10,12b
RADARSAT-1	25/01/2008	13/03/2008	492	446	48	yes	-
RADARSAT-1	25/01/2008	24/05/2008	1239	1015	120	no	-
RADARSAT-1	13/03/2008	24/05/2008	746	568	72	yes	-

Figures 5a and 5b show the coherence for an ENVISAT ASAR pair collected between December 5, 2007 and May 28, 2008. White shade represents a high coherence and dark colours represent low coherence. The coherence is highest in urban areas and significantly decreases when image acquisitions are during the vegetative growth season (May to November). Additionally, although best results were obtained with image acquisition dates with a difference of less than one year, it was possible to obtain information from longer acquisition separations. With one D-InSAR pair, usable results were obtained for a time difference of just under three years. Due to temporal decorrelation and high perpendicular baselines, the ERS-2 data for the Toluca valley were not useful for this study. Only one ERS-1 pair was of use. The remaining D-InSAR pairs used in this study are from either ENVISAT ASAR or RADARSAT-1 images.

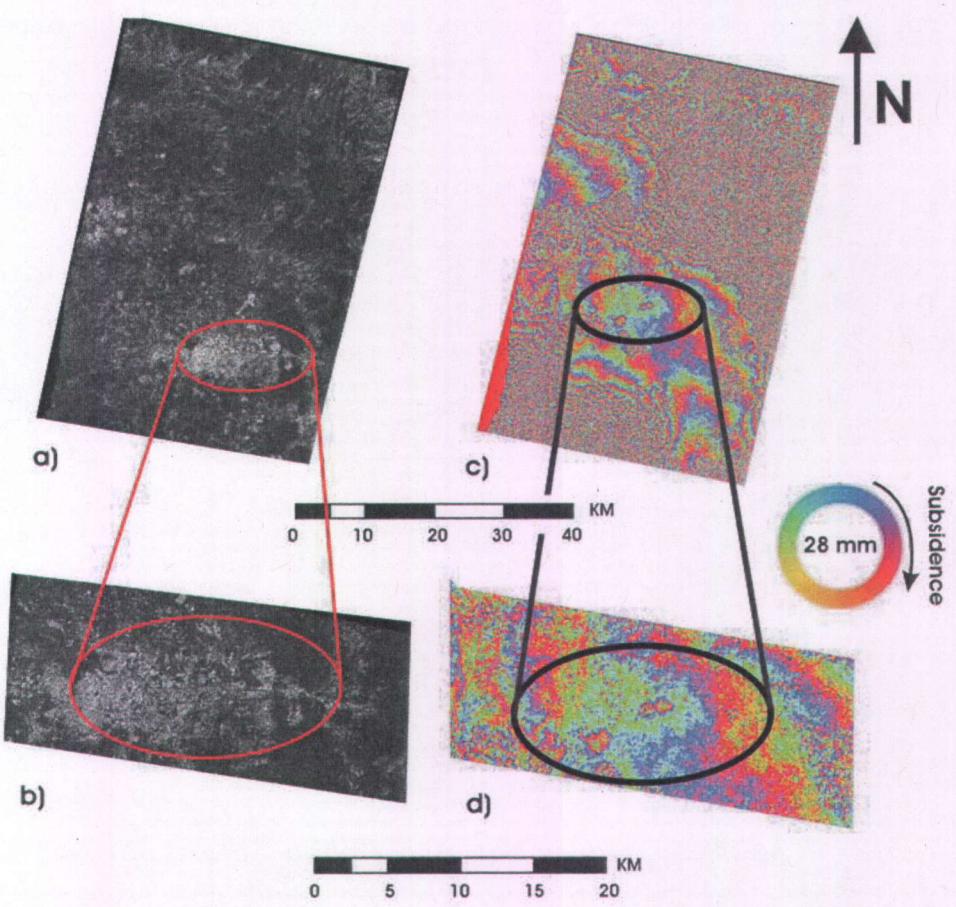


Figure 5: Coherence of the Toluca Valley in a) and b) and corresponding differential interferogram of the same region in c) and d) for ENVISAT ASAR InSAR pair (December 5th 2007 and May 28th, 2008). b) and d) are enlargements of a) and c) respectively.

Figures 5c and 5d show the interferogram of the image pair (December 5, 2007 and May 28, 2008) with Figure 5d as a close up zoom of 5c. Large fringes in Figure 5c indicate areas where coherence is sufficient for detecting land movement. Small scattered colours represent areas where information can not be used. Due to low coherence outside of the urban areas, it is impossible to obtain useful information in these regions where land use is mostly characterized by vegetative growth. Atmospheric effects caused variations in the interferograms, however, prominent subsidence zones were observed throughout the data set. Circled in 5c and 5d is a region of interest where subsidence is detected and measured. Knowing that ENVISAT ASAR uses C-band radar (wavelength of 5.6 cm), preliminary estimates of the land movement are obtained. A complete red-green-blue fringe or 2π phase cycle represents a surface displacement of $\lambda/2$ (2.8 cm) along the LOS direction, where λ is the operating wavelength of the SAR sensor. Field measurements reinforce these findings as we show below. Future discussion focuses on this area where the subsidence area is mapped.

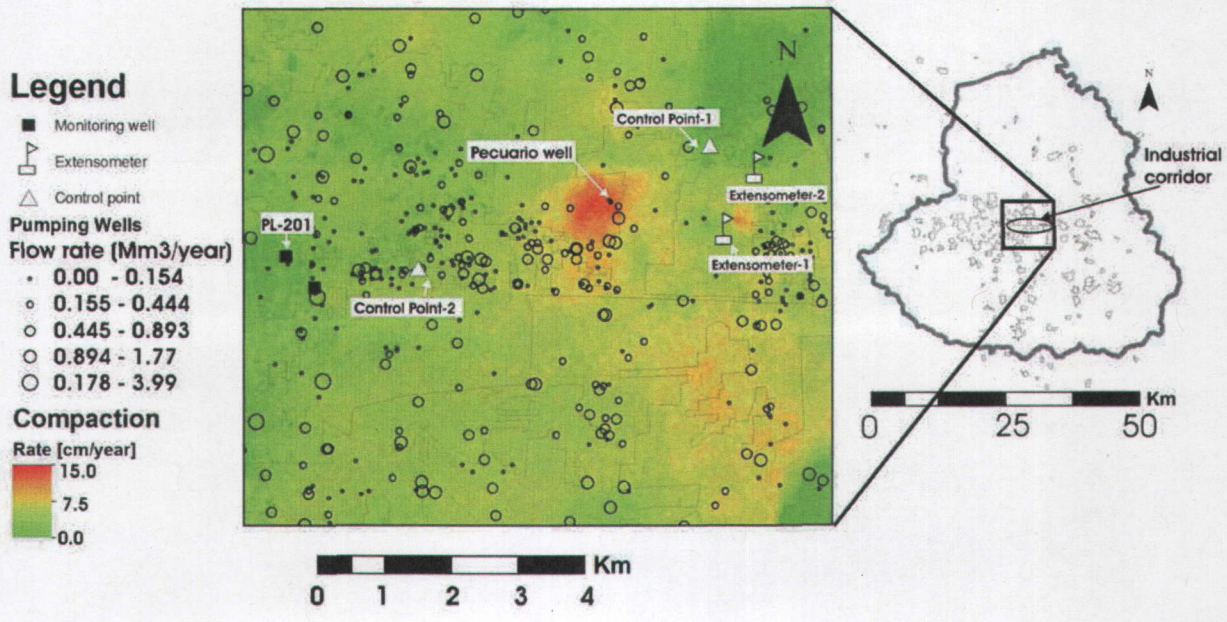


Figure 6: ENVISAT-ASAR height deformation map of the Toluca Valley basin obtained from Figure 5d showing the location of extensometers, control points, monitoring wells, pumping wells with rates. InSAR measured subsidence rates are between December 2007 and May 2008. Corresponding baseline and pass are in Tables 2 and 3.

The region of maximum subsidence is red in colour in Figure 6; this area is detected throughout the entire data set; therefore it is not caused by atmospheric disturbances. In this image the highest subsidence rate is estimated at approximately 15 cm/year. Due to the nature of the terrain and the factors influencing subsidence, the deformation is assumed to be vertical; however, it is possible there is a negligible amount of horizontal deformation in the Toluca Valley. A series of pumping wells are located around the region of maximum subsidence. Although no detailed geological information is available for this region, it is probable that there are highly compressible clays in this area of maximum subsidence since few pumping wells are directly in the centre of the zone. Other smaller regions with subsidence are also detected in the vicinity of the industrial corridor. The south-east corner of Figure 6 has a series of moderate subsidence zones on the order of 5-8 cm/year; and another subsidence zone, between the two extensometers, has a compaction rate in the 8-12 cm/year range for this time frame.

The control point that was most used for measuring the subsidence is Control Point-1 (Figure 6). This point was chosen because from field observations and almost all of the InSAR results, the area around Control Point-1 shows no variation of land movement. When results from Control-point 1 were incoherent, possibly due to errors in unwrapping or atmospheric effects, Control Point-2 was used as the reference.

Three points in the industrial corridor are examined more closely in this section: Extensometer 1, Extensometer 2, and the Pecuario well. Due to delays in obtaining subsidence maps, no field data is available from the Pecuario well location. However, the two other locations do have extensometers, and from December 2006 to July 2008, a pressure transducer at Extensometer 1 measured the water level every 12 hours. The nearby monitoring well, PL-201, is also used as a reference.

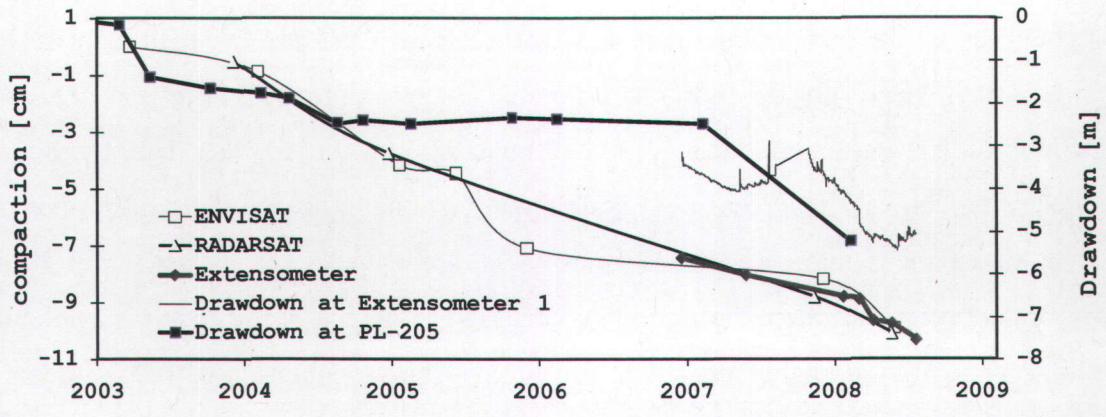


Figure 7: D-InSAR measured subsidence by ENVISAT ASAR and RADARSAT-1 and extensometer and water level at Extensometer-1 and PL-205 between March 2003 and May 2008.

In Figures 7-10, the compaction rate represents the slope of the lines, excluding water levels. Figures 7, 8, and 10 use data respectively from Extensometer 1, Extensometer 2, and Pecuario well. Figure 9 uses data from Extensometer 1. Except for figure 9, InSAR results are from March of 2003 to May of 2008 and extensometer readings begin in December 2006.

Good correlation between ENVISAT ASAR and RADARSAT-1 D-InSAR results and the readings from Extensometer-1 is seen in Figure 7. Between November of 2003 and May 2008 a total of over 10 cm of subsidence is measured by ENVISAT ASAR. The results are backed up by the good correlation of later measurements of RADARSAT-1 and the extensometer. In Figure 7, incomplete data was the cause for the gap in the water level data from August 2007 until November 2007. At Extensometer-1, approximately 1 metre of drawdown (decrease in water level) gives 1 cm of compaction. Subsidence at Extensometer-2 is observed in Figure 8. Good correlation exists between the two D-InSAR results. The extensometer data slope coincides relatively well with the D-InSAR results. The order of subsidence is similar to Extensometer-1's values with approximately 9 cm between November 2003 and May 2008 and approximately 1 metre of drawdown gives 2 cm of subsidence. From Figures 7 and 8 it can be inferred that the industrial corridor clay compacts in a relatively linear fashion with varying compaction rates as a

function of differing drawdown and geo-mechanical properties. Hydraulic head drawdown at PL-205 does dot decrease significantly between 2004 and 2007 yet subsidence occurrence do steadily occur. This can be explained by the fact that PL-205 is located approximately 2 Km North of Extensometer 1, thus giving only a regional tendency. Local drawdown is more representative at Extensometer-1, unfortunately however, this data only spans 2 years.

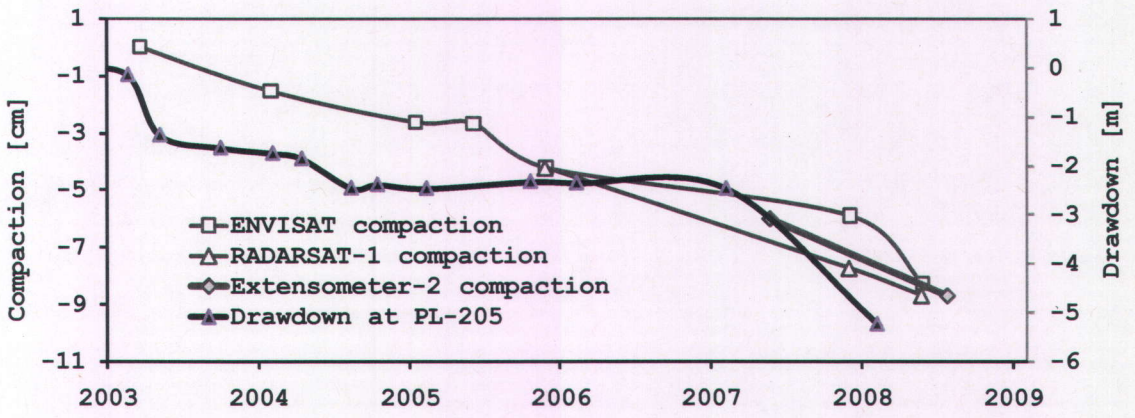


Figure 8 : D-InSAR measured subsidence by ENVISAT ASA and RADARSAT-1 at Extensometer-2 and water level at PL-201 between March 2003 and May 2008.

At the Extensometer-1 location, D-InSAR data from January 1996 to May 2008 are compared with historical groundwater level data (Figure 9). Between 1996 and 2008 a total of 30 cm of subsidence is estimated at the Extensometer-1 location. SAR images were unavailable between April 1996 and March 2003, therefore estimated subsidence rates are based on the 1996 and 2003-2008 data. Based on water levels between 1996 and 2003 and the 2003-2008 subsidence record it is quite possible that the actual total subsidence between 1996 and 2003 is underestimated because the water levels drop at higher rates in the period 1997-2003 than in the period 2003-2008.

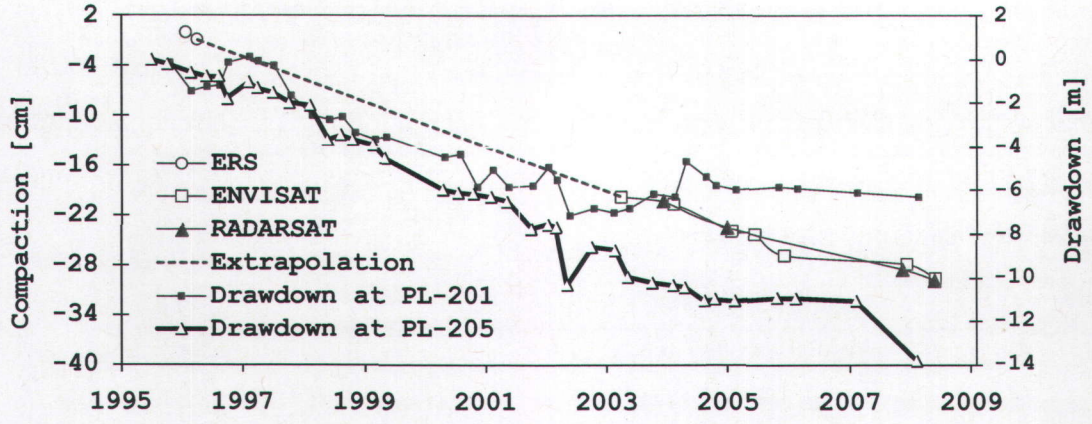


Figure 9: D-InSAR measured subsidence by ENVISAT ASAR and RADARSAT-1 between March 2003 and May 2008 and ERS-1 D-INSAR results from 1996. Water levels at PL-201 from 1995 to 2008 are also included. The extrapolation between 1996 and 2003 is based on average rates in 1996 and 2003-2008.

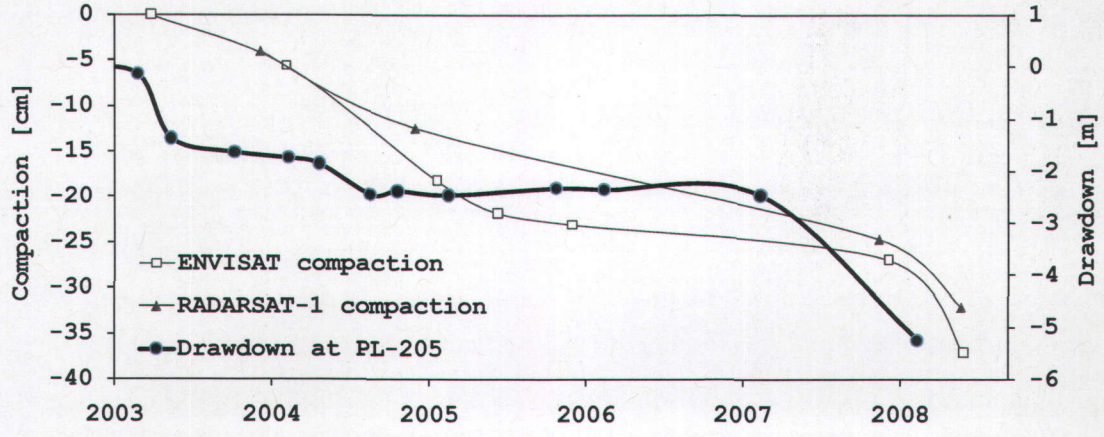


Figure 10: D-InSAR measured subsidence by ENVISAT ASAR and RADARSAT-1 and water level at the Pecuario well location between March 2003 and May 2008.

The Pecuario well location (Figure 10) is more sensitive to drawdown than the other locations with 1 metre of drawdown leading to approximately 8 cm of compaction. According to D-InSAR results, the Pecuario well location has over 37 cm of total subsidence between November 2003 and May 2008. This point is close to the area where the highest subsidence rates are detected and it is estimated that the maximum total subsidence in the valley for the same period is in the 40 cm range. A groundwater deficit in the valley first occurred in 1962 and heavy pumping in the industrial corridor began in

the late 1980's, therefore, based on the water level decline, D-InSAR, and extensometer readings, it is reasonable to assume that the maximum total subsidence since 1962 for this location is over 2.0 m. The maximum subsidence rates in the valley are in the order of 15 cm/year however the areas with maximum subsidence are not stationary, and thus maximum rates can decrease in time at a specific location.

Figure 11 shows the evolution of the Pecuario subsidence area in six interferometric pairs from March 2003 until May 2008. Observing images a) to f), one can see that the centre of maximum subsidence varies with time. Generally the subsidence rates do not exceed 15 cm/year. The varying subsidence rates can be attributed to varying pumping rates and varying geology. A larger extent in subsidence zones is noticed between 2003 and 2005. Caution should be taken with frame c) because it does not correspond to other subsidence rates. Atmospheric effects most likely contribute to this error.

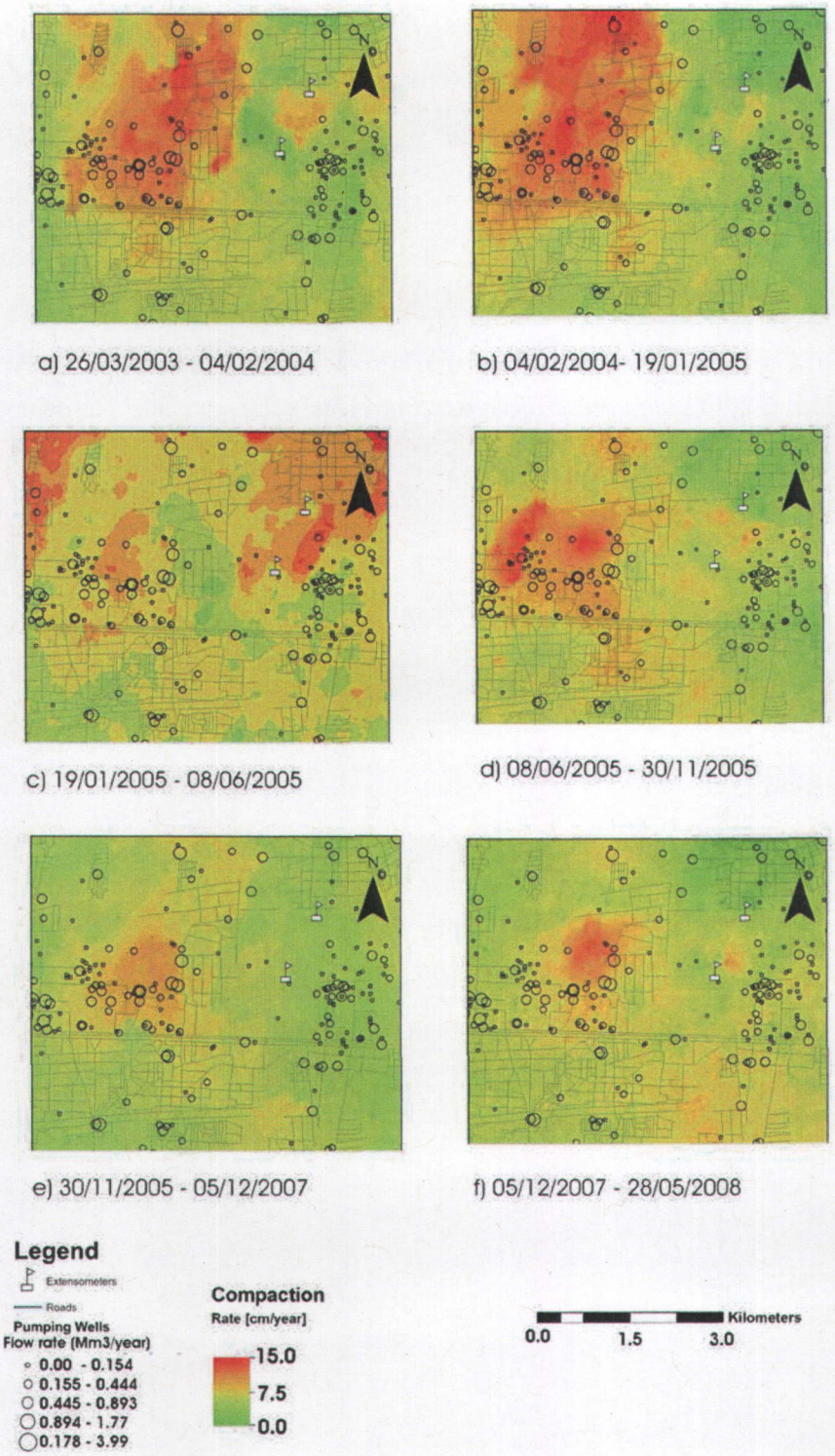


Figure 11: Evolution of the Pecuario subsidence area as observed by 6 ENVISAT-ASAR interferometric pairs from March 2003 until May 2008. Refer to Tables 2 and 3 for pass and baseline.

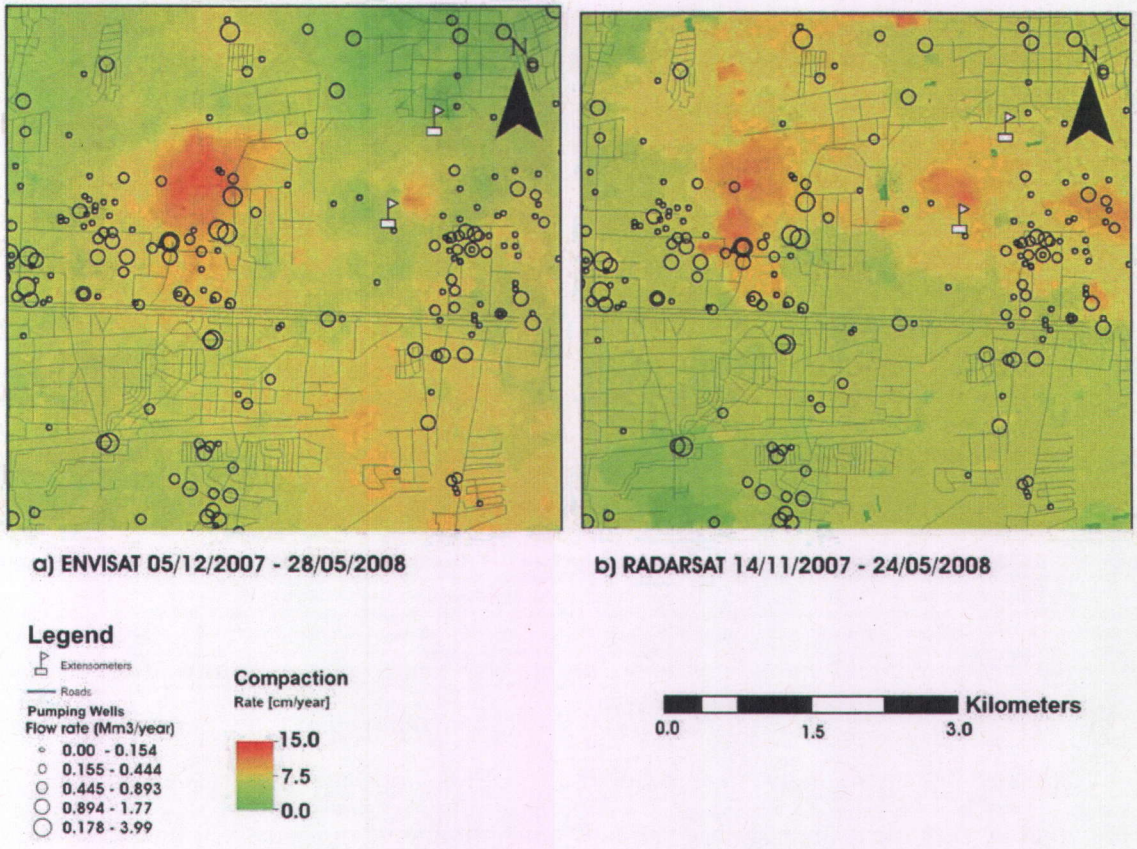


Figure 12: Comparison of ENVISAT ASAR and RADARSAT-1 InSAR results in the maximum subsidence areas and similar time frame. Refer to Tables 2 and 3 for pass and baselines.

When comparing D-InSAR results from ENVISAT ASAR and RADARSAT-1 (Figure 12) one can see that the maximum subsidence areas are in similar locations with similar magnitudes, however there are differences in the spatial extent of the subsidence. The spatial variation can be attributed to the fact that the dates compared do not exactly match, baselines are relatively high with the RADARSAT-1 pair (Table 3), and atmospheric effects are also likely.

For the RADARSAT-1 InSAR pairs it was found that the unwrapped phase and deformation maps had better accuracy when using shorter baselines. Compared to ENVISAT ASAR and extensometer readings, the RADARSAT-1 deformation was over estimated when using baselines greater than 800 m, and more reliable when using baselines of less than 600 m. In general, the ENVISAT ASAR mission has shorter

baselines than RADARSAT-1 and thus baselines were not an issue in obtaining useful interferograms and subsidence maps with ENVISAT ASAR. The differences in spatial extent of calculated subsidence (Figure 12) probably originates from the larger baselines used by RADARSAT-1, however atmospheric effects are also a probable factor.

5 DISCUSSION AND CONCLUSION

Due to the compressible clay content and the excessive groundwater pumping in the basin, subsidence is observed in the Toluca Valley. It is shown that D-InSAR processing combined with water level and extensometer field data can be useful for monitoring subsidence.

D-InSAR has facilitated sporadic monitoring of subsidence in the Toluca Valley since 1996 and continuous monitoring since 2003. The urbanized part of the valley had the best D-InSAR results where man-made reflectors, such as buildings and cement structures were abundant. In these areas, usable results were obtained from pairs with up to 3 years separation, however best results were obtained when the time difference was less than 1 year. Vegetative cover was a major factor in obtaining usable results; best results were obtained in the drier season - November to the end of April - when vegetative growth is least. For all D-InSAR image pairs, high baseline values, atmospheric effects, temporal decorrelation, and vegetative cover were the limiting factors in obtaining a maximum number of usable interferograms (Table 3, Figures 5 and 11).

When comparing ENVISAT ASAR with RADARSAT-1 results, it was found that when using shorter baselines and time differences between images, the RADARSAT-1 results detected very similar subsidence locations and magnitude to ENVISAT ASAR. In the case of RADARSAT-1, the baselines tented to be larger than ENVISAT ASAR (Table 3), and baselines below 800 m were useful yet baselines with values below 600 m produced more reliable results. The ENVISAT ASAR mission had shorter baselines than RADARSAT-1; and thus more useful pairs. Differences in the results (Figure 12) can also be attributed to atmospheric effects.

Errors in the measured subsidence from the field data could exist since the extensometers do not reach bedrock. However, comparing the D-InSAR results with the extensometers, we notice that there is mostly a direct correlation. Figures 7 and 8 show that the ENVISAT ASAR and RADARDAT-1 compaction results follow the extensometer measurements very closely. It can also be stated that the industrial corridor clay compacts in a relatively linear fashion with varying compaction rates as a function of the geology and drawdown. Although clay is found at deeper depths (>300m) (Figure 2), the results imply that the compaction is occurring in the upper 110 m portion of the valley. These results further validate the InSAR technique and the usefulness of the water level data and the extensometers.

While little subsidence is located on the eastern edge of the valley, the Lerma groundwater pumping system plays an important role in the subsidence by capturing most of the recharge water arriving from the Sierra Las Cruces. This has the effect of preventing the central part of the valley from recharging, thus decreasing the water levels and increasing subsidence. According to Figure 3 the subsidence probably first started occurring in 1962 when a groundwater deficit first appeared.

Several areas of interest, where subsidence is detected, exist in and around the industrial corridor. The industrial corridor has a high concentration of both pumping wells and compressible clays. In 3 different locations it was found that 1 m of drawdown lead to between 1 and 8 cm of compaction, implying that varying clay characteristics yields varying compaction rates. In some areas, the maximum subsidence reaches more than 15 cm/year. The Pecuario well location has detected varying compaction rates with a total compaction of 37 cm in a 5 year span. The total maximum subsidence for a point location in the valley between November 2003 and May 2008 is approximately 40 cm.

Observing Figures 7, 8 and 10, hydraulic head and compaction data from 2007 and 2008, it is noticed that there is approximately a 4 month delay between a decrease in hydraulic head and compaction.

Although the maximum subsidence rate changes in magnitude and location (Figure 11), it is estimated that the total maximum subsidence in the valley since 1962 is over 2.0 metres. Comparing the total subsidence to other cities with subsidence problems such as Mexico City (up to 8.7 m), Houston (2.8 m), Shanghai (2.6 m), or Venice (0.25 m); although these cities have different hydrological and geological properties, the Toluca values are similar to values of some cities found on river flood plains such as Houston and Shanghai.

Acknowledgments

We are grateful to the Canadian Space Agency and the Geological Survey of Canada for providing the RADARSAT-1 data and we acknowledge the European Space Agency for providing ERS and ENVISAT ASAR data at cost of reproduction under project C1P 3821. We are appreciative of the Canadian Centre for Remote Sensing for providing support with the InSAR technique and comments (V. Singhroy and N. Short) and the Comision National del Agua for their logistical support on the field. We are also thankful to the Ministère des Relations Internationales, CONACyT, the Autonomous University of the State of México (UAEM), INRS-ETE, NSERC (a discovery grant held by Richard Martel), AUCC/IDRC, and the Ministère d'Éducation du Québec for their financial support.

References

Amelung, F., Galloway, D. L., Bell, J.W., Zebker, H. A., & Laczniak, R. J. (1999). Sensing the ups and downs of Las Vegas: InSAR reveals structural control of land subsidence and aquifer-system deformation. Geology, 27, 483–486.

Ariel y Consultores (1996). Hydrodynamic modeling study and design optimization of the monitoring well networks for the aquifers of Caldera, San Luis Potosi and Toluca (Part 3: Aquifer of Toluca) Estudio de Simulacion Hidrodinamica y Diseno Optimo de las Redes de Observacion de los acuiferos de Calera, San Luis Potosi y Toluca (Tomo 3: Acuifero de Toluca). CNA (Comisión Nacional del Agua) México, DF, Unitecnia 308

Cabral Cano, E., Dixon, T., Sanchez Zamora, O., Diaz Molina, O., & Correa Mora, F. (2003). Ground subsidence in Mexico City imaged by InSAR, GPS and gravimetry. In, Geological Society of America. Seattle, USA: vol.35, no.4, pp.77

Carnec, C., & Fabriol, H. (1999). Monitoring and modeling land subsidence at the Cerro Prieto geothermal field, Baja California, Mexico, using SAR interferometry. Geophysical Research Letters, 26, 1211-1214

CNA, Comision Nacional del Agua. (2008) Registro de Lecturas Piezométricas por el Valle de Toluca Marzo 2008

Calderhead A. I., Martel, R. Rivera, A., Garfias, J., Therrien, R., A spatially variable approach to quantifying the groundwater budget with an increasing storage deficit in the Toluca Valley, Mexico. Environ. Res. Lett. (Submitted 2009)

Chatterjee, R.S., Fruneau, B., Rudant, J.P., Roy, P.S., Frison, P.L., Lakhera, R.C., Dadhwal, V.K., & Saha, R. (2006). Subsidence of Kolkata (Calcutta) City, India during the 1990s as observed from space by Differential Synthetic Aperture Radar Interferometry (D-InSAR) technique. Remote Sensing of Environment, 102, 176-185

Colesanti, C., & Wasowski, J. (2006). Investigating landslides with space-borne Synthetic Aperture Radar (SAR) interferometry. Engineering Geology, 88, 173-199

Cummings, I. & Wong, F., 2004. Introduction to Fundamentals of Synthetic Aperture Radar, Processing of Synthetic Aperture Radar Data – A DSP Perspective, Artech House, Inc, Boston MA.USA.

Farina, P., Avila-Olivera, J.A., & Garduno-Monroy, V.H. (2007). Structurally-controlled Urban subsidence along the Mexican Volcanic Belt (MVB) monitored by InSAR. In, European Space Agency, (Special Publication) ESA SP

Farr, T. G., et al. (2007), The Shuttle Radar Topography Mission, Rev. Geophys., 45, RG2004, doi:10.1029/2005RG000183.

Fatland, D.R., & Lingle, C.S. (2002). InSAR observations of the 1993-95 Bering Glacier (Alaska, U.S.A.) surge and a surge hypothesis. Journal of Glaciology, 48, 439-451

Franceschetti, G. and Lanari, R., 1999. Synthetic Aperture Radar Processing. CRC Press, Boca Raton, FL, USA.

Galloway, D.L., Hudnut, K.W., Ingebritsen, S.E., Phillips, S.P., Peltzer, G., Rogez, F., & Rosen, P.A. (1998). Detection of aquifer system compaction and land subsidence using interferometric synthetic aperture radar, Antelope Valley, Mojave Desert, California. Water Resources Research, 34, 2573-2585

Hilley, G.E., Burgmann, R., Ferretti, A., Novali, F., & Rocca, F. (2004). Dynamics of slow-moving landslides from permanent scatterer analysis. Science, 304, 1952-1955

Hoffmann, J., Zebker, H.A., Galloway, D.L., & Amelung, F. (2001). Seasonal subsidence and rebound in Las Vegas Valley, Nevada, observed by synthetic aperture radar interferometry. Water Resources Research, 37, 1551-1566

IMTA, 2003. Censo del utilización del agua en el valle de Toluca. Instituto Mexicano de Tecnologia del Agua.

JPL (2008). Jet propultion Lab - What is SAR Anyway? http://southport.jpl.nasa.gov/

Lesser and Asociados, S.A. (1992). Diagnostic study of the aquifer of the Valley of Toluca to implement a program for the extraction of groundwater. Estudio para el Diagnostico del acuifero del Valle de Toluca, para implementar la reglamentacion de la extraccion del agua subterranea

Li, S., Benson, C., Gens, R., & Lingle, C. (2008). Motion patterns of Nabesna Glacier (Alaska) revealed by interferometric SAR techniques. Remote Sensing of Environment, 112, 3628-3638

Lopez-Quiroz, P., Doin, M.P., Tupin, F., Briole, P., & Nicolas, J.M. (2007). Mexico City subsidence: Spatio-temporal analysis using interferometry, AGU Joint Assembly. Acapulco, Mexico: May 22-25

Lu, Z., & Kwoun, O.I. (2008). Radarsat-1 and ERS InSAR analysis over southeastern coastal Louisiana: Implications for mapping water-level changes beneath swamp forests. IEEE Transactions on Geoscience and Remote Sensing, 46, 2167-2184

Massonnet, D., Rossi, M., Carmona, C., Adragna, F., Peltzer, G., Feigl, K., & Rabaute, T. (1993). The displacement field of the Landers earthquake mapped by radar interferometry. Nature, 364, 138-142

Massonet, D., Briole, P., & Arnaud, A. (1995). Deflation of Mount Etna monitored by spaceborne radar interferometry. Nature, 375, 567–570.

Massonnet, D., & Feigl, K.L. (1998). Radar interferometry and its application to changes in the earth's surface. Reviews of Geophysics, 36, 441-500

MDA, 2007. EV-InSAR Users Guide, Version 4.0. MDA Geospatial Services, Nepean, Ontario. Canada.

MDA, 2009 Radarsat-2 information website, http://www.radarsat2.info/ - Frequently Asked Questions section.

Mora, O., Mallorqui, J. J., & Broquetas, A. (2003). Linear and nonlinear terrain deformation maps from a reduced set of interferometric SAR images. IEEE Transactions on Geoscience and Remote Sensing, 41(10), 2243–2252.

Peltzer, G., & Rosen, P. (1995). Surface displacement of the 17 May 1993 Eureka Valley, California, earthquake observed by SAR interferometry. Science, 268, 1333-1336

Peyret, M., Djamour, Y., Rizza, M., Ritz, J.F., Hurtrez, J.E., Goudarzi, M.A., Nankali, H., Cheiry, J., Le Dortz, K., & Uri, F. (2008). Monitoring of the large slow Kahrod landslide in Alborz mountain range (Iran) by GPS and SAR interferometry. Engineering Geology, 100, 131-141

Pinel, V., Hooper, A., De La Cruz-Reyna, S., Reyes-Davila, G., & Doin, M.P. (2008). Study of the deformation field of two active Mexican stratovolcanoes (Popocatepetl and Colima Volcano) by time series of InSAR data. In, European Space Agency, (Special Publication) ESA SP

Rignot, E., Gogineni, S., Joughin, I., & Krabill, W. (2001). Contribution to the glaciology of northern Greenland from satellite radar interferometry. Journal of Geophysical Research D: Atmospheres, 106, 34007-34019

Roctest (2009) R-4 magnetic reed switch probe extensometer system, Roctest

http://www.roctest.com/modules/AxialRealisation/img_repository/files/documents/R4-E5013D-W.pdf

Rocca, F., Prati, C., & Ferretti, A. (1997, March 17–21). An overview of ERSSAR interferometry. Proceedings of the 3rd ERS symposium on space at the service of our environment (pp. xxvii–xxxvi). Florence, Italy: European Space Agency (ESA).

Salvi, S., Atzori, S., Tolomei, C., Allievi, J., Ferretti, A., Rocca, F., Prati, C., Stramondo, S., & Feuillet, N. (2004). Inflation rate of the Colli Albani volcanic complex retrieved by the permanent scatterers SAR interferometry technique. Geophysical Research Letters, 31, L12606 12601-12604

Sarychikhina, O., Mellors, R., & Glowacka, E. (2007). Aplication of insar to the study of ground deformation in the Mexicali Valley, B. C., Mexico. In, European Space Agency, (Special Publication) ESA SP

Stramondo, S., Tesauro, M., Briole, P., Sansosti, E., Salvi, S., Lanari, R., Anzidei, M., Baldi, P.,

Fornaro, G., Avallone, A., Buongiorno, M.F., Franceschetti, G., & Boschi, E. (1999). The September 26, 1997 Colfiorito, Italy, earthquakes: Modeled coseismic surface displacement from SAR interferometry and GPS. Geophysical Research Letters, 26, 883-886

Strozzi, T. & Wegmüller, U. (1999) Land subsidence in Mexico City mapped by ERS differential SAR interferometry. Geoscience and Remote Sensing Symposium, 1999. IGARSS apos;99 Proceedings. IEEE 1999 International Volume 4, Issue, 1999 Page(s):1940 - 1942 vol. 4

Strozzi T., Wegmüller, U., Werner, C., Wiesmann, A. and Spreckels, V. (2003) JERS SAR interferometry for land subsidence monitoring, IEEE Trans. Geosci. Remote Sensing, 41, 1702-1708

Terzaghi, K. (1925). Earthworks mechanics based on soil physics. Erdbaumechanik auf bodenphysikalisher Grundlage

Walker, W.S., Kellndorfer, J.M., LaPoint, E., Hoppus, M., & Westfall, J. (2007). An empirical InSAR-optical fusion approach to mapping vegetation canopy height. Remote Sensing of Environment, 109, 482-499

Wegmüller, U., Werner, C., Strozzi, T., & Wiesmann, A. (2006). APPLICATION OF

SAR INTERFEROMETRIC TECHNIQUES FOR SURFACE DEFORMATION MONITORING. In, 3rd IAG / 12th FIG Symposium. Baden, Austria: May 22-24

Wdowinski, S., Kim, S.W., Amelung, F., Dixon, T.H., Miralles-Wilhelm, F., & Sonenshein, R. (2008). Space-based detection of wetlands' surface water level changes from L-band SAR interferometry. Remote Sensing of Environment, 112, 681-696

Winebrenner, D.P., Joughin, I.R., & Fahnestock, M.A. (1997). Interferometric SAR for observation of glacier motion and firn penetration. European Space Agency, (Special Publication) ESA SP, 983-985

Zebker, H.A.; Rosen, P.A. & Hensley, S. (1997), "Atmospheric effects in inteferometric synthetic aperture radar surface deformation and topographic maps", Journal of Geophysical Research 102: 7547–7563

List of tables

Table 1: Acquired images between 1995 and 2008 118

Table 2: InSAR pair acquisition dates, perpendicular baseline (b perp.) and parallel baseline (b paral.) in metres, and time difference in days (d_days) are listed. Also listed are the figure numbers where results from subsidence maps are presented in this study. 122

List of figures

Figure 1: Location map of the Toluca Valley and the industrial corridor within the Republic of Mexico and the State of Mexico. Cross section A-B is shown is Figure 2. A deformation map is in the centre of the valley (Modified from Calderhead et al., 2009). 113

Figure 2: 2D view of the conceptual model for the Toluca Valley Basin. Cross section A-B is located on Figure 1. (Modified from Calderhead et al., 2009) 114

Figure 3: Observed and expected groundwater recharge, pumping, and deficit from 1970 to 2050. From 1970 to 1999 actual recharge values are shown. From 2000 to 2050 average expected recharge including climate change is shown. Recharge, discharge and deficit projections are based on Calderhead et al. (2009). The deficit is the sum of the recharge and the discharge. Modified from Calderhead et al. (2009) 115

Figure 4: Schematic drawing of the magnetic probe extensometer. Piezometric surface variations with time and location of pressure transducer are also represented. Drawing is not to scale. 120

Figure 5: Coherence of the Toluca Valley in a) and b) and corresponding differential interferogram of the same region in c) and d) for ENVISAT ASAR InSAR pair (December 5th 2007 and May 28th, 2008). b) and d) are enlargements of a) and c) respectively. 123

Figure 6: ENVISAT-ASAR height deformation map of the Toluca Valley basin obtained from Figure 5d showing the location of extensometers, control points, monitoring wells, pumping wells with rates. InSAR measured subsidence rates are between December 2007 and May 2008. Corresponding baseline and pass are in Tables 2 and 3. 124

Figure 7: D-InSAR measured subsidence by ENVISAT ASAR and RADARSAT-1 and extensometer and water level at Extensometer-1 and PL-201 between March 2003 and May 2008 126

Figure 8 : D-InSAR measured subsidence by ENVISAT ASA and RADARSAT-1 at Extensometer-2 and water level at PL-201 between March 2003 and May 2008 127

Figure 9: D-InSAR measured subsidence by ENVISAT ASAR and RADARSAT-1 between March 2003 and May 2008 and ERS-1 D-INSAR results from 1996. Water levels at PL-201 from 1995 to 2008 are also included. The extrapolation between 1996 and 2003 is based on average rates in 1996 and 2003-2008. 128

Figure 10: D-InSAR measured subsidence by ENVISAT ASAR and RADARSAT-1 and water level at the Pecuario well location between March 2003 and May 2008. 128

Figure 11: Evolution of the Pecuario subsidence area as observed by 6 ENVISAT-ASAR interferometric pairs from March 2003 until May 2008. Refer to Tables 2 and 3 for pass and baseline. 130

Figure 12: Comparison of ENVISAT ASAR and RADARSAT-1 InSAR results in the maximum subsidence areas and similar time frame. Refer to Tables 2 and 3 for pass and baselines..... 131

Chapitre 4: Simulating pumping-induced regional land subsidence in a complex aquifer system

Résumé

Le pompage des eaux souterraines a provoqué l`affaissement des sols dans de nombreuses zones urbaines à travers le monde. Depuis les années 1970, des modèles numériques de plus en plus sophistiqués ont été développés afin de simuler l`affaissement des sols induits par le pompage de l`eau souterraine. Une des limites principales de la représentation adéquate de la subsidence est le manque de données représentatives. Une approche multidisciplinaire est présentée ici pour quantifier la subsidence dans un système d`aquifère avec une stratigraphie complexe. La méthodologie consiste en: (1) le couplage du principe de la compaction instantanée 1D de Terzhagi avec l'équation de l`écoulement des eaux souterraines avec le modèle HydroGeoSphere; (2) la validation du nouveau modèle, et (3) La mise en œuvre du modèle pour la vallée de Toluca. Differential Interferometric Synthetic Aperture Radar (D-InSAR), un modèle géologique 3D, des extensomètres, le suivi du rabattement, et l`utilisation des données disponible, sont utilisées pour contraindre le modèle. L'écoulement des eaux souterraines et la subsidence régionale et locale sont observés. La subsidence mesurée avec D-InSAR, les extensomètres, et les simulations numériques se ressemble relativement bien. Il est constaté que la partie supérieure de l'aquifère est la partit le plus compressible. D-InSAR montre que les taux de subsidence peuvent atteindre jusqu'à 15-20 cm/an dans certains endroits, les taux d'affaissement sont variables dans le temps et l'espace. Des simulations montrent que, depuis la subsidence régionale a commencé au début des années 1960, il y a eu jusqu'à 2 m de subsidence dans le couloir industriel, la où le pompage dans les couches argileuses se trouvent.

Simulating pumping-induced regional land subsidence in a complex aquifer system

A I Calderhead[1], R Therrien[2], A Rivera[3], R Martel[1], J Garfias[4]

[1] Institut national de la recherche scientifique - Centre Eau, Terre & Environnement, 490 de la Couronne, Québec, QC G1K 9A9, Canada

[2]Département de géologie et de génie géologique, Université Laval, Québec, QC G1K 7P4, Canada

[3]Geological Survey of Canada, Natural Resources Canada, 490 de la Couronne, Quebec, QC G1K 9A9, Canada

[4]Universidad Autónoma del Estado de México, Facultad de Ingeniería (CIRA), Cerro de Coatepec, s/n, C.U., Toluca, MEX 50130, México

Abstract

Groundwater pumping has caused land subsidence in many urban areas around the world. Since the 1970's, increasingly sophisticated numerical models have been developed to simulate land subsidence induced by groundwater pumping. A major limitation to the proper representation of land subsidence, however, remains the lack of representative data. A multidisciplinary approach is presented here to quantifying land subsidence in a heavily pumped aquifer system with complex stratigraphy. The methodology consist in: (1) coupling Terzhagi's 1D instantaneous compaction principle to the groundwater flow equation using the HydroGeoSphere model; (2) validating the new model; and (3) Model setup for the Toluca Valley, Mexico and calibration. Differential Interferometric Synthetic Aperture Radar (D-InSAR), a generated 3D-geological model, extensometers, monitoring wells, and available literature, are used to constrain the model. The model is used to simulate pumping induced land subsidence within the complex stratigraphy of the Toluca Valley basin, Mexico. Regional and local groundwater flow and subsidence patterns are observed. The D-InSAR measured subsidence, extensometers, and numerical simulations of subsidence agree relatively well. It is found that the upper portion of the aquifer is the most compressible part. D-InSAR shows that although subsidence rates can reach up to 30 cm per year in certain locations, the magnitudes are variable in time and

space. Simulations show that since regional subsidence began in the early 1960's there has been up to 2m of subsidence in the industrial corridor, where heavy pumping and thick clay layers are found. This study shows that multidisciplinary approach is useful in estimating and constraining the vertical component of the inelastic skeletal specific storage.

1 INTRODUCTION

Many cities around the world experience land subsidence due to their geologic setting and decreasing groundwater levels. Population growth, and intensifying industry and agriculture are often the principal reason for the increasing groundwater demand and resulting subsidence problems. Coupled groundwater flow and compaction models are useful tools to analyze land subsidence and they represent one of the best methods available for predicting subsidence.

Since the emergence of numerical groundwater flow models in the 1970s, several have coupled compaction to groundwater flow. Since Gambolati and Helm's pioneering work in the early 1970's (Gambolati, 1972; Helm, 1975), most models have represented compaction by applying Terzhagi's 1D compaction principle with a finite difference solution method (Helm, 1975, Rivera et al. 1991; Hoffman et al., 2003b; Liu and Helm 2008); however, Biot's 3D derivation (Biot, 1941)) is sometimes used (Safai, and Pinder, 1979; Lewis and Shrefler, 1978), usually with the finite element solution method. Over the years, various compaction aspects have also been included in models such as dependence of compaction on hydraulic conductivity (e.g. Rudolph and Frind, 1991; Rivera et al., 1991), time delays (e.g. Hoffman et al., 2003a), and effects of moving water tables (e.g. Leake and Galloway, 2007; and Liu and Helm 2008).

The availability of field data remains a major limitation to model applications and to the reliability of their predictions. Except for a few heavily studied major urban centers such as Mexico City, Venice, the Antelope Valley, California, and Shanghai, subsidence data is often incomplete mostly because extensometer installations needed to measure land

subsidence are expensive. Even where extensometers exist, there is often a lack of long term monitoring data needed for model calibration. Over the last two decades, however, the emergence of synthetic aperture radar interferometry (InSAR) has revolutionized subsidence studies. InSAR can monitor land movement at the regional scale, with sub-centimeter vertical precision, thus providing data to calibrate subsidence models even where a few extensometer field subsidence data is available. Due to little interaction between remote sensing communities and hydrogeologists, only a handful of subsidence studies have combined groundwater flow and compaction numerical models with remote sensing techniques and field data. Amelung et al. (1999) has contrasted clay thickness maps with D-InSAR subsidence patterns and Galloway et al. (1998) and Hoffman et al. (2003a) have presented finite difference delayed-compaction models constrained by D-InSAR results and field data for several subsiding locations in Nevada and California. There is a need to further explore the use of InSAR data to calibrate numerical model that simulate land subsidence.

This paper extends the HydroGeoSphere (HGS) (Therrien et al., 2009) finite element groundwater flow and transport model by accounting for instantaneous compaction. The coupling of the flow model with compaction is verified and the model is demonstrated by reproducing land subsidence caused by pumping in the Toluca Valley, Mexico. Simulations are constrained by remote sensing and field data for the complex aquifer system of the Toluca Valley. Hoffmann et al. (2003a) demonstrates that D-InSAR is useful for deriving the total inelastic skeletal storage coefficient (S'_{sk}) of an aquifer. Their approach, however, does not consider the vertical variability of S'_{sk}. In complex aquifer systems, such as in the Toluca Valley, Mexico, with vertically variable material properties, assigning inelastic skeletal storage coefficient for individual clay layers becomes more problematic and requires other sources of data. This work extends the general approach used by Galloway et al. (1998), Amelung et al. (1999), and Hoffmann et al. (2003a) by using D-InSAR subsidence estimates and further constrains the groundwater flow-compaction model with a 3D geologic model to derive S'_{sk} for individual clay layers. Additionally, multiple remote sensors are used over a 5-year period, thus increasing confidence in D-InSAR estimates.

2 BACKGROUND

With the objective of representing land subsidence in the Toluca Valley, Mexico, a compaction module was added to the multipurpose 3D finite element groundwater flow model HGS. The compaction component is based on Terzhaghi's 1D effective stress principle as applied most recently by Hoffmann et al. (2003b), Leake and Galloway (2007b), and Liu and Helm (2008).

The total stress, σ, at any point in a porous medium is given by the geostatic load of the overlying saturated and unsaturated sediments. According to Terzaghi (1925), changes in the effective stress can result from changes in the total stress or changes in pore pressure according to

$$\sigma'_{ij} = \sigma_{ij} - p \qquad (1)$$

where σ'_{ij} [$M \cdot L^{-2}$] is a component of the effective stress tensor, σ_{ij} [$M \cdot L^{-2}$] is a component of the total stress tensor, and p [$M \cdot L^{-2}$] is the fluid pore pressure.

If layers forming an aquifer system are assumed to be horizontal and laterally extensive with respect to their thickness, the changes in pore-pressure gradients will be primarily vertical. If it is further assumed that the resulting strains are also primarily vertical, with z being the vertical coordinate, the following one-dimensional form of equation 1 can be used:

$$\sigma'_{zz} = \sigma_{zz} - p \qquad (2)$$

An important assumption is that the total stress remains constant in time, that is, $\Delta\sigma_{zz} = 0$. Thus, the method presented applies only to sediment compaction in confined aquifers subject to a constant geostatic load.

Saturated groundwater flow systems are commonly described with hydraulic head as opposed to pore pressure. Total hydraulic head is the sum of the pressure head and the elevation head,

$$h = \frac{p}{\rho_w g} + h_z \qquad (3)$$

where h [L] is the total hydraulic head, ρ_w = the density of water [$M \cdot L^{-3}$] g is the gravitational acceleration constant [$M \cdot T^{-2}$], and h_z [L] is the elevation head referenced to an arbitrary datum.

A change in effective stress resulting from a given head change generally differs in confined and unconfined aquifers. In an unconfined aquifer, a change in head corresponds to a draining or re-wetting of pore space and results in a change in the geostatic load or the total stress on the underlying sediments as well as the pore pressure. The change in effective stress caused by a head change in the saturated portion of an unconfined aquifer can be described as (Poland and Davis, 1969):

$$\Delta\sigma'_{zz} = -\rho_w g(1 - n + n_w)\Delta h \qquad (4)$$

where $\Delta\sigma'_{zz}$ is the change in vertical effective stress (positive for increase), n [-] is the aquifer porosity, n_w [-]is the moisture content in the unsaturated zone above the water table, as a fraction of total volume, and Δh is the change in hydraulic head.

It should be noted that changes in head in an unconfined aquifer constitute a mass change in that aquifer. This represents a change in the total stress for all underlying confined aquifers. In a confined aquifer, the total stress changes negligibly with changes in pore pressure as water is released from or is taken into storage by the saturated porous medium as a result of the compression or expansion of the medium and (or) the water. The change in water density associated with the expansion or compression of the water is negligible. Thus the change in effective stress for a given change in head can be expressed as (Poland and Davis, 1969)

$$\Delta\sigma'_{zz} = -\rho_w g \Delta h \qquad (5)$$

The HGS compaction module is designed to simulate instantaneous compaction and storage changes in confined aquifer systems and is thus based on equation 5. For compressible layers in the saturated part of an unconfined aquifer, where hydraulic head variations are occurring, this approach will overestimate the change in effective stress, and thus overestimates sediment compaction by the factor equal to $(1 - n + n_w)^{-1}$ (see Equation 4).

Changes in effective stress ($\Delta\sigma'_{zz}$) cause compaction and expansion of the sediments constituting many aquifer systems. In this paper, the term compaction is used to describe a reduction in the thickness of a horizontal compressible layer. A negative compaction implies an expansion or increased thickness of the compressible layer. Neglecting horizontal displacements, the one-dimensional compressibility ($\overline{\alpha}$) [Pa^{-1} or $M{\cdot}L^{-1}T^{-2}$] can be defined as

$$\overline{\alpha} = \frac{-\frac{db}{b}}{d\sigma'_{zz}} \qquad (6)$$

where *db* is the change in thickness of a control volume with initial thickness b.

If the change in effective stress is due only to a change in the pore pressure, equation 5 can be used to express equation 6 as:

$$\rho_w g \overline{\alpha} b = S'_{sk}\, b = S'_k = \frac{db}{dh} \qquad (7)$$

where S'_{sk} [L^{-1}] is the skeletal specific storage, equal to $\rho_w g \overline{\alpha}$, S'_k [-] is the skeletal storage coefficient, equal to $S'_{sk}b$, and *dh* [L] is the change in hydraulic head.

Laboratory consolidation tests on sediment cores and measurements of aquifer-system compaction obtained from borehole extensometers indicate that compressibility, and thus the skeletal specific storage, can assume very different values depending on whether or not the effective stress exceeds the previous maximum effective stress, termed the preconsolidation stress (Johnson and others, 1968; Riley, 1969; Jorgensen, 1980).

For some sediments, inelastic compaction is approximately proportional to the logarithm of the effective stress (Jorgensen, 1980). However, in many cases applicable to aquifer-system compaction where incremental changes in effective stress are typically small (e.g. the Toluca Valley - Figure 1), the relationship (equation 7) can be linearized as

$$\Delta b = S'_k \, \Delta h \qquad (8)$$

where S'_k is the skeletal storage coefficient. To account for the marked change of the skeletal specific storage when the effective stress exceeds the preconsolidation stress, two separate values are often used:

$$S'_{sk} = \begin{cases} S'_{ske} \;\; for \;\; \sigma'_{zz} < \sigma'_{zz(pre)} \\ S'_{skv} \;\; for \;\; \sigma'_{zz} \geq \sigma'_{zz(pre)} \end{cases} \qquad (9)$$

where S'_{ske} [L^{-1}] is the elastic skeletal specific storage, S'_{skv} [L^{-1}] is the inelastic, or virgin, skeletal specific storage, and $\sigma'_{zz\ (pre)}$ [$M \cdot L^{-2}$] is the preconsolidation effective stress.

Compressibility ($\overline{\alpha}$), elastic skeletal specific storage (S'_{ske}) and inelastic skeletal specific storage (S'_{skv}) can be obtained from consolidation experiments by using both the inferred inelastic (C_c) and the elastic (C_s) compression indices obtained by plotting the void ratio e [-] (volume of voids/ total volume) against the log effective stress (e - $log\ \sigma'_{zz}$ curve) (Figure 1).

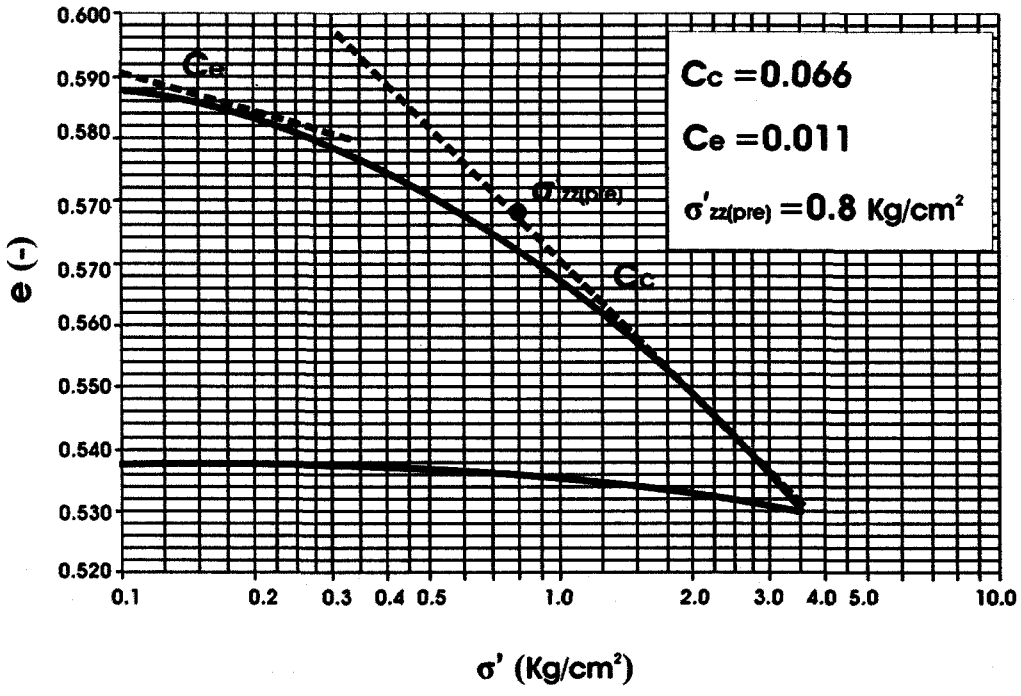


Figure 1: Example of compression test results of a Toluca Valley clay (from UAEM, 2008)

The slope of the inelastic compaction curve is defined as the compression index C_c.

$$C_c = \frac{e_0 - e}{\log \frac{\sigma'_{zz}}{\sigma_0}} = \frac{-de}{d(\log \sigma'_{zz})} \qquad \text{for} \quad \sigma'_{zz} > \sigma'_{zz(pre)} \tag{10}$$

The derivative of void ratio with respect to effective stress is given by:

$$\frac{de}{d\sigma'_{zz}} = \frac{de}{d(\log \sigma'_{zz})} \frac{0.434}{\sigma'_{zz}} = C_c \frac{0.434}{\sigma'_{zz}} \tag{11}$$

On the basis of the definition for aquifer compressibility (Fetter 2001), and using equations (11), we obtain:

$$\bar{\alpha}_c = -\frac{dV/V}{d\sigma'} = \frac{de}{(1+e)d\sigma'_{zz}} = 0.434 \frac{C_c}{(1+e)\,\sigma'_{zz}} \tag{12}$$

where dV is the change in aquifer volume, V is the original volume, and $d\sigma'$ is the change in effective stress. Combining equations 7 and 12, we obtain:

$$S'_{skv} = \rho g \bar{\alpha}_c = 0.434 \frac{C_c \rho g}{(1+e_0)\sigma'_{zz}} \qquad \text{for } \sigma'_{zz} > \sigma'_{zz(pre)} \tag{13}$$

In the above formula, the compression index C_c can be used only when σ'_{zz} is greater than the pre-consolidation stress. Otherwise, the expansion index C_s can be used instead of C_c to obtain:

$$S'_{ske} = \rho g \bar{\alpha}_e = 0.434 \frac{C_s \rho g}{(1+e_0)\sigma'_{zz}} \qquad \text{for } \sigma'_{zz} < \sigma'_{zz(pre)} \tag{14}$$

If the effective stress remains less than the preconsolidation stress, a further increase in effective stress (or decrease in hydraulic head) causes a small elastic compaction in both coarse- and fine-grained sediments. This compaction is recoverable if the effective stress returns to its initial value. If the effective stress remains consistently above or below the preconsolidation stress, the compressibility and skeletal specific storage are a function of the effective stress (Figure 1).

For stresses greater than the preconsolidation stress, S'_{skv} is used, and S'_{ske} is used for stresses less than the preconsolidation stress (Figure 1). To a certain extent, this approach linearizes the nonlinear stress/compaction relation with respect to the preconsolidation stress. By observing figure 1 and other e - $log\ \sigma'_{zz}$ curves from consolidation tests of Toluca Valley clays, the resulting constitutive law represented by equation 8 is a reasonable estimate for these clays, however it only approximates the true stress/compaction relation of the sediments. The consolidation and subsidence process depends on the rate in migration of the decrease in pressure head through the compressible layers and is controlled by the hydraulic diffusivity. The resulting subsidence is the integrated response of the pressure decrease migrating upward through the sediment sequence since pumping began. Thus a delay term is often required in the

conceptualization of the compaction process. Observing delays between a decrease in head and clay compaction (e.g. figure 11), it is noticed that, at Extensometer-1, there appears to be approximately a 4 month delay. There is no other data to suggest the 4 month delay in compaction is due processes that occurred at an earlier time. It can be further argued that the Toluca valley clays are significantly different than the Mexico City clays, where delayed responses are dominant. Additionally, considering the length of time that the simulations represent (~ 100 years), the 4 month delay in compaction is considered insignificant and the use of an instantaneous compaction coupling is considered sufficient for the purpose of representing and predicting consolidation and subsidence of the Toluca Valley.

3 METHODOLOGY

The methodology used for this study includes (1) coupling compaction to the groundwater equation; (2) validating the model; and (3) Setting up and calibrating the model for the Toluca Valley

3.1 Coupling compaction to the groundwater flow equation

The following equation is used to describe HGS`s modified version of three-dimensional transient subsurface flow for a fully saturated porous medium (Therrien et al., 2009):

$$-\nabla q + \sum \Gamma_{ex} \pm Q = S_s \frac{\partial h}{\partial t} \qquad (15)$$

with the fluid flux q [$L \cdot T^{-1}$] given by:

$$q = -K \nabla h \qquad (16)$$

and where the hydraulic head h is defined in equation 3. S_s is the specific storage [L^{-1}] and the hydraulic conductivity, K [$L \cdot T^{-1}$], is given by:

$$K = \frac{\rho_w g}{\mu} k \qquad (17)$$

where g is the gravitational acceleration constant, μ [$M \cdot L^{-1} \cdot T^{-1}$] is the viscosity of water, k [L^2] is the permeability tensor of the porous medium and ρ_w [$M \cdot L^{-3}$] is the density of water.

Fluid exchange with the outside of the simulation domain, as specified from boundary conditions, is represented by Q [$L^3 \cdot L^{-3} \cdot T^{-1}$], which is a volumetric fluid flux per unit volume representing a source (positive) or a sink (negative) to the porous medium system. In Equation 15, Γ_{ex} [$L^3 \cdot L^{-3} \cdot T^{-1}$] represents the volumetric fluid exchange rate between the subsurface domain and all other types of domains of the HGS model and it is expressed per unit volume of the other domain types. HGS can simulate several processes; however, except for wells these other capabilities are not used here.

The term on the right hand side of equation 15 describes the rate of flow into or out of storage per unit volume of aquifer material. The compaction formulation presented below was previously implemented in the finite difference code MODFLOW (Leake and Pudic, 1991; Hoffman et al., 2003b, Leake and Galloway, 2007). If the aquifer system includes compressible sediments, this term can be multiplied by (1 – γ*), where γ* [-] is the fraction, by volume, of compressible interbeds in the aquifer system. The storage of the compressible interbeds is represented by a second term added to the right hand side. Equivalently, the water entering the flow system from interbeds can be added to the source term Q.

The flow per unit volume for the compressible material [$L \cdot T^{-1}$] is as follows:

$$\bar{q} = \gamma^* S'_{sk} \frac{\partial h}{\partial t} \qquad \text{with} \qquad S'_{sk} = \begin{cases} S'_{ske} & for\ h > h_{\min} \\ S'_{skv} & for\ h \le h_{\min} \end{cases} \qquad (18)$$

where h_{min} is the lowest previous head or the equivalent preconsolidation stress expressed in terms of preconsolidation head. S'_{sk} is the skeletal specific storage, which assumes an elastic or inelastic (virgin) value depending on whether the head is above or below h_{min}. It

is assumed that $h_{\min}$ defines the preconsolidation stress in terms of a preconsolidation head. Note that this is equivalent to equation 9, with the assumption that the total stress remains constant, and therefore assumes that the water levels in any overlying unconfined aquifers remain approximately constant. Similarly, the compaction of these interbeds can be determined directly from equation 8.

Thus, combining the compaction term to the governing groundwater flow equation yields:

$$-\nabla \cdot q + \sum \Gamma_{ex} \pm Q = [(1-\gamma^*) * S_s + \gamma * S'_{sk}] \frac{\partial h}{\partial t} \qquad (19)$$

The coupling ignores time-delays from slow dissipation of head transients within the interbeds and assumes that heads everywhere equilibrate instantaneously with the head in the surrounding aquifer. Although delays can be important in certain clays (e.g. Mexico City), the Toluca Valley clays exhibit rapid compaction response to head decline. For an example see Figure 11 for comparison between hydraulic head and compaction at Extensometer-1.

Discretization

HGS uses the control volume finite element method with fully implicit time-weighting (Therrien et al., 2009). Based on equation 19 the following discretized porous medium flow equation, with compaction, is obtained:

$$\left[(1-\gamma^*) S_s (h_i^{L+1} - h_i^L) + \gamma * q^*_i\right] \frac{v_i}{\Delta t} = \sum_{j \in \eta i} \gamma^*_{ij} (h_j^{L+1} - h_i^{L+1}) - \left(\sum \Gamma_{ex}^{L+1}\right) v_i \pm Q_i^{L+1} \qquad (20)$$

where :

$$q^*_i = S'^{L+1}_{ki} \left(h_i^{L+1} - h_{\min}^L\right) + S'_{ske} \left(h_{\min}^L - h_i^L\right) \qquad (21)$$

with

$$S'^{L+1}_{ki} = \begin{cases} S'_{ske} & Elastic\ storage\ for\ h_i^{L+1} > h_{\min}^{L} \\ S'_{skv} & Inelastic\ storage\ for\ h_i^{L+1} \le h_{\min}^{L} \end{cases} . \quad (22)$$

and where h_i is the head for control volume i as defined in equation 3 and

$$\gamma_{ij} = \int_v \nabla N_i \cdot K \cdot \nabla N_j dv \quad (23)$$

for the interpolation functions N defined for the 3-D porous medium elements and where the control volume associated with a given node is given by:

$$v_i = \int_v N_i dv . \quad (24)$$

Because an implicit representation is used, equation 20 is non linear and an iterative solution is required. The Picard method is used to linearize the equation.

3.2 HGS model verification

Both the MODFLOW-SUB package and HGS's flow solution accuracy have been verified by analytical solutions (Hoffmann et al., 2003b; Therrien et al., 2009) and have been successfully applied to several case studies. The new compaction module of HGS is thus verified by comparing a sample problem solution to MODFLOW-SUB.

The scenario, selected from Hoffmann et al. (2003b), simulates the effects of seasonally fluctuating stresses on heads in an aquifer and on subsidence history. A confined aquifer with a thickness of 500 m and a storage coefficient (S) of 1.44×10^{-3} was simulated in a single model cell (Figure 2). The cell extends 1,000 m in both horizontal dimensions and 500 m vertically. No-flow boundaries were specified on the sides and bottom of the cell. Starting heads and preconsolidation heads were specified as 0 m. A 20-meter thick, laterally extensive clay lens is interbedded in this aquifer. The compressible material was assigned values of 5×10^{-5} m^{-1} and 5×10^{-3} m^{-1} for elastic (S'_{ske}) and inelastic (S'_{skv}) skeletal specific storage, respectively, and 1.125×10^{-10} m/s for vertical hydraulic

conductivity (K'_z). The stresses were modulated by seasonal pumping and recharge during 5 years: for 6 months, 118.3 m^3/d was withdrawn by pumping followed by a 6-month period during which 20 percent (23.66 m^3/d) of the extracted water was recharged through the well; this cycle was repeated 5 times in the simulation. The model setup is shown in Figure 2.

The HGS simulation uses a finite element model and heads are therefore simulated at nodes, and not at cell centers like MODFLOW. For HGS a 3D brick element with 8 nodes is used. Pumping rates are equally distributed between all 8 nodes, as opposed to MODFLOW where only one rate is applied at the cell center.

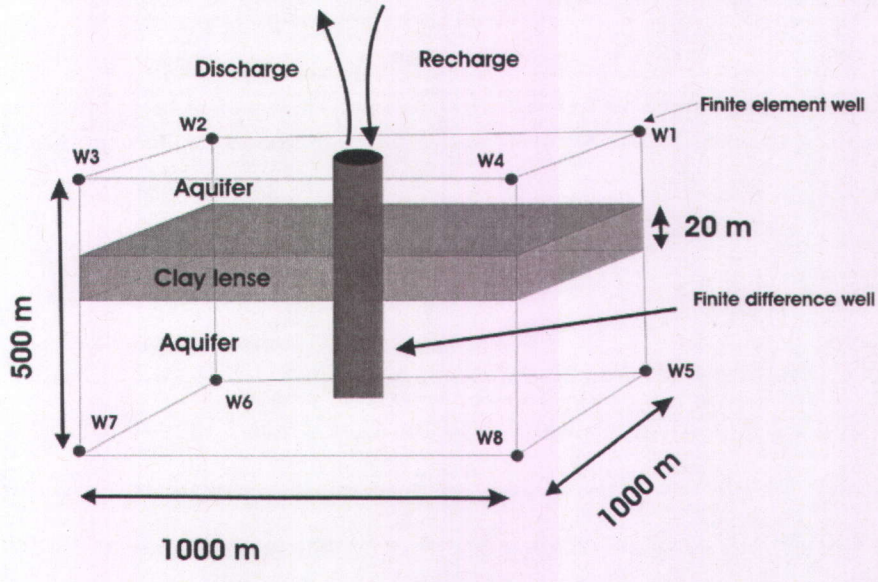


Figure 2: Verification problem - Model configuration used to simulate seasonally fluctuating stresses. The only sources and sinks of water in the system are the discharge or recharge through the well and the storage in the interbed and aquifer. The finite difference model uses a single well for recharge and discharge and the finite element uses the 8 corners of the block as wells (w1-w8), with the pumping and injection rates respectively divided by 8 for each well.

The resulting computed head at each node is equal for both models and is the head shown in Figure 3. On the other hand, nodal compaction has to be added up vertically to obtain the total subsidence shown in Figure 3 (i.e. the compaction is added up for two nodes that have the same x,y coordinates).

The resulting hydraulic heads and compaction of the layer for MODFLOW-SUB and HGS-compaction are shown in Figure 3. For each model, we observe that both the

hydraulic heads and the compaction values are identical. By matching the coupling equations and the time weighting scheme (implicit) identical results were achieved with both models.

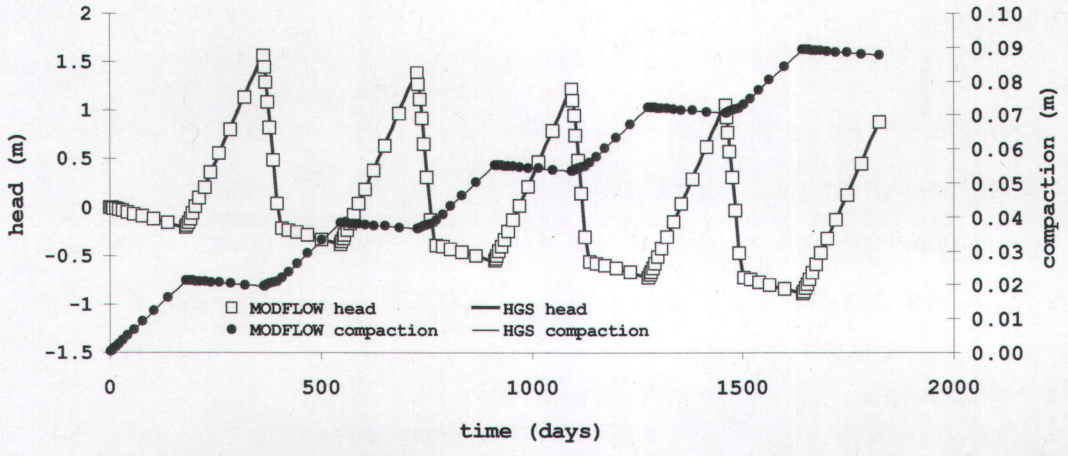


Figure 3: verification results showing hydraulic head and total compaction for the HGS and MODFLOW simulations

4 TOLUCA VALLEY BACKGROUND

The Toluca Valley basin (Figures 4 and 5a) covers an area of approximately 2100 Km^2. The basin is adjacent to the Mexico City Valley, with the Sierra Las Cruces forming a natural border between the two basins. The Toluca Valley's geographic position in the center of the country and proximity to Mexico City, as well as its rapidly developing infrastructure, have allowed the city to grow into a major industrial zone for the country.

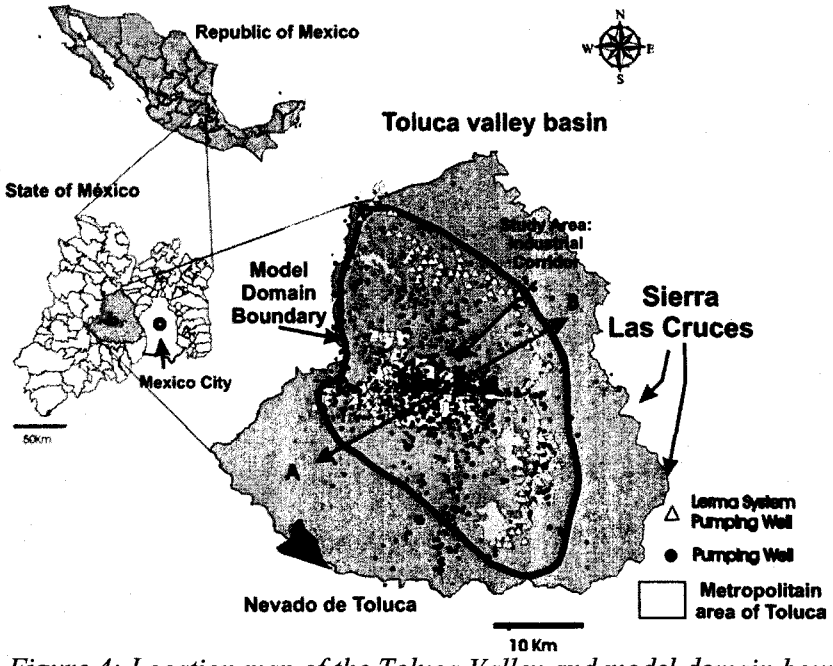


Figure 4: Location map of the Toluca Valley and model domain boundary within the Republic of Mexico and the State of Mexico. Over 935 pumping wells are in operation in the Valley, including the 230 Lerma system wells pumping water to the Mexico City Basin.

According to the 2005 census (INEGI, 2005), the metropolitan area of Toluca, including 12 neighbouring municipalities, is the fifth most populous metropolitan area in Mexico and the largest within the State of México. The total population of the Toluca Valley in 2005 was just over 1.7 million people (INEGI, 2005). From 1960 to 2005, the population of the valley has doubled approximately every 20 years (INEGI, 1960-2005).

The following sub-sections describe the available data and associated pre-processing: Geological information is used to generate a 3D geological model; and the D-InSAR technique is used to obtain subsidence maps

Geology

Volcanic andesitic rock from a Miocene-age buried volcano in the centre of the valley forms the basement in the basin (Figure 5A). The bedrock forms a bowl in the centre of the valley, reaching depths greater than 600 m and cropping out to the surface at the edges of the valley. The andesitic volcano formation of the Nevado de Toluca core is located to the West. The bedrock is overlain by a confining layer of pure lacustrine clays

and by the Chalma formation aquifer, composed of a mixture of sand, gravel and clay. The Tarango formation aquifer, deposited after the Chalma formation, extends from the flanks of the Sierra Las Cruces Mountains in the East across the basin floor to the foot of the Nevado of Toluca volcano. This formation is a heterogeneous mixture of volcaniclastic materials (Lesser and Asociados, 1992). The basaltic and ash flows of the Chichinautzin formation were deposited in the eastern portion of the Toluca Valley and act as an aquifer. In the upper middle portion of the valley, where most of the groundwater pumping occurs, complex interlayering of lacustrine clay (aquitard) and alluvium deposits (aquifer) are found. The industrial corridor, adjacent to the Lerma River (Figure 4, 5A), is located on what used to be a flood plain. Occasionally, during heavy rainfall, parts of the industrial corridor become a flood plain, yielding more compressible sediment. The complex sequence of layers in this area is shown schematically in Figure 5B.

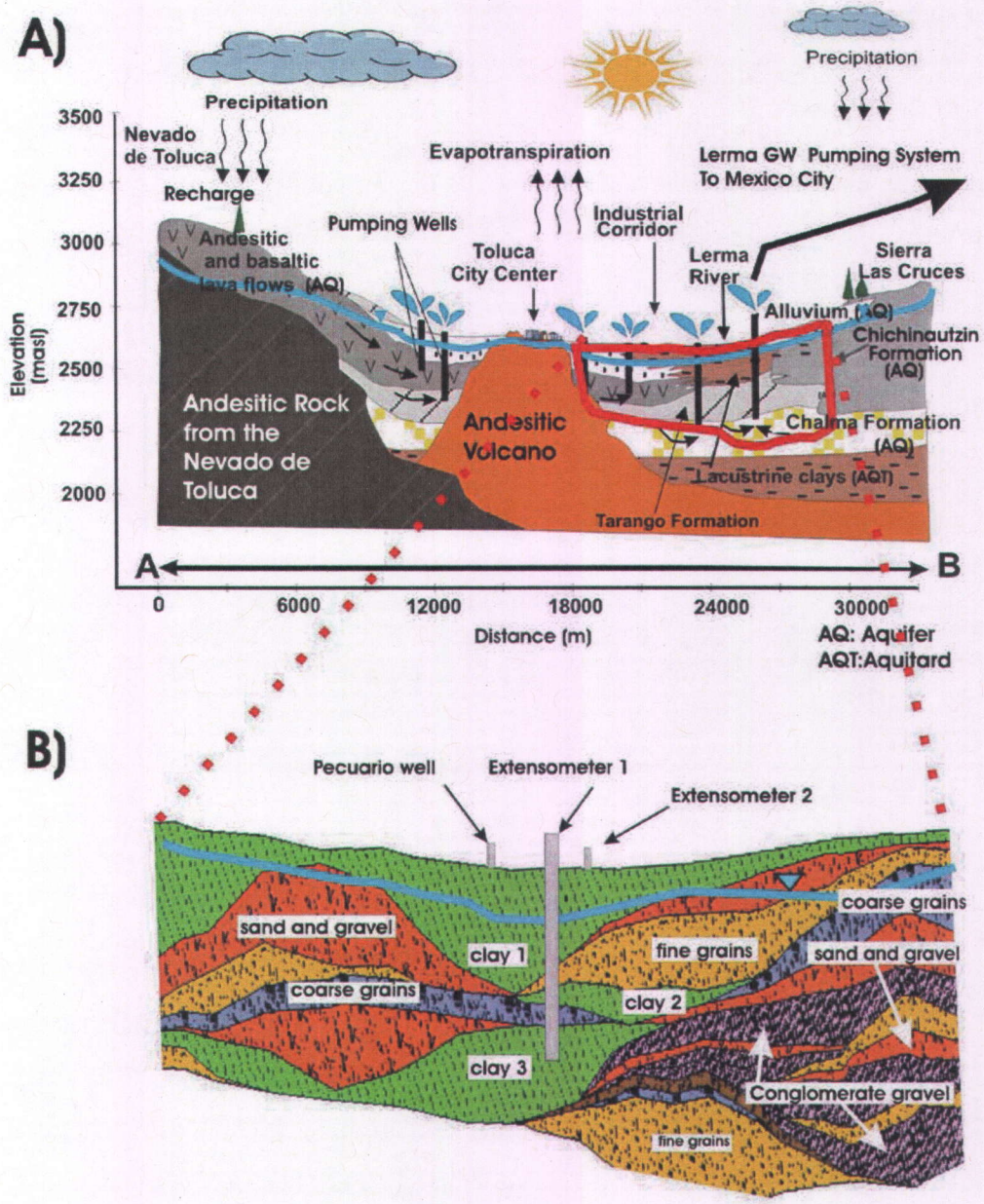


Figure 5: 5A: 2D view of the conceptual model for the Toluca Valley Basin including geologic layers (Modified from Calderhead et al. (2009a)) and 5B: a close up of the industrial corridor study area with a generated cross section. Locations of observation points in B are located in plane view on Figures 8 and 15. Cross section A-B is located on figure 4.

Clay materials are known to be significantly more compressible than other common materials such as sand, gravel, or consolidated rock. It is thus important to delineate the clay layer boundaries for a proper representation of a compaction model. Amelung et al. (1999) describe the correlation between InSAR derived subsidence and aggregate clay thickness (the sum of clay layer thicknesses at a given xy-location). There are several

types of clays in the Toluca valley, varying from very low compressibility ($\overline{\alpha} = 2e^{-8}\ Pa^{-1}$) to moderately high compressibility ($\overline{\alpha} = 3e^{-6}\ Pa^{-1}$). From the geological model presented in the previous section, four distinct clay layers are delineated in addition to the computed aggregate clay thickness. Figure 6 presents the 2 major (Figures 6A and 6B), and aggregate (Figure 6C) clay layers.

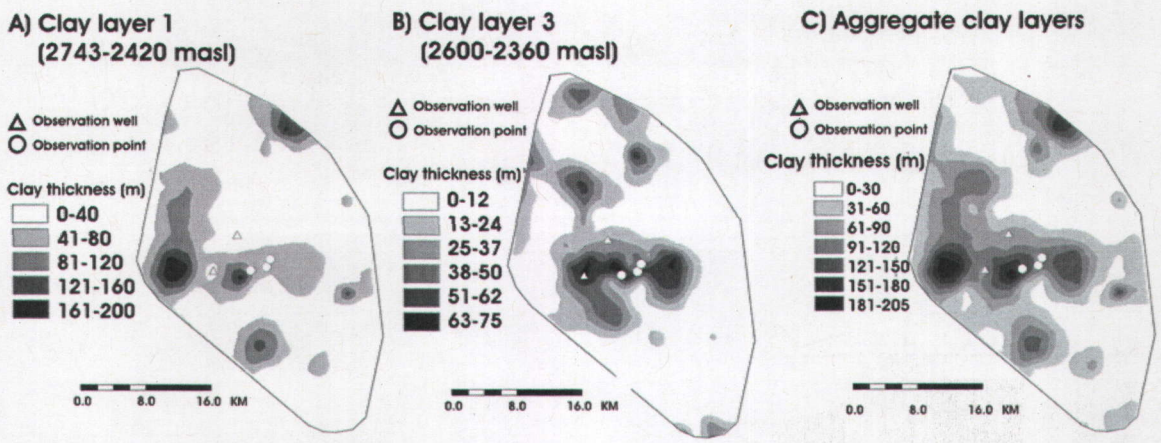


Figure 6: Clay layer thickness (6A and 6B) and aggregate clay thickness (6C)

Water budget

The rainy season generally occurs during the months of April through to October. Annually, the basin valley receives an average of 695 *mm* of precipitation (Lesser y Asociados SA 1992), whereas the higher altitudes receive larger amounts of rain, in the range of 1,200 *mm/year*. Annual precipitation cycles and amounts in the basin have been relatively constant since the first year of available data in 1942 (Lesser y Asociados SA 1992). Recharge values, needed for the flow simulations, are based on meteorological data between 1970 and 1999 (Figure 7). An average recharge value is used for the period 2000-2010 (CNA 2006).

Based on 48 multilevel piezometers operating in the Toluca Valley since 1969, CNA (2008) documents drawdown within the valley over a 4 decade period. Drawdown is induced by over 935 pumping wells with varying pumping rates located throughout the Toluca Valley (Figure 10A). For simplification purposes, 167 representative wells at

selected locations are used to represent all pumping occurrences. Based on IMTA (2003) and Calderhead et al. (2009a), total pumping is distributed evenly between the 167 representative wells.

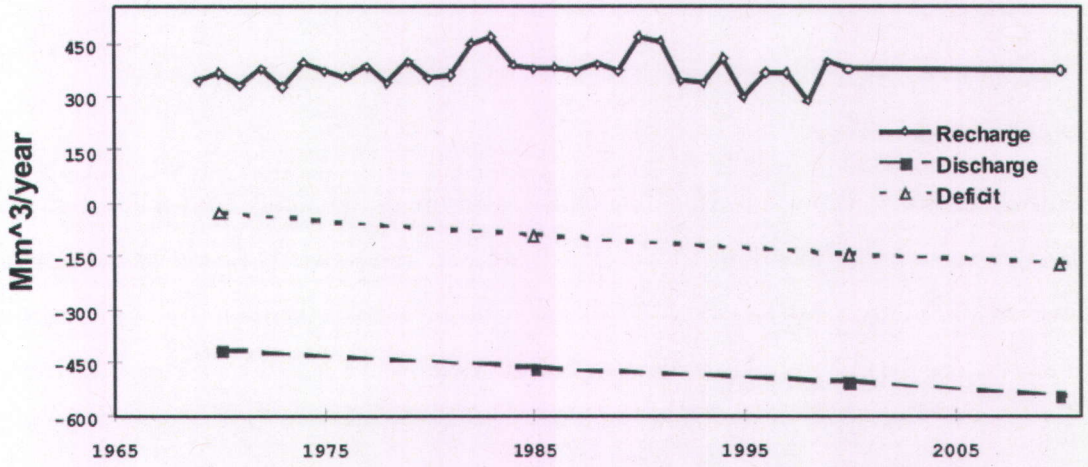


Figure 7: Groundwater recharge, discharge (natural and anthropogenic), and deficit from 1970 to 2010. From 1970 to 1999 actual recharge values are shown. From 2000 to 2010 an average expected recharge is shown. Recharge, discharge and deficit values are based on Calderhead et al. (2009a).

By backwards extrapolating, Calderhead et al. (2009a) show that there has been a water budget deficit in the Toluca Valley since the early 1960's (Figure 7) and this deficit continues to increase with time. Considering the increasing deficit within the basin, it was determined that over a long time (> 10 years), seasonal head fluctuations did not have a significant impact on the total subsidence. Therefore, only yearly, as opposed to monthly or daily, recharge, discharge, and budget deficits were used for the simulations. With the assumption of the increasing deficit, subsidence (not uplift or clay expansion) is the dominant process and therefore more importance is given to the inelastic skeletal specific storage (S'_{skv}) as opposed to the elastic skeletal specific storage (S'_{ske}).

Subsidence measurements

Although several previous studies of the Toluca Valley have described the location and orientation of fractures (Figueroa, 1990; 2004) and the compressibility of clays near the surface (Consultec, 1978; Minor, 2007), a very limited amount of quantitative subsidence

data is available from the literature. Field data was obtained by installing two borehole extensometers in regions with noticeable subsidence down to depths of 120m and gathering data over a two-year period. Consolidation tests were performed on clay samples taken from representative locations. And finally, D-InSAR was used to locate and quantify magnitudes of subsidence zones. Borehole extensometers and D-InSAR data are briefly described below.

Borehole extensometers

The objective of installing the extensometers was to obtain accurate field measurements of subsidence at point locations. Two R-4 magnetic reed switch probe extensometer systems, manufactured by Roctest® (Roctest, 2009), were installed in the Industrial Corridor (Figure 5B). Boreholes with a 15 cm diameter were bored by a rotary drill and reached depths of 115 and 78 meters for Extensometer-1 and Extensometer-2, respectively. For this study, reading frequencies from the extensometers varied from 1 to 6 months and spanned two years beginning in July of 2006 and ending in July of 2008.

InSAR

InSAR derived subsidence maps are used to estimate and decrease the uncertainty associated with of specific storage values. The interferograms and deformation maps are useful for locating compacting regions and quantifying the amount of subsidence. SAR images were obtained from ERS-1, ENVISAT ASAR, and RADARSAT-1 between 1996 and 2008. Calderhead et al. (2009b) present the complete D-InSAR results for the Toluca Valley. Figure 10B shows an example of an interferogram of two images taken 70 days apart in late 2007 and early 2008.

5 MODEL SETUP AND CALIBRATION

This section presents the model setup and describes the calibration process.

5.1 Model setup

To deal with the complex stratigraphy of the Toluca Valley, a processing chain uses borehole logs for generating a representative regional 3D geologic model. A total of 211 geologic well logs (Figure 8A: 151 Lerma pumping wells, 48 multi-level piezometers, and 12 additional wells) from the Toluca Valley basin were used to create the 3D geologic model domain. The 22 geologic types ranging from clays and fine sands to coarse gravel and volcanic fractured rock were simplified into 10 material types. Based on the well data and existing cross sections, the GMS 6.5 software uses a sequence of algorithms (GMS, 2009) for assigning consecutive layer horizons, creating cross sections between boreholes and finally generating the solids. In total, 34 solid layers (Figure 8B and 8C) were generated. Careful examination of the stratigraphy of each well combined with comparisons of existing cross sections (Ariel and Consultores, 1996) were necessary to obtain a simplified, yet detailed, geologic representation of the basin. While preserving the general geologic topography, the 34 layers with 10 material types were further simplified to 14 layers with 6 material types. Using the GridBuilder software (McLaren, 2005), the final 2D mesh of 27225 nodes (Figure 8D), representing the horizontal extent of the simulation domain, was generated with a mesh refinement around the location of 167 representative wells. The topography of the 14 geologic horizons was sequentially extracted at each node by 15 2D mesh layers. The 3D mesh (Figure 8F) is created by superposing the 15 2D mesh layers in the 3rd dimension (Figure 8E). The 3D mesh has a total of 408375 nodes and 760284 elements.

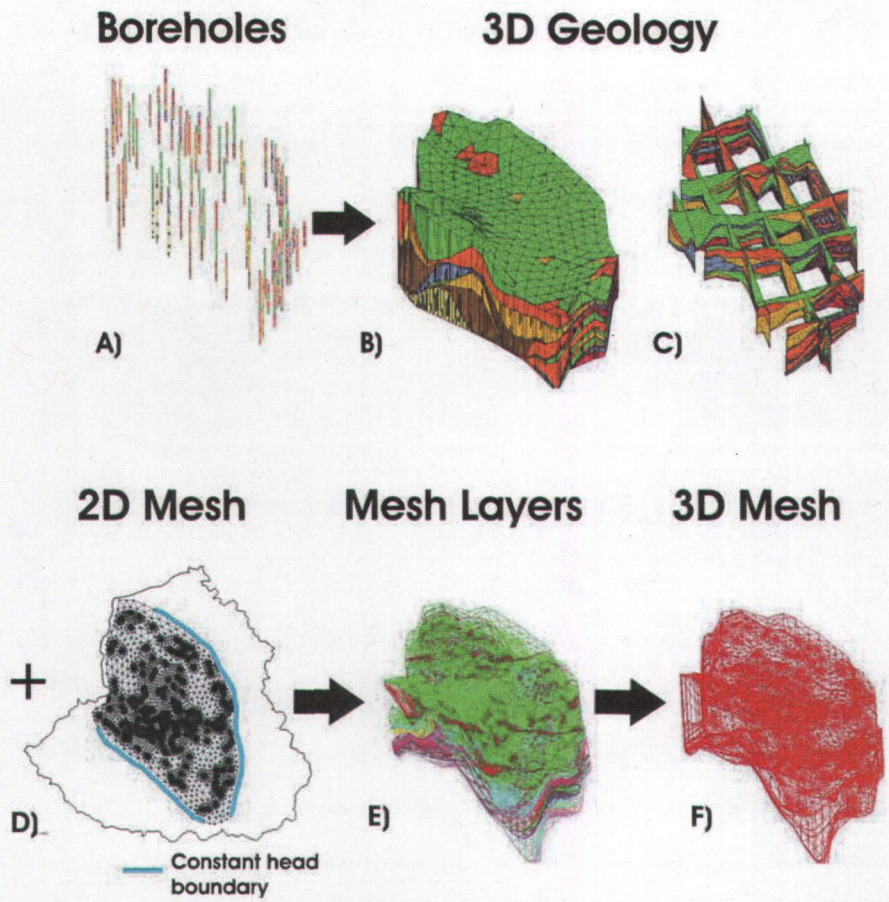


Figure 8: Processing chain for obtaining the 3D finite-element model domain. Boreholes (A) are used to generate 3D geology (B and C), then using the geologic layers and the 2D mesh (D), the topography of the geological layers are extracted (E). Finally the 3D mesh (F) is generated

Table 1 presents the boundary conditions, initial conditions, pumping incrementation, and the solution method. Table 2 gives a description of the material properties used for the simulations.

Table 1: Problem setup

SIMULATION SETUP	DESCRIPTION
Boundary Conditions	
Uniform vertical recharge	135 mm/year
Constant head boundary	Nodes at top of layer 1; See Figure 8D for xy location of boundary
Initial conditions	
Hydraulic head	Estimated hydraulic head values from 1950 (based on CNA (2008)
Simulations begin date	January 1st,1950
Total pumping	
1950-1969	312 Mm^3/year
1970-1977	346 Mm^3/year
1978-1993	401 Mm^3/year
1994-2004	456 Mm^3/year
2005-2010	494 Mm^3/year
Solution	
Solution method	Picard Iteration
Absolute convergence criteria	1.0e-4
Maximum iteration	15
Initial timestep	1 day
Maximum timestep	100 days

Table 2: Description of material properties for the Toluca Valley.

Layer number (from top to bottom)	Description	Average thickness	Hydraulic Conductivity	Specific Storage	Porosity	Fraction of compressible materials	Elastic skeletal specific storage	Inelastic skeletal specific storage
		b [m]	K [m/s]	Ss [1/m]	θ [-]	γ* [-]	S'ke [1/m]	S'kv [1/m]
Layer 1	clays 1	45,9	2,0E-06	7,0E-03	0.40	0,7	9,2E-07	3,7E-06
Layer 2	sand and gravel	18,0	4,0E-04	8,9E-03	0.35	1,00E-04	3,6E-08	1,4E-07
Layer 3	fine grains	16,9	3,0E-05	3,4E-03	0.30	1,00E-04	8,4E-08	3,4E-07
Layer 4	clay 2	2,1	2,0E-06	7,0E-03	0.35	0.7	3,0E-07	4,2E-07
Layer 5	fine grains	17,1	6,0E-05	3,4E-03	0.35	1,00E-04	8,6E-08	3,4E-07
Layer 6	coarse grains	19,0	1,0E-03	4,0E-03	0.35	1,00E-04	3,3E-08	1,3E-07
Layer 7	sand and gravel	10,6	4,0E-04	8,9E-03	0.35	1,00E-04	2,1E-08	8,5E-08
Layer 8	volcanic solids	6,7	6,0E-04	1,7E-03	0.30	1,00E-04	1,7E-12	6,7E-12
Layer 9	clays 3	21,9	5,0E-07	7,0E-03	0.35	0,7	2,1E-07	4,4E-06
Layer 10	conglomerate	7,3	6,0E-05	3,0E-03	0.30	1,00E-04	1,8E-12	7,3E-12
Layer 11	sand and gravel	6,8	4,0E-04	8,9E-03	0.35	1,00E-04	1,4E-08	5,4E-08
Layer 12	clays 4	3,7	6,0E-06	7,0E-03	0.35	0,7	1,9E-07	7,5E-07
Layer 13	fine grains	9,8	6,0E-05	3,4E-03	0.35	1,00E-04	4,9E-08	2,0E-07
Layer 14	sand and gravel	2,0	4,0E-04	8,9E-03	0.35	1,00E-04	4,0E-09	1,6E-08
Zones A-G	High compressibility areas of Layer 1	30,0	2,0E-06	7,0E-03	0.35	1,00E-04	1,0E-06	2,4E-06

5.2 Calibration

The model was set up by using field data for assigning the aquifer and aquitard physical properties (Table 2), initial hydraulic head conditions, and boundary conditions. Several points, or numerical observation wells, were used to monitor the calibration process. Namely, the points used were located at Extensometer-1, Extensometer-2 and the Pecuario well, located in the region where most of the compaction is observed. This is also where a significant amount of InSAR work was focused.

Initial simulations showed that the hydraulic heads were not decreasing and compaction was not increasing as rapidly as measured in the field. Certain parameters of the model were adjusted to achieve an acceptable degree of calibration.

Pumping location and rates were used to calibrate the hydraulic heads. This is described further in the following section. Increasing the specific storage (S_s) values of the non-clay layers by an order of magnitude greater than field observations significantly improved the calibration of head and compaction. The values shown in table 2 are approximately one order of magnitude greater than those measured in the field. Finally, the inelastic skeletal specific storage (S'_{skv}) was fine tuned to match the observed field compaction. The

calibration of hydraulic head and inelastic skeletal specific storage S'skv are described in more detail in the following sections. A description of the drawdown and compaction agreement is also discussed.

Head calibration

Calibrating the hydraulic head involved both using hydraulic head and drawdown values from multilevel piezometers located throughout the valley and by varying pumping. The total pumping rate of the entire valley (based on Calderhead et al., 2009a) however remained constant for all simulation. A higher grid resolution was placed on the industrial corridor where a large portion of the pumping and the largest drawdowns are observed. Yearly total pumping was estimated in 5 to 15 year increments (Table 1), the simulated drawdown is shown in Figure 9. The general trend follows the hydraulic head and drawdown values at PL-201, PL-205, and the limited information at Extensometer-1. Seasonal head variations could be of interest, however, considering that the groundwater levels are in a steady decline, only yearly data has been considered.

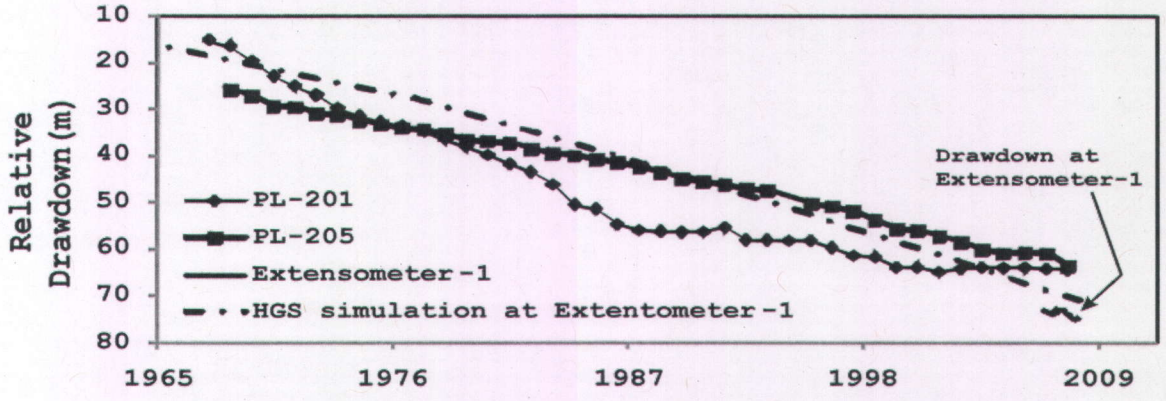


Figure 9: Measured and simulated relative drawdown at Extensometer 1 contrasted with relative drawdown of nearby long-term monitoring wells PL-201 and PL-205 (see figure 15 for locations).

Estimating S'_{sk} for an individual clay layer

Figure 10A shows pumping locations, and pumping rates, overlaying the generated aggregate clay thickness (from Figure 6); and Figure 10B is a representative D-InSAR

interferogram of the entire valley showing localized subsidence zones over a 70 day period. Figure 10B suggests that there is very limited interferometric coherence – or detectable surface movement - in the North-East and South-West corners, thus limiting its usefulness. However, usable results are obtained throughout the central part of the valley, where subsidence is the largest. Note that the interferogram is not optimised for parameter retrieval in zone E; this zone of maximum subsidence is studied in more detail in the results section. For the 70 day period between December 5th and February 13th, zones A though G are 'hotspots' with very clear subsidence patterns observed. If one observes the zoom on zone A (Figure 10B), two colour cycles (clockwise: yellow-blue-red; see legend of Figure 10B) are observed and represent a total subsidence of 56 mm for the given period. This translates to subsidence rates of 29 cm/year. As noted by Calderhead et al. (2009b) in their D-InSAR study of the Toluca Valley, maximum subsidence rates depend on the geological context, the pumping rates, and the season and are therefore often variable in space, time, and magnitude. Considering this, actual maximum yearly subsidence at a specific location is closer 15 cm/year.

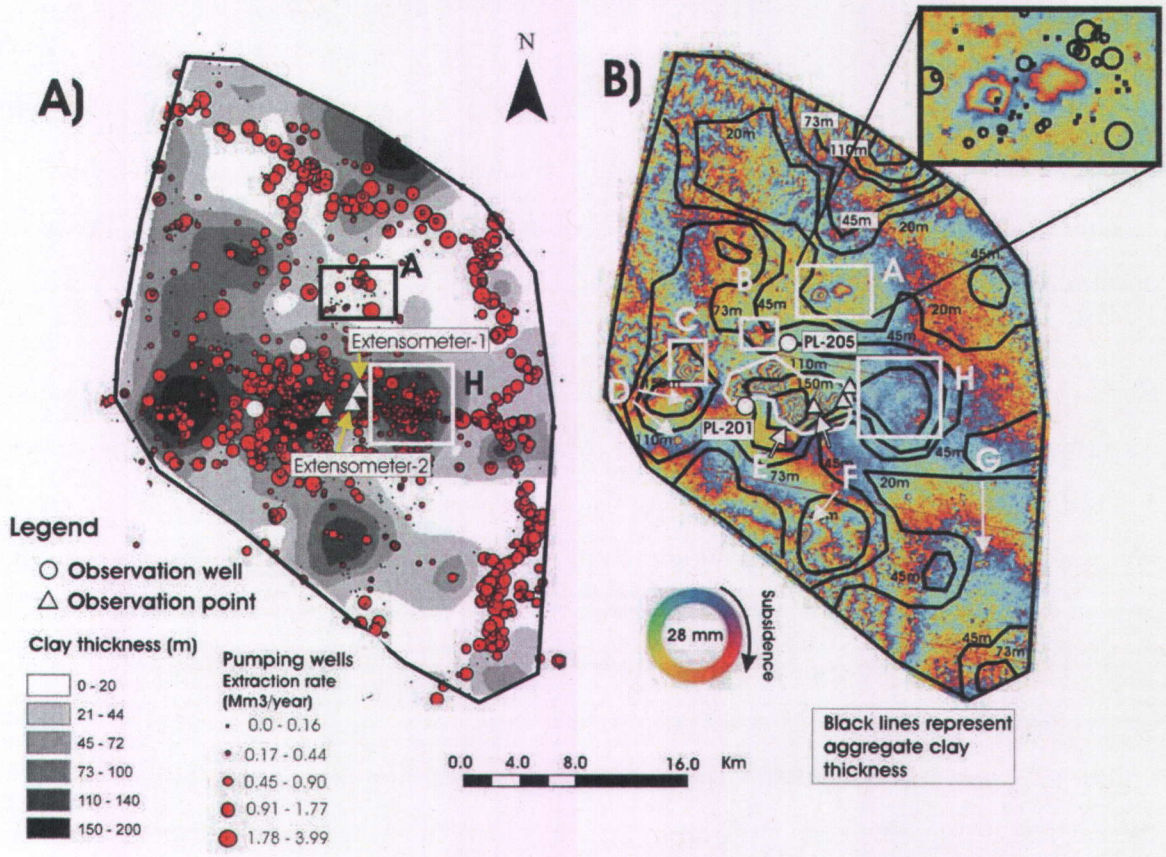


Figure 10: A) Aggregate clay thickness and pumping occurences B) Differential Interferogram of the Toluca Valley with a time interval of 70 days. ENVISAT ASAR images were acquired on December 5th 2007 and February 13, 2008. A blue-red-yellow cycle represents subsidence (2.8cm), conversely blue-yellow-red would represent uplift. Lines of equal aggregate thickness (from 9A) are also shown on the map. Note that topographic errors are seen on the edges of the valley and should not be interpreted as subsidence. Subsidence should only be inferred from zones A-G.

Using clay layer thicknesses (Figures 6, 9A), interferograms (e.g. Figure 10B), pumping data (IMTA, 2003) (Figure 10A) and hydraulic head measurements, S'_{ki} can be constrained for an individual layer *i*, belonging to a system of N layers. S'_k represents the skeletal storage coefficient of the entire aquifer system of N layers at a given location on the xy plane, and is given by:

$$S'_k = \sum_{i=1}^{N} S'_{ki} = \sum_{i=1}^{N} S'_{ski} b_i \qquad (25)$$

where b_i is the thickness of layer i. Using data obtained from borehole logs, the fraction of compressible interbeds (λ_i) can be estimated for all N layers. A layers with no clay content is assigned a value of 0, conversely a layer with pure clay is assigned a value of 1. The borehole logs assist in assigning the fraction of clay in each layer (Table 2). Assuming the given fraction of compressible interbeds for each layer, it is then possible to estimate S'_{sk} for individual clay layers (S'_{ski}).

Borehole logs, clay compressibility data from the Toluca Valley (UAEM, 2007) and empirically derived compressibility tables (Marsily, 1986) assist in assigning S'_{sk} values to the layers. Only layers with clay content are considered compressible and all other layers are considered to have negligible compressibility. According to Figures 5B and 6, of the 14 material layers, the most influential layers in terms of compressibility are layers 1 and 9. The others are considered to either be of negligible compressibility or too small of a layer to have a significant impact. Field data is not available for zone H, shown in Figure 10B, however the InSAR data is useful in constraining S'_{ski} for this zone: although there is a high aggregate clay thickness (Figure 6C) and significant groundwater pumping (Figure 10A) in zone H, all usable interferograms from 1996-2008 show very little to no subsidence in this zone. Observing Figure 6 further, we notice that the thickness of clay layer 3 (Layer 9) is significant (40-80 m) in zone H, implying that the S'_{ski} value for this layer is most likely small and that Layer 1 has the highest S'_{ski} and is the dominant compressible layer in this region. This phenomenon could be explained by the fact that older and deeper clays of clay layer 3 tend to be less compressible than more recent clays in Layer 1. This in turn could explain why the extensometers readings, with data from the top 120m of the system, coincide with the InSAR results and show that the large majority of compaction is occurring in the upper portion of the aquifer.

Thus the large majority of the total S'_{sk} (equation 26) is attributed to layer 1. By using the 3D geological model, pumping occurrences, and D-InSAR results, we are able to isolate the most compressible clay structure and assign more probable values to individual layers. Thus the uncertainty associated with the estimation is reduced to better constrain

the S'_{sk} values. Table 2 is a summary of the assigned material properties used for the simulation.

Head and compaction agreement

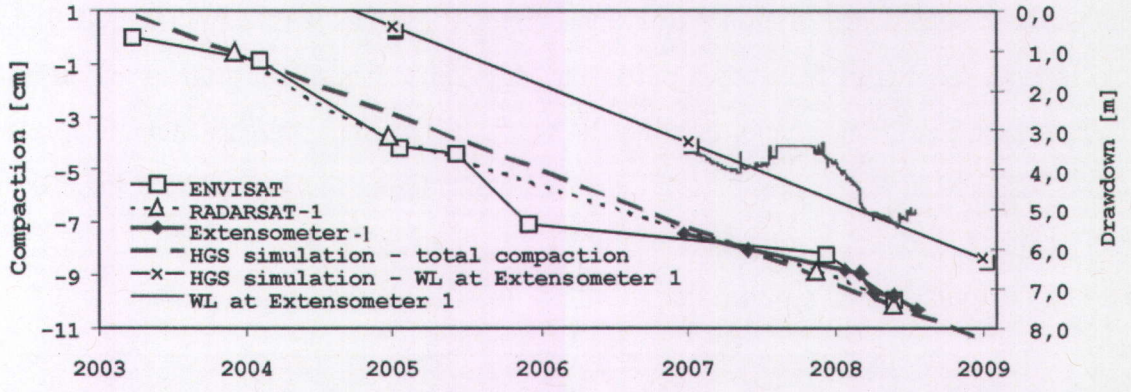


Figure 11: Simulated and measured total compaction at Extensometer 1 by ENVISAT ASAR, RADARSAT-1, Extensometer-1, and HGS simulation. Simulated and measured drawdown (WL) at Extensometer-1 are also included.

At Extensometer-1, similar subsidence patterns are observed from ENVISAT ASAR, RADARSAT-1, Extensometer-1, and the HGS compaction simulation (Figure 11). From December 2006 to July 2008, a pressure transducer at Extensometer 1 measured the hydraulic head every 12 hours. From Figure 11, it is seen that approximately 1 metre of drawdown leads to 1 cm of compaction. Additional hydraulic head data at extensometer 1 would enhance the calibration process.

6 RESULTS

Three locations in the industrial corridor, where drawdown has been monitored over a 40-year period and noticeable subsidence is observed, are examined more closely: Extensometer-1 (seen in the calibration section above), Extensometer 2, and the Pecuario well location (Figures 11, 12, and 13 respectively). Two of the three observation points have 2 years of extensometer data. Due to delays in obtaining subsidence maps, only D-InSAR data is available for the Pecuario well location; on-site surveys at this location are

not available. The nearby monitoring wells, PL-201 and PL-205, are used for long term monitoring of hydraulic head or drawdown at an approximate depth of 150 m.

Subsidence at Extensometer-2 is observed in Figure 12. The extensometer data slope coincides relatively well with the D-InSAR results and the numerical model. The magnitude of subsidence is similar to Extensometer-1's values with approximately 9 cm of compaction between November 2003 and May 2008. Considering the proximity of Extensometer 2 to Extensometer 1, hydraulic head is assumed to decrease at a rate similar to that observed at Extensometer 1 (Figure 9). Considering the similar head decline at both locations, and that compaction magnitudes are similar for both locations (Figure 11 and 12); the total skeletal specific storage values are also assumed to be similar.

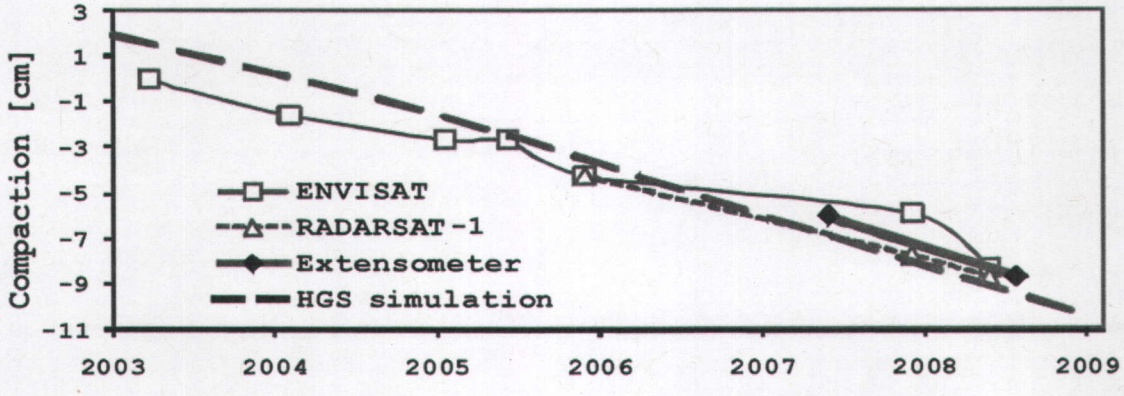


Figure 12: Total compaction as a function of time at Extensometer 2 location. Shown are compaction observed with the extensometer, compaction measured by ENVISAT ASAR and RADARSAT-1, and compaction simulated with HGS.

Skeletal specific storage (S'_{sk}) appears higher at the Pecuario well location (Figure 13) because the same amount of drawdown in this region (1 m) produces more compaction (8 cm) than elsewhere. According to the D-InSAR results, the Pecuario well location has had over 37 cm of total subsidence between November 2003 and May 2008. This point is close to the area where the highest subsidence rates are detected and it is estimated that the maximum total subsidence in the valley for the same period is in the order of 40 cm.

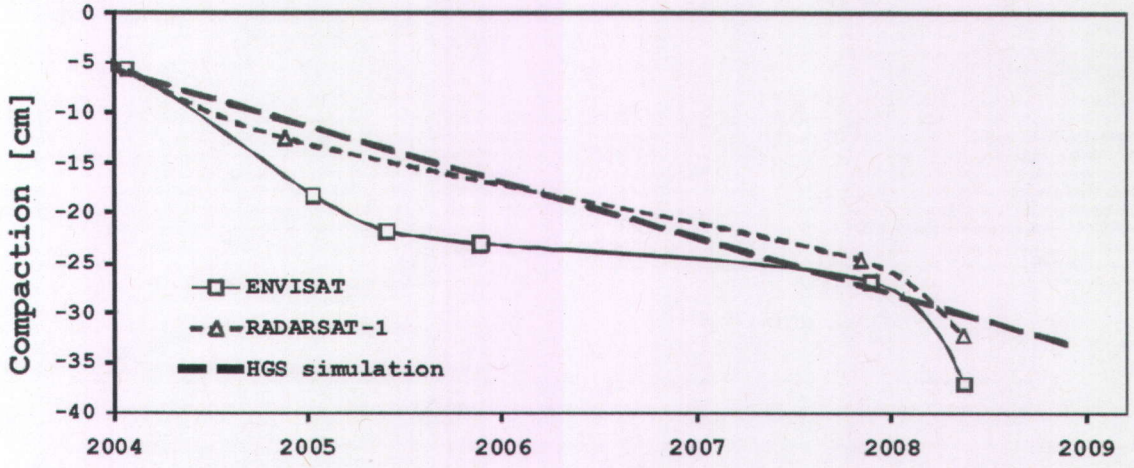


Figure 13: Total compaction at the Pecuario well location measured by ENVISAT ASAR RADARSAT-1, and the numerical model between March 2003 and January 2009.

From Figures 11-13, it can be inferred that, from 2003 to 2008, the industrial corridor clay compacted in a relatively linear fashion with varying compaction rates as a function of differing drawdown and geo-mechanical properties. It can be argued that the linearized approach used by HGS is applicable to the Toluca Valley since the clays are not as compressible as some other clays (e.g. Mexico City).

Although most of the D-InSAR data available for the Toluca Valley are from 2003 to 2008, one D-InSAR pair was obtained from the 1996 ERS-1 archives. The simulated compaction rates in 1996 at Extensometer-1 agree with the subsidence map generated with the ERS-1 sensor images (Figure 14). Between 1996 and 2008 a total of 30 cm of subsidence is estimated at the Extensometer-1 location.

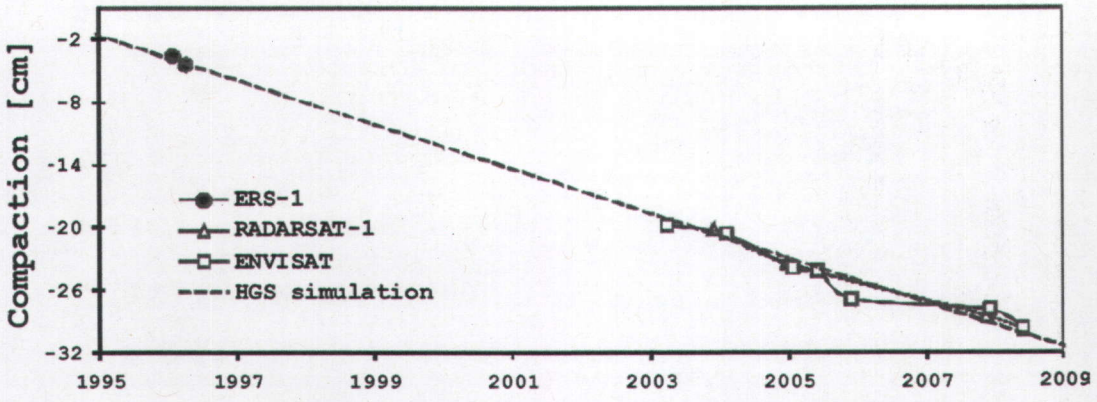


Figure 14: Total compaction at Extensometer-1 measured by ENVISAT ASAR, RADARSAT-1, ERS-1, and simulated by HGS between 1996 and 2008.

Figure 15A shows the HGS compaction result superimposed on a D-InSAR subsidence map for the period from December 5th 2007 to May 28, 2008. Simulations do not exactly match subsidence occurrences however the region of maximum subsidence is in the same location for both methods. Magnitudes are slightly higher with D-InSAR, possibly because the measurements were taken during the dry season, when maximum drawdown and subsidence occurs. Seasonal compaction patterns could have been simulated, however, since there is a growing groundwater deficit over a 50 year period, subsidence occurrences on a larger time scale were preferred.

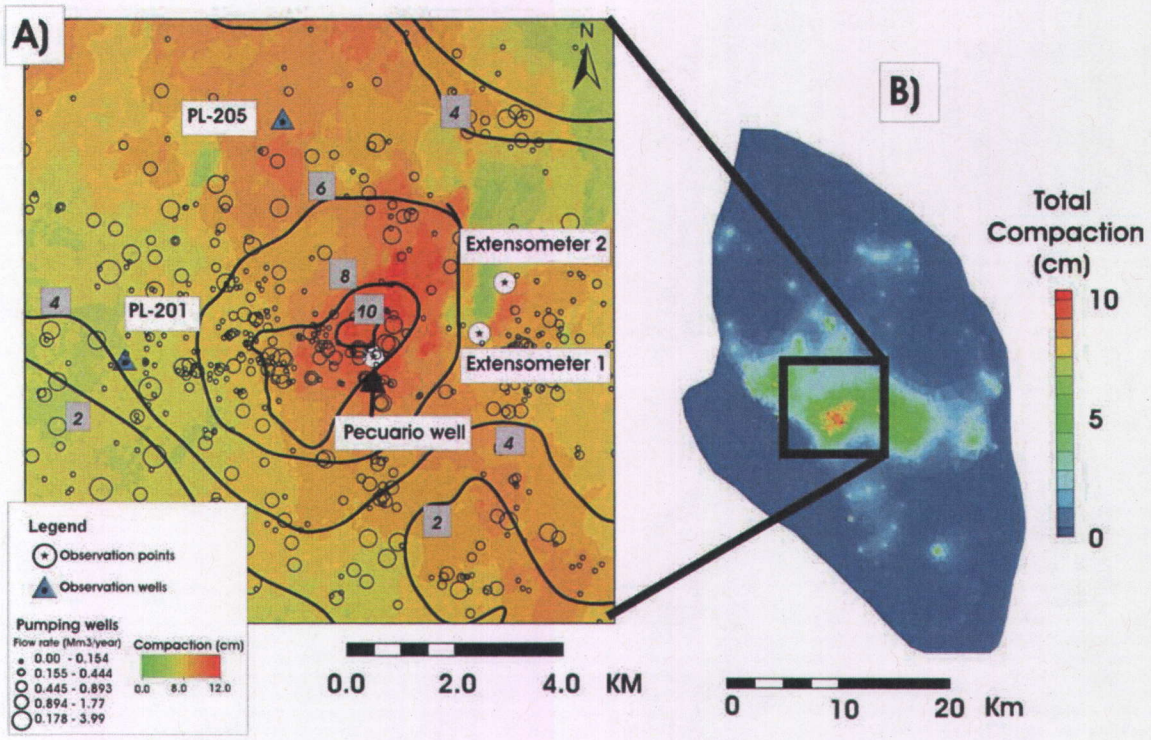


Figure 15: A) HGS simulation (solid black lines) superimposed on D-InSAR subsidence map (colour infilling) in the 175 days from December 5th 2007 to May 28, 2008. Locations of pumping wells with pumping rates are also indicated. Lables for the lines are compaction in cm. B) HGS simulation results for the entire valley for the same time period

The groundwater deficit in the valley first occurred in the early 1960's and has increased steadily ever since. From the simulations, minor compaction occurrences are observed in 1963 (Figure 16) and total compaction reaches 2 metres by 2009. As seen in figures 10-15 the simulation results agree reasonably well with the measured compaction occurrences between 2003 and 2008. There is a lack, however, of regional subsidence data before 2003 with only a handful of studies examining subsidence occurrences in the Toluca Valley over the past 40 years (Consultec, 1978; Figueora, 1990; 2004). These studies are mostly limited to the formation of fractures and none examine regional subsidence. Nevertheless, assuming the model is representative of the groundwater budget and material properties before 2003, it is estimated that the model is also representative of the subsidence occurrences before 2003.

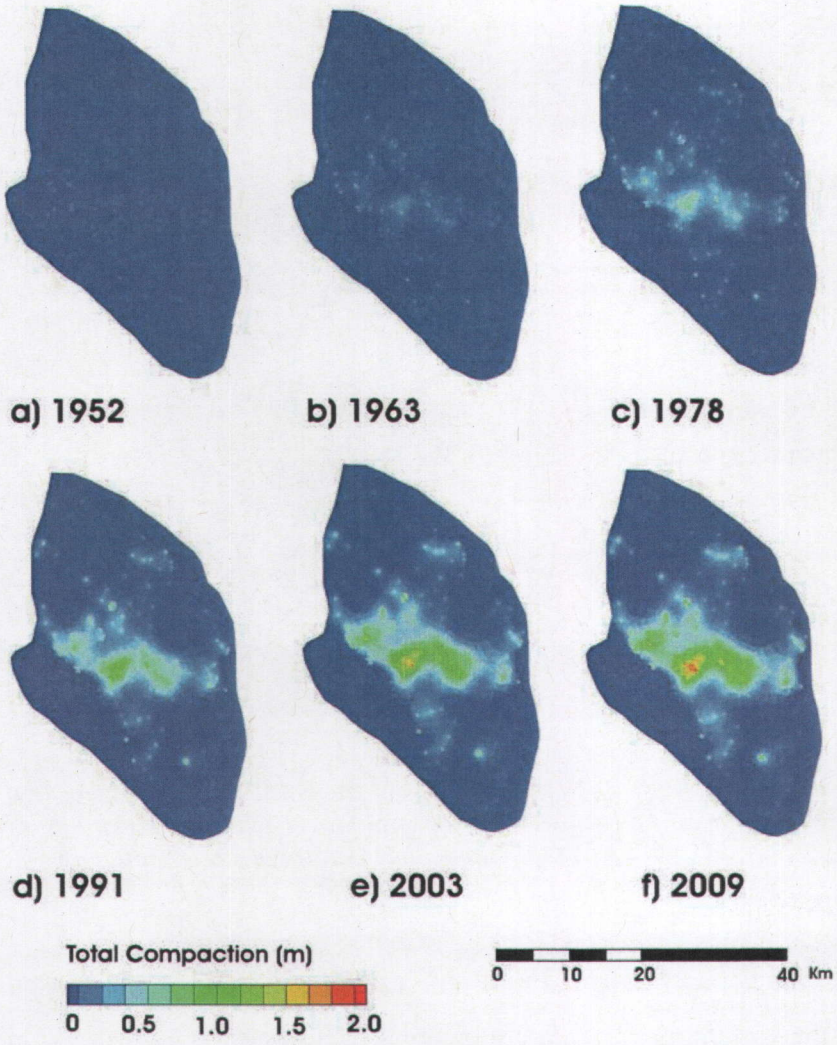


Figure 16: Evolution of regional land subsidence in the Toluca Valley from 1960 to 2009 simulated with HGS.

The simulation results agree with increased pumping over time, the subsidence occurrences have proportionally increased and are located in areas where compressible clay thickness is high. Maximum subsidence rates in the valley are in the order of 30 cm/year, however the areas with maximum subsidence are spatially variable (Calderhead et al. 2009a), and thus rate magnitudes will vary in time at a specific location.

7 DISCUSSION AND CONCLUSION

Limitations exist for the new HGS-compaction numerical model in representing subsidence. Both the solution approach and the use of representative data are major

factors in obtaining reliable model results. However, the rapid decrease in head in 2008 (Figure 11) followed 4-5 months later by a rapid compaction rate can lead one to think that the compaction delays in the Toluca valley system are relatively fast compared to other systems (e.g. Mexico City), thus, based on the limited data, an instantaneous compaction representation for the Toluca Valley is acceptable. It should also be noted that what has been defined as clay layers in the model setup often implies interlayering with coarse alluvial deposits, often with relatively thin clay layers, implying that the migration of the pressure head to the surrounding aquifer can be relatively fast. A longer time span of compaction data coupled with hydraulic head information will enhance the understanding of the clay behaviour.

Using the linearized form of the constitutive law introduces representation errors. Leake and Prudic (1991) have estimated the error of this method by comparing the linearized equations of computed compaction with a more complex treatment of computed compaction using S'_{skv} proportional to log σ'_{zz}. Their results indicate that using the linearized form overestimates compaction by approximately one-half the percentage increase in effective stress.

The new numerical model has helped in reproducing subsidence of the Toluca Valley. The new HGS-compaction code gives very reasonable estimates for instantaneous subsidence in confined aquifers; however there is room for improving the estimates by including aspects such as dependence on hydraulic conductivity, non-linear deformation, time delays, effects of moving water tables, and extending to a 3D representation of deformation.

The industrial corridor of the Toluca Valley has both compressible clay and heavy groundwater pumping with the model showing up to 2 meters of subsidence occurring over the last 50 years. Although there is a groundwater deficit in the Toluca Valley Basin, the steady increase in the extent and magnitude of regional subsidence is observed from 1952 to 2009. It is found that the upper clay layer of the aquifer system is the most

compressible unit. This information assists in assigning better estimates of the S'_{sk} values to the system.

Although an extensive groundwater level monitoring system has been in place in the Toluca Valley since the late 1960s, more detailed information on the underlying geologic parameters would greatly enhance the predictive capability of the numerical model. A better 3D geological model could be achieved by including more borehole logs and consolidation tests. According to the InSAR results and the numerical model, it appears that most of the compaction is occurring in the upper 120 m of the aquifer. To enhance confidence, additional extensometers reaching immobile bedrock would increase our confidence in subsidence measurements at specific locations. Benchmarks should also be used to monitor the subsidence. Additionally, a more detailed census on the groundwater pumping tendencies occurring in the Toluca valley would enhance the understanding of groundwater flow. Seasonal subsidence information could be of interest, however, considering that the groundwater levels are in a steady decline, only yearly data has been considered.

While not discussed in detail, the D-InSAR data was very useful, especially in locating areas with significant subsidence and extracting the specific storage (S'_{sk}) values from individual layers. InSAR, whether its differential (D-InSAR) or permanent scatter (PS-InSAR), has a large potential for mapping subsidence. The study would have been very difficult to undertake without the satellite data. With a steady increase in the number of InSAR capable satellites being launched, more data and software will likely become available. Although several factors influence the suitability of InSAR use for deformation mapping, the usefulness of InSAR is bound to improve.

Based on the available data, the results appear to be reliable. The multidisciplinary approach of using a 3D geological model, pumping estimates, hydraulic head measurements, D-InSAR, and extensometers to constrain the numerical model enables a very reasonable representation of the system.

Acknowledgements

We are thankful to the Ministère des Relations Internationales du Quebec, CONACyT, the Autonomous University of the State of México (UAEM), INRS-ETE, NSERC (a discovery grant held by Richard Martel), AUCC/IDRC, and the Ministère d'Éducation du Québec for their financial support. We are appreciative of Geoffrey Edwards from Laval University and Vern Singhroy from the Canadian Centre for Remote Sensing for providing support with InSAR software and techniques; and Sergio Murillo from the Comision National del Agua for the logistical support on the field. We are grateful to the Canadian Space Agency and the Geological Survey of Canada for providing the RADARSAT-1 data and finally, we acknowledge the European Space Agency's contribution for providing ERS and ENVISAT ASAR data at cost of reproduction under project C1P 3821.

References

Amelung, F., Galloway, D. L., Bell, J.W., Zebker, H. A., & Laczniak, R. J. (1999). Sensing the ups and downs of Las Vegas: InSAR reveals structural control of land subsidence and aquifer-system deformation. Geology, 27, 483–486.

Ariel y Consultores (1996). Hydrodynamic modeling study and design optimization of the monitoring well networks for the aquifers of Caldera, San Luis Potosi and Toluca (Part 3: Aquifer of Toluca) Estudio de Simulacion Hidrodinamica y Diseno Optimo de las Redes de Observacion de los acuiferos de Calera, San Luis Potosi y Toluca (Tomo 3: Acuifero de Toluca). CNA (Comisión Nacional del Agua) México, DF, Unitecnia 308

Biot, M.A. (1941) General theory of three dimensional consolidation. Journal of Applied physics. 12:155-164

Calderhead A. I., Martel, R. Rivera, A., Garfias, J., Therrien, R., An increasing groundwater budget deficit induced by urbanization, industrialization, and climate change in the Toluca Valley, Mexico. Hydrological Processes (Submitted 2009a)

Calderhead, A. I., Martel, R., Allasset, P-J., Rivera, A., Garfias, J, Land subsidence

induced by groundwater pumping, monitored by C-band D-InSAR and field data in the Toluca Valley, Mexico. Canadian Journal of Remote Sensing (accepted 2009b)

CNA, (2006) Datos climatológico, Servicio Meteorológico Nacional, Comisión Nacional del Agua.

CNA (2008) Registro de Lecturas Piezométricas por el Valle de Toluca Marzo 2008

Consultec (1978). Study of the behavior of fractures in the upper Lerma river basin reports I-III . Estudio del compotamiento de grietas en el valle del Alto Rio Lerma. Informes I-III.

Fetter, C.W., 2001. Applied Hydrogeology. 4th Ed. New Jersey: Prentice Hall Inc.

Figueroa Vega, G. E., (1990) Estudio sobre el comportamiento reciente del acuifero de la ciudad de Toluca y su relacion con el problema de agrietamientos de la zona poniente de la misma. CEAS, The state of Mexico, May 1990

Figueroa Vega, G. E, (2004) El agrietamiento de la ciudad de Toluca, Consejo consultivo de Agua, December 2004.

Galloway, D.L., Hudnut, K.W., Ingebritsen, S.E., Phillips, S.P., Peltzer, G., Rogez, F., & Rosen, P.A. (1998). Detection of aquifer system compaction and land subsidence using interferometric synthetic aperture radar, Antelope Valley, Mojave Desert, California. Water Resources Research, 34, 2573-2585

Gambolati, G., 1972. A three-dimensional model to compute land subsidence. Bullet. Int. Ass. Hydrolog. Sci. 17 (1972), pp. 219–226.

GMS, 2009. GMS 6.5 User guide, GMS - Salt lake City, Utah.

Harbaugh, A.W., Banta, E.R., Hill, M.C., and McDonald, M.G., 2000, MODFLOW-2000, the U.S. Geological Survey modular ground-water model—User guide to modularization concepts and the ground-water flow process: U.S. Geological Survey Open-File Report 00-0092, 121 p.

Helm, D. C., 1975. One-dimensional simulation of aquifer system compaction near Pixley, California, 1, Constant parameters, Water Resour. Res., 11, 465–478,

Hoffmann, J., Galloway, D. and Howard, A. J., 2003a. Inverse Modeling of Interbed Storage Parameters Using Land Subsidence Observations, Antelope Valley, California. Water Resource Research, Vol. 39, No.2, 1231.

Hoffmann, J., Leake, S.A., Galloway, D.L., and Wilson, A.M, 2003b, MODFLOW-2000 ground-water model—User guide to the Subsidence and Aquifer-System Compaction (SUB) Package: U.S. Geological Survey Open-File Report 03–233, 46 p.

IMTA, 2003. Censo del utilización del agua en el valle de Toluca. Instituto Mexicano de Tecnologia del Agua.

INEGI, 1960. Censo general de población y vivienda 1960. Instituto Nacional de Estadística, Geografía e Informática.

INEGI, 1970. Censo general de población y vivienda 1970. Instituto Nacional de Estadística, Geografía e Informática.

INEGI, 1980. Censo general de población y vivienda 1980. Instituto Nacional de Estadística, Geografía e Informática.

INEGI, 1990. Censo general de población y vivienda 1990. Instituto Nacional de Estadística, Geografía e Informática.

INEGI, 2000. Censo general de población y vivienda 2000. Instituto Nacional de Estadística, Geografía e Informática.

INEGI, 2001. Instituto Nacional de Estadística, Geografía e Informática, Sinthesis of geographic information for the state of Mexico. Síntesis de información Geográfica del Estado de Mexico

INEGI, 2005. Censo general de población y vivienda 2005. Instituto Nacional de Estadística, Geografía e Informática.

Johnson, A.I., Moston, R.P., and Morris, D.A., 1968, Physical and hydrologic properties of water-bearing deposits in subsiding areas in California: U.S. Geological Survey Professional Paper 497-A, 71 p.

Jorgensen, D.G., 1980, Relationships between basic soils-engineering equations and basic ground-water flow equations: U.S. Geological Survey Water-Supply Paper 2064, 40 p.

Leake, S.A., and Prudic, D.E., 1991, Documentation of a computer program to simulate aquifer-system compaction using the modular finite-difference ground-water flow model: U.S. Geological Survey Techniques of Water-Resources Investigations, book 6, chap. A2, 68 p.

Leake, S.A., and Galloway, D.L., 2007, MODFLOW ground-water model—User guide

to the Subsidence and Aquifer-System Compaction Package (SUB-WT) for water-table aquifers: U.S. Geological Survey, Techniques and Methods 6–A23, 42 p.

Lesser and Asociados, S.A. (1992). Diagnostic study of the aquifer of the Valley of Toluca to implement a program for the extraction of groundwater. Estudio para el Diagnostico del acuifero del Valle de Toluca, para implementar la reglamentacion de la extraccion del agua subterranea

Lewis RW, Schrefler B (1978) Fully coupled consolidation model of subsidence of Venice. Water Resources Res 14 (2):223–230

Liu, Y., and D. C. Helm (2008), Inverse procedure for calibrating parameters that control land subsidence caused by subsurface fluid withdrawal: 1. Methods, Water Resour. Res., 44, W07423, doi:10.1029/2007WR006605.

Marsily, G. de Quantitative Hydrogeology. Groundwater Hydrology for Engineers Ed. Academic Press, New-York (1986)

McLaren, R.G. (2005) User Guide: GRID BUILDER A pre-processor for 2-D, triangular element,finite-element programs, University of Waterloo - Groundwater Simulations Group.

Minor Villar, A-M. 2007. Determinación del esfuerzo de corte de los distintos tipos de arcilla del Valle de Toluca bajo diferentes condiciones de humedad. Masters Thesis, UAEM, March 2007

Municipio de Toluca (1999). ANÁLISIS DE PELIGROS POR REMOCIÓN EN MASA EN LA COLONIA RANCHO LA MORA Y LA DELEGACIÓN DE SAN PEDRO TOTOLTEPEC. Municipal Report 1999

Neuman, S.P., Preller, C., and Narasimhan, T.N., 1982, Adaptive explicit-implicit quasi three-dimensional finite element model of flow and subsidence in multiaquifer systems: Water Resources Research, v. 18, no. 5, p. 1551–1561.

Poland, J.F., and Davis, G.H., 1969, Land subsidence due to withdrawals of fluids, in Varnes, D.J., and Kiersch, G., eds.: Geological Society of America Reviews in Engineering Geology, v. 2, p. 187–269.

Riley, F.S., 1969, Analysis of borehole extensometer data from central California: International Association of Scientific Hydrology Publication 89, p. 423–431.

Rivera, A., E. Ledoux and G. de Marsily, 1991. Nonlinear modeling of groundwater flow

and total subsidence of the Mexico city aquifer-aquitard system. FISOLS (IV Inter. Symposium on Land Subsidence); 12-17 may 1991 Houston Texas, USA. IAHS Publication no. 20; pp 45-58.

Roctest (2009) R-4 magnetic reed switch probe extensometer system, Roctest http://www.roctest.com/modules/AxialRealisation/img_repository/files/documents/R4-E5013D-W.pdf

Rudolph, D. L., and Frind E. O., 1991. Hydraulic response of highly compressible aquitards during consolidation. Water Resources Research, 27 (1), 17-28.

Safai, N. M., and G. F. Pinder, 'Vertical and horizontal land deformation in a desaturating porous medium', Adv. Water Resours., 2, 19-25 (1979).

Terzaghi, K. (1925). Earthworks mechanics based on soil physics. Erdbaumechanik auf bodenphysikalisher Grundlage, Franz Deuticke, Vienna

Therrien, R., .G. McLaren, E.A. Sudicky, S.M. Panday (2009) User Guide: HydroGeoSphere - A Three-dimensional Numerical Model Describing Fully-integrated Subsurface and Surface Flow and Solute Transport, University of Waterloo

UAEM, 2007. Compilation of clay compressibilities of the Toluca Valley, Mexico.

UAEM, 2008. Universidad Autonoma del Estado de Mexico, Faculdad de Ingeneria, Laboratorio de Materiales. Report on consolidation and linear contraction tests- August, 2007

List of tables

Table 1: Problem setup 171

Table 2: Description of material properties for the Toluca Valley. 171

List of figures

Figure 1: Example of compression test results of a Toluca Valley clay (from UAEM, 2008) 155

Figure 2: Verification problem - Model configuration used to simulate seasonally fluctuating stresses. The only sources and sinks of water in the system are the discharge or recharge through the well and the storage in the interbed and aquifer. The finite difference model uses a single well for recharge and discharge and the finite element uses the 8 corners of the block as wells (w1-w8), with the pumping and injection rates respectively divided by 8 for each well. 161

Figure 3: verification results showing hydraulic head and total compaction for the HGS and MODFLOW simulations 162

Figure 4: Location map of the Toluca Valley and model domain boundary within the Republic of Mexico and the State of Mexico. Over 935 pumping wells are in operation in the Valley, including the 230 Lerma system wells pumping water to the Mexico City Basin. 163

Figure 5: 5A: 2D view of the conceptual model for the Toluca Valley Basin including geologic layers (Modified from Calderhead et al. (2009a)) and 5B: a close up of the industrial corridor study area with a generated cross section. Locations of observation points in B are located in plane view on Figures 8 and 15. Cross section A-B is located on figure 4. 165

Figure 6: Clay layer thickness (6A and 6B) and aggregate clay thickness (6C) 166

Figure 7: Groundwater recharge, discharge (natural and anthropogenic), and deficit from 1970 to 2010. From 1970 to 1999 actual recharge values are shown. From 2000 to 2010 an average expected recharge is shown. Recharge, discharge and deficit values are based on Calderhead et al. (2009a). 167

Figure 8: Processing chain for obtaining the 3D finite-element model domain. Boreholes (A) are used to generate 3D geology (B and C), then using the geologic layers and the 2D mesh (D), the topography of the geological layers are extracted (E). Finally the 3D mesh (F) is generated 170

Figure 9: A) Aggregate clay thickness and pumping occurences B) Differential Interferogram of the Toluca Valley with a time interval of 70 days. ENVISAT ASAR images were acquired on December 5th 2007 and February 13, 2008. A blue-red-yellow cycle represents subsidence (2.8cm), conversely blue-yellow-red would represent uplift. Lines of equal aggregate thickness (from 9A) are also shown on the map. 175

Figure 10: Measured and simulated relative drawdown at Extensometer 1 contrasted with relative drawdown of nearby long-term monitoring wells PL-201 and PL-205 (see figure 15 for locations)..... 173

Figure 11: Simulated and measured total compaction at Extensometer 1 by ENVISAT ASAR, RADARSAT-1, Extensometer-1, and HGS simulation. Simulated and measured drawdown (WL) at Extensometer-1 are also included..... 177

Figure 12: Total compaction as a function of time at Extensometer 2 location. Shown are compaction observed with the extensometer, compaction measured by ENVISAT ASAR and RADARSAT-1, and compaction simulated with HGS 178

Figure 13: Total compaction at the Pecuario well location measured by ENVISAT ASAR RADARSAT-1, and the numerical model between March 2003 and January 2009. 179

Figure 14: Total compaction at Extensometer-1 measured by ENVISAT ASAR, RADARSAT-1, ERS-1, and simulated by HGS between 1996 and 2008... 180

Figure 15: A) HGS simulation (solid black lines) superimposed on D-InSAR subsidence map (colour infilling) in the 175 days from December 5th 2007 to May 28, 2008. Locations of pumping wells with pumping rates are also indicated. Lables for the lines are compaction in cm. B) HGS simulation results for the entire valley for the same time period 181

Figure 16: Evolution of regional land subsidence in the Toluca Valley from 1960 to 2009 simulated with HGS. 182

Chapitre 5: Groundwater pumping scenarios for minimizing land subsidence in the Toluca Valley, Mexico: tools for policy design

Résumé

Des scénarios de gestion des eaux souterraines sont examinés avec l'utilisation d'un modèle tridimensionnel d`écoulement d`eaux souterraines couplé à un module de compaction instantané. Plusieurs scénarios sont examiné dans vallée de Toluca, Mexique en faisant varier 4 paramètres principaux: la recharge, les exportations vers d'autres bassins, la consommation locale, et de la relocalisation des centres de pompage. Il est évident que poursuivre au rythme actuel de consommation d'eau amènera à un affaissement de plus de 1,4 m sur une période de 40 ans (2010-2050). Arrêter complètement les exportations vers la ville de Mexico n'est pas le facteur le plus important dans le contrôle de la subsidence, car le système de pompage se situe principalement dans une région à faible teneur en argile. Toutefois, en diminuant les exportations de la moitié et en déplaçant les centres de pompage à des endroits avec une faible teneur en argile ont un effet positif sur le budget global de l'eau et la subsidence. En se basant sur les résultats de simulations, il semble qu'une grande partie de la subsidence aurait pu être évité s`il y avait une politiques pour limiter le pompage dans les régions avec une concentration élevé de matériaux compressibles (argiles). L'approche adoptée dans cette étude pourrait être appliquée à d'autres régions ayant des problèmes similaires, en vue de déterminer l'option la plus viable pour l'approvisionnement en eau.

Sustainable development and management for minimizing land subsidence of an over-pumped volcanic aquifer system: tools for policy design

A I Calderhead[1], R Martel[1], J Garfias[2], A Rivera[3], R Therrien[4]

[1] Institut national de la recherche scientifique - Centre Eau, Terre & Environnement, 490 de la Couronne, Quebec, QC G1K 9A9, Canada

[2]Universidad Autónoma del Estado de México, Facultad de Ingeniería (CIRA), Cerro de Coatepec, s/n, C.U., Toluca, MEX 50130, México

[3]Geological Survey of Canada, Natural Resources Canada, 490 de la Couronne, Quebec, QC G1K 9A9, Canada

[4]Département de géologie et de génie géologique, Université Laval, Québec, QC G1K 7P4, Canada

Abstract

Groundwater management scenarios for the Toluca Valley, Mexico, are examined with a three dimensional groundwater flow model coupled to a one dimensional compaction module. Several scenarios are tested by varying 4 main parameters: recharge, exports to other basins, local consumption, and relocating pumping centers and quantifying their impact on land subsidence in the Valley. It is apparent that continuing at current rates of water consumption will lead to subsidence of over 1.4m over a 40 year period (2010-2050). Completely stopping exports to Mexico City is not the most important factor in controlling subsidence because the pumping system is mostly located in regions with low clay content, where subsidence is lower. However, decreasing exports by half and relocating the pumping centres to low-clay-content areas does have a positive effect on the overall water budget and subsidence. Based on simulation results, it appears that much of the land subsidence could have been avoided had water policies been applied to restrict pumping in regions of compressible materials (clay). The approach taken in this study could be applied to other locations with similar problems in order to determine the most viable option for water supply.

1 INTRODUCTION

Growing cities are forced to increase their clean water supply in order to meet the demand from households and industries. When possible, increasing local pumping is an economically viable option. However, a direct consequence of heavy groundwater pumping in aquifers that are in hydraulic connection with thick compressible clays is the formation of fractures and land subsidence. Clay compaction yields to costly infrastructure repair. The Toluca Valley has experienced such problems since it became, in the 1960's, an important fresh water supply for the nearby, effervescent Mexico City.

The Toluca Valley's water resource and land subsidence problems are of interest because the basin was formally seen as an important source of water to the Mexico City basin, yet today the Toluca Valley basin can no longer support its own growth let alone provide for Mexico City's. Exporting water to Mexico City has had a negative outcome in the case of Toluca, however, importing to the Toluca basin could become a viable alternative, if better management practises are taken into account.

The use of numerical models to represent and predict subsidence (e.g. Gambolati 1972; Helm, 1975; Leake and Galloway, 2007) has greatly enhanced the understanding and predictive capabilities of subsiding systems. It should be noted, however, that the theoretical assumptions and modeling approximations combined with a lack of representative geological, geomechanical, and hydraulic data can sometimes lead to numerical predictions that are not always reliable. Nonetheless, the application of consolidation theory to numerical models remains the best approach for examining and predicting subsidence. Studies examining water resource management options (e.g. Rejani et al., 2008; Loukas et al, 2007, Sayan and Yazicigil, 2004) rarely consider land subsidence. Studies that have examined future subsidence (e.g. Rivera, 1991; Ortega-Guerrero et al., 1999; Teatini et al., 2006) usually focus on groundwater pumping as the major factor influencing subsidence. Climate change (e.g. Larson et al., 2001),

optimizing pumping locations (e.g. Bayer et al 2009), and inter-basin water transfer are rarely considered. No studies have considered a combination of the above factors.

In view of the strategic importance of these resources in the region, and the conflicting evidence of potential impacts of excessive groundwater withdrawals and land subsidence, the main goal of this paper is to develop a groundwater flow/compaction model of the aquifer system based on extensive characterization and calibration studies. The resulting model is then used to evaluate the consequences of alternative groundwater pumping and management scenarios.

The paper uses a previously calibrated finite-element 3D groundwater flow and 1D instantaneous compaction model of the Toluca Valley, Mexico (Calderhead et al., 2009) and simulates various scenarios for determining the extent of land subsidence in the period from 2010 to 2050. The four parameters considered are: varying recharge (with respect to climate change), export/import water volumes to/from adjacent basins, local pumping volumes, and relocating pumping wells within the valley.

Geographic Setting

The Toluca Valley basin (Figure 1) covers an area of approximately 2116 km^2 in the south-centre of Mexico. The basin is adjacent to the Mexico City Valley, with the Sierra Las Cruces forming both a topographic and a hydraulic border between the two basins. The Toluca Valley's proximity to Mexico City and rapidly developing infrastructure has allowed the city to grow into a major industrial zone for the country. The industrial corridor (Figure 1) located to the East of downtown Toluca has a high concentration of industrial activity and is the area where most of the subsidence occurs.

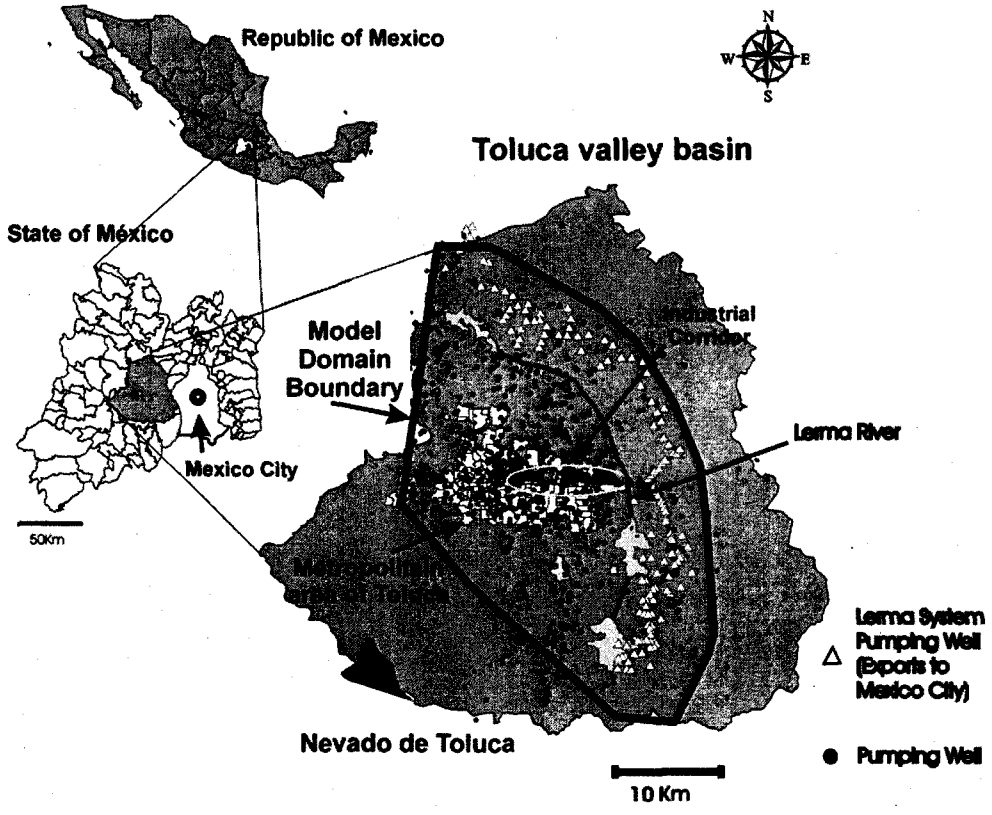


Figure 1: Location map of the Toluca Valley and model domain boundary within the Republic of Mexico and the State of Mexico. Over 935 pumping wells are in operation in the Valley, including the Lerma System wells exporting water to Mexico City. The simulated region boundaries are shown in figures 5 to 8.

Population growth

The total population of the Toluca Valley in 2005 was just over 1.7 million people and it is expected to increase to over 2.2 million by 2050 (Figure 2). From 1960 to 2005, the population of the valley has doubled approximately every 20 years (Figure 2). Based on United Nations projections (UNEP, 2008), the population of the valley will reach a plateau around 2050 with a population of approximately 2.2 million people.

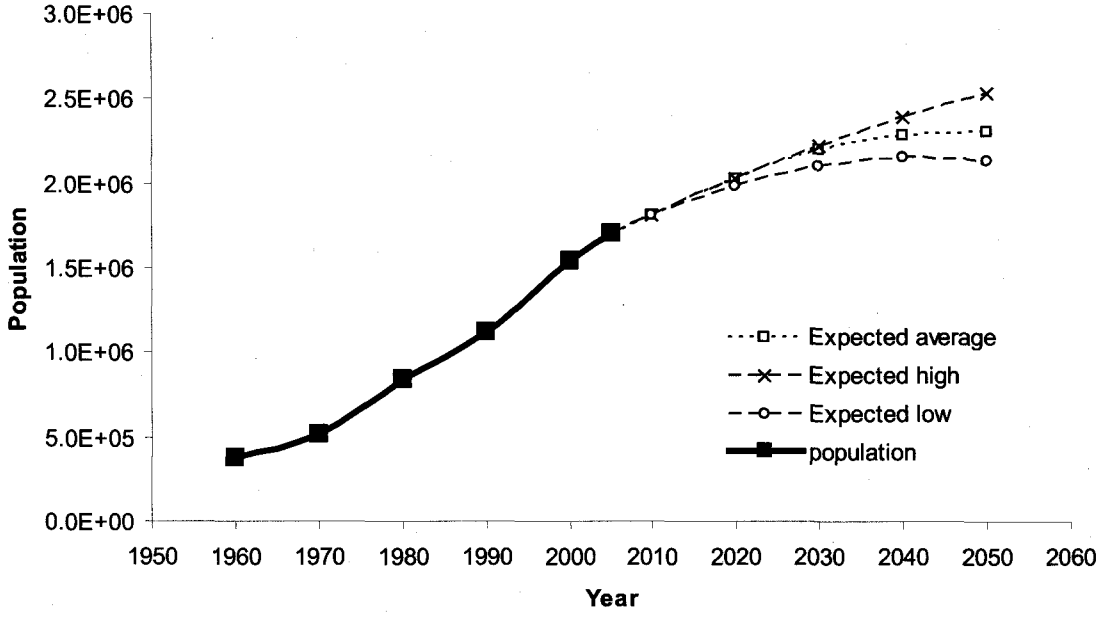


Figure 2: Recorded and expected population of the Toluca Valley from 1960-2050 (based on INEGI, 1960-2005 and UNEP, 2008)

Hydrogeology and Groundwater pumping

The Toluca Valley basin consists of two aquifer systems; an alluvial aquifer in the upper portion and a fractured aquifer at the bottom. In the upper aquifer there are layers of clays that induce a local confinement. Before the 1960's, groundwater levels in the Toluca Valley were either near surface or emerged above the land surface (Lesser y Asociados, 1992). Since the late 1960's, Mexico City began importing water on a large scale from other basins, including the Toluca Valley, to accommodate its water shortages. The Toluca Valley has continued to grow over the last four decades and presently, more than 935 pumping wells in the Toluca Valley are pumping over 469 Mm^3/year (million cubic meters per year) (Calderhead et al., 2009a). Over one third of the total pumping comes from the Lerma system wells: a groundwater pumping system consisting of 396 pumping wells located along the upper section of the Lerma River. The system captures a large portion of the recharge water entering from the Sierra Las Cruces, and is then exported to Mexico City at a rate of approximately 6.0 m^3/s (CNA, 2007).

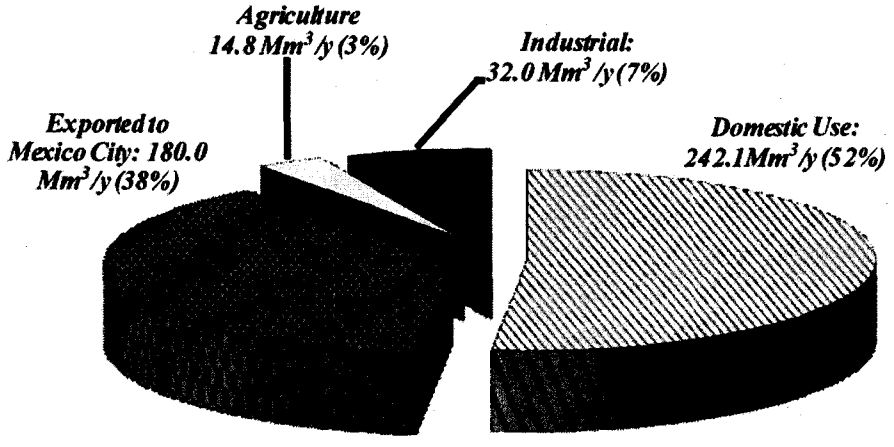


Figure 3: Groundwater use in the Toluca Valley based on IMTA (2003) and modified from Calderhead et al. (2009a)

As of the latest water use census (IMTA, 2003), water consumption is divided as follows (Figure 3): The majority of the groundwater pumped is for domestic/household use (52%), the second most important share (38%) is exported to Mexico City (at 6.0 m^3/s). Industrial (7%), and agricultural (3%) uses presently account for a relatively small percentage of the total volume.

2 METHODOLOGY

Model setup

Simulations are based on the previously calibrated 3D-flow and 1-D compaction finite-element numerical model of the Toluca Valley, Mexico (Calderhead et al., 2009c). A 3D geologic model domain (Figure 4A) is created from 211 borehole logs and available cross sections. While preserving the general geologic topography, the generated 34 layers with 10 material types were simplified to 14 layers with 6 material types. The topography of the 14 geologic horizons was sequentially extracted at each node by 15 2D mesh layers. Using the GridBuilder software (McLaren, 2005), the final 2D mesh of 27225 nodes (Figure 4B), representing the horizontal extent of the simulation domain, was generated with a mesh refinement around the location of 167 representative wells. The 3D mesh (Figure 4D) is created by superposing the 15 2D mesh layers in the 3rd dimension (Figure 4C). The 3D mesh has a total of 408375 nodes and 760284 elements. Table 1

presents the boundary conditions, initial conditions, pumping increments, and the solution method. Table 2 presents the material properties for the 14 layers.

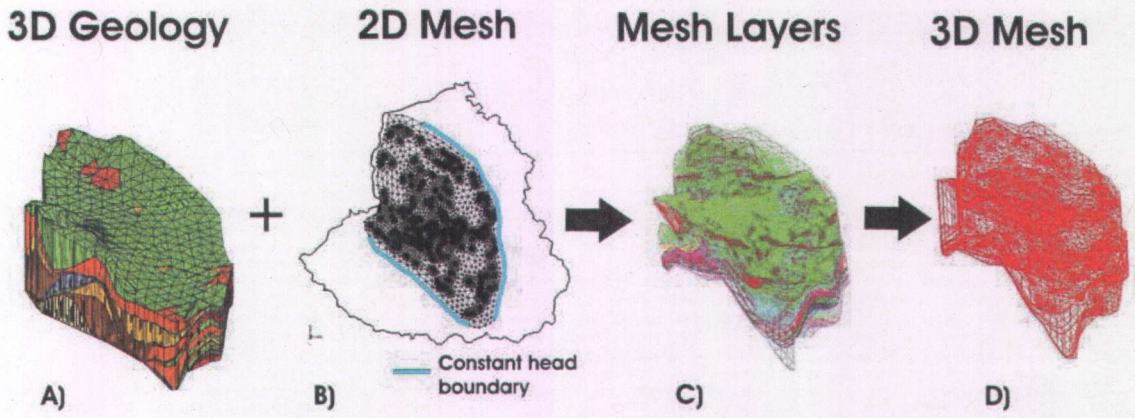


Figure 4: Processing chain for obtaining the 3D finite-element model domain. The 3D geology (A) is generated with the use of borehole logs and available cross sections, then using the 2D mesh (B) and the topography of the geologic layers, 15 topographically variable 2D layer meshes are extracted (C) and used to generate the 3D mesh (D). Location of the constant head boundary is also shown in B. Modified from Calderhead et al., 2009c.

Table 1: Problem setup

SIMULATION SETUP	DESCRIPTION
Boundary Conditions	
Uniform vertical recharge	135 mm/year
Constant head boundary	Nodes at top of layer 1; See Figure 4B for xy location of boundary
Initial conditions	
Hydraulic head	Estimated hydraulic head values from 1950 (based on CNA (2008)
Simulations begin date	January 1st,1950
Total pumping	
1950-1969	312 Mm^3/year
1970-1977	346 Mm^3/year
1978-1993	401 Mm^3/year
1994-2004	456 Mm^3/year
2005-2010	494 Mm^3/year
2011-2020	534 Mm^3/year
2021-2030	571 Mm^3/year
2031-2040	599 Mm^3/year
2041-2050	618 Mm^3/year
Solution	
Solution method	Picard Iteration
Absolute convergence criteria	1.0e-4
Maximum iteration	15
Initial timestep	1 day
Maximum timestep	100 days

Table 2: Description of layer material properties for the Toluca Valley (after Calderhead et al, 2009c).

Layer number (from top to bottom)	Description	Average thickness	Hydraulic Conductivity	Specific Storage	Porosity	Fraction of compressible materials	Elastic skeletal specific storage	Inelastic skeletal specific storage
		b [m]	K [m/s]	Ss [1/m]	θ [-]	γ* [-]	S'ke [1/m]	S'kv [1/m]
Layer 1	clays 1	45,9	2,0E-06	7,0E-03	0.40	0,7	9,2E-07	3,7E-06
Layer 2	sand and gravel	18,0	4,0E-04	8,9E-03	0.35	1,00E-04	3,6E-08	1,4E-07
Layer 3	fine grains	16,9	3,0E-05	3,4E-03	0.30	1,00E-04	8,4E-08	3,4E-07
Layer 4	clay 2	2,1	2,0E-06	7,0E-03	0.35	0.7	3,0E-07	4,2E-07
Layer 5	fine grains	17,1	6,0E-05	3,4E-03	0.35	1,00E-04	8,6E-08	3,4E-07
Layer 6	coarse grains	19,0	1,0E-03	4,0E-03	0.35	1,00E-04	3,3E-08	1,3E-07
Layer 7	sand and gravel	10,6	4,0E-04	8,9E-03	0.35	1,00E-04	2,1E-08	8,5E-08
Layer 8	volcanic solids	6,7	6,0E-04	1,7E-03	0.30	1,00E-04	1,7E-12	6,7E-12
Layer 9	clays 3	21,9	5,0E-07	7,0E-03	0.35	0,7	2,1E-07	4,4E-06
Layer 10	conglomerate	7,3	6,0E-05	3,0E-03	0.30	1,00E-04	1,8E-12	7,3E-12
Layer 11	sand and gravel	6,8	4,0E-04	8,9E-03	0.35	1,00E-04	1,4E-08	5,4E-08
Layer 12	clays 4	3,7	6,0E-06	7,0E-03	0.35	0,7	1,9E-07	7,5E-07
Layer 13	fine grains	9,8	6,0E-05	3,4E-03	0.35	1,00E-04	4,9E-08	2,0E-07
Layer 14	sand and gravel	2,0	4,0E-04	8,9E-03	0.35	1,00E-04	4,0E-09	1,6E-08

Focus is placed on projections of four parameters: recharge, pumping volumes for local use, export volumes to Mexico City and/or importing from less populated basins, and relocating pumping wells within the valley. For simplicity, and to avoid excessive computation time, 173 representative wells are used with a relaxed mesh to simulate the more than the 935 pumping wells; and 14 material layers are used to simplify the complex geology of the Toluca Valley (Calderhead et al., 2009c). Pumping rates are representative of the total pumping. Although higher pumping rates from fewer wells can locally lead to a misrepresentation of the drawdown and subsidence, the regional extent of the drawdown and subsidence is generally representative of the observed behaviour (Calderhead et al., 2009c).

Table 3 summarizes the variations of recharge used in the simulations. Projections involved using the HELP3 recharge model of the Toluca Valley (Calderhead et al. 2009a). Recharge was assumed to change as a function of climate change as outlined in the IPCC 2007 report (IPCC, 2007). Historical data and climate change predictions for the area were input into the model from 1970 to 2050 as shown in table 3. Recharge variations are not the focus of this study; for more information on recharge predictions for the Toluca Valley, see Calderhead et al. (2009a).

To consider past pumping volumes of groundwater for local use, historical studies were used (OEE, 1970; Ariel and Consultores, 1996; CNA, 2002; IMTA, 2003) and projections for future consumption were made using several assumptions. Projections of domestic use of groundwater are based on the population growth (INEGI 1960-2005). Over a 40 year period (2010-2050) projected annual population growth rates gradually decrease by 1.36 (1.34 to -0.2) for the average case (UNEP, 2008), 0.34 (1.34 to 1.0) for the worst case, and 1.64 (1.34 to -0.5) for the best case. Pumping for domestic was assumed to increase proportionally to the population increases.

The State of Mexico presently contributes to 9.7% of Mexico's Gross Domestic Product (GDP) (INEGI, 2009). If it is assumed that this percentage remains constant in time and that the Toluca Valley's percentage of GDP remains constant in time, then Toluca's

projected industrial use of water can also be based on Mexico's projected GDP (Hawksworth, 2006). Between 1989 and 1999, agriculture using irrigation fluctuated around 153 000 ha with no significant increase or decrease (INEGI 2001); therefore it is assumed that agricultural use of water remains constant.

Export volumes to Mexico City have not increased in the last 10 years (Legoretta, 1997; CNA, 2007), therefore a constant export volume (6.0 m^3/s) is assumed for the average projection. It is believed that legal action between the State of Mexico and Mexico City (Metropoli, 2008) will deter water exports from the Toluca Valley basin, and even decrease or stop altogether because the state of Mexico will be more protective of its water resources. Toluca and Mexico City are now faced with building new pumping well networks to provide for the growing water demand. As was done with the Toluca Valley over 40 years ago, adjacent basins are being drawn upon to provide for the more populated regions. The upper portion of the Balsas river basin (Systema Cutzamala) and areas around Valle de Bravo are currently being used or are seen as good possibilities to provide for Mexico City and Toluca (GEM, 2000).

Figure 5 shows the simulated pumping wells used for the various scenarios presented in table 4. Clay thicknesses are used to locate desirable areas for moving valley pumping wells (scenarios 7 and 8). The removed valley wells are mostly located in the urbanized part of the valley where clay thickness is high.

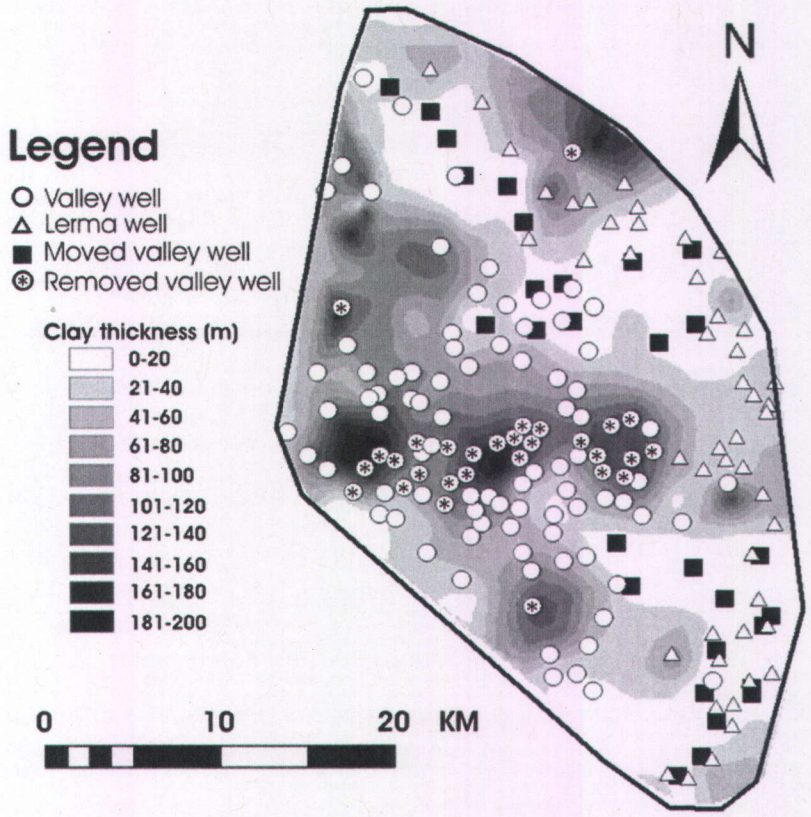


Figure 5: Simulated pumping wells with aggregate clay thickness

Table 3: Summary of the observed and expected groundwater recharge and pumping from 1970 to 2050.'-' implies data is not relevant. Recharge estimates are based on Calderhead et al. (2009a) and IPCC (2007).

			1970	1985	2000	2010	2020	2030	2040	2050
Recharge [Mm^3/year]	Historical Recharge		385,0	373,9	376,2	-	-	-	-	-
	Average		-	-	-	373,0	370,0	367,0	364,0	361,0
	Worst case		-	-	-	358,4	340,8	323,2	305,6	288,0
	Best case		-	-	-	377,8	379,6	381,4	383,2	385,0
Total pumping [Mm^3/year]	Domestic use	Historical	-157,68	-212,232	-266,8	-	-	-	-	-
		Average	-	-	-	-305,3	-345,6	-382,6	-409,9	-428,7
		Wost case	-	-	-	-248,0	-294,8	-344,8	-398,4	-456,9
		Best case	-	-	-	-396,1	-426,4	-448,9	-461,5	-463,1
	Exports to Mexico City	Historical	-189,2	-189,2	-189,2					
		Average	-	-	-	-189,2	-189,2	-189,2	-189,2	-189,2
		Wost case	-	-	-	-252,3	-252,3	-252,3	-252,3	-252,3
		Best case	-	-	-	-94,6	-94,6	-94,6	-94,6	-94,6
Relocation of wells	Well locations: See figure 4	Scenarios 1-6 (table 2)	curent	curent	curent	curent	curent	curent	curent	curent
		Scenarios 7,8 (table 2)	curent	curent	curent	**moved**	**moved**	**moved**	**moved**	**moved**

The following section explains the different combinations of the parameters in Table 3 that make up the scenarios.

Scenarios

Scenarios 1-3 (Table 4) examine worst case, best case, and average expected values based on table 3. Recharge (based on Calderhead et al., 2009a; and IPCC (2007)) and pumping are assigned their respective scenario based on table 3 with pumping divided into (A) exports to Mexico City and (B) local use. The pumping is divided into these two categories because local pumping is seen more as a function of a growing population whereas exports to Mexico City are largely considered to be a political issue and legal battles could potentially lead to decreasing exports. Exports to Mexico City are expected to increase (8 m^3/s) in the worst case scenario, decrease (3 m^3/s) in the best case scenario and remain constant (6 m^3/s) in the average expected scenario. A probable scenario is that pumping to Mexico City decreases thus scenarios 4 and 5 decrease exports to 0 m^3/s and 3 m^3/s respectively while keeping average estimates for all other parameters. Scenario 6 examines the possibility of decreasing pumping in Toluca (-25%) and Mexico City (-50%) to a more sustainable rate. Scenarios 7 and 8 make use of the clay thickness model (Figure 5) for moving pumping wells in areas with high clay content to areas with lower clay content. Scenario 7 assumes average expected pumping and scenario 8 decreases pumping rates to scenario 6 values. By decreasing pumping for local use within the valley, scenarios 6 and 8 imply inter-basin water transfer from surrounding basins.

Table 4: Pumping scenarios 2010-2050

Scenario	Lerma pumping (to Mexico City)	Toluca Pumping	Recharge	Description
1	33% increase	worst case	worst case	Worst case expected with 33% increased Lerma pumping
2	50% decrease	best case	best case	Best case expected with 50% decrease in Lerma pumping
3	constant at $6m^3/s$	average	average case	Average case with Lerma pumping constant at $6m^3/s$
4	Stop Lerma pumping ($0m^3/s$)	average	average case	Average case with stopping Lerma pumping
5	50% decrease	average	average case	Average case with a 50% decrease in Lerma pumping
6	50% decrease	decrease by 25%	average case	Decrease Lerma pumping by 50% and decrease Toluca Basin pumping by 25%
7	constant at $6m^3/s$	average	average case	Move pumping centres to locations with less clay (see figure 4)
8	50% decrease	decrease by 25%	average case	Move pumping centres to locations with less clay (see figure 4) and decrease Toluca Basin pumping by 25% and Lerma Pumping by 50%

3 RESULTS

Figure 6 presents the drawdown distribution, beginning from 1950 levels, for scenario 3 between 1962 and 2050. The regional drawdown began around 1962 and increases over the years because of the increasing groundwater budget deficit. By 1990 there is already a marked drawdown of over 40 m in the centre of the valley. This progresses significantly over the following 60 years by increasing to over 120 m, in the industrial corridor, by 2050. The simulated groundwater level decline between 1970 and 2009 agrees quite well with observed field data (Calderhead et al., 2009c).

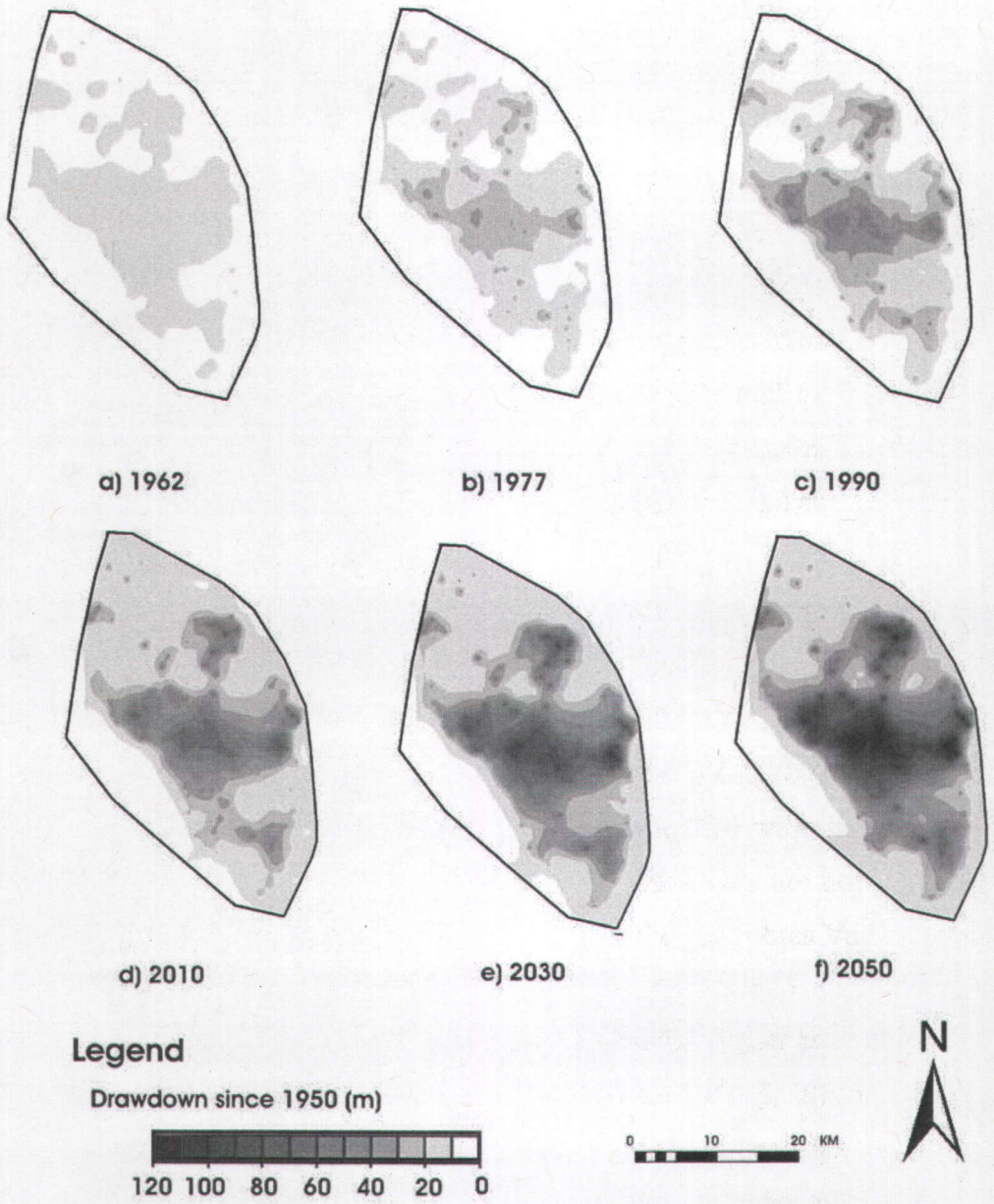


Figure 6: Simulated drawdown from 1950 levels in the valley between 1962 and 2050 (scenario 3).

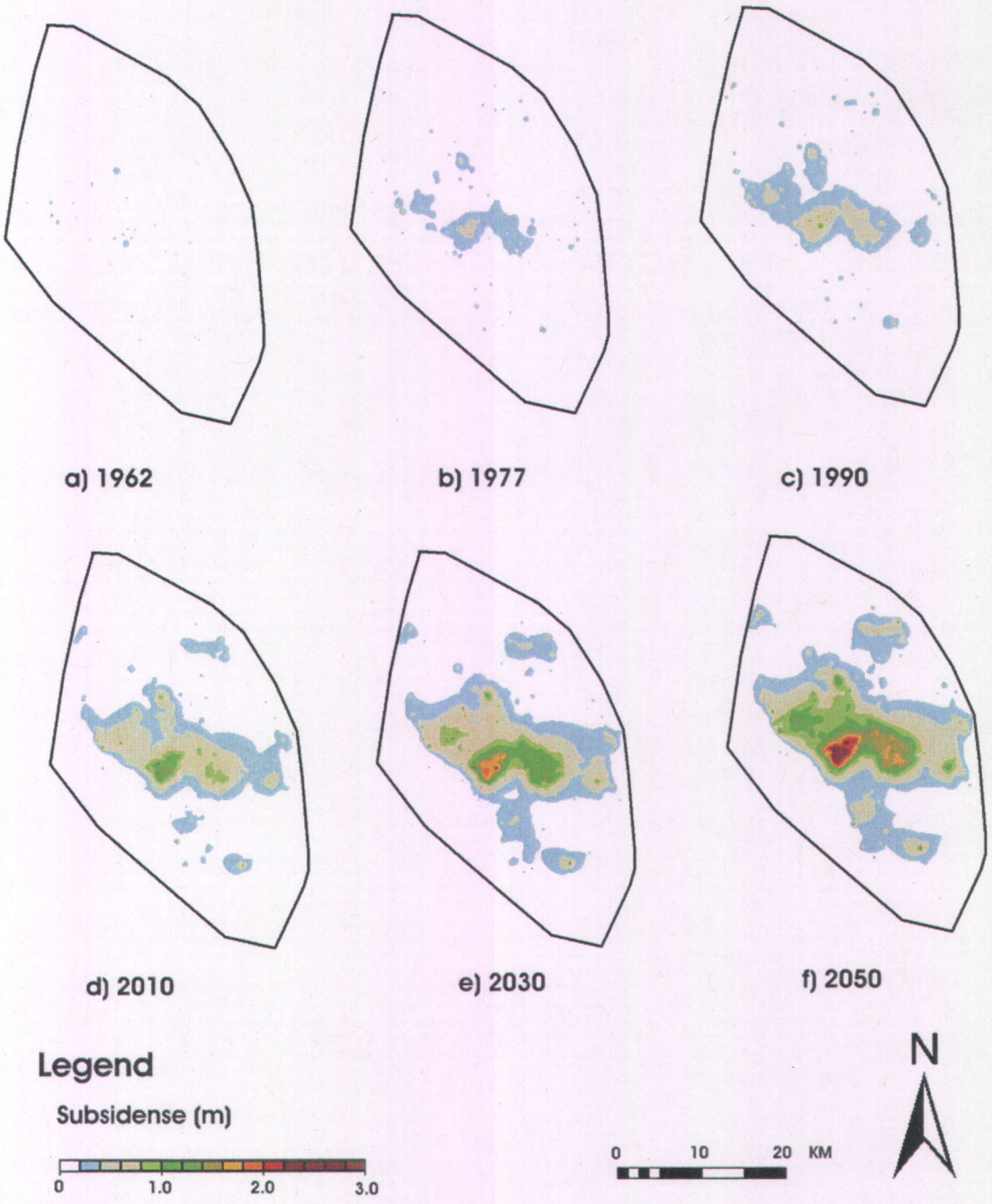


Figure 7: Total subsidence distribution between 1962 and 2050 (scenario 3).

Figure 7 shows the progression of total subsidence occurrences in the Toluca Valley. Results from 1962 to 2050 are based on the average expected scenario (scenario 3). Simulations begin in 1950 and only small occurrences of subsidence (< 0.4 m) are

observed in 1962. The occurrences are progressively larger from that point on and reach a maximum total subsidence of 3.8 m in 2050. The area of maximum subsidence is located in the industrial corridor (Figure 1) where high pumping rates, high drawdown, and thick compressible clay layers are observed.

Although very few studies have examined regional land subsidence in the Toluca Valley, remote sensing techniques and field data were used to calibrate the model (Calderhead et al., 2009b and Calderhead et al., 2009c) giving more confidence in the 2010 case (Figure 7d).

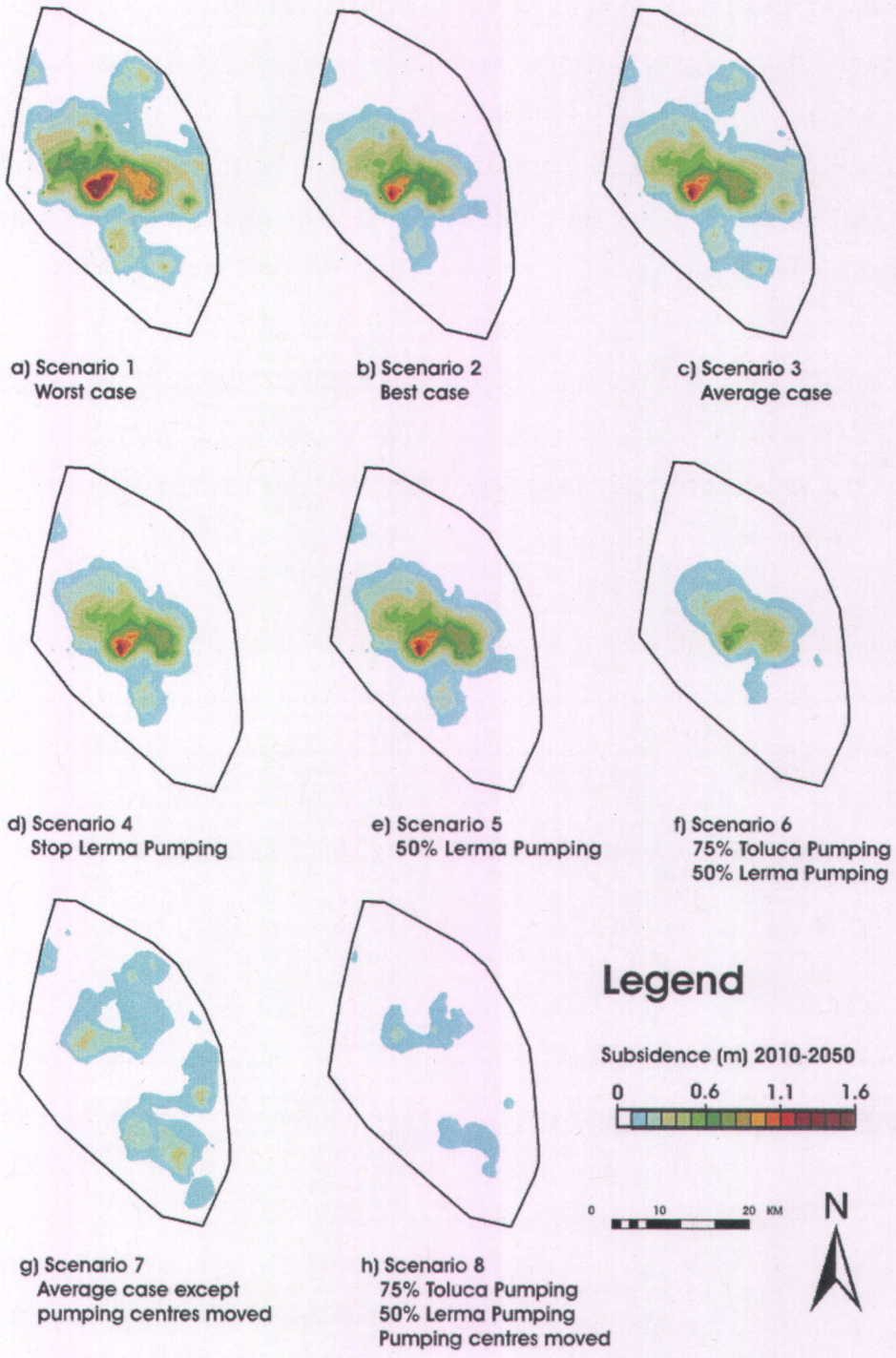


Figure 8: Simulation results for scenarios 1-8 showing total subsidence between 2010 and 2050.

Although pumping began before the 1960's it is estimated that regional land subsidence did not begin until heavy water exporting began in the late 1960's.

Figure 8 presents the total compaction results between 2010 and 2050 for the 8 scenarios. Scenarios 1-3 demonstrate the effects of worst, best, and average case scenarios for the climate change and pumping parameters. Maximum total subsidence reaches 2.2 m for the worst case scenario (scenario 1), 1.4 m for the best case scenario (scenario 2), and 1.6 m for the average expected subsidence (scenario 3). Compared to other scenarios, the spatial extent of the affected area is similar and the differences in subsidence magnitude are within 0.8 m for the 40 year period.

Comparing scenarios 3, 4 and 5 is of interest. There are only subtle differences between stopping exports (scenario 4) and cutting exports in half (scenario 5). However, there are noticeable differences between constant exports (scenario 3) and cutting exports in half (scenario 5).

The most marked change in subsidence occurs when moving the pumping centres (scenarios 7 and 8) away from compressible clays. Total compaction can be drastically reduced by simply moving the pumping centres to different locations within the valley. The most desirable results (scenario 8) show a localized maximum subsidence of < 0.3 m in 2050, otherwise there is only limited subsidence throughout the valley.

4 DISCUSSION

It is possible that the theoretical assumptions and modeling approximations, combined with a lack of representative geological, geomechanical, and hydraulic data has lead to unreliable numerical predictions. However, the calibration process for the Toluca valley flow and subsidence model (discussed more thoroughly in Calderhead et al., 2009c), increases our confidence in the simulation results.

Although the major factors controlling subsidence were varied in the simulations, for simplicity, some parameters that have an influence (e.g. geomechanical properties, extent of clay layers) were not varied. There is also uncertainty in the chosen parameters. For instance the population growth is based on UN estimates for the country. An earthquake

or a volcanic eruption in the valley would greatly throw off the population growth curve; hence the results should be viewed with caution.

Climate change plays only a minor role in the occurrence of subsidence (Table 3). The most important parameters controlling subsidence are export volumes to Mexico City, local pumping volumes, and relocating pumping wells within the valley. It is apparent that continuing at the current rates of water consumption will lead to more subsidence. Even in the best case scenario (scenario 2), maximum subsidence occurrences over a 40 year period (2010-2050) will reach 1.4 m.

Considering that the system pumping groundwater to Mexico City is mostly located in regions with low clay content and little difference is observed between scenarios 4 and 5, completely stopping exports to Mexico City (scenario 4) is not necessary for controlling the subsidence. However, decreasing exports by half, decreasing domestic-use pumping, and relocating wells, does have a positive effect on the overall water budget and subsidence. It can be argued that all scenarios will require inter-basin water transfer at a later date because the water budget deficit is not sustainable.

Importing water from adjacent basins becomes necessary when decreasing pumping within the valley. However, inter-basin water transfer alone is not sufficient for controlling the subsidence. It is shown that a very effective way of controlling subsidence is by relocating the pumping centres to other locations with low clay content. Had pumping not occurred in the in the most compressible layers and a pumping system been in place to pump water to the urbanized part of the valley, much of the land subsidence could have been avoided. When planning water imports to the Toluca Valley from untapped basins, one could learn from the past and avoid drilling new wells in locations with thick compressible clay units - whether for exporting or local use.

It is probably not feasible to stop, or even decrease, pumping in the urbanized part of the valley. A costly infrastructure project would be required to import the water into the basin and supply the water to users in the urbanized part of the valley. Considering the

likelihood of pumping continuing at current or greater rates, wells within the valley will probably be drilled to greater depths, further tapping the non-renewable resources and drawing on deeper, less potable water.

Simulating scenarios with the numerical model is a viable tool when considering water management for limiting subsidence occurrences. The approach can be useful to other cities currently considering expanding their water supply and results can be used by decision makers for better management practices.

Acknowledgements

We are thankful to the Ministère des Relations Internationales du Quebec, INRS-ETE, NSERC (a discovery grant held by Richard Martel), the Autonomous University of the State of México (UAEM), CONACyT, AUCC/IDRC, and the Ministère de l'Éducation du Québec for their financial support. We are appreciative of Sergio Murillo from the Commission National del Agua for logistical support on the field.

References

Ariel y Consultores (1996). Hydrodynamic modeling study and design optimization of the monitoring well networks for the aquifers of Caldera, San Luis Potosi and Toluca (Part 3: Aquifer of Toluca) Estudio de Simulacion Hidrodinamica y Diseno Optimo de las Redes de Observacion de los acuiferos de Calera, San Luis Potosi y Toluca (Tomo 3: Acuifero de Toluca). CNA (Comisión Nacional del Agua) México, DF, Unitecnia 308.

Bayer, P., Duran, E., Baumann, R., Finkel, M. (2009) Optimized groundwater drawdown in a subsiding urban mining area. Journal of Hydrology 365 (1-2), pp. 95-104.

Calderhead A. I., Martel, R. Rivera, A., Garfias, J., Therrien, R., An increasing groundwater budget deficit induced by urbanization, industrialization, and climate change in the Toluca Valley, Mexico. Hydrological processes. (Submitted 2009a).

Calderhead, A. I., Martel, R., Allasset, P-J., Rivera, A., Garfias, J, Land subsidence

induced by groundwater pumping, monitored by C-band D-InSAR and field data in the Toluca Valley, Mexico. Canadian journal of remote sensing (accepted, 2009b).

Calderhead A. I., Martel, R. Rivera, A., Garfias, J., Therrien, R., Simulating pumping-induced regional land subsidence in a complex aquifer system. Advances in water resources (to submit in November 2009c).

CNA, 2002. Determinacion de la disponibilidad de agua en el acuifero Valle de Toluca. CNA (Comisión Nacional del Agua) México, DF, Unitecnia: 26.

CNA 2007. Base de datos de los Aquiferos Nacional y Regional. Comisión Nacional del Agua.

Gambolati, G., 1972. A three-dimensional model to compute land subsidence. Bullet. Int. Ass. Hydrolog. Sci. 17 (1972), pp. 219–226.

Hawksworth J. 2006. The World in 2050: How big will the emerging market economies get and how can the OECD compete?, Pricewaterhouse Coopers, London, UK.

Helm, D. C., 1975. One-dimensional simulation of aquifer system compaction near Pixley, California, 1, Constant parameters, Water Resour. Res., 11, 465–478,

IMTA, 2003. Censo del utilización del agua en el valle de Toluca. Instituto Mexicano de Tecnologia del Agua.

INEGI, 1960. Censo general de población y vivienda 1960. Instituto Nacional de Estadística, Geografía e Informática.

INEGI, 1970. Censo general de población y vivienda 1970. Instituto Nacional de Estadística, Geografía e Informática.

INEGI, 1980. Censo general de población y vivienda 1980. Instituto Nacional de Estadística, Geografía e Informática.

INEGI, 1990. Censo general de población y vivienda 1990. Instituto Nacional de Estadística, Geografía e Informática.

INEGI, 2000. Censo general de población y vivienda 2000. Instituto Nacional de Estadística, Geografía e Informática.

INEGI, 2001. Instituto Nacional de Estadística, Geografía e Informática, Sinthesis of geographic information for the state of Mexico. Síntesis de información Geográfica del Estado de Mexico.

INEGI, 2005. Censo general de población y vivienda 2005. Instituto Nacional de

Estadística, Geografía e Informática.

INEGI, 2009 Instituto Nacional de Estadística, Geografía e Informática, Sinthesis of geographic information for the state of Mexico. Aportación al Producto Interno Bruto (PIB) nacional/ Contribution to Gross Domestic Product (GDP) http://cuentame.inegi.org.mx.

IPCC, 2007. Climate Change 2007: The Physical Science Basis. Contribution of Working Group I to the Fourth Assessment Report of the Intergovernmental Panel on Climate Change [Solomon, S., D. Qin, M. Manning (eds.)].

OEE, 1970. Los acuíferos del alto Lerma pub. No. 7, . report for Oficina de estudios especiales (OEE) de la CHCVM-SRH.

Larson, K.J., H. Basagaoglu, M.A. Marino. (2001) Prediction of optimal safe ground water yield and land subsidence in the Los Banos-Kettleman City area, California, using a calibrated numerical simulation model. Journal of Hydrology 242 (1-2), pp. 79-102.

Leake, S.A., and Galloway, D.L., 2007, MODFLOW ground-water model—User guide to the Subsidence and Aquifer-System Compaction Package (SUB-WT) for water-table aquifers: U.S. Geological Survey, Techniques and Methods 6–A23, 42 p.

Legorrreta J. 1997. Rainfall, the key to the future of the Valley of Mexico. La Jornada Ecologica, 5(58): 1-12.

Lesser y Asociados, S.A. (1992). Diagnostic study of the aquifer of the Valley of Toluca to implement a program for the extraction of groundwater. Estudio para el Diagnostico del acuifero del Valle de Toluca, para implementar la reglamentacion de la extraccion del agua subterránea.

Loukas, A.; N. Mylopoulos; L. Vasiliades. 2007. A Modeling System for the Evaluation of Water. Resources Management Strategies in Thessaly, Greece. Water Resour Manage (2007) 21:1673–1702

McLaren, R.G. (2005) User Guide: GRID BUILDER A pre-processor for 2-D, triangular element,finite-element programs, University of Waterloo - Groundwater Simulations Group.

Metropoli, 2008. Pierde Edomex batalla legal sobre acuíferos. In: Metropoli (Editor). Metropoli, Mexico, Mexico, last accessed June 4th 2008.

http://www.metropoli.org.mx/modules.php?name=News&file=article&sid=3439.

Municipio de Toluca (1999). ANÁLISIS DE PELIGROS POR REMOCIÓN EN MASA EN LA COLONIA RANCHO LA MORA Y LA DELEGACIÓN DE SAN PEDRO TOTOLTEPEC. Municipal Report 1999.

Ortega-Guerrero, A., D. Rudolph , and J. Cherry (1999), Analysis of Long-Term Land Subsidence Near Mexico City: Field Investigations and Predictive Modeling, Water Resour. Res., 35(11), 3327-3341.

Rejani, R. Madan K. Jha ; S. N. Panda ; R. Mull. 2008. Simulation Modeling for Efficient Groundwater Management in Balasore Coastal Basin, India. Water Resour Manage, 22:23–50.

Sakiyan, J. and Yazicigil, H. 2004. Sustainable development and management of an aquifer system in western Turkey. Hydrogeology Journal, 12:66–80.

Terzaghi, K. (1925). Earthworks mechanics based on soil physics. Erdbaumechanik auf bodenphysikalisher Grundlage, Franz Deuticke, Vienna.

Teatini, P., M. Ferronato, G. Gambolati, and M. Gonella (2006), Groundwater pumping and land subsidence in the Emilia-Romagna coastland, Italy: Modeling the past occurrence and the future trend, Water Resour. Res., 42, W01406, doi:10.1029/2005WR004242.

Therrien, R., .G. McLaren, E.A. Sudicky, S.M. Panday (2009) User Guide: HydroGeoSphere - A Three-dimensional Numerical Model Describing Fully-integrated Subsurface and Surface Flow and Solute Transport.

UNEP. 2008. Mexico's Annual population Growth Rate. United Nations Environment Programme data, http://www.unep.org/.

List of tables

Table 1: Problem setup 206

Table 2: Description of layer material properties for the Toluca Valley (after Calderhead et al, 2009). 206

Table 3: Summary of the observed and expected groundwater recharge and pumping from 1970 to 2050.'-' implies data is not relevant. Recharge estimates are based on Calderhead et al. (2009a) and IPCC (2007). 209

Table 4: Pumping scenarios 2010-2050 211

List of figures

Figure 1: Location map of the Toluca Valley and model domain boundary within the Republic of Mexico and the State of Mexico. Over 935 pumping wells are in operation in the Valley, including the Lerma System wells exporting water to Mexico City. The simulated region boundaries are shown in figures 5 to 8. 202

Figure 2: Recorded and expected population of the Toluca Valley from 1960-2050 (based on INEGI, 1960-2005 and UNEP, 2008) 203

Figure 3: Groundwater use in the Toluca Valley based on IMTA (2003) and modified from Calderhead et al. (2009a) 204

Figure 4: Processing chain for obtaining the 3D finite-element model domain. The 3D geology (A) is generated with the use of borehole logs and available cross sections, then using the 2D mesh (B) and the topography of the geologic layers, 15 topographically variable 2D layer meshes are extracted (C) and used to generate the 3D mesh (D). Location of the constant head boundary is also shown in B. Modified from Calderhead et al., 2009c..... 205

Figure 5: Simulated pumping wells with aggregate clay thickness 209

Figure 6: Simulated drawdown from 1950 levels in the valley between 1962 and 2050 (scenario 3)..... 212

Figure 7: Total subsidence distribution between 1962 and 2050 (scenario 3). 213

Figure 8: Simulation results for scenarios 1-8 showing total subsidence between 2010 and 2050..... 215

ANNEXES

ANNEXE A – ARTICLES DE CONFÉRENCES

ANNEXE A 1 – IAH/CNC 2006, VANCOUVER

A STUDY OF GROUNDWATER RESOURCES AND LAND SUBSIDENCE IN THE TOLUCA VALLEY, MEXICO

Angus I. Calderhead, Institut National de la Recherche Scientifique, University of Quebec, Québec, Québec, Canada
Richard Martel, Institut National de la Recherche Scientifique, University of Quebec, Québec, Québec, Canada
Jaime Garfias, Centro Interamericano de Recursos del Agua – Universidad Autónoma del Estado de México, Toluca, State of Mexico, México

ABSTRACT
The Toluca valley, situated within the high plateau of Central Mexico, experiences heavy groundwater extraction. Currently there is a net loss (recharge – extraction) of 166 M m^3 per year of groundwater within the upper Lerma basin aquifers. Ongoing work involves quantifying and predicting land subsidence associated with the lowering water tables and the high clay content found in the metropolitan area and the industrial corridor of Toluca.

RÉSUMÉ
La vallée de Toluca, située sur le haut plateau du centre du Mexique subit beaucoup d'extraction d'eau souterraine. Présentement il y a une perte d'eau (recharge – extraction) de plus de 166 M m^3 /année dans le bassin du haut Lerma. Les travaux en cours permettront la quantification et la prédiction de l'affaissement des sols associée (subsidence) à la baisse des niveaux d'eau et à la présence d'argiles retrouvée dans la zone métropolitaine et le corridor industriel de Toluca.

1. INTRODUCTION

The sustained growth in population in the Toluca Valley and neighboring Mexico City has primarily depended on the continuous development of both local and regional water resources for industrial, agricultural and domestic use. The Upper Lerma Basin, covering an area of approximately 2000 Km^2 (figure 1), is the focus of this study. Currently there is a significant net loss of water within the Upper Lerma Basin primary due to groundwater pumping, and the discrepancy is increasing with time. Stress on the aquifer has caused significant changes on the regional water flow patterns, a general reversal in the direction of hydraulic gradients, the disappearance of artesian springs and wetlands, and noticeable land subsidence within the basin.

This paper focuses on the excessive groundwater extraction occurring in the valley. We examine various changes in regional flow patterns, and ever decreasing groundwater levels throughout the valley. We examine modifications in the regional groundwater flow. We also estimate the current water balance deficit occurring in the upper Lerma basin.

A follow up study will include the quantification and prediction of aquifer compaction in the Toluca valley. Neighbouring Mexico City's land subsidence problems have been well documented. However, no comprehensive studies exist for the Toluca Basin. Of concern in this region is the total magnitude of the land subsidence and the future subsidence rate that is likely to result from current groundwater extraction.

2. BACKGROUND

2.1 Geographic setting

The Toluca Valley is located in a region known as the Highlands of Mexico in the central portion of the state of Mexico at an elevation of aproximately 2,580 ma.s.l. (Fig. 1).



Figure 1: Geographic setting of the Toluca Basin with respect to the State of Mexico and the Republic of Mexico

The upper basin of the Rio Lerma has an approximate area of 2000 km^2. It is located entirely in the state of Mexico. The entire Lerma River is 560 km long and crosses 5 states before ending in the Pacific Ocean.

The Toluca valley is where the Lerma river's headwaters originate; this valley is an important urban center with major industry occurring along with significant agricultural activities. Industrialization has led to an increase in the number of inhabitants over the course of the last four decades.

2.2 Climate

The following section gives an overview of the major climate parameters. Precipitation, Temperature, and Evapotranspiration were examined by looking at 39 climate stations located throughout the valley. Data was somewhat irregular and sometimes incomplete, however averages were obtained from the years between 1946 and 2000 (SICHEM 2004). See Figure 2 for the average annual precipitation, temperature and evapotraspiration recorded by a climate station located in the central plane of the valley. Climate stations in higher altitudes had considerably different data and will be discussed in the following sections.

2.2.1 Precipitation

Total annual rainfall varies from 1,300 mm in the highest areas to 750 mm in the center of the valley. The most intense rainfall is in the highest sectors, where 80 to 120 mm can fall in a single day. Rainfall over the rest of the area is between 60 to 80 mm/day. Approximately 90% of the rainfall occurs between May and October (SICHEM 2004).

2.2.2 Temperature

In the Toluca valley the annual average temperature ranges from 12 to 16 °C, with May being the warmest month (14–15 deg C) and January the coldest (11–12 deg C), while in the mountainous areas the annual average is 12–14 deg C, with a minimum in the Nevado de Toluca (annual means from 2 to 5 deg C) (SICHEM, 2004).

2.2.3 Evapotranspiration

Estimates of real evapotranspiration, using Turc's Method, range from 754 to 453 mm, with an average of about 579 mm, where maximum values were recorded in April and May and minimum ones in January and December (SICHEM, 2004).

2.2.4 Infiltration

Vertical recharge due to infiltration has been estimated to be between 2 % and 11% of total precipitation (Lesser 1992, CNA 1996b, CNA 2000, GTZ-CAN 2004).

Current work involves discretizing the infiltration pattern throughout the valley using discretized soil, precipitation and evapotranspiration data. This will be used to obtain a more accurate recharge rate occurring in the valley. We have also installed a network of pressure transducers that take a water level reading twice daily. These levels will also enable us to better measure the recharge due to infiltration.

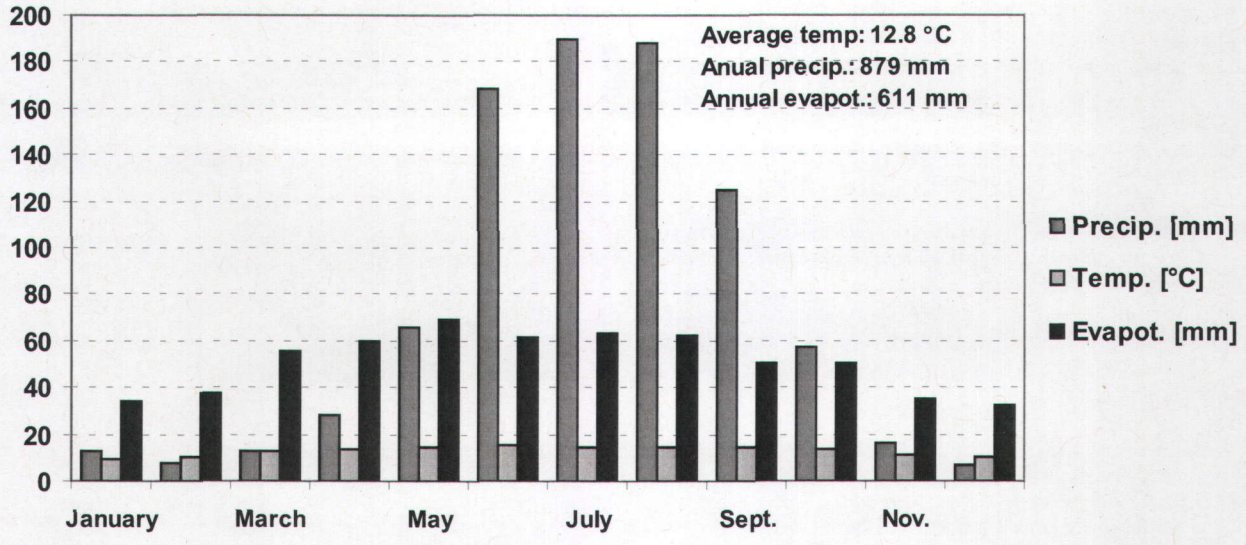


Figure 2: Annual precipitation, temperature, and evapotranspiration at a climate station in the central plain of the Toluca Basin. Averages taken for the years between 1971 and 1999.

2.3 Geology

The Lerma River Basin is located within the Transmexican volcanic belt in central Mexico (CNA 1996a). This region was a tectonically active zone in the Upper to Mid-Tertiary period (around 23 million years ago) forming a series of northwest-southeast trending fault systems throughout much of southern Mexico (DGCOH 1992).

deposited in the Pliocene period (around 3 million years ago) and extends from the flanks of the Sierra de las Cruces mountains in the east across the basin floor to the foot of the Nevado of Toluca volcano (Figures 1 and 3) (DGCOH 1992). This formation is a heterogeneous mixture of volcaniclasitc materials (DGCOH 1992). The basaltic flows of the Chichinautzin formation were deposited in the eastern portion of the Lerma River Basin in the Pleistocene and Holocene periods (CNA 1996b). This formation is composed of volcanic flow and ash materials and has a lower fracture density than the Tarango formation (DGCOH 1992).

The Nevado de Toluca volcano see (figures 1 and 3) is primarily composed of dacite and andesite lava flows with a core of andesite. During the Pleistocene, cinder cones formed atop the flanks of the volcano after which andesitic and basaltic lava flows were deposited in the Holocene (CNA 1996b). Basaltic lava flow materials from the Sierra de las Cruces mountain chain along the eastern edge of the basin, and the Nevado de Toluca volcano to the west, are interbedded with erosional deposits from the surrounding mountains. These sediments are further overlain by younger fluvial deposits from the Lerma River and lacustrine sediments from the ancient lakes that extended throughout the basin interior (Figure 3) (CNAb 1996).

Volcanic alluvium, eroded from the flanks of the surrounding highlands, is composed of sand and gravel (DGCOH 1992). Lacustrine materials, consisting of fine sand, silt and clay (DGCOH 1992) were deposited in the Late Pliocene, above the alluvium (CNA 1996b). The fluvial sediments are composed of fine to coarse sand sized particles and are interbedded with the lake sediments (DGCOH 1992). Alluvium thickness increases towards the basin interior to a maximum depth of 200 m (CNA 1996b).

2.4 Population density

The largest single factor controlling future growth and development of the State of Mexico is considered to be the availability of water for irrigation of agricultural fields, potable drinking water and industrial use (Diez Perez 1998).

Figure 4 demonstrates the rapid growth occurring in the Toluca valley, an area of approximately 2000 km^2 where since the 1960's the population has approximately doubled every 20 years This growth has had a deep impact on the groundwater resources in the Toluca Valley.

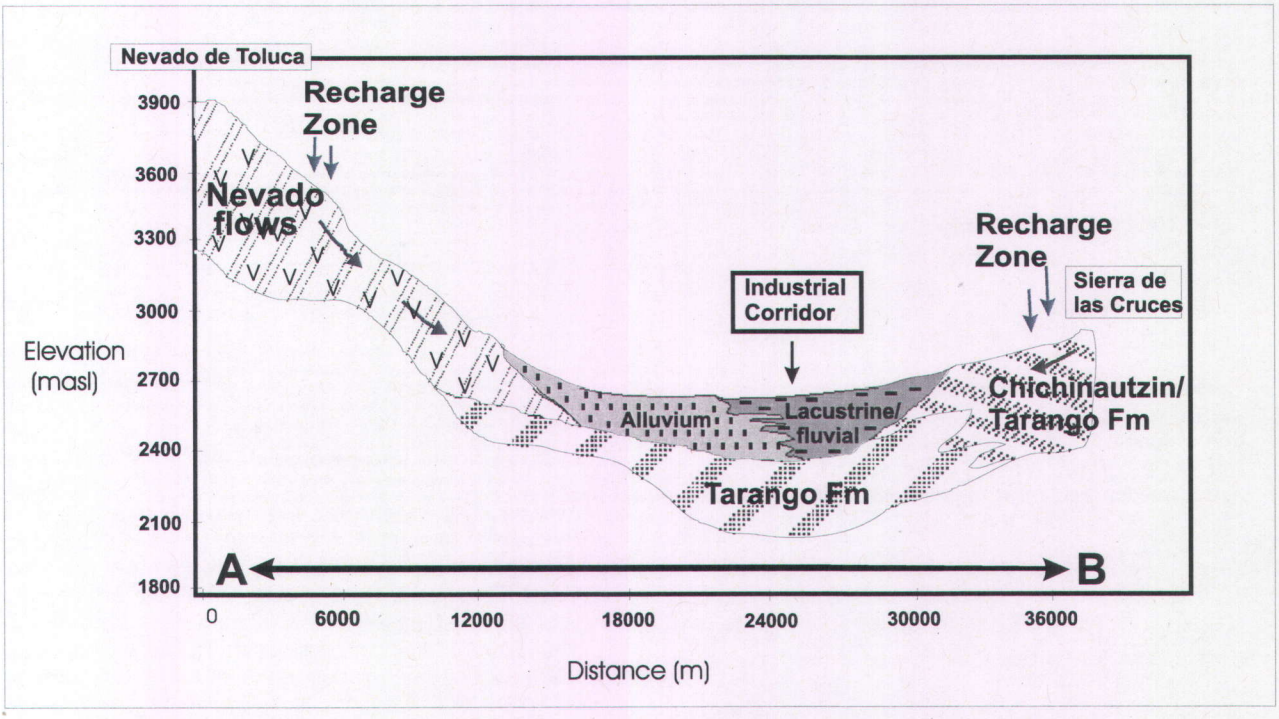


Figure 3: General basin geology: west-east cross-section (A-B) (see figure 1) through the southern Lerma River Basin from Nevado de Toluca volcano to the foothills of the Sierra de las Cruces mountains. The primary recharge areas and general direction of groundwater flow are also indicated in the diagram. Modified from Rudolph et al. (2006) and CNA (1996b).

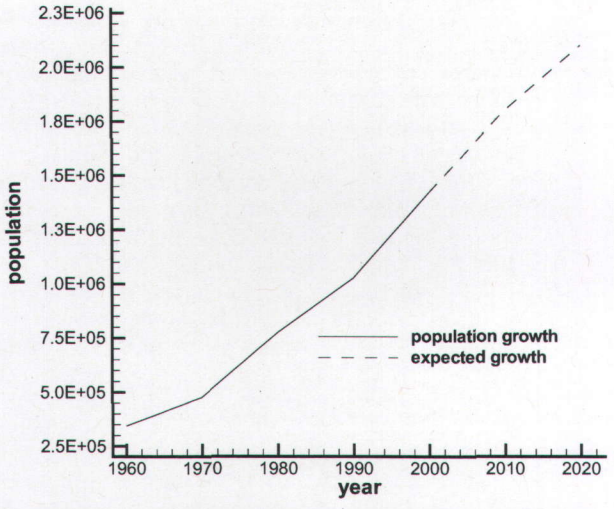


Figure 4: Population growth in the Toluca valley. Data from INEGI 1960, INEGI 1970, INEGI 1980, INEGI 1990, INEGI 2000.

If the population continues to increase at the same rate as the current one, there is no question that there will be a shortage of water in the foreseeable future. This problem is similar to the problems of Mexico City where, ironically, in the late 1960's Mexico City started importing water from the Toluca Basin, now the Toluca basin can no longer support its own or Mexico City's water demands. The end result is that people will either have to move away from the urban center or water will have to be imported from abroad.

3. HYDROGEOLOGY AND GROUNDWATER EXPLOITATION

The following section is divided as follows: regional flow, population density, groundwater extraction, water balance in the Toluca valley, and regional depletion of groundwater levels and reversal of vertical hydraulic gradients.

3.1 Regional flow

Precipitation in the higher altitudes infiltrates to recharge the Lower aquifer unit of the Tarango formation, where the volcanic sediments are exposed to the surface. Recharge to the Upper aquifer system is thought to be along the flanks of the highlands surrounding the Lerma River Basin, and in the basin interior where the Lower aquifer is covered by low permeability clay (DGCOH, 1992).

Infiltration from the Nevado de Toluca volcano travels east, below the valley floor, towards the location of the ancient lakes and the Lerma River (Gobierno del Estado de Mexico 1993, Lesser 1992). Groundwater flows from the volcano also travels to the north towards Ixtlahuaca (Lesser 1992). Recharge waters within the eastern mountain chain of Las Cruces, flow west to the foot of the range, towards the Laguna Almoloya and the Lerma River (Gobierno del Estado de Mexico 1993).

3.2 Groundwater extraction

Groundwater extracted in the Lerma River Basin is divided between local use and exports to Mexico City. Locally, water is used as a potable water resource, irrigation of land and supplies industrial practices. In a 2002 census, a total of 448,476,824 m^3 was calculated to have been extracted during that year through the 930 wells and springs that are tapped within the whole basin (IMTA 2003). Most of the extraction is occurring in the metropolitan area of Toluca and the Industrial corridor.

The Industrial Corridor is located on the main highway between Mexico City and Toluca. The Corridor is a newly developed and highly concentrated industrial zone. After the destructive 1985 earthquake in Mexico City, many industries, previously located in the Valley of Mexico were displaced to the Toluca Basin to more stable ground (Garfias Soliz 1997).

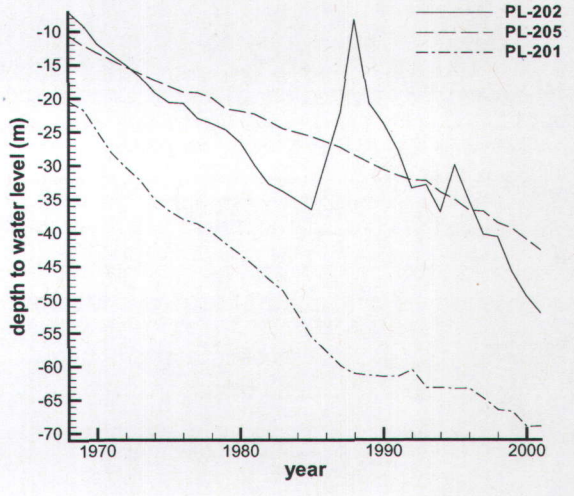


Figure 5. Hydraulic head at wells located within the Industrial corridor. Measurements were taken at least 4 times per year since 1968.

There is a high concentration of deep production wells in the Industrial Corridor that provide water to meet the needs of industrial production. The most significant hydraulic head decreases over the last 4 decades have occurred around the City of Toluca and the Industrial corridor. The lowering of the hydraulic heads is noted in Figure 5 where 3 monitoring wells have recorded significant decreases in water levels over the past 35 years. Drawdown rates of over 1.4m/year are common in this area. Measurements were taken from the lower aquifer at a depth of approximately 150 m. The well PL-202 has a peak occurring in the late 80's, this abnormality is associated with an artificial recharge program that occurred some time between 1984 and 1990 near the well. Other than the peak in the mid to late 80's, the groundwater levels continue to lower.

3.3 Water balance in the Toluca Valley

With excessive extraction occurring in the Toluca valley an accurate water budget of the system has become an important parameter in determining ways of managing the aquifer's resource and minimizing negative impacts. Several attempts have been made to properly determine the water budget, with varying success.

The water budget can be written as:

$$P + Q_{on} = ET + \Delta S + Q_{off} \qquad (1)$$

(from Healy and Cook (2002))

where P is precipitation plus irrigation; Q_{on} and Q_{off} are surface and subsurface water flow into and out of the basin; ET is the sum of bare-soil and open-water evaporation and plant transpiration; ΔS is change in water storage; and all components are given as rates.

Table 1. Assessments of the availability of water in the Toluca Valley Aquifer. All values in Millions of m^3/year. Modified from CNA, 2000.

Source	1970	1996	2000	*2003
Entrants				
Groundwater (Nevado)	-	94.5	94.6	94.6
Groundwater (Las Cruces)	-	63	63.07	63.07
Vertical recharge	-	98	177	177
Total Entrants	**342.1**	**256.5**	**336.76**	**336.76**
Flow out of the Basin				
Groundwater outflow	2	-	-	-
extraction	353.9	327.4	422.34	449
Evapotranspiration	-	14.7	-	-
Natural discharge (rivers and springs)	-	-	53.6	53.6
Total output	**359.9**	**342.1**	**475.95**	**502.6**
Water Balance Deficit	**-13.8**	**-85.5**	**-139.19**	**-165.84**

- no data

* 2000 data except for extraction

Several studies have examined the water balance in the Toluca Valley including OEE (1970); Lesser (1992); CNA (1996b); CNA (2000); and most recently GTZ-CNA (2004). Some of the studies are incomplete and lacking a detailed analysis. However, a more rigorous estimate of recharge and discharge has been estimated in the 1996 and 2000 studies respectively. Table 1 displays four studies that have examined the water balance of the Toluca Valley Basin.

The CNA (1996b) study is used to estimate recharge and discharges such as groundwater discharge and river and stream discharge. IMTA's (2003) study, determined that 449M m^3/year was extracted from the valley, and this value was used for the extraction parameter. This rate has a considerable effect on the water balance.

Using the data from the 2000 study and modifying the extraction rates using the IMTA (2003) data, the water balance deficit would be placed at 166 M m^3 /year. This deficit will only continue to rise due to the expected population increase.

3.4 Regional depletion of groundwater levels and reversal of vertical hydraulic gradients

Regional groundwater flow was previously primarily from south to north from the Toluca Basin to the Ixtlahuaca/Atlacomulco Basin (CNA 1996b). Increased pumping of deep wells throughout the basins has, however, altered groundwater flow directions in the Lerma River Basin forming a depression cone in the metropolitan area of the valley.

Historically, groundwater levels in the Lerma River Basin were near-surface and emerged above the land surface in the vicinity of the ancient lakes on the eastern basin floor (Lesser 1992). Evidence of flowing artesian conditions has been documented by the National Water Commission (CNA) through water level measurements in deep monitoring wells in the middle of the basin. Lowering of the regional water levels, presumably due to heavy groundwater extraction in the basin, has been recorded in many studies (Gobierno del Estado de Mexico 1997, DGCOH 1992, DGCOH 1997, UAEM 1993, CNA 1997, CNA 1996b, CNA 2000, GTZ-CNA 2004).

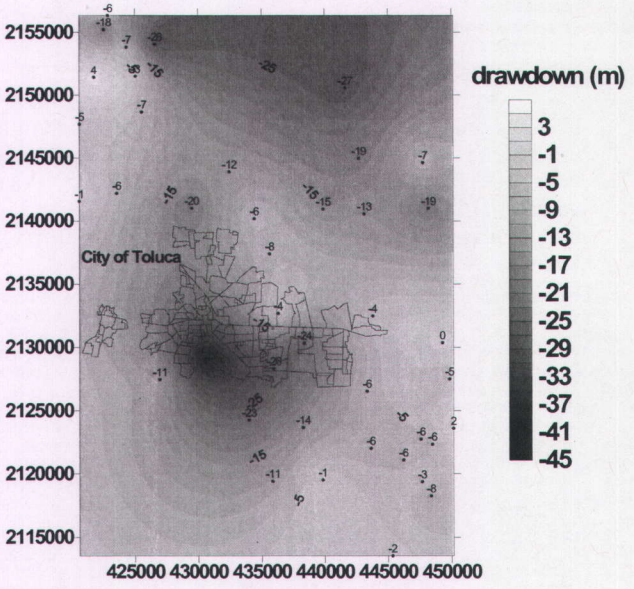


Figure 6: Difference in hydraulic heads between 1970 and 2004. Measurements were taken in the lower aquifer at the 150 m depth. Ticks represent UTM coordinates and are marked every 5 km on the X and Y axis.

The CNA has recorded hydraulic heads with the use of multilevel piezometers of depths ranging from 10m to 150m from 1968 to 2006 in over 50 wells within the Toluca Basin. This valuable data has enabled researchers and water management experts to evaluate the ongoing depletion of groundwater in the Toluca Basin. The drawdown occurring between 1970 and 2004 throughout the valley is displayed in Figure 6. The metropolitan area of Toluca is also noted in the figure.

We notice a systematic decrease throughout almost the entire valley with maximum drawdowns (43 m) occurring around the City of Toluca.

The Systema Lerma, situated along the upper section of the Lerma river, gathers a large portion of the recharge water entering from the sierra las Cruces (figure 1).

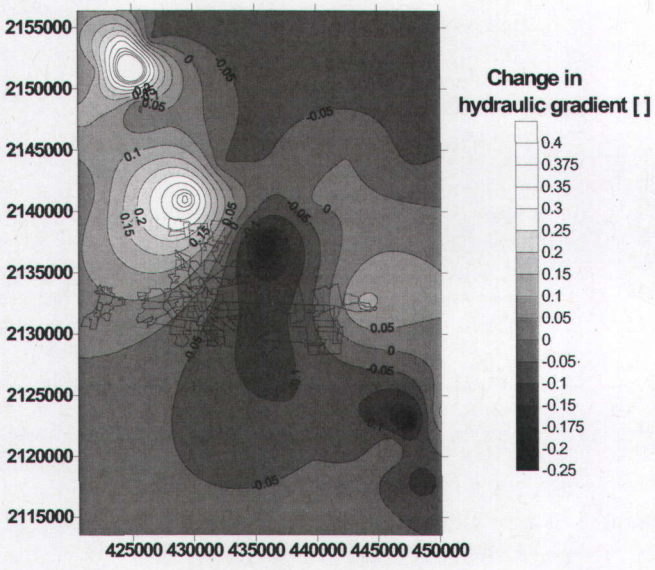


Figure 7: Change in hydraulic gradient between 1970 and 2004. Gradients were taken between upper and lower aquifers and the gradient values of 2004 subtracted from the values of 1970 to obtain the differences. Gradients were obtained between 150 m to 15 m depth. Positive values show an increase in gradients upward and negative values show an increase in gradients downward. Ticks represent UTM coordinates and are marked every 5 km on the X and Y axis.

There is evidence of downward hydraulic gradients between the shallowest and deeper wells. As a general rule the hydraulic gradients in 2004 were downward and in 1970 were more upward, neutral or only slightly downward. The resulting difference shows that a majority of the region has had an increase in downward vertical hydraulic gradients (Figure 7). In the North West part of the valley, away from the City of Toluca, upward gradients were stronger. The strongest decreases in hydraulic gradients were noticed close to the metropolitan area of Toluca.

4. LAND SUBSIDENCE

This next section examines land subsidence. A more detailed paper on subsidence will be presented once all data is assembled and treated. The land subsidence section is divided into: Background of subsidence in the Toluca Valley, Theory, and Ongoing Work.

4.1 Background of subsidence in the Toluca Valley

Directly related to the drop in groundwater levels is the occurrence of land subsidence throughout the valley. We have observed several sites in the Toluca Valley where land subsidence is occurring. This takes place in the form of vertical land movement and the occurrence of fractures, usually in areas where there is heavy groundwater extraction. The village of San Pedro Totoltepec, 7km East from the center of Toluca and adjacent to the industrial corridor, has experienced severe land subsidence in the past 10 years. Many buildings have cracked walls or foundations, and several houses are no longer livable.

The clay content combined with heavy groundwater extraction in the central part of the Toluca basin is conducive for land subsidence and the occurrence of fractures (ICGA 1977a). Several sites, especially in and around the industrial corridor have had severe problems associated with land subsidence. The lacustrine clay and alluvial deposits reach 150 m in thickness in these areas implying that there is a large potential for compaction.

Very few studies have been carried out on subsidence in the Toluca valley. However, some studies examined the effects of the fractures on the structures of the valley (ICGA 1977a, ICGA 1977b Consultec 1978, Consultec 1979).

The dependency on the semiconfined aquifer system within the Toluca Valley will likely remain high or even increase into the future. Due to this fact, accurate predictions of long-term land subsidence phenomena will be crucial.

4.2 Theory

Subsidence is often caused by groundwater extraction. Groundwater pumping entails a drop in the pressure head or hydraulic head and an increase in effective stress. This was first noted by Meinzer and Hard (1925) and Meinzer (1928). At the same period Terzaghi (1925) established that :

$$\sigma = \bar{\sigma} - p \qquad (2)$$

σ = total stress

$\bar{\sigma}$ = effective stress

p = water pressure (positive for compression)

Terzaghi's one-dimensional theory was then developed by Biot (1941) who considered consolidation as a three dimensional phenomenon. Biot's formulation has a simultaneous solution for two variables : water pressure and deformation within the matrix. In this case horizontal and vertical displacement can be obtained at each point within the 3 dimensional domain. Biot's approach is probably the best way for calculating surface deformation but it is mathematically intensive because it accounts for the two parameters (water pressure and deformation) in three dimensions. Biot's approach was later extended to encompas anisotropic material properties (Biot 1955); Caroll 1979)).

4.3 Ongoing work

Ongoing work includes the examination of regional land subsidence with the use of InSAR (Synthetic Aperture Radar Interferometry) images obtained from the European Space agency's ERS-1, ERS-2 and Envisat Satellites.

InSAR (Synthetic Aperture Radar Interferometry) is a new remote sensing method used in several fields to measure displacements on the ground. The development of the InSAR techniques, using radar satellites, gives us the possibility of measuring vertical displacements of the ground surface with a precision of one centimetre to a few millimetres on areas extended with very good space details (10-100 km^2) (Amelung et al. 1996, Galloway 1998, Hoffman et al. 2001, Hoffman 2003). Data from years 1995, 1996, 2001, 2002, and 2006 will be used to produce subsidence maps of the Toluca Valley.

The study of land compaction will be done on a regional scale on Toluca valley. Our findings will be verified by in-situ extensometers (Roctest ltd. R-4, Montreal Canada) installed in the industrial corridor where the most significant drops in groundwater levels are found. From field observations, San Pedro Totoltepec has had at least 2 m in subsidence in some areas over the past 10 years. This is where the first extensometer has been installed. This extensometer measures compaction in the upper 80 m of the clay and alluvium. The second extensometer has yet to be installed but will be placed throughout the clay and alluvium media (up to 150 m) to use the bedrock as a benchmark for measuring vertical movement.

The final aspect of this study will be to incorporate a subsidence module (based on either a 1-D Terzaghi model or a 3-D Biot model) into the HydroGeosphere finite element model (Therrien and Sudicky 1996) whereby future land subsidence occurrences will be simulated and predicted.

5. CONCLUSIONS

We have seen that heavy groundwater extraction is occurring in the Toluca valley and will likely continue and even increase in the future. A modification of the groundwater flow system including the lowering of water levels, the reversal of vertical hydraulic gradients, the disappearance of springs and the occurrence of land subsidence are all indications that the current rates of pumping are not sustainable. There is currently a water budget deficit of over 166 M m^3/year in the Toluca basin.

Deep monitoring wells have experienced a drop of over 1.4 m/year, the highest drawdown's being in and around the metropolitan area of Toluca and the industrial corridor.

The occurrence of land subsidence in the industrial corridor and the metropolitan area of the city of Toluca is of concern. Ongoing work will add to the quantification and prediction of land subsidence occurring in the Toluca Valley.

6. ACKNOWLEDGEMENTS

The writers would like to acknowledge the financial support and contributions from the Ministere de l'Education- Quebec, The Association of Universities and Colleges of Canada, the International Development Research Center, the Ministère des Relations International – Quebec, and INRS. From our partners in Mexico, we would like to thank the Universidad Autónoma del Estado de Mexico and the Comisión Nacional del Agua.

7. REFERENCES

Amelung F., Galloway, D.L., Bell, J.W., Zebker, H.A., and Laczniak, R.J., (1996). Sensing the ups and downs of Las Vegas: Insar reveals structural control of land subsidence and aquifer-system deformation. *Geology.* 27(6) pp. 483-486

Biot, M.A. (1941) General theory of three dimensional consolidation. *Journal of Applied physics.* 12:155-164

Biot, M.A. (1955) Theory of elasticity and consolidation for porous anisotropic solid. *Journal of Applied Physics.* 26(2): 182-185. February 1955.

Carroll, M.M., (1979) An effective stress law for anisotropic clactic deformation, *Journal of Geophysical Research*. 84(13):7510-7512,

Consultec, S.A. (1979). Estudio del comportamiento de grietas en el valle del Alto Lerma. Para la CAVM. SARH.

Consultec, S.A. (1978). Estudio del comportamiento de grietas en el valle del Alto Lerma. Para la CAVM. SARH.

CNA (Comisión Nacional del Agua) (1996a) *Estudio para el diseño de Redes de Monitoreo de los acuíferos de los Valles de Toluca y Atlacomulco-Ixtlahuaca, en el Estado de México; Tomo I: Informe y Tomo II: Anexos.* México, DF, Unitecnia, 66 pp

CNA (Comisión Nacional del Agua) (1997) *Actualización de Mediciones Piezométricas de los acuíferos Reactivados en los Valles de Toluca y Atlacomulco-Ixtlahuca, en el Estado de México*, México, DF, Unitecnia, 26 pp

CNA (Comisión Nacional del Agua) (1996b) *Estudio de Simulación Hidrodinámica y Diseño Óptimo de las Redes de Observación de los acuíferos de Calera, San Luis Potosí y Toluca (Tomo 3: Acuífero de Toluca)*, México, DF, Unitecnia, 308 pp

CNA (2002) Comisión Nacional del Agua, Determinación de la disponibilidad de agua en el acuífero valle de Toluca, Estado de México,

DGCOH (1992) *Estudio Hidrogeológico Regional de los Valles de Toluca e Ixtlahuaca: Tomo I* (Regional hydrogeologic study of the Valleys of Toluca and Ixtlahuaca: Part I), 214 p

DGCOH (1997) *Estudio de Evolución de Niveles Piezométricos en la Cuenca del Alto Lerma para el periodo 1985-1997: Informe Final* (Study of the evolution of piezometric levels in the Upper Lerma

Basin from the period 1985–1997), 47 p
Diez Perez, J.A. (1998) Análisis de las zonas de recarga de acuíferos mediante la percepción remota: Aplicación a la cuenca de Almoloya del Río. M.Sc. Thesis. UAEM:CIRA. 142 pp,
Galoway, D.L., Hudnut, K.W., Ingebritsen, S.E., Phillips, S.P., Peltzer, G., Rogez, F., and P.A. Rosen. (1998) Detection of aquifer-system campaction and land subsidence using interferometric synthetic aperture radar. Antelope Valley. Mojave Dert, California. Water Resources research, 34(10):2573-2585
Gobierno del Estado de México (1993) *Atlas Ecológico de la Cuenca Hidrográfica del Río Lerma: Tomo I: Cartografía,* Comisión Coordinadora para la Recuperación Ecológica de la Cuenca del Río Lerma, 126 p
Gobierno del Estado de México (1997) *Atlas Ecológico de la Cuenca Hidrográfica del Río Lerma; Tomo III (Impacto de las actividades productivas en el suelo) y (Un recurso escaso, valioso y necesario: El agua)* Comisión Coordinadora para la Recuperación Ecológica de la Cuenca del Río Lerma, 138 p
GTZ-CNA, (2004) Deutsche Gesellschaft fur Technische Zusammenarbeit - Comisión National del Agua, Modelo de Simulación Hidrodinámica del Acuífero del Valle de Toluca, Estado de México.
Healy, R.W., and Cook, P.G., (2002), Using groundwater levels to estimate recharge: *Hydrogeology Journal*, 10:91-109
Hoffmann, J., Galloway. D.L., Zebker, H.A., and Amelung, F. (2001) Seasonal subsidence and rebound in Las Vegas, Nevada, observed by synthetic apertura radar interferometry. *Water Resources Research*. 37(6): 1551-1556.
Hoffman J., (2003). The application of satellite radar interferometry to the study of land subsidence over developed aquifer systems. Ph.D. Thesis, Stanford University
IMTA (2003) - Instituto Mexicano de Tecnologia del Agua, Censo del utilización del agua en el valle de Toluca.
Ingenieros Civiles y Geólogos Asociados, S.A. Actualización del levantamiento de grietas en los valles de Toluca e Ixtlahuaca-Atlacomulco, CAVM-SARH, 1977.
Ingenieros Civiles y Geólogos Asociados, S.A. Investigaciones geofísicas para la detección degrietas en los valles de Toluca e Ixtlahuaca-Atlacomulco CAVM-SARH, 1977.
INEGI (1960) Instituto Nacional de Estadística, Geografía e Informática, Censo general de población y vivienda 1960.
INEGI (1970) Instituto Nacional de Estadística, Geografía e Informática, Censo general de población y vivienda 1970.
INEGI (1980) Instituto Nacional de Estadística, Geografía e Informática, Censo general de población y vivienda 1980.
INEGI (1990) Instituto Nacional de Estadística, Geografía e Informática, Censo general de población y vivienda 1990.
INEGI (2000) Instituto Nacional de Estadística, Geografía e Informática, Censo general de población y vivienda 2000.
Lesser y Asociados, S.A. Estudio para el diagnóstico del acuífero valle de Toluca, para implementar la reglamentación de la extracción del agua subterránea. GEM, 1992.
Meinzer, O.E.. Compressibility of Artesian Aquifers. Econ. Geology. 23 (3): 263-291, 1928.
Meinzer, O.E., and H. A. Hard. (1925) The artesian water supply of the Dakota sandstone in North Dakota with special reference to the Edegeley quadrangle. Water-Supply paper 520-E. U.S. Geological Survey,
Rudolph, D. L., Sultan, R. , Garfias J., McLaren R. G., Significance of enhanced infiltration due to groundwater extraction on the disappearance of a headwater lagoon system: Toluca Basin, Mexico *Hydrogeology Journal* 14: 115 - 130
Oficina de estudios especiales (OEE) de la CHCVM-SRH los acuíferos del alto Lerma pub. No. 7, 1970.
SICHEM, Sistema de Information para las cuencas hidrologicas del estado de Mexico, 2004.
Sultan R (2001) Impacts on wetland hydrology from extensive groundwater Extraction: Lerma River Basin, Mexico. M.Sc., University of Waterloo, 225 p
Terzaghi, K., 1925, Erdbaumechanik, Franz Deuticke, Vienna
Therrien, R., Sudicky, E.A., (1996) Three dimensional analysis of variably saturated flow and solute transport In discretely fractured porous media. *Jour. Contam. Hydrology*, 23, 1-44.
UAEM (1993) Problemática Ambiental de los Recursos Hídricos en la Cuenca Alta del Río Lerma Seminario Ambiental sobre el Ambiente 1:170–181

ANNEXE A 2 – IEEE IGARSS 2009, CAPE TOWN

C-BAND D-INSAR AND FIELD DATA FOR CALIBRATING A GROUNDWATER FLOW AND LAND SUBSIDENCE MODEL

Angus I. Calderhead[1], Richard Martel[1], Alfonso Rivera[2], Jaime Garfias[3], Pierre-Jean Alasset[4]

[1]Institut national de la recherche scientifique - Centre Eau, Terre & Environnement (INRS-ETE)
[2]Geological Survey of Canada, Natural Resources Canada, (GSC)
[3]Universidad Autónoma del Estado de México, Facultad de Ingeniería (CIRA)
[4]C-CORE

7.1.1.1 ABSTRACT

Differential Synthetic Aperture Radar Interferometry (D-InSAR) is a powerful technique used for detecting and measuring surface deformation with sub-centimetre accuracy. Using C-band data from three different satellites, the D-InSAR technique is used to calibrate a coupled groundwater flow and land subsidence numerical model. Additionally, D-InSAR results from different sensors are compared and contrasted. When comparing D-InSAR results with extensometers and water levels, a direct correlation is nociced. For all D-InSAR image pairs, large baselines, atmospheric effects, temporal decorrelation, and vegetative cover were limiting factors in obtaining a maximum number of usable interferograms. The total maximum subsidence for a point location in the valley between November 2003 and May 2008 is approximately 40 cm reaching a maximum total subsidence of over 2.0 metres since 1962. When contrasting the ENVISAT ASAR and RADARSAT-1 data, subsidence rates were similar yet the distribution had significant differences. Additionally, ENVISAT's shorter baselines led to more accurate results.

Index Terms — D-InSAR, land subsidence, groundwater RADARSAT-1, ENVISAT ASAR, Toluca, Mexico

1. INTRODUCTION

Excessive groundwater pumping from geologic structures composed of compressible clays leads to land subsidence potentially causing significant damage to buildings and infrastructure. An effective way of limiting this damage is by characterising and predicting future land subsidence. Differential Synthetic Aperture Radar Interferomerty (D-InSAR) is a powerful technique used for detecting surface deformation on the sub-centimeter scale (Franceschetti and Lanari, 1999). The calibration of coupled groundwater flow-compaction models by D-InSAR has been investigated by Galloway et al. [1] and Hoffmann [2]. The objective of this work is to calibrate a coupled groundwater flow and land subsidence numerical model, with emphasis placed on a clay layers individual skeletal specific storage (S_{sk}). Additionally, D-InSAR results from different sensors are compared and contrasted.

The region of interest was focused on the Toluca Valley, Mexico and unwrapping was concentrated in the industrial corridor where noticeable land subsidence is observed. Field work involved obtaining historical and current groundwater levels, geologic information and quantifying subsidence at point locations. Field data and D-InSAR interferograms and subsidence maps are applied to the coupled groundwater flow and compaction model to constrain individual clay layer compressibilities and determine when subsidence began and to what degree the groundwater level decline and geologic properties have affected the subsidence rates. Additionally, D-InSAR results from ENVISAT ASAR and RADARSAT-1 are compared and contrasted with the objective of determining the suitability of one sensor over the other.

2. BACKGROUND

2.1 D-InSAR

D-InSAR uses two SAR images of the same area taken from slightly different positions at two different times, measures the difference in phase between 2 scene images (master and slave images) in a co-registered pixel by pixel basis and removes the topographic phase component using a Digital Elevation Model (DEM) producing an image known as a differential interferogram. This is measured in radians of phase difference and, due to the cyclic nature of phase, is recorded as repeating fringes which each represent a full 2π cycle (half of satellite wavelength, i.e. 2.8 cm of line of sight displacement in the C-band case).

In practice, the phase is also affected by several other factors, which together make the raw phase return in any one SAR image essentially arbitrary, with no correlation from pixel to pixel. To get any useful information from the phase, some of these effects must be isolated and removed. The phase difference of an InSAR data pair ($\Delta\phi$) separated by a spatial and temporal baseline can be described as follows (Massonnet & Feigl, 1998; Mora et al., 2003; Rocca et al., 1997):

$$\Delta\phi = \delta\phi_{flat} + \delta\phi_{top} + \delta\phi_{disp} + \delta\phi_{atm} + \delta\phi_{noise} \pm n \times 2\pi \qquad (1)$$

$$\Delta\phi = \frac{4\pi \cdot B_{\perp} \cdot r}{\lambda \cdot \rho \cdot tg\theta} + \frac{4\pi \cdot B_{\perp} \cdot h}{\lambda \cdot \rho \cdot \sin\theta} + \frac{4\pi \cdot \delta\rho}{\lambda} + \delta\phi_{atm} + \delta\phi_{noise} \pm n \cdot 2\pi \qquad (2)$$

where, $\delta\phi_{flat}$, $\delta\phi_{top}$, $\delta\phi_{disp}$, $\delta\phi_{atm}$, and $\delta\phi_{noise}$ represent phase difference from the spatial baseline of the data pair assuming a flat Earth, topographic unevenness of the terrain, ground displacement along the radar line-of-sight, atmospheric disturbance resulting from spatio-temporal variation in the atmosphere, and random noise resulting from radar instrument and temporal decorrelation between two images of the pair respectively. In the term, $n \cdot 2\pi$, n is a discrete number, including 0 and represents the number of phase cycles in the wrapped phase difference ($\Delta\phi$). λ, θ, ρ, $B_\perp$, r, h and δ_ρ are radar wavelength, look angle, slant range distance of the master image, perpendicular baseline component of the data pair, slant range difference of the data pair due to orbital separation, topographic height of the given point, and ground displacement parallel to radar line of sight (LOS).

2.2 Compaction

Groundwater pumping is known to cause compaction, also known as land subsidence when compressible materials, such as clays, are present. According to Terzaghi (1925), changes in the effective stress can result from changes in the total stress or changes in pore pressure (equation 3). The total stress is given by the geostatic load of the overlying saturated and unsaturated sediments. If it is assumed that the resulting strains are primarily vertical (*zz*), it can be stated that:

$$\sigma'_{zz} = \sigma_{zz} - p \qquad (3)$$

where:

σ'_{zz} is the vertical component of the effective stress tensor,
σ_{zz} is the vertical component of the total stress tensor, and
p is the fluid pore pressure.

For some sediments, inelastic compaction is approximately proportional to the logarithm of the effective stress (Jorgensen, 1980). However, in many cases applicable to aquifer-system compaction where incremental changes in effective stress are typically small (e.g. the Toluca Valley), the relationship can be linearized as

$$\Delta b = S'_k \, \Delta h \qquad (4)$$

where:

Δb is the change in thickness of the sediment layer
S'_k is the skeletal storage coefficient
Δh is the change in hydraulic head

To account for the marked change of the skeletal specific storage when the effective stress exceeds the preconsolidation stress, two separate values are often used:

$$S'_k = \begin{cases} S'_{ske} & for\ \sigma'_{zz} < \sigma'_{zz(pre)} \\ S'_{skv} & for\ \sigma'_{zz} \geq \sigma'_{zz(pre)} \end{cases} \qquad (5)$$

where:

S'_{ske} is the elastic skeletal specific storage,
S'_{skv} is the inelastic, or virgin, skeletal specific storage, and
$\sigma'_{zz\,(pre)}$ is the vertical preconsolidation effective stress component.

3. MATERIALS

3.1 SAR images and software

The interferograms and deformation maps are generated from ERS-1, ERS-2, ENVISAT ASAR, and RADARSAT-1 C-band Single Look Complex (SLC) SAR images over the Toluca Valley, Mexico. In addition to the SLC SAR data, a DEM from the Shuttle Radar Topography Mission [8] was used to remove the topographic phase from the interferogram. Forty four D-InSAR pairs were obtained with only 31 of those results with usable interferograms and subsidence maps (Table 1).

Table 1: Toluca Valley usable interferograms from ERS-1, ENVISAT ASAR, and RADARSAT-1 (b perp. B paral. and d_days are respectively the perpendicular baseline parallel baseline and the difference in acquisition time in days)

Mission	Date 1	Date 2	b perp.	b paral.	d_days
ERS-1	1996-01-28	1996-04-07	26	22	70
ENVISAT ASAR	2003-03-26	2004-02-04	74	77	315
ENVISAT ASAR	2003-07-09	2004-02-04	505	126	210
ENVISAT ASAR	2004-02-04	2004-04-14	310	73	70
ENVISAT ASAR	2004-02-04	2004-12-15	64	14	315
ENVISAT ASAR	2004-02-04	2005-01-19	120	46	350
ENVISAT ASAR	2004-04-14	2004-12-15	374	87	245
ENVISAT ASAR	2004-12-15	2005-01-19	56	32	35
ENVISAT ASAR	2005-01-19	2005-06-08	243	125	140
ENVISAT ASAR	2005-01-19	2005-11-30	94	40	315
ENVISAT ASAR	2005-06-08	2005-11-30	149	85	175
ENVISAT ASAR	2005-11-30	2007-12-05	217	88	735
ENVISAT ASAR	2007-12-05	2008-02-13	29	33	70
ENVISAT ASAR	2007-12-05	2008-04-23	85	86	140
ENVISAT ASAR	2007-12-05	2008-05-28	185	2	175
ENVISAT ASAR	2008-02-13	2008-04-23	172	41	70
ENVISAT ASAR	2008-02-13	2008-05-28	323	108	105
ENVISAT ASAR	2008-04-23	2008-05-28	151	149	35
RADARSAT-1	2003-12-05	2004-03-10	592	456	96
RADARSAT-1	2003-12-29	2004-03-10	459	412	72
RADARSAT-1	2003-12-29	2004-12-23	841	659	360
RADARSAT-1	2004-03-10	2004-08-01	695	636	144
RADARSAT-1	2004-03-10	2004-11-29	698	617	264
RADARSAT-1	2004-08-01	2004-12-23	312	389	144
RADARSAT-1	2004-11-29	2007-11-14	1125	595	625
RADARSAT-1	2004-12-23	2007-11-14	44	78	1056
RADARSAT-1	2007-11-14	2008-01-25	521	452	72
RADARSAT-1	2007-11-14	2008-03-13	28	5	120
RADARSAT-1	2007-11-14	2008-05-24	754	654	192
RADARSAT-1	2008-01-25	2008-03-13	492	446	48
RADARSAT-1	2008-03-13	2008-05-24	746	568	72

For all D-InSAR image pairs, high baseline values, atmospheric effects, temporal decorrelation, and vegetative cover were the limiting factors in obtaining a maximum number of usable interferograms. The urbanized part of the valley had the best results where man made reflectors, such as buildings were abundant. In these areas, usable results were obtained from pairs with up to 3 years difference, however best results were obtained with a time difference less than 1 year. Vegetative cover was a major factor in obtaining usable results; best results were obtained in the drier season (November to the end of April) when vegetative growth is least.

3.2 Field data acquisition

Due to the compressible clay content and the excessive groundwater pumping in the basin, subsidence is observed in the Toluca Valley. According to groundwater level and geologic data, subsidence probably first started occurring in 1962 when a water budget deficit first appeared. As discussed in section 2.2, hydraulic head change and geo-mechanical properties have a direct consequence on the amount of subsidence. The following section briefly describes the field data acquisition.

A 3D geological model with 14 layers was generated from 267 borehole logs enabling a 3D representation of individual and aggregate (Figure 2A) clay layer thicknesses. Historical

geodetic information and accurate field subsidence measurements were not available for the Toluca valley therefore 2 extensometers, measuring total compaction with high accuracy (< 2mm) were installed at 2 locations in the industrial corridor.

Long-term monitoring of water levels in the basin was available from 1969 to present. Wells PL-201 and PL-205 are the closest long term monitoring wells to the region of interest. Additionally, the water level at Extensometer-1 (Figure 2A) is measured every 12 hours by a pressure transducer and data is available from December 2006 to July 2008.

4. RESULTS

4.1 Calibration

Figure 1A shows pumping occurrences overlaying the generated aggregate clay thickness and Figure 1B is a representative D-InSAR interferogram of the entire valley showing localized subsidence zones over a 70 day period. From Figure 1B, the interferogram is not optimised for parameter retrieval in zone E; this zone of maximum subsidence is studied in more detail in the unwrapping section. For the 70 days between December 5th, 2007 and February 13th, 2008, zones A though G are 'hotspots' with very clear subsidence patterns observed. If one observes the zoom on zone A (Figure 1B), two colour cycles (clockwise: yellow-blue-red; see legend of Figure 1B) are observed and represent a total subsidence of 56 mm for the given period. This translates to subsidence rates of 29 cm/year. However, as noted by Calderhead et al.'s (2009) D-InSAR study of the Toluca Valley, depending on the geological context and the pumping rates, the maximum subsidence rates are often variable in space, time, and magnitude.

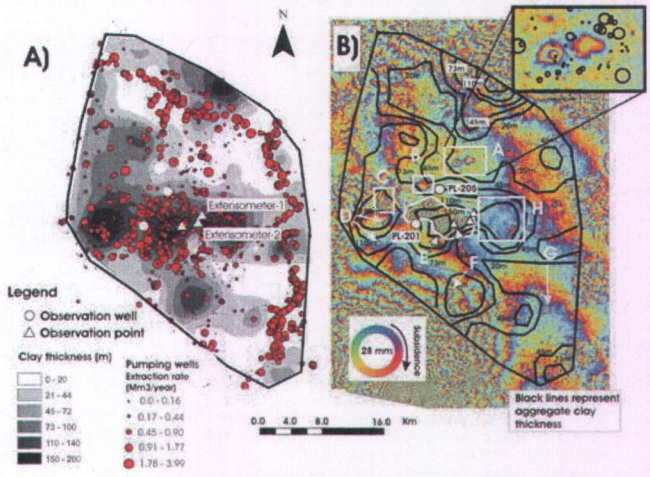


Figure 1: A) Aggregate clay thickness and pumping occurrences B) Differential Interferogram of the Toluca Valley with a time interval of 70 days. ENVISAT ASAR images were acquired on December 5th 2007 and February 13, 2008.

Using empirically derived compressibility tables (Marsily, 1986), only layers with clay content are considered compressible, all other layers are considered to have negligible compressibility. When observing zone H of Figure 1B, no field data is available for this region however the InSAR data is useful in constraining S'_{sk}. Although there is a high aggregate clay thickness and significant groundwater pumping (Figure 1A), the usable interferograms from 1996-2008 (Table 1) show very little to no subsidence in this region. From the 3D geological model, it is noticed that Layer 4's thickness is significant (40-80 m) in zone H, implying that S'_{sk4}'s value is small and that layer 1's S'_{ski} is the dominant compressible layer in this region. This phenomenon could be explained by the fact that older and deeper clays tend to be less compressible than more recent clays. This in turn could explain why the extensometers readings, with data from the top 120m of the system, coincide with the InSAR results: the large majority of compaction is occurring in the upper portion of the aquifer. Table 2 summarizes the compressibilities used for the model.

Table 2: Description of material properties for the Toluca Valley.

Layer number (from top to bottom)	Description	Average thickness	Elastic skeletal specific storage	Inelastic skeletal specific storage
		b [m]	S'_{ke} [1/m]	S'_{kv} [1/m]
Layer 1	clays 1	45,86	9,17E-07	3,67E-06
Layer 2	sand and gravel	18,05	3,61E-08	1,44E-07
Layer 3	fine grains	16,86	8,43E-08	3,37E-07
Layer 4	clay 2	2,09	1,04E-07	4,18E-07
Layer 5	fine grains	17,12	8,56E-08	3,42E-07
Layer 6	coarse grains	19,00	3,32E-08	1,33E-07
Layer 7	sand and gravel	10,61	2,12E-08	8,49E-08
Layer 8	volcanic solids	6,72	1,68E-12	6,72E-12
Layer 9	clays 3	21,91	1,10E-06	4,38E-06
Layer 10	conglomerate	7,32	1,83E-12	7,32E-12
Layer 11	sand and gravel	6,79	1,36E-08	5,44E-08
Layer 12	clays 4	3,73	1,87E-07	7,46E-07
Layer 13	fine grains	9,83	4,92E-08	1,97E-07
Layer 14	sand and gravel	2,00	4,00E-09	1,60E-08
Zones A-G	compressibility areas of Layer 1	30,00	6,00E-07	2,40E-06

The unwrapped D-InSAR interferograms are used to calibrate the 1-D compaction-3D groundwater flow model to simulate land subsidence. Figure 2 shows the compaction results from ENVISAT ASAR, RADARSAT-1, Extensometer-1, and the model simulation at Extensometer 1. Simulated and measured hydraulic head at Extensometer-1 are also included.

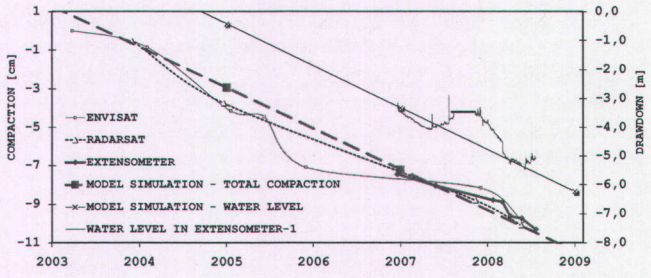


Figure 2: Simulated and measured total compaction at the Extensometer-1 site by ENVISAT ASAR, RADARSAT-1, Extensometer-1, and HGS simulation. Simulated and measured hydraulic head at the Extensometer-1 site are also included.

4.2 Comparison of ENVISAR ASAR and RADARSAT-1

When comparing D-InSAR results from ENVISAT ASAR and RADARSAT-1 (Figure 3) one can see that the maximum subsidence areas are in similar locations with similar magnitudes, however there are differences in the spatial extent of the subsidence.

The spatial variation can be attributed to the fact that the dates compared do not exactly match, baselines are relatively high with the RADARSAT-1 pair (Table 1), atmospheric effects are likely, and unwrapping errors are possible. Compared to ENVISAT ASAR and extensometer readings, the RADARSAT-1 deformation was overestimated when using baselines greater than 800 m, and more reliable when using baselines of less than 600 m.

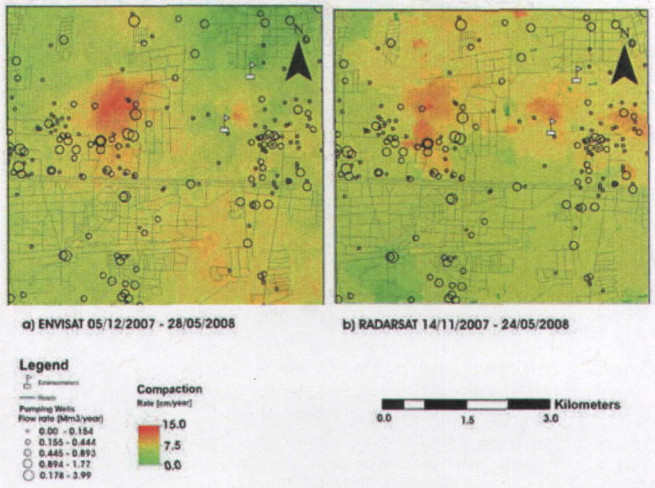


Figure 3: Comparison of ENVISAT ASAR and RADARSAT-1 InSAR results in the maximum subsidence areas and similar time frame. Refer to Table 1 for pass and baselines.

5. CONCLUSION

Both ENVISAT ASAR and RADARDAT-1 D-InSAR compaction results follow the extensometer measurements very closely. Errors in the measured subsidence from the field data could exist since the extensometers do not reach bedrock. However, it is found that the majority of the subsidence occurs in the upper portion of the aquifer, where the extensometers are located.

Results from D-InSAR interferograms have been applied to the compaction model by helping constrain individual clay layer compressibilities. By using the 3D geological model, pumping occurrences, and D-InSAR results, it is possible to isolate the most compressible clay structure and assign more probable values to individual layers.

When comparing ENVISAT ASAR and RADARSAT-1 results, it was found that when using shorter baselines and time differences between images, the RADARSAT-1 InSAR results detected very similar subsidence locations and magnitude to ENVISAT-ASAR. In general, the ENVISAT ASAR mission had shorter baseline differences than the RADARSAT-1 mission; and thus more useful pairs. Differences in the results can also be attributed to atmospheric effects ($\delta\phi_{atm}$) and difficulties in unwrapping.

These results further validate the InSAR technique and the usefulness of D-InSAR, extensometers, 3D geological models, and coupled numerical models in representing land subsidence.

ACKNOWLEDGMENTS

We are thankful to the Ministère des Relations Internationales du Quebec, INRS-ETE, AUCC/IDRC, the Ministère d'Éducation du Québec, NSERC (a discovery grant held by Richard Martel), CONACyT, and the Autonomous University of the State of México (UAEM) for their financial support. We are grateful to the Canadian Space Agency and the Geological Survey of Canada for providing the RADARSAT-1 data and we acknowledge the European Space Agency for providing ERS and ENVISAT ASAR data at cost of reproduction under project C1P 3821. Finally, we are appreciative of the Comision National del Agua for their logistical support in the field.

REFERENCES

[1] Galloway, D.L., Hudnut, K.W., Ingebritsen, S.E., Phillips, S.P., Peltzer, G., Rogez, F., & Rosen, P.A. (1998). Detection of aquifer system compaction and land subsidence using interferometric synthetic aperture radar, Antelope Valley, Mojave Desert, California. *Water Resources Research, 34*, 2573-2585

[2] Hoffmann, J. D. L. Galloway, and H. A. Zebker, Inverse modeling of interbed storage parameters using land subsidence observations, Antelope Valley, California, Water Resources Research, Vol. 39, No. 2, 1031, Feb. 2003.

[3] Massonnet, D., & Feigl, K.L. (1998). Radar interferometry and its application to changes in the earth's surface. *Reviews of Geophysics, 36*, 441-500

[4] Mora, O., Mallorqui, J. J., & Broquetas, A. (2003). Linear and nonlinear terrain deformation maps from a reduced set of interferometric SAR images. IEEE Transactions on Geoscience and Remote Sensing, 41(10), 2243–2252.

[5] Rocca, F., Prati, C., & Ferretti, A. (1997, March 17–21). An overview of ERSSAR interferometry. Proceedings of the 3rd ERS symposium on space at the service of our environment (pp. xxvii–xxxvi). Florence, Italy: European Space Agency (ESA).

[6] Terzaghi, K. (1925). Earthworks mechanics based on soil physics. *Erdbaumechanik auf bodenphysikalisher Grundlage*

[7] Jorgensen, D.G., 1980, Relationships between basic soils-engineering equations and basic ground-water flow equations: U.S. Geological Survey Water-Supply Paper 2064, 40 p.

[8] Farr, T. G., et al. (2007), The Shuttle Radar Topography Mission, *Rev. Geophys.*, 45, RG2004, doi:10.1029/2005RG000183.

[9] Calderhead, A. I., Martel, R., Alasset, P-J., Rivera, A., Garfias, J, Land subsidence induced by groundwater pumping, monitored by C-band D-InSAR and field data in the Toluca Valley, Mexico. International Journal of Remote Sensing (Submitted 2009)

[10] Marsily, G. de, Quantitative Hydrogeology. Groundwater Hydrology for Engineers Ed. Academic Press, New-York (1986)

ANNEXE A 3 – IAH/CNC 2009, HALIFAX

Pumping-induced regional land subsidence: calibrating a flow and compaction model with remote sensors and field data

Angus I. Calderhead
Institut National de la Recherche Scientifique, University of Quebec, Québec, Québec, Canada
Richard Martel
Institut National de la Recherche Scientifique, University of Quebec, Québec, Québec, Canada
ALFONSO RIVERA
GEOLOGICAL SURVEY OF CANADA, NATURAL RESOURCES CANADA, 490 DE LA COURONNE, QUEBEC, QC CANADA
RENÉ THERRIEN
DÉPARTEMENT DE GÉOLOGIE ET DE GÉNIE GÉOLOGIQUE, UNIVERSITÉ LAVAL, QUÉBEC, QC G1K 7P4, CANADA
Jaime Garfias
Centro Interamericano de Recursos del Agua – Universidad Autónoma del Estado de México, Toluca, State of Mexico, México

ABSTRACT
The Toluca Valley, Mexico experiences heavy groundwater pumping and significant land subsidence. This study examines pumping induced regional land subsidence of the Toluca Valley. The study is divided as follows: (1) obtaining remote sensing data, field data, and all available literature for the Toluca Valley; (2) coupling compaction to the groundwater flow equation with the HGS model; and (3) constraining the model with available data to eventually examine several pumping scenarios for minimizing future land subsidence. It is apparent that continuing at the current rates of the water consumption will lead to more subsidence. Average estimates predict a maximum subsidence in the valley that will reach 1.2 m in the next 40 years.

RÉSUMÉ
La Valle de Toluca, Mexique subit un pompage d'eau souterraine et connaît un problème de subsidence important. Cette étude examine l'affaissement des sols résultant de l'extraction d'eau souterraine dans la vallée de Toluca. L'étude se divise par (1) obtenir toutes les données (satellitaire, terrain, littérature) disponibles; (2) coupler la compaction a l'équation d'écoulement avec HydroGeoSphere; (3) contraindre le modèle avec les données disponibles et examiner plusieurs scenarios pour minimiser l'affaissement à venir. Il est évident que si l'on continue au taux de consommation d'eau présente, il y aura d'avantage d'affaissement. Les prédictions moyennes estimes que l'affaissement maximal dans la vallée sera environs 1.2 m dans les prochaines 40 années.

8. INTRODUCTION

In many urban settings, excessive groundwater pumping from aquifers composed of compressible clays leads to land subsidence, potentially causing significant damage to buildings and infrastructure.

Numerical models serve as important tool in analysing subsidence patterns. Terzhaghi's 1D effective stress principle coupled to groundwater flow has most recently been applied by Hoffmann et al. (2003), Leake and Galloway (2007), and Lui and Helm (2008). The objective of this study is to examine land subsidence occurrences in the Toluca Valley, Mexico. A newly coupled finite element 1-D instantaneous compaction and 3D groundwater flow model, Hydrogeosphere (HGS) (Therrien et al., 2009) is used for the analysis. The model is coupled, verified and then applied to the Toluca Valley. Field data, remote sensing techniques, and available literature are used for constraining the new model, and finally several pumping scenarios for minimizing future land subsidence are examined.

The Toluca Valley presently exports 38% ($6m^3/s$) of its groundwater resources to Mexico City (CNA, 2007). The Toluca Valley's water resource and land subsidence problems are of

interest because the basin was formally seen as an important source of water to the Mexico City basin, yet today the Toluca Valley can no longer support its own growth let alone provide for Mexico City's. Inter-basin water transfer is examined as both a problem (exports) and a solution (imports) to the ongoing subsidence.

In contrast to Mexico City's well documented subsidence, very little compaction information has been documented in the Toluca Valley even though subsidence occurrences have been noticed since the early 1970's. Remote sensing information (Synthetic Aperture Radar (SAR) images) in the last 10 years has added to the overall understanding of the subsidence occurrences.

9. COMPACTION BACKGROUND

According to Terzaghi (1925) (equation 1), changes in the effective stress can result from changes in the total stress or changes in pore pressure. The total stress is given by the geostatic load of the overlying saturated and unsaturated sediments.

$$\sigma'_{ij} = \sigma_{ij} - p \qquad (1)$$

where

σ'_{ij} is a component of the effective stress tensor, σ_{ij} is a component of the total stress tensor, and p is the fluid pore pressure.

A change in effective stress resulting from a given head change generally differs in confined and unconfined aquifers. In an unconfined aquifer, a change in head corresponds to a draining or re-wetting of pore space and results in a change in the geostatic load or the total stress on the underlying sediments as well as the pore pressure. The change in effective stress caused by a head change in the saturated portion of an unconfined aquifer can be described as (Poland and Davis, 1969):

$$\Delta\sigma'_{zz} = -\rho_w g(1 - n + n_w)\Delta h \qquad (2)$$

where

$\Delta\sigma'_{zz}$ = the change in vertical effective stress (positive for increase),
n = the aquifer porosity,
n_w = the moisture content in the unsaturated zone above the water table, as a fraction of total volume, and
Δh = the change in hydraulic head.

It should be noted that changes in head in an unconfined aquifer constitute a mass change in that aquifer. This represents a change in the total stress for all underlying confined aquifers. In a confined aquifer, the total stress changes negligibly with changes in pore pressure as water is released from or is taken into storage by the saturated porous medium as a result of the compression or expansion of the medium and (or) the water. The change in water density associated with the expansion or compression of the water is negligible. Thus the change in effective stress for a given change in head can be expressed as (Poland and Davis, 1969)

$$\Delta\sigma'_{zz} = -\rho_w g \Delta h \qquad (3)$$

In Hydrogeosphere the compaction module is designed to simulate instantaneous compaction and storage changes in confined aquifer systems and is thus based on equation 3. For compressible layers in the saturated part of an unconfined aquifer where hydraulic-head variations are occurring, this approach will overestimate the change in effective stress, and thus overestimate sediment compaction by the factor $(1 - n + n_w)^{-1}$ (see Equation 2).

Changes in effective stress ($\Delta\sigma'_{zz}$) cause compaction and expansion of the sediments constituting many aquifer systems. In this paper, the term compaction is used to describe a reduction in the thickness of a horizontal compressible layer. A negative compaction implies an expansion or increased thickness of the compressible layer. Removing horizontal displacements, the one-dimensional compressibility ($\bar{\alpha}$) can be defined as

$$\bar{\alpha} = \frac{-\frac{db}{b}}{d\sigma'_{zz}} \tag{4}$$

where

db is the change in thickness of a control volume with initial thickness b.

If the change in effective stress is due only to a change in the pore pressure, equation 3 can be used to express equation 4 as:

$$\rho_w g \bar{\alpha} b = S'_{sk}\, b = S'_k = \frac{db}{dh} \tag{5}$$

where

S'_{sk} is $\rho_w g \bar{\alpha}$, the skeletal specific storage S'_k is $S'_{sk}b$, the skeletal storage coefficient, and *dh* is the change in hydraulic head.

Laboratory consolidation tests on sediment cores and measurements of aquifer-system compaction obtained from borehole extensometers indicate that the compressibility, and thus the skeletal specific storage, can assume very different values depending on whether or not the effective stress exceeds the previous maximum effective stress, termed the preconsolidation stress (Johnson and others, 1968; Riley, 1969; Jorgensen, 1980).

For some sediments inelastic compaction is approximately proportional to the logarithm of the effective stress (Jorgensen, 1980). However, in many cases applicable to aquifer-system compaction where incremental changes in effective stress are typically small (e.g. the Toluca Valley), the relationship (equation 5) can be linearized as

$$\Delta b = S'_k\, \Delta h \tag{6}$$

where:

Δb is the change in thickness of the sediment layer
S'_k is the skeletal storage coefficient
Δh is the change in hydraulic head

To account for the marked change of the skeletal specific storage when the effective stress exceeds the preconsolidation stress, two separate values are often used:

$$S'_k = \begin{cases} S'_{ske} & for\ \sigma'_{zz} < \sigma'_{zz(pre)} \\ S'_{skv} & for\ \sigma'_{zz} \geq \sigma'_{zz(pre)} \end{cases} \tag{7}$$

where:

S'_{ske} is the elastic skeletal specific storage, S'_{skv} is the inelastic, or virgin, skeletal specific storage, and $\sigma'_{zz\,(pre)}$ is the preconsolidation effective stress.

10. METHODOLOGY

3.1 Toluca Valley data

The Toluca Valley basin (Figures 1) covers an area of approximately 2100 Km^2. The basin is adjacent to the Mexico City Valley, with the Sierra Las Cruces forming a natural border between the two basins. The Toluca Valley's geographic position in the center of the country and proximity to Mexico City, as well as its rapidly developing infrastructure, have allowed the city to grow into a major industrial zone for the country.

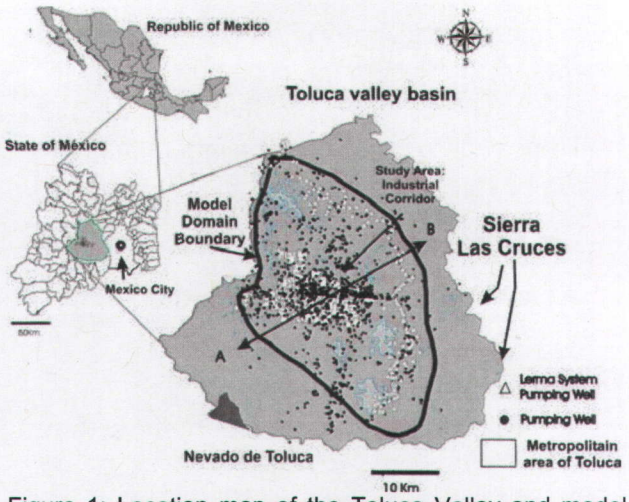


Figure 1: Location map of the Toluca Valley and model domain boundary within the Republic of Mexico and the

State of Mexico. Over 935 pumping wells are in operation in the Valley, including the 230 Lerma system wells that are located along the Lerma river on the eastern edge of the valley.

Heavy groundwater pumping for local use and exports to Mexico City have caused a significant groundwater deficit over the last 45 years. A comprehensive recharge and discharge model (Calderhead et al. 2009a) shows that the deficit will continue to increase (Figure 2).

Very little compaction data was available from the literature thus efforts were made to obtain subsidence data from two bore holes equipped with one extensometer each and from D-InSAR subsidence maps.

Extensometers

The objective of installing the extensometers was to obtain accurate field measurements at point locations. Two R-4 magnetic reed switch probe extensometer systems by Roctest® (Roctest, 2009) were installed in the Industrial Corridor (Figure 4A). Boreholes with a 15 cm diameter were bored by a rotary drill and reach 115 and 78 meters depth respectively for Extensometer-1 and Exsensometer-2. For this study, reading frequencies from the extensometers varied from 1 to 6 months and spanned two years beginning in July of 2006 and ending in July of 2008.

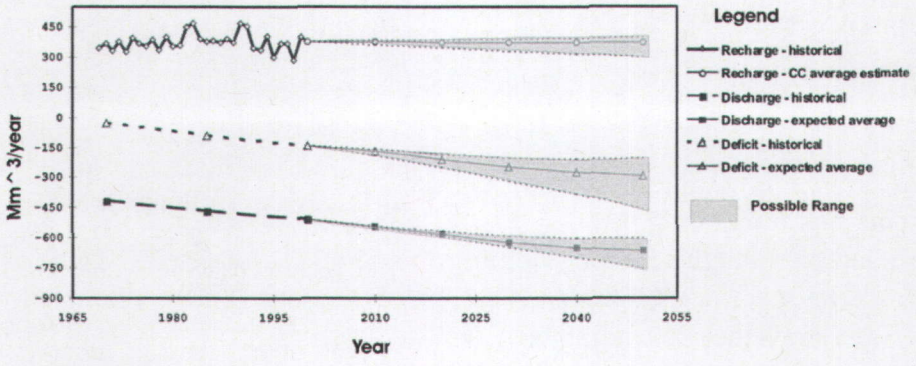


Figure 2: Observed and expected groundwater recharge, pumping, and deficit from 1970 to 2050. From 1970 to 1999 actual recharge values are shown. From 2000 to 2050 average expected recharge including climate change (IPCC, 2007) is shown. Recharge, discharge and deficit projections are based on Calderhead et al. (2009a). The deficit is the sum of the recharge and the discharge. Modified from Calderhead et al. (2009a)

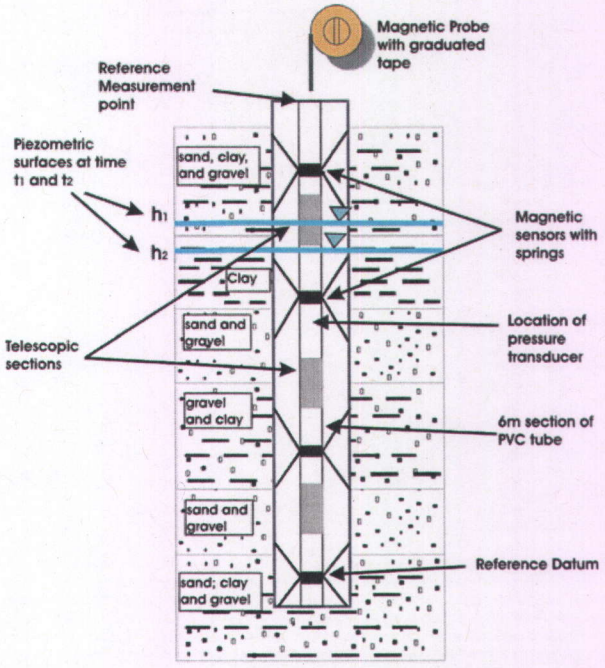


Figure 3: Schematic drawing of the magnetic probe extensometer. Piezometric surface variations with time and location of pressure transducer are also represented. Drawing is not to scale.

D-InSAR

Over the last two decades, the immergence of differential synthetic aperture radar interferometry (D-InSAR) as a tool for monitoring land movement, at the regional scale with sub-centimeter vertical precision, has revolutionized subsidence studies. D-InSAR provides the possibility to calibrate subsidence models even with little field subsidence data available.

InSAR derived subsidence maps are used to constrain the compaction model. The interferograms and deformation maps are useful for locating compacting regions and quantifying subsidence magnitudes. SAR images were obtained from ERS-1, ENVISAT ASAR, and RADARSAT-1 between 1996 and 2008 (Table 1). Calderhead et al. (2009b) presents the complete InSAR results for the Toluca Valley. Table 2 summarises the 31 interferograms used to derive compaction rates.

Figure 4A shows pumping occurrences overlaying the aggregate clay thickness; and Figure 4B is a representative D-InSAR interferogram of the entire valley showing localized subsidence zones over a 70 day period. From Figure 4B, there is very limited coherence in the North-East and South-West corners, thus limiting its usefulness. However, usable results are obtained throughout the central part of the valley. Note that the interferogram is not optimised for parameter retrieval in zone E; this zone of maximum subsidence is studied in more detail in the results section. For the 70 days between December 5th and February 13th, zones A though G are 'hotspots' with very clear subsidence patterns observed. If one observes the zoom on zone A (Figure 4B), two colour cycles (clockwise: yellow-blue-red; see legend of Figure 4B) are observed and represent a total subsidence of 56 mm for the given period. This translates to subsidence rates of 29 cm/year. However, as noted by Calderhead et al.'s (2009b) D-InSAR study of the Toluca Valley, depending on the geological context and the pumping rates, the maximum subsidence rates are often variable in space, time, and magnitude.

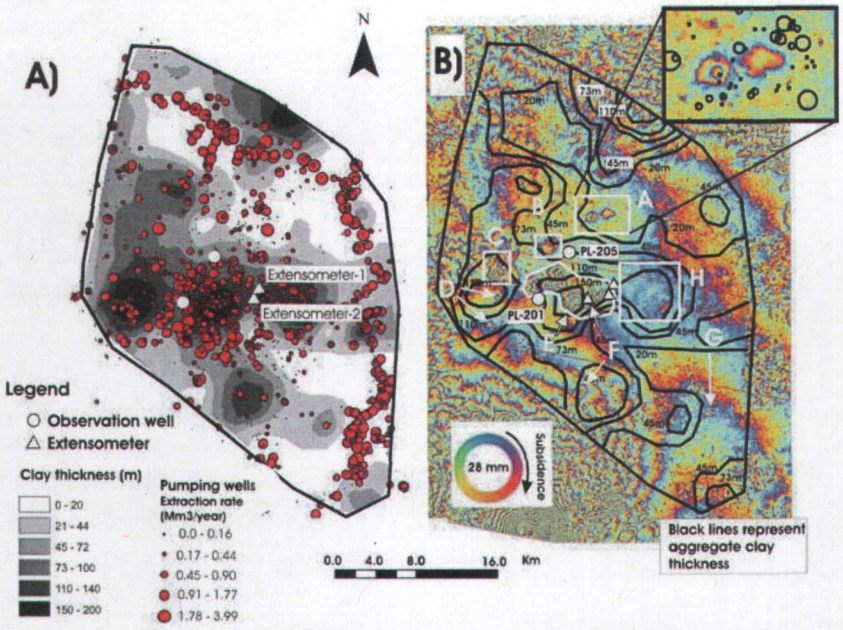


Figure 4: A) Aggregate clay thickness and pumping occurrences B) Differential Interferogram of the Toluca Valley with a time interval of 70 days. ENVISAT ASAR images were acquired on December 5th 2007 and February 13, 2008. Lines of equal aggregate thickness are overlain also shown on the map.

Figure 4A shows pumping occurrences overlaying the aggregate clay thickness; and Figure 4B is a representative D-InSAR interferogram of the entire valley showing localized subsidence zones over a 70 day period. From Figure 4B, there is very limited coherence in the North-East and South-West corners, thus limiting its usefulness. However, usable results are obtained throughout the central part of the valley. Note that the interferogram is not optimised for parameter retrieval in zone E; this zone of maximum subsidence is studied in more detail in the results section. For the 70 days between December 5th and February 13th, zones A though G are 'hotspots' with very clear subsidence patterns observed. If one observes the zoom on zone A (Figure 4B), two color cycles (clockwise: yellow-blue-red; see legend of Figure 4B) are observed and represent a total subsidence of 56 mm for the given period. This translates to subsidence rates of 29 cm/year. However, as noted by Calderhead et al.'s (2009b) D-InSAR study of the Toluca Valley, depending on the geological context and the pumping rates, the maximum subsidence rates are often variable in space, time, and magnitude.

3.2 Coupling Compaction to groundwater flow

With the objective of representing land subsidence in the Toluca Valley, Mexico, a compaction module was added to the multipurpose 3D finite element groundwater flow model HGS. The following equation is used to describe HGS`s modified version of three-dimensional transient subsurface flow for a fully saturated porous medium (Therrien et al., 2009):

$$-\nabla q + \sum \Gamma_{ex} \pm Q = S_s \frac{\partial h}{\partial t} \qquad (8)$$

with the fluid flux q given by:

$$q = -K \nabla h \qquad (9)$$

and the hydraulic head h. The hydraulic conductivity, K, is given by:

$$K = \frac{\rho_w g}{\mu} k \qquad (10)$$

where g is the gravitational acceleration constant, μ is the viscosity of water, k is the permeability tensor of the porous medium and ρ is the density of water.

Fluid exchange with the outside of the simulation domain, as specified from boundary conditions, is represented by Q, In Equation 8, Γ_{ex} represents the volumetric fluid exchange rate between the subsurface domain and all other types of domains supported by the HGS model and it is expressed per unit volume of the other domain types. The definition of Γ_{ex} (positive for flow into the porous medium) depends on the conceptualization of fluid exchange between the domains.

If the aquifer system includes compressible sediments, this term can be multiplied by $(1 - \gamma^*)$, where γ^* is the fraction, by volume, of compressible interbeds in the aquifer system.

Thus, combining the compaction term to the governing equation yields:
(11)

$$-\nabla \cdot q + \sum \Gamma_{ex} \pm Q = [(1-\gamma^*) * S_s + \gamma * S'_{sk}] \frac{\partial h}{\partial t}$$

11. RESULTS

Simulating the hydraulic head involved using hydraulic head values from multilevel piezometers located throughout the valley. More detail was placed on the industrial corridor where the largest drawdowns are observed. The simulated hydraulic head at Extensometer 1 follows the general hydraulic head pattern of PL-201, PL-205, and Extensometer 1 (Figure 5).

At the Extensometer-1 location, similar subsidence patterns are observed from ENVISAT ASAR, RADARSAT-1, Extensometer-1, and the HGS compaction simulation (Figure 6). Assuming instantaneous

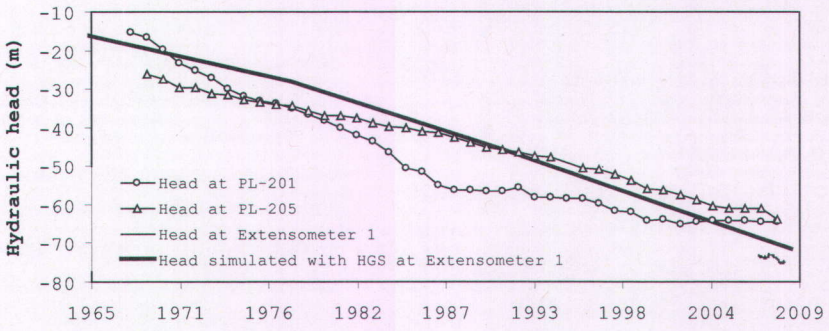


Figure 5: Measured and simulated hydraulic head values at Extensometer 1 contrasted with nearby long term monitoring wells PL-201 and PL-205

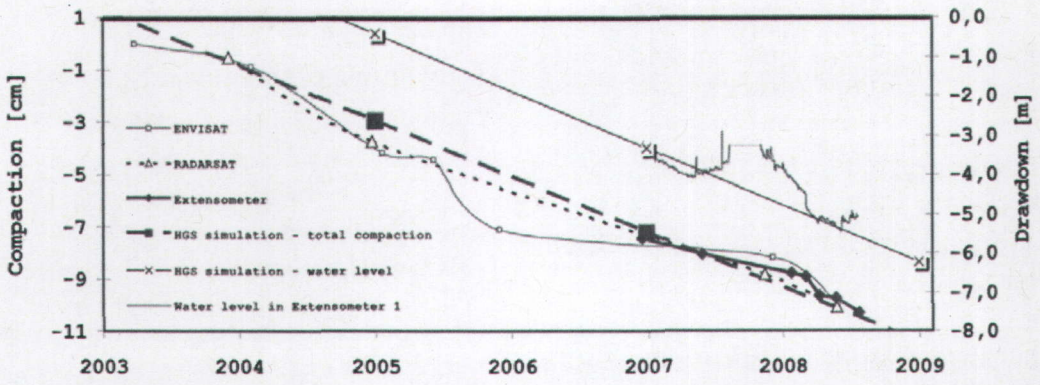


Figure 6: Simulated and measured total compaction at Extensometer 1 by ENVISAT ASAR, RADARSAT-1, Extensometer-1, and HGS simulation. Simulated and measured hydraulic head at Extensometer-1 are also included.

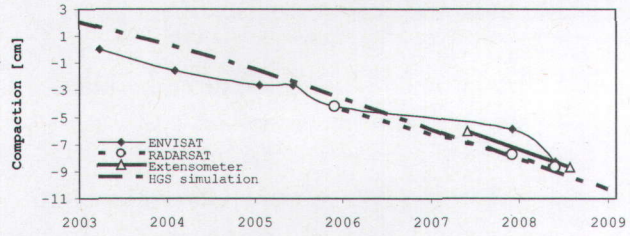


Figure 7: Subsidence at the Extensometer 2 location measured by ENVISAT ASAR, RADARSAT-1, Extensometer 2, and HGS between March 2003 and May 2008.

compaction, approximately 1 meter of drawdown leads to 1 cm of compaction. Subsidence at Extensometer-2 is observed in Figure 7. The extensometer data slope coincides relatively well with the D-InSAR results and the numerical model. The order of subsidence is similar to Extensometer-1's values with approximately 9 cm of compaction between November 2003 and May 2008. Considering the proximity of Extensometer 2 to Extensometer 1, hydraulic head decline is assumed to decrease at a similar rate to Extensometer 1 (Figure 6). Considering head decline, compaction magnitudes are similar for both locations; the total skeletal specific storage values are also assumed to be similar.

Scenarios 1-3 (Table 2) examine worst case, best case, and average expected values based on table 1. Recharge and discharge are assigned with their respective scenario based on table 1 with pumping divided into (A) exports to Mexico City and (B) local use. Exports to Mexico City are expected to increase (8 m^3/s) in the worst case scenario, decrease (3 m^3/s) in the best case scenario and remain constant (6 m^3/s) in the average expected scenario.

A probable scenario is that pumping to Mexico City decreases thus scenarios 4 and 5 decrease exports to 0 m^3/s and 3 m^3/s respectively while keeping average estimates for all other parameters. Scenario 6 examines the possibility of decreasing pumping in Toluca (-25%) and Mexico City (-50%) to a more sustainable rate. Scenarios 7 and 8 make use of the clay thickness model (Figure 4A) for moving pumping wells in areas with high clay content to areas with lower clay content. Scenario 7 assumes average expected pumping and scenario 8 decreases pumping rates to scenario 6 values. By decreasing pumping for local use within the valley, scenarios 6 and 8 imply inter-basin water transfer from surrounding basins.

Scenario	Lerma pumping (to Mexico City)	Toluca Pumping	Recharge	Description
1	33% increase	worst case	worst case	Worst case expected with 33% increased Lerma pumping
2	50% decrease	best case	best case	Best case expected with 50% decrease in Lerma
3	constant at 6m3/s	average	average case	Average case with Lerma pumping constant at 6m3/s
4	Stop Lerma pumping (0m3/s)	average	average case	Average case with stopping Lerma pumping
5	50% decrease	average	average case	Average case with a 50% decrease in Lerma pumping
6	50% decrease	decrease by 25%	average case	Decrease Lerma pumping by 50% and decrease Toluca Basin pumping by 25%
7	constant at 6m3/s	average	average case	Move pumping centres to locations with less clay
8	50% decrease	decrease by 25%	average case	Move pumping centres to locations with less clay and decrease Toluca Basin pumping by 25% and Lerma Pumping by 50%

Table 2: Pumping scenarios 2010-2050

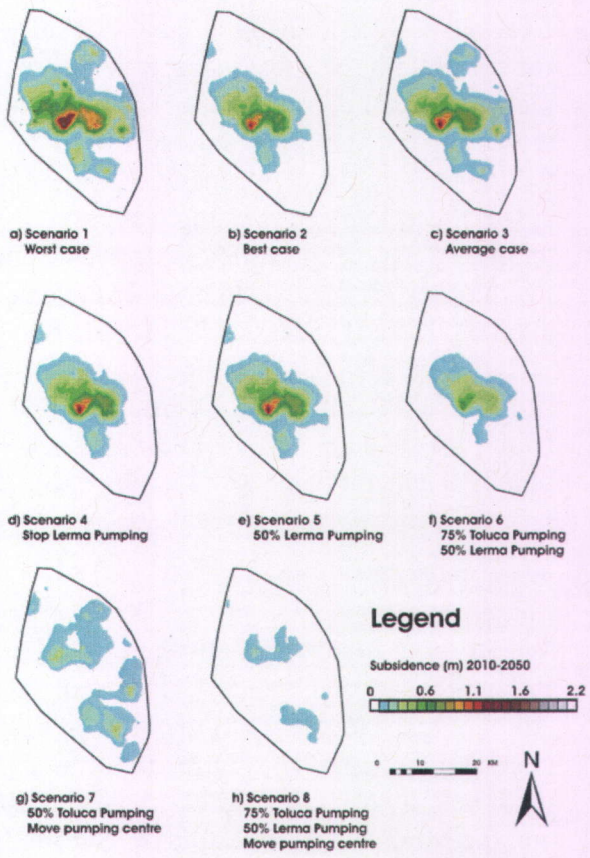


Figure 8: Subsidence scenarios 2010-2050 (see Figure 1 for location of the simulated domain)

Figure 8 presents the total compaction results between 2010 and 2050 for the 8 scenarios. Maximum total subsidence reaches 2.2 m for the worst case scenario (scenario 1), 1.4 m for the best case scenario (scenario 2), and 1.6 m for the average expected subsidence (scenario 3). Comparing scenarios 3, 4 and 5 is of interest. There are only subtle differences between stopping exports (scenario 4) and cutting exports in half (scenario 5). However, there are noticeable differences between constant exports (scenario 3) and cutting exports in half (scenario 5).

The most marked change in subsidence occurs when moving the pumping centres (scenarios 7 and 8) away from compressible clays. Total compaction can be drastically reduced by simply moving the pumping centres to different locations within the valley. The most desirable results (scenario 8) show a localized maximum subsidence of < 0.3 m in 2050, otherwise there is only limited subsidence throughout the valley.

12. DISCUSSSION AND CONCLUSION

Limitations exist for the new HGS-compaction numerical model in representing subsidence. Using the linearized form of the constitutive law introduces errors into the calculations (Narasimhan and Witherspoon, 1977, and Bethke and Corbett, 1988). Leake and Prudic (1991) have estimated the error of this method by comparing the linearized equations of computed compaction with a more complex

treatment of computed compaction using S'_{skv} proportional to log σ'_{zz}. Their results indicate that using the linearized form overestimates compaction by about one-half the percentage increase in effective stress. Hoffman et al. (2003) estimates that if the effective stress increases by 10 percent, compaction would be overestimated by about 5 percent. For sediments relatively deep below the land surface, a given decline in head will result in a smaller percentage increase in effective stress than for shallower sediments. The new HGS-compaction code gives very reasonable estimates for instantaneous subsidence in confined aquifers, however there is room for improving the estimates by including aspects such as dependence on hydraulic conductivity, non-linear deformation, time delays, effects of moving water tables, and extending to a 3D representation of deformation.

The D-InSAR data was very useful in calibrating the subsidence model. InSAR has a large potential for mapping subsidence. With a steady increase in the number of InSAR capable satellites becoming available, more data and software will become available. As mentioned by Calderhead et al. (2009b), several factors influence the suitability of InSAR use for deformation mapping: 1- Perpendicular baselines between satellite acquisitions have upper limits (generally < 600 m); 2- atmospheric effects: spatial variability of the atmosphere changes with time thus fringes are produced by atmospheric effects; 3- temporal decorrelation: vegetation growth or movement is a common cause for InSAR decorrelation; 4- Resolution of the sensors and the DEM: higher spatial resolution leads to more accurate results; 5- band type and wavelength – the band type of the sensor can be a factor in obtaining usable results.

It is apparent that continuing at the current rates of water consumption will lead to more subsidence. Even in the best case scenario (scenario 2), maximum subsidence occurrences over a 40 year period will reach 1.4 m.

Considering that the Lerma pumping system is mostly located in regions with low clay content and little difference is observed between scenarios 4 and 5, completely stopping exports to Mexico City (scenario 4) is not necessary for controlling the subsidence. However, decreasing exports by half (scenarios 2, 5, 6, and 8) does have a positive effect on the overall water budget and subsidence. It can be argued that all scenarios will require inter-basin water transfer at a later date because the water budget deficit is not sustainable.

Inter-basin water transfer alone is not sufficient for controlling the subsidence. It is shown that the best way of controlling subsidence is by relocating the pumping centres to other locations with low clay content. Had a pumping system been in place to pump water to the urbanized part of the valley (scenarios 7 and 8), much of the land subsidence could have been avoided. Even if scenarios 7 and 8 are not undertaken, when planning water imports to the Toluca Valley from other basins, one can learn from past mistakes and avoid drilling new wells in locations with thick compressible clay units - whether for exporting or local use.

ACKNOWLEDGEMENTS

We are thankful to the Ministère des Relations Internationales du Quebec, CONACyT, the Autonomous University of the State of México (UAEM), INRS-ETE, NSERC (a discovery grant held by Richard Martel), AUCC/IDRC, and the Ministère d'Éducation du Québec for their financial support. We are appreciative of Sergio Murillo from the Comision National del Agua for logistical support on the field. We are grateful to the Canadian Space Agency and the Geological Survey of Canada for providing the RADARSAT-1 data and finally, we acknowledge the European Space Agency`s

contribution for providing ERS and ENVISAT ASAR data at cost of reproduction under project C1P 3821.

REFERENCES

Bethke, C.M., and Corbett, T.F., 1988. Linear and nonlinear solutions for one-dimensional compaction flow in sedimentary basins: Water Resources Research, v. 24, p. 461–467.

Calderhead A. I., Martel, R. Rivera, A., Garfias, J., Therrien, R., 2009a. An increasing groundwater budget deficit induced by urbanization, industrialization, and climate change in the Toluca Valley, Mexico. Journal of hydrology (Submitted)

Calderhead, A. I., Martel, R., Allasset, P-J., Rivera, A., Garfias, J,. 2009b. Land subsidence induced by groundwater pumping, monitored by C-band D-InSAR and field data in the Toluca Valley, Mexico. International Journal of Remote Sensing (Submitted)

CNA, 2007. Base Aquiferos Nacional y Regional. Comisión Nacional del Agua- database.

Galloway, D.L. and Hoffmann J. 2007 The application of satellite differential SAR interferometry-derived ground displacements in hydrogeology. Hydrogeology Journal (2007) 15: 133–154

Hoffmann J, Leake SA, Galloway DL, Wilson AM, 2003. MODFLOW-2000 ground-water model-user guide to the subsidence and aquifer-system compaction (SUB) package. USGS Open-File Rep 03-233.

IMTA, 2003. Censo del utilización del agua en el valle de Toluca. Instituto Mexicano de Tecnologia del Agua.

INEGI, 2009. Instituto Nacional de Estadística, Geografía e Informática, Sinthesis of geographic information for the state of Mexico. Aportación al Producto Interno Bruto (PIB) nacional/ Contribution to Gross Domestic Product (GDP)http://cuentame.inegi.org.mx

IPCC, 2007. Climate Change 2007: The Physical Science Basis. Contribution of Working Group I to the Fourth Assessment Report of the Intergovernmental Panel on Climate Change [Solomon, S., D. Qin, M. Manning (eds.)].

Johnson, A.I., Moston, R.P., and Morris, D.A. 1968. Physical and hydrologic properties of water-bearing deposits in subsiding areas in California: U.S. Geological Survey Professional Paper 497-A, 71 p.

Jorgensen, D.G., 1980. Relationships between basic soils-engineering equations and basic ground-water flow equations: U.S. Geological Survey Water-Supply Paper 2064, 40 p.

Leake, S.A., and Prudic, D.E., 1991. Documentation of a computer program to simulate aquifer-system compaction using the modular finite-difference ground-water flow model: U.S. Geological Survey Techniques of Water-Resources Investigations, book 6, chap. A2, 68 p.

Leake, S.A., and Galloway, D.L., 2007. MODFLOW ground-water model—User guide to the Subsidence and Aquifer-System Compaction Package (SUB-WT) for water-table aquifers: U.S. Geological Survey, Techniques and Methods 6–A23, 42 p.

Legorrreta, J., 1997. Rainfall, the key to the future of the Valley of Mexico. *La Jornada Ecologica*, **5**(58): 1-12.

Liu, Y., and D. C. Helm 2008., Inverse procedure for calibrating parameters that control land subsidence caused by subsurface fluid withdrawal: 1. Methods, *Water Resour. Res.*, 44, W07423, doi:10.1029/2007WR006605.

Narasimhan, T.N., and Witherspoon, P. A. 1977. Numerical model for land subsidence in shallow ground-water systems, Internat. Assoc. Sci. Hydrology Pub. 121, p. 133-144.

Poland, J.F., and Davis, G.H., 1969. Land subsidence due to withdrawals of fluids, *in* Varnes, D.J., and Kiersch, G., eds.: Geological Society of America Reviews in Engineering Geology, v. 2, p. 187–269.

Riley, F.S., 1969. Analysis of borehole extensometer data from central California: International Association of Scientific Hydrology Publication 89, p. 423–431.

Roctest, 2009. R-4 magnetic reed switch probe extensometer system, Roctest http://www.roctest.com/modules/AxialRealisation/img_repository/files/documents/R4-E5013D-W.pdf

Terzaghi, K. 1925. Earthworks mechanics based on soil physics. Erdbaumechanik auf bodenphysikalisher Grundlage, Franz Deuticke, Vienna

Therrien, R., McLaren, .G. Sudicky, E.A., Panday, S.M. 2009 User Guide: HydroGeoSphere - A Three-dimensional Numerical Model Describing Fully-integrated Subsurface and Surface Flow and Solute Transport

ANNEXE B *Résumé des modèles numériques couplés*

Annexe B: Summary of coupled groundwater flow and compaction numerical models

Author	Model Name	Variables in space			Numerical method		Constitutive Relation	Case study	Verified
		aquifer	aquitard	deformation	flow	deformation			
Gambolati (1972)		N/a			-	N/A(linear)	compressibility	Venise	No
Gambolati et al. 1973,1974		X ,Y	Z	Z	FE	DF (linear)	compressibility		Yes
Helm (1975)	COMPAC	Z	Z	Z	FD	DF (non linear)	Terzaghi		Yes
Trescot et al. (1976)		X ,Y	-	-	FD	n/a (linear)	-	none	No
Narasimhan and Witherspoon (1977)		X ,Y	Z	Z			Terzaghi		
Safai, and Pinder (1979)		X ,Y,Z			FE				
Newman et al (1982)	FLUMPS	X ,Y			FE	FE (non linear)		California	
Gambolati et al. (1986)	MAINFLW	X ,Y	Z	-	FE	n/a (linear)	-	none	No
Chorley and Frind (1978)	-	X ,Y	Z	-	FE	n/a (linear)	-	none	Yes
Herrera et al. (1976) (1977) (1981)	-	X ,Y	Z	-	FE	n/a (linear)	-	-	No
Verujijt and Barends (1987)	-	n/a	Z	Z	n/a	FE (linear)	Terzaghi	none	Yes
Lewis and Shrefler (1987)	PLASCON	X ,Y	Z	X ,Y	FE	FE (non linear)	Biot	Venice	No
Bear and Corapcioglu (1981) (1982)	-	X ,Y	X ,Y	X ,Y	N/A	N/A (linear)	-	none	No
Cruikshank (1984)		X ,Y	Z	-	FD	FD (non linear)	-	Pixley	No
Rivera et al. (1991)	NEWSAM	X ,Y	Z	Z	FD	FD (non linear)	Terzaghi	Mexico	Yes
Leake and Prudic, (1991)	IBS1(MODFLOW)	X ,Y	Z	Z	FD	FD (non linear)	Terzaghi	many	Yes
Shrefler and Zhan (1993)	-	X ,Y	X ,Y	X ,Y	FE	FE (non linear)	Biot	none	Yes

Teatini, Gambolati & Tosi (1995)		X ,Y,Z	Z	Z	FE	FE (non linear)	Terzhagi	Venice	yes
Yeh et al. (1996)	-	X ,Y	X ,Y	X ,Y	FE	FE (non linear)	Biot	none	Yes
Shearer (1998)	IDP (MODFLOW)	X ,Y	Z	Z	FD	FD (non linear)	Terzaghi	Hangu, China	Yes
Guvanasen and Chan (2000)	MOTIF	X ,Y,Z	X ,Y,Z	X ,Y,Z	FE	FE	Biot	none	Yes
Lipnikov (2002)	-	X ,Y	X ,Y	X ,Y,Z	FE/FD	FE/FD	Biot	None	No
Chen et. al. (2003)		X ,Y,Z	Z	Z		FD	Terzaghi	Suzhou, China	Yes
Hoffmann et al. (2003b)	SUB (MODFLOW 2000)	X ,Y	Z	Z	FD	FD	Terzaghi	Many	Yes
Leake and Galloway (2007)	SUB-WT	X,Y	Z	Z	FD	FD	Terzaghi	Many	Yes
Liu and Helm (2008)		X,Y	Z	Z	FD	FD	Terzaghi		Yes
This thesis	HydroGeoSphere	X ,Y,Z	Z	Z	FE	FE (non linear)	Terzaghi	Toluca	Yes

References

Bear, J., and Y. Corapcioglu, Mathematical model for regional land subsidence due to pumping, Part. 1: integrated aquifer equations based on vertical displacement only, *Water Resources Research*, 17(4):937-946, 1981.

Bear, J., and Y. Corapcioglu, Mathematical model for regional land subsidence due to pumping, Part. 2: Integrated aquifer equations for vertical and horizontal displacements, *Water Resources Research*, 17(4):947-958, 1981.

Chen CX, Pei SP, Jiao JJ (2003) Land subsidence caused by groundwater exploitation in Suzhou City, China. Hydrogeol Journal 11, 275-287

Chorley, D., and E. Frind (1978), An Iterative Quasi-Three-Dimensional Finite Element Model for Heterogeneous Multiaquifer Systems, Water Resour. Res., 14(5), 943-952.

GAMBOLATI, G. 1972. A three dimensional model to compute land subsidence. Bull. Internat. Assoc. Hydrol. Sci., v. 17, no. 2, p. 219-226.

GAMBOLATI, G., and FREEZE, R. A. 1973. Mathematical simulation of the subsidence of Venice, 1, Theory. Water Resources Research, v. 9, no. 3, p. 721-733.

Gambolati, G. Perdon A. M., and Ricceri G. (1984) A coupled finite element model of flow in porous layered media. Finite Elements in Water Resources, 5th International Conference, 1984, Burlington, Vermont. pp. 25-36

Gambolati, Giuseppe, Sartoretto, Flavio, and Uliana, Fiore, 1986, A conjugate gradient finite element model of flow for large multiaquifer systems: Water Resources Research, v. 22, no. 7, p. 1003–1015.

Guvanasena, V., Tin Chan (2000) A three-dimensional numerical model for thermohydromechanical deformation with hysteresis in a fractured rock mass. International Journal of Rock Mechanics and Mining Sciences 37. 89-106

Harbaugh, A.W., Banta, E.R., Hill, M.C., and McDonald, M.G., 2000, MODFLOW-2000, the U.S. Geological Survey modular ground-water model—User guide to modularization concepts and the ground-water flow process: U.S. Geological Survey Open-File Report 00-0092, 121 p.

Helm, D. C., 1975. One-dimensional simulation of aquifer system compaction near Pixley, California, 1, Constant parameters, Water Resour. Res., 11, 465–478,

Helm, D. C., 1994. Horizontal aquifer movement in a Theis-Theim confined system. Water Resources Research, 30(4): 953-964. April 1994.

Herrera, I., and R. Yates, Integrodifferential equations for systems of leaky aquifers, 3, A numerical method of unlimited applicability, Water Resour. Res., 13(4), 725-732,1977.

Hoffmann, J., Leake, S.A., Galloway, D.L., and Wilson, A.M, 2003b, MODFLOW-2000 ground-water model—User guide to the Subsidence and Aquifer-System Compaction (SUB) Package: U.S. Geological Survey Open-File Report 03–233, 46 p.

Leake, S.A., and Prudic, D.E., 1991, Documentation of a computer program to simulate aquifer-system compaction using the modular finite-difference ground-water flow model: U.S. Geological Survey Techniques of Water-Resources Investigations, book 6, chap. A2, 68 p.

Leake, S.A., and Galloway, D.L., 2007, MODFLOW ground-water model—User guide to the Subsidence and Aquifer-System Compaction Package (SUB-WT) for water-table aquifers: U.S. Geological Survey, Techniques and Methods 6–A23, 42 p.

Lewis RW, Schrefler B (1978) Fully coupled consolidation model of subsidence of Venice. Water Resources Res 14(2):223–230.

Liu, Y., and D. C. Helm (2008), Inverse procedure for calibrating parameters that control land subsidence caused by subsurface fluid withdrawal: 1. Methods, *Water Resour. Res.*, 44, W07423, doi:10.1029/2007WR006605.

Neuman, S.P., Preller, C., and Narasimhan, T.N., 1982, Adaptive explicit-implicit quasi three-dimensional finite element model of flow and subsidence in multiaquifer systems: Water Resources Research, v. 18, no. 5, p. 1551–1561.

NARASIMHAN, T.N., and WITHERSPOON, P. A. 1977. Numerical model for land subsidence in shallow ground-water systems, Internat. Assoc. Sci. Hydrology Pub. 121, p. 133-144.

Rivera, A., E. Ledoux and G. de Marsily, 1991. Nonlinear modeling of groundwater flow and total subsidence of the Mexico city aquifer-aquitard system. *FISOLS* (*IV Inter. Symposium on Land Subsidence*); 12-17 may 1991 Houston Texas, USA. IAHS Publication no. 20; pp 45-58.

Rudolph, D. L., and Frind E. O., 1991. Hydraulic response of highly compressible aquitards during consolidation. WaterResources Research, 27 (1), 17-28.

Safai, N. M., and G. F. Pinder, 'Vertical and horizontal land deformation in a desaturating porous medium', *Adv. Water Resours., 2,* 19-25 (1979).

Schrefler, B. A., and X. Zhan,'A fully coupled model for water and airflow in deformable porous media', Water *Resour.* Res., 29, 155-167 (1993).

Shearer T.R. 1998, A numerical model to calculate land subsidence, applied at Hangu in China, Engineering Geology 49 (1998) 85-93.

Teatini, P., Gambolati, G., and Tosi, L. (1995). ''A new three-dimensional non-linear model of the subsidence at Venice.'' *Proc., 5th Int. Symp. on Land Subsidence, IAHS Publ. No. 234*, International Association of Hydrological Sciences, Wallingford, U.K., 353–361.

Trescott, P. C, Pinder, G. F. & Larson, S. P. (1976) Finite difference model for aquifer simulations in two dimensions with results of numerical experiments. *USGS Techniques of Water Research Investigations no. 7.*

Verujijt and Barends (1987) Mechanics of fluids in layered soils, in Advances in Transport Phenomena in Porous Media. NATO ASI series. EDS. J. Bear and Y Corapciouglu, pp. 241-266.

Yeh, H.D., Lu, R.H. and Yeh, G.T., 1996, Finite element modelling for land displacements due to pumping. International Journal for Numerical and Analytical Methods in Geomechanics, 20, 79–99.

ANNEXE C – Autres travaux de terrain

ANNEXE C : Autres travaux de terrain fait dans le contexte de monitoring à long terme mais pas présenté dans les résultats de cette thèse.

Même si les résultats de certains travaux de terrain ne sont pas complètement utilisés dans cette thèse, l'étudiant, l'INRS, la CNA, ainsi que l'UAEM ont collaboré pour installer deux puits d'observation ainsi qu'un système de capteur de pression automatique. Les résultats de ces travaux ne sont pas présenté dans cette thèse, par contre les travaux seront utile pour la population de la vallée à long terme.

Installation de deux puits d'observation ainsi qu'un système de capteur de pression automatique

Deux puits d'observation ont été installés dans la vallée de Toluca pour complémenté la base de donne sur le système de multi-piézomètres (CNA, 2008) et font partie du réseau de capteurs de pression automatique décrite plus bas. Ces donnes assisteront aux mesures de la recharge, l'extraction d'eau souterraine, ainsi que le comportement hydrique dans la vallée de Toluca. Les deux puits ont été installés dans des endroits géographiquement opposé dans la vallée. Le puits de Santiago Tianguistenco (figure 1) se situe au sud est du bassin et le puits du CIRA (figure 3) se situe dans la partie nord-ouest du bassin. Dans les deux cas, les forages ont atteint 80 m de profondeur et la partie ouverte permettant l'entré d'eau a 40 m de longueur commençant a 40 m de profondeur.

De plus, l'équipe de la CNA et l'étudiant ont installé un réseau de capteur de pression automatique pour prendre des mesures de niveau d'eau à toutes les 12 heures. Ces capteurs de pression serviront à évaluer les niveaux d'eau dynamique dans la vallée. Les capteurs ont été installées dans des ancien puits de production par contre avant la mise en place des capteurs ces puits ont été inspectés à l'aide d'une camera vidéo (figure 5) afin de vérifier l'intégrité du tubage d'acier et l'état général des parois.

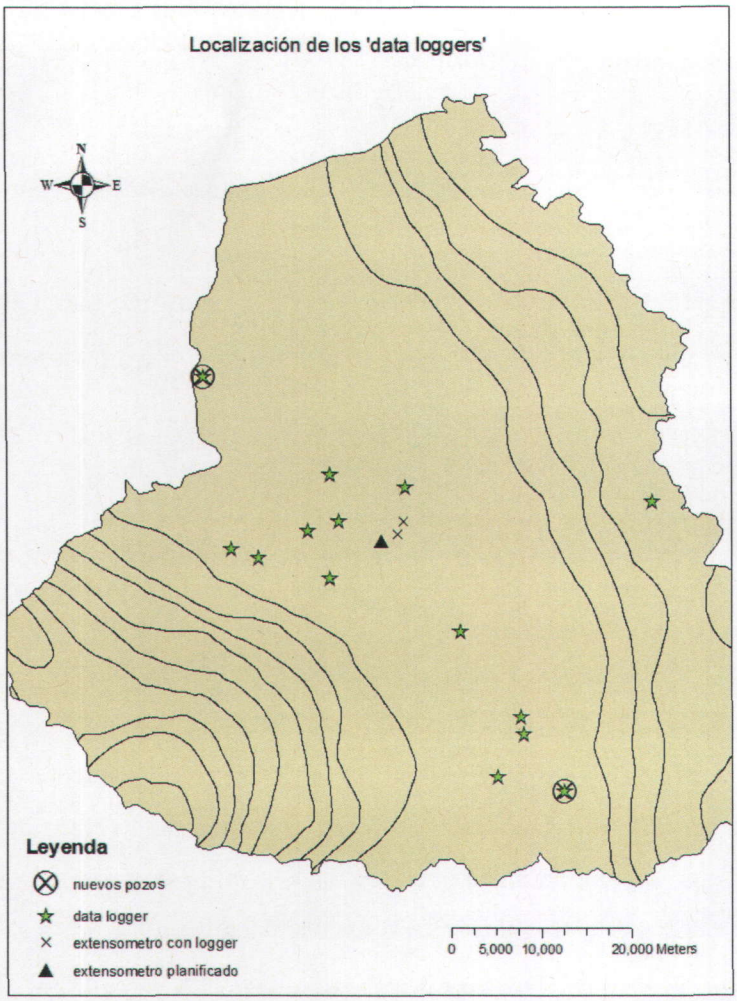


Figure 1 : Distribution du réseau de capteur de pression dans la Vallée de Toluca

La plupart des capteurs de pression sont distribué dans les plaines de la Vallée de Toluca, qui couvre une superficie d'environs 2100 km^2 et se situe à une altitude d'environ 2650 m. Le réseau de capteurs de pression fournit de l'information importante sur la recharge ainsi que les baisses de niveau d'eau dans la vallée. La CNA planifie d'ajouter d'autres capteurs de pression au réseau. Les extensomètres qui contiennent des capteurs de pression sont aussi indiqués par une croix. La localisation l'altitude et la profondeur sont compilé au tableau 1.

Tableau 1 : La localisation, l'altitude, et la profondeur des puits du système d'acquisition de pression automatique.

Nombre del pozo		Localización (UTM) X	Y	Altitud (masl)	Well depth (m)	fecha	nivel del agua (ref bara) (m)	dist. entre bara y brocal (m)	nivel del agua (ref bara) (m)	# del logger	profondidad del logger abajo del nivel de agua (m)	distancia entre bara y logger (m)	Altitud of logger (masl)	frequency of data collection
PMPA-14	CIRA	425073	2144992	2661	80	12-janv-06	19,885	0,1	19,985	SN (CIRA/INRS)	-7,605	27,49	2653	cada 12 horas, empieza al 0:00:00
PMPA-06	Barcel	432610	2133858	2630	101	11-janv-06	30,08	0,05	30,13	SN (CNA)	-35	65,08	2595	cada 12 horas, empieza al 0:00:00
PMPA-03	DGCOH 51-A	448413	2118942	2588	31	18-janv-06	21,504	0,05	21,554	SN 51498 (CIRA/INRS)	-7	28,504	2559,5	cada 12 horas, empieza al 0:00:00
PMPA-04	DGCOH 44-A	448202	2120249	2586	114	18-janv-06	28,92	0,039	28,959	SN 48134 (CNA)	-20	48,92	2536	cada 12 horas, empieza al 0:00:00
PMPA-12	San Miguel Totoltepec	439761	2136995	2595	99,5	19-janv-06	37,571	0	37,571	SN 48091 (CNA)	-20	57,571	2538	cada 12 horas, empieza al 0:00:00
PMPA-13	San Cristobal Huichochitlan	434237	2137905	2614	73	19-janv-06	41,235	0,045	41,28	SN 48145 (CNA)	-20	61,235	2553	cada 12 horas, empieza al 0:00:00
	San Carlos, Metepec	434222	2130367	2635	67,6	19-janv-06	64,43	not applicable	64,43	SN 08395 (CIRA/INRS)	-2,57	67	2568	cada 12 horas, empieza al 0:00:00
PMPA-11	Celanece	434855	2134561	2626	85,43	21-janv-06	71,135	0,089	71,224	SN 48106 (CNA)	-10	81,135	2545	cada 12 horas, empieza al 0:00:00
PMPA-09	San Buenaventura	429011	2131870	2705	132	21-janv-06	38,193	0,055	38,248	SN 48147 (CNA)	-20	58,193	2647	cada 12 horas, empieza al 0:00:00
PMPA-02	DGCOH 75-A	446517	2115861	2575	123	2006-01-26	18,335	0,07	18,405	SN 48104 (CNA)	-20	38,335	2575	cada 12 horas, empieza al 0:00:00
PMPA-05	Marquesa	457855	2135953	3033	>200 m	2006-01-26	143,15	0	143,15	SN 48136 (CNA)	-20	163,15	2870	cada 12 horas, empieza al 0:00:00
PMPA-1	Santiago Ocatenco	451355	2114805	2635	80	2006-03-06	30,685	0,075	30,76	SN 44943 (CIRA/INRS)	-7	37,685	2598	cada 12 horas, empieza al 0:00:00
PMPA-10	Lodo Prieto	426999	2132502	2735	173	31/0502007	brocal	52,71	52,71		30,57	83,28		cada 12 horas, empieza al 0:00:00
PMPA-07	Izcalli Cuahutemoc	443779	2126472	2580	140	2006-02-09	43,61		43,61	(CNA)	-20	63,61		cada 12 horas, empieza al 0:00:00
PMPA-16	Extensometer 1 Casa San Pedro	439666	2134469	2660	132	2006-11-15	--	--	42,551	CIRA				cada 12 horas, empieza al 0:00:00
PMPA-15	Extensometer 2 (Coca-Cola)	439197	2133532	2631	120	2006-07-10	--	--	32,79	CIRA	6.59 (6 junio 2007)			cada 12 horas, empieza al 0:00:00
PMPA-14	CIRA (barometro)	425073	2144992	2661	80	12-janv-06	19,885	0,1		SN (CIRA/INRS)	9,915	9,97	2651	every 12 hours stratiing at 0:00:00
PMPA-03	DGCOH 51-A (barometro)	448413	2118942	2630	101	11-janv-06	30,08	0,05		SN (CNA)	28,08	2	2658,08	every 12 hours stratiing at 0:00:00

ANNEXE D – Résultats des tests de consolidation

Universidad Autónoma del Estado de México
Facultad de Ingeniería.
Laboratorio de Materiales.

Ciudad Universitaria, Toluca Méx., a 09 de Julio de 2007.

DR. MARTÍN CARLOS VERA ESTRADA
DIRECTOR DE LA FIUAEM.
P R E S E N T E.

At´n. DR. CARLOS DÍAZ DELGADO.
COORDINADOR DEL CIRA.

Por este conducto, le informo a usted que a la fecha se han concluido los trabajos de campo y laboratorio del primer sondeo ubicado en el BORDO DE CONFINAMIENTO DE LA LAGUNA, ALMOLOYA DEL RÍO, para el proyecto de Investigación Universidad de Québec-FICIRA-UAEM, a cargo del Dr. Jaime Garfias.

Únicamente se realizo el ensaye en una de las tres muestras obtenidas, debido a que se localizaron arenas limosas en dos de ellas.

Es importante indicar que la muestra ensayada es de un Limo de Alta Compresibilidad. No se localizaron arcillas en el sondeo realizado. Los valores de LL e IP están fuera de los rangos considerados para el Índice de compresión (Cc), con el que se pretenden correlacionar, según lo tratado en la tesis de licenciatura "Determinación del esfuerzo de corte de los distintos tipos de arcilla del Valle de Toluca, bajo diferentes condiciones de Humedad", de Ing. Ana María Minor Villar (FIUAEM, Marzo 2007).

El monto de los trabajos realizados se muestra en la siguiente tabla.

Concepto	Cantidad	P.U.	Importe
Perforación en suelo	22	$ 350,00	$ 7 700,00
Traslado de brigada y equipo de perforación	1	800,00	800,00
Muestreo con tubo Shelby	3	400,00	1 200,00
Densidad de sólidos, contenido de agua, granulometría y límites de consistencia	1	825,00	825,00
Consolidación unidimensional	1	1 500,00	1 500,00
Tiempo extraordinario día sábado 23 de Junio	1	350,00	350,00
		Sub-total	$ 12 375,00

Están pendientes la realización de los trabajos de perforación en dos puntos:

- **Puente vehicular entre San Mateo Atenco y San Pedro Tultepec.**
- **Puente vehicular carretera Toluca-Temoaya sobre Río Lerma.**

Es importante que se soliciten los permisos así como las medidas de protección, ante las autoridades municipales o estatales correspondientes, además de que se asigne a una persona del CIRA, para que acompañe a la brigada durante los trabajos de perforación e indique las profundidades de muestreo.

Para cualquier duda o aclaración de la presente, quedamos de usted:

A T E N T A M E N T E
PATRIA, CIENCIA Y TRABAJO
" 2007, 50 Aniversario Luctuoso del Poeta Enrique Carniado"

M. EN I. SERGIO ALEJANDRO DÍAZ CAMACHO.
RESPONSABLE DEL ÁREA DE INVESTIGACIÓN
DEL LABORATORIO DE MATERIALES

ING. MARIA ESTHER ANTONIO SALINAS.
JEFA DEL LABORATORIO DE MATERIALES

LABORATORIO DE MATERIALES DE LA FACULTAD DE INGENIERIA DE LA U.A.E.M.

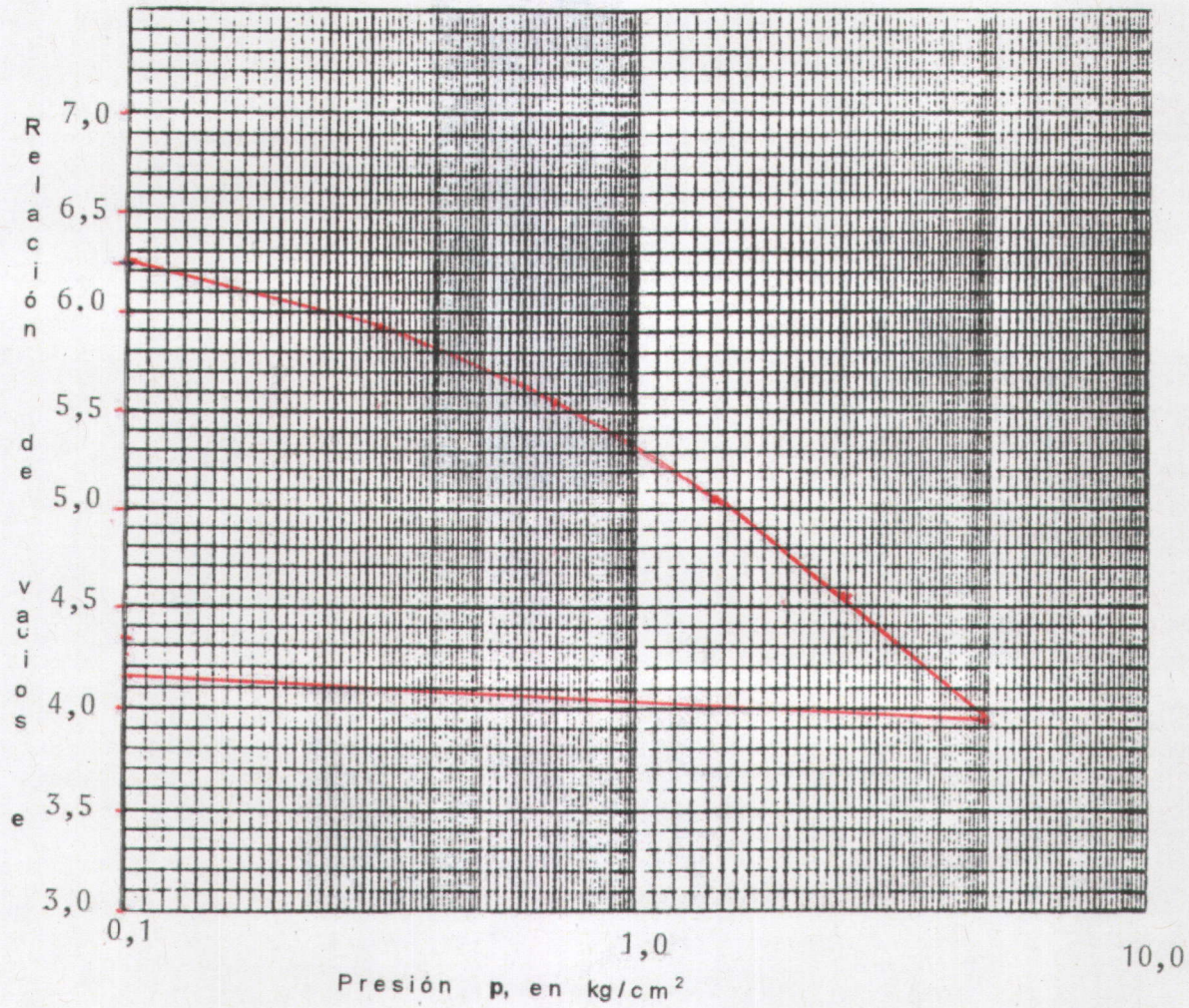
CURVA DE COMPRESIBILIDAD

Compañía: PROYECTO DE INVESTIGACION UNIVERSIDAD DE QUEBEC-FICIRA-UAEM.

Obra: DETERMINACIÓN DE LOS VALORES DE COMPRESIBILIDAD DE LAS ARCILLAS DEL VALLE DE TOLUCA.

Muestra No.	Profundidad (m)	Ss	Wi (%)	Wf (%)	ei	ef	Gi (%)	Gf (%)
SPT-1	1,5-1,9	2,14	289,04	216,44	6,453	4,349	95,84	100,0

PRESION EFECTIVA: 0,870 kgf/cm^2



Fecha de reporte; 2007 Jul 09

Laboratorista	Jefa del Laboratorio de Materiales	El Director
Efraín Vallejo Toledano	Ing. Maria Esther Antonio Salinas	Dr. Martín Carlos Vera Estrada.

Universidad Autónoma del Estado de México.
Facultad de Ingeniería
Laboratorio de Materiales.

RESULTADOS DEL ENSAYE DE CONSOLIDACIÓN UNIDIMENSIONAL.

Compañía:	PROYECTO DE INVESTIGACIÓN UNIVERSIDAD DE QUÉBEC-FICIRA-UAEM
Nombre:	**DETERMINAR LOS VALORES DE COMPRESIBILIDAD DE LAS ARCILLAS DEL VALLE DE TOLUCA.**
Ubicación:	PRESA DE ALMOLOYA DEL RIO, ESTADO DE MÉXICO.

DATOS DE LA MUESTRA

No. de ensaye:	CIRA-01	CÁLCULOS		ANTES DE LA PRUEBA		DESPUÉS DE LA PRUEBA	
Muestra No.	1	Ws (g)=	14,60	Vvi (cm^3)=	44,034	Ss=	2,14
S.P.T. No.	1	Whi (g)=	56,80	Vwi (cm^3)=	42,20	γhf (kg/m^3)=	1 266
Profundidad (m)	1,5-1,9	Wwi (g)=	42,20	γhi (kg/m3)=	1 117	Wf (%) =	216,44
Densidad de sólidos:	2,14	Whf (g)=	46,20	Wi (%) =	289,04	Gf (%) =	100,00
Área del anillo cm^2	25,428	Vi (cm^3)=	50,856	Gi (%) =	95,84	ef (%) =	4,349
Altura del anillo cm	2,00	Vf (cm^3)=	36,507	ei (%) =	6,453		
σ_o kg/cm2	0,180	Vs (cm^3)=	6,822				
Peso anillo + suelo (antes) gr:	187,30						
Peso anillo + suelo (después) gr:	176,70						
Peso anillo + suelo seco (gr):	145,10						
Peso anillo	130,50						

JEFE DE SECCIÓN	JEFA DEL LABORATORIO	DIRECTOR
C. EFRAÍN VALLEJO TOLEDANO	ING. MA. ESTHER ANTONIO SALINAS.	DR. MARTÍN CARLOS VERA ESTRADA.

Universidad Autónoma del Estado de México.
Facultad de Ingeniería
Laboratorio de Materiales.

INFORME DEL ENSAYE DE DENSIDAD DE SÓLIDOS

Compañía :	PROYECTO DE INVESTIGACIÓN UNIVERSIDAD DE QUÉBEC-FICIRA-UAEM	Reporte No.	DENS-CIRA-01
Obra:	**DETERMINAR LOS VALORES DE COMPRESIBILIDAD DE LAS ARCILLAS DEL VALLE DE TOLUCA.**	No. de Orden:	INVEST-01
		Fecha de Muestreo:	2007-06-13
Ubicación:	PRESA DE ALMOLOYA DEL RIO, ESTADO DE MÉXICO.	Fecha de Reporte:	2007-07-04

MATERIAL QUE PASA LA MALLA No. 4				
ENSAYE No.	CIRA-01	CIRA-01		
Sondeo No:	SPT-1	SPT-1		
Profundidad:	1,50-1,90	1,50-1,90		
MATRAZ No.	2	4		
Temperatura t °C	18	18		
Wmws gr	683,1	682,2		
Wmw gr	669	666,9		
Ws gr	26,6	28,4		
Ws + Wmw - Wmws	12,5	13,1		
K	0,9986	0,9986		
Ss	2,13	2,16		

DENSIDAD DE SUELOS (promedio) **2,14**

Ws : Peso del suelo seco

Wmw : Peso del matraz + agua a t

Wmws : Peso del matraz + agua + muestra a t

$$Ss = \frac{Ws\ K}{Ws + Wmw - Wmws}$$

K : Densidad del agua a t

Observaciones:	Muestra obtenida con tubo shelby.

Notas: **Los resultados son válidos sólo para los elementos ensayados.**
Este informe sólo es válido en su forma original. No debe ser reproducido, sin la aprobación por escrito del Laboratorio de Materiales de la Facultad de Ingeniería de la UAEM.

Jefe de sección.	Jefa del Laboratorio de Materiales	Director
C. Efraín Vallejo Toledano.	Ing. María Esther Antonio Salinas	Dr. Martín Carlos Vera Estrada.

Universidad Autónoma del Estado de México.
Facultad de Ingeniería.
Laboratorio de Materiales.
Cerro de Coatepec S/N, Ciudad Universitaria, Toluca México. C.P. 50130.
Tel. (722) 2 14 08 55, 2 14 05 34 Ext. 260. Fax Ext. 110.

INFORME DE CLASIFICACION DE MATERIALES TERREOS.

No. Presup.: VEST-01 Ensaye No. CIRA-01 No. Informe: IDEN-CIRA-01-2007 Hoja:

Muestra No:	01; Sondeo S.P.T.-1; Profundidad: 1,50 m a 1,90 m.
Fecha de toma de la muestra:	2007-Jun-13. Muestreo realizado por personal del Laboratorio de Materiales.
Fecha de realización de ensayes:	2007-Jun-23.
Fecha de Reporte:	2007-Jul-04.
Compañía:	PROYECTO DE INVESTIGACIÓN UNIVERSIDAD DE QUÉBEC-FICIRA-UAEM
Obra:	**DETERMINAR LOS VALORES DE COMPRESIBILIDAD DE LAS ARCILLAS DEL VALLE DE TOLUCA.**
Ubicación:	PRESA DE ALMOLOYA DEL RIO, ESTADO DE MÉXICO.

FRAGMENTOS DE ROCA (PORCIENTO EN PESO)	GRANDES (75 cm a 200 cm)	0%
	MEDIANOS (de 20 cm a 75 cm)	0%
	CHICOS (de 7,6 cm a 20 cm)	0%
SUELOS (PORCIENTO EN PESO)	PASA LA MALLA DE 7,6 cm (3")	100%

Tabla 1. Resultados del análisis granulométrico

Pulg.	mm	% parcial retenido	% que pasa
2"	50,0	0	100
1 ½"	37,5	0	100
1"	25,0	0	100
¾"	19,0	0	100
½"	12,7	0	100
3/8"	9,50	0	100
No. 4	4,75	0	100
No. 10	2,000	0	100
No. 20	0,850	1	99
No. 40	0,425	2	97
No. 60	0,250	3	94
No.100	0,150	4	90
No.200	0,075	5	85

D_{10} = Sin Dato D_{30} = Sin Dato
D_{60} = Sin Dato **en mm**

Cu = **No aplica** Cc = **No aplica**

GRAVAS (G) ARENAS (S) FINOS (F)

GRAFICA DE COMPOSICIÓN GRANULOMÉTRICA

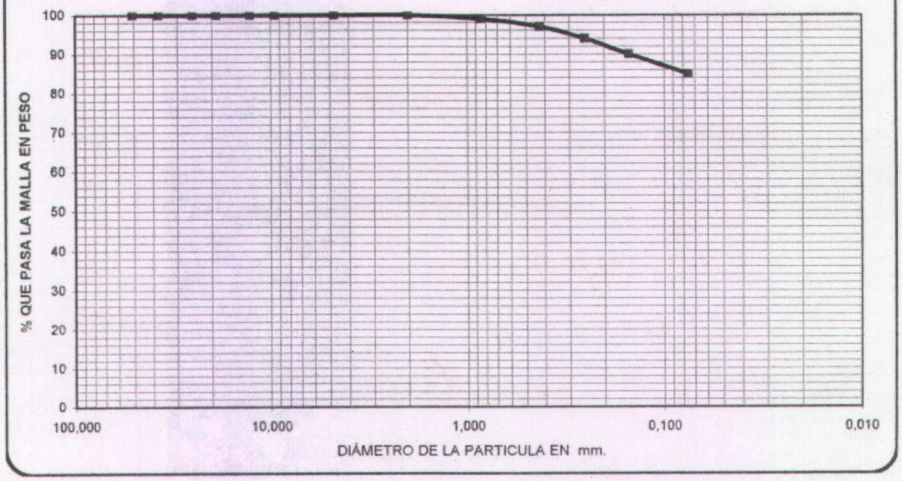


Tabla 2: Características del material retenido hasta la malla 4,75 mm (No. 4)

Tamaño Máximo:	9,5 mm	Aristas:	No aplica	Grado de alteración:	No aplica
Forma:	No aplica	Dureza:	No aplica	Textura superficial:	No aplica

Tabla 3: Resultados de los límites de consistencia

Límite Líquido (%)	167,3
Límite Plástico (%)	152,0
Índice Plástico (%)	15,3
Contracción Lineal (%)	5,7

Tabla 4: Resultados de la masa Volumétrica.

Masa Volumétrica Seca Suelta kg/m^3	

Contenido de agua del lugar: **175,0%**

Clasificación S.U.C.S	MH

Métodos de ensaye incluidos en el proceso "SERVICIOS DE EXTENSIÓN DEL LABORATORIO DE MATERIALES", CERTIFICADO CON LA NORMA ISO 9001:2000

NMX–C–416–ONNCCE–2003. INDUSTRIA DE LA CONSTRUCCIÓN–GEOTECNIA- Muestreo de estructuras térreas y métodos de prueba. Capítulo 2: Muestreo Capítulo 3: Procedimiento para la preparación de muestras. Capítulo 4. Determinación del contenido de agua. Capítulo 5. Determinación del análisis granulométrico. Capítulo 6: Determinación de los límites de consistencia. Capítulo 7: Determinación de la contracción lineal.

Notas: Los resultados son válidos sólo para los elementos ensayados.
Este informe sólo es válido en su forma original. No debe ser reproducido, sin la aprobación por escrito, del Laboratorio de Materiales de la Facultad de Ingeniería de la UAEM.

OBSERVACIONES:	Material color gris-café. Muestra obtenida con tubo shelby.

Jefe de sección.	Jefa del Laboratorio de Materiales	Director
C. Efraín Vallejo Toledano.	Ing. María Esther Antonio Salinas.	Dr. Martín Carlos Vera Estrada.

Universidad Autónoma del Estado de México.
Facultad de Ingeniería.
Laboratorio de Materiales.
Cerro de Coatepec S/N, Ciudad Universitaria, Toluca Méx., C.P. 50130
Tel. (722) 2 14 08 55, 2 15 45 12 Ext. 256-254. Fax: Ext. 110

INFORME DE LOS ENSAYES DE LÍMITES DE CONSISTENCIA Y CONTRACCIÓN LINEAL.

PRUEBA EN MATERIAL TAMIZADO POR LA MALLA No. 40

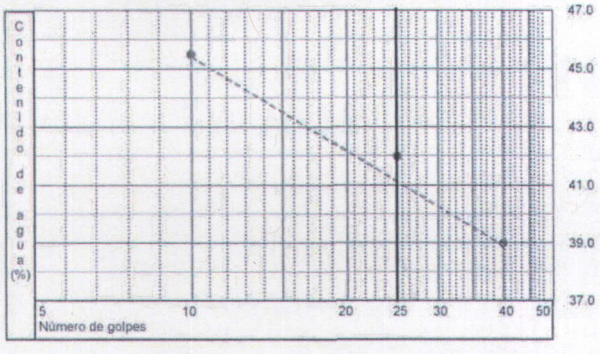
Ord. Trab.: INVEST-01 Ensaye No. CIRA-02 No. Informe: LIMI0CIRA-02-2008 Hoja: 1/16

Muestra No:	01, Tipo: Alterada; Sondeo SPT-1; Profundidad: 9,00 m .
Fecha de toma de la muestra:	2007-Oct-15. Muestreo realizado por personal del Laboratorio de Materiales.
Fecha de ensaye:	2007-Nov-07.
Fecha de reporte:	2007-Nov-14.
Compañía:	PROYECTO DE INVESTIGACIÓN UNIVERSIDAD DE QUÉBEC-FICIRA-UAEM
Obra:	DETERMINAR LOS VALORES DE COMPRESIBILIDAD DE LAS ARCILLAS DEL VALLE DE TOLUCA.
Ubicación:	RIO LERMA, TEMOAYA, ESTADO DE MÉXICO.

LIMITE LIQUIDO.

Número de golpes	Vidrio de reloj No.	Masa húmeda + vidrio Wm + T (1) g	Masa seca + vidrio Wd + T (2) g	Masa del vidrio de reloj T (3) g	Contenido de agua Ww (4) 4 = 1 - 2 g	Masa de suelo seca Ws (5) 5 = 2 - 3 g	Contenido de Agua w (6) 6 = 4 / 5 x 100 %
40	17	45,47	40,21	26,72	5,26	13,49	39,0
25	16	51,94	44,50	26,78	7,44	17,72	42,0
20							
10	14	48,24	41,52	26,74	6,72	14,78	45,5

LÍMITE PLÁSTICO	Vidrio de reloj No.	Masa húmeda + vidrio Wm + T (7) g	Masa seca + vidrio Wd + T (8) g	Masa del vidrio de reloj T (9) g	Contenido de agua Ww (10) 10 = 7 - 8 g	Masa de suelo seca Ws (11) 11= 8 - 9 g	Contenido de Agua w (12) 12 = 10 /11 x 100 %
	13	30,91	30,00	26,89	0,91	3,11	29,3
	13	30,91	30,00	26,89	0,91	3,11	29,3

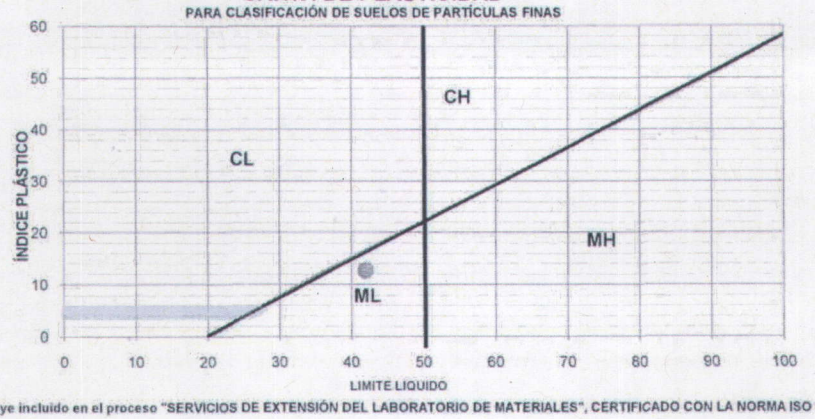


CONTRACCIÓN LINEAL	
MOLDE No.	30
Lectura inicial mm (13)	99,7
Lectura final mm (14)	94,9
% CL = 100 - ((14)/(13) x 100)	4,8

RESULTADOS	
Límite Líquido LL (%)	42,0
Límite Plástico LP (%)	29,3
Índice Plástico LP (%)	12,7
Contracción lineal (%)	4,8
CLASIFICACIÓN DEL SUELO FINO:	ML

CARTA DE PLASTICIDAD

PARA CLASIFICACIÓN DE SUELOS DE PARTÍCULAS FINAS



Método de ensaye incluido en el proceso "SERVICIOS DE EXTENSIÓN DEL LABORATORIO DE MATERIALES", CERTIFICADO CON LA NORMA ISO 9001:2000

NMX–C–416–ONNCCE–2003. INDUSTRIA DE LA CONSTRUCCIÓN–GEOTECNIA- Muestreo de estructuras térreas y métodos de prueba.
Capítulo 6: Determinación de los límites de consistencia. Capítulo 7: Determinación de la contracción lineal.

OBSERVACIONES: Material color gris en condición húmeda.

Notas: **Los resultados son válidos sólo para los elementos ensayados.**
Este informe sólo es válido en su forma original. No debe ser reproducido, sin la aprobación por escrito, del Laboratorio de Materiales de la Facultad de Ingeniería de la UAEM.

Jefe de Sección	Responsable de Servicios de Extensión	Jefe del Laboratorio de Materiales
C. Efraín Vallejo Toledano	Ing. José Saturnino Pérez Fajardo	M. en I. Sergio Alejandro Díaz Camacho.

Universidad Autónoma del Estado de México.
Facultad de Ingeniería.
Laboratorio de Materiales.
Cerro de Coatepec S/N, Ciudad Universitaria, Toluca México. C.P. 50130.
Tel. (722) 2 14 08 55, 2 14 05 34 Ext. 260. Fax Ext. 110.

INFORME DE CLASIFICACION DE MATERIALES TERREOS.

No. Ord. Trab.: INVEST-01 Ensaye No. CIRA-02 No. Informe: IDEN-0CIRA-02-2007 Hoja: 2/16

Muestra No:	01, Tipo: Alterada; Sondeo SPT-1; Profundidad: 9,00 m .
Fecha de toma de la muestra:	2007-Oct-15. Muestreo realizado por personal del Laboratorio de Materiales.
Fecha de realización de ensayes:	2007-Nov-05.
Fecha de Reporte:	2007-Nov-14.
Compañía:	PROYECTO DE INVESTIGACIÓN UNIVERSIDAD DE QUÉBEC-FICIRA-UAEM
Obra:	**DETERMINAR LOS VALORES DE COMPRESIBILIDAD DE LAS ARCILLAS DEL VALLE DE TOLUCA.**
Ubicación:	RIO LERMA, TEMOAYA, ESTADO DE MÉXICO.

FRAGMENTOS DE ROCA (PORCIENTO EN PESO)	GRANDES (75 cm a 200 cm)	0%
	MEDIANOS (de 20 cm a 75 cm)	0%
	CHICOS (de 7,6 cm a 20 cm)	0%
SUELOS (PORCIENTO EN PESO)	PASA LA MALLA DE 7,6 cm (3")	100%

Tabla 1. Resultados del análisis granulométrico

Pulg.	mm	% parcial retenido	% que pasa
2"	50,0	0,0	100,0
1 ½"	37,5	0,0	100,0
1"	25,0	0,0	100,0
¾"	19,0	0,0	100,0
½"	12,7	0,0	100,0
⅜"	9,50	0,0	100,0
No. 4	4,75	0,0	100,0
No. 10	2,000	0,3	99,7
No. 20	0,850	7,9	91,8
No. 40	0,425	5,1	86,7
No. 60	0,250	3,7	83,0
No.100	0,150	2,3	80,7
No.200	0,075	3,8	76,9

D_{10} = Sin dato D_{30} = Sin dato
D_{60} = Sin dato en mm

Cu = No aplica Cc = No aplica

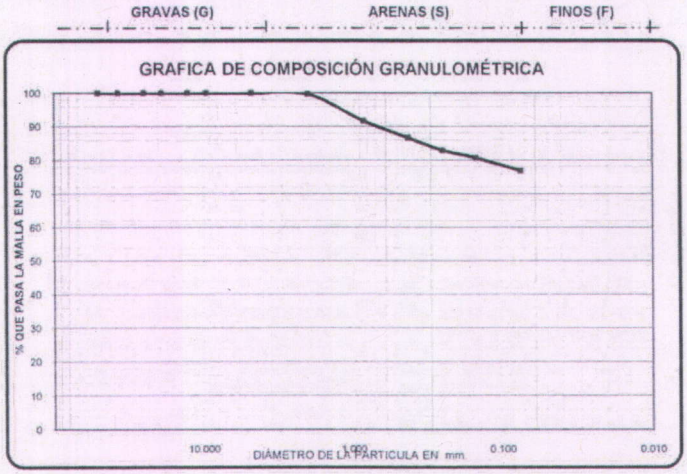


Tabla 2: Características del material retenido hasta la malla 4,75 mm (No. 4)

Tamaño Máximo:	No aplica	Aristas:	No aplica	Grado de alteración:	No aplica
Forma:	No aplica	Dureza:	No aplica	Textura superficial:	No aplica

Tabla 3: Resultados de los límites de consistencia

Límite Líquido (%)	42,0
Límite Plástico (%)	29,3
Índice Plástico (%)	12,7
Contracción Lineal (%)	4,8

Tabla 4: Resultados de la masa Volumétrica.

Masa Volumétrica Seca Suelta kg/m^3	No se determinó

Contenido de agua del lugar: **70,5%**

Clasificación S.U.C.S	ML

Métodos de ensaye incluidos en el proceso "SERVICIOS DE EXTENSIÓN DEL LABORATORIO DE MATERIALES", CERTIFICADO CON LA NORMA ISO 9001:2000

NMX–C–416–ONNCCE–2003. INDUSTRIA DE LA CONSTRUCCIÓN–GEOTECNIA- Muestreo de estructuras térreas y métodos de prueba. Capítulo 2: Muestreo Capítulo 3: Procedimiento para la preparación de muestras. Capítulo 4. Determinación del contenido de agua. Capítulo 5. Determinación del análisis granulométrico. Capítulo 6: Determinación de los límites de consistencia. Capítulo 7: Determinación de la contracción lineal.

Notas: Los resultados son válidos sólo para los elementos ensayados.
Este informe sólo es válido en su forma original. No debe ser reproducido, sin la aprobación por escrito, del Laboratorio de Materiales de la Facultad de Ingeniería de la UAEM.

OBSERVACIONES:	Material color gris en condición húmeda.

Jefe de sección.	Responsable de Servicios de Extensión	Jefe del Laboratorio de Materiales
C. Efraín Vallejo Toledano	Ing. José Saturnino Pérez Fajardo	M. en I. Sergio Alejandro Díaz Camacho.

Universidad Autónoma del Estado de México.
Facultad de Ingeniería.
Laboratorio de Materiales.
Cerro de Coatepec S/N, Ciudad Universitaria, Toluca Méx., C.P. 50130
Tel. (722) 2 14 08 55, 2 15 45 12 Ext. 256-254. Fax: Ext. 110

INFORME DE LOS ENSAYES DE LÍMITES DE CONSISTENCIA Y CONTRACCIÓN LINEAL.

PRUEBA EN MATERIAL TAMIZADO POR LA MALLA No. 40

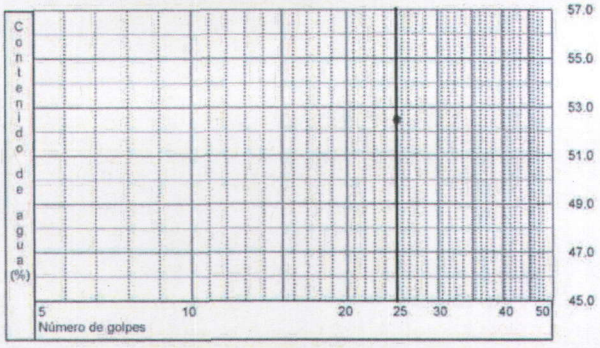
Ord. Trab.: INVEST-01 Ensaye No. CIRA-03 No. Informe: LIMI0CIRA-03-2008 Hoja: 3/16

Muestra No:	02, Tipo: Alterada; Sondeo SPT-1; Profundidad: 15 m .
Fecha de toma de la muestra:	2007-Oct-15. Muestreo realizado por personal del Laboratorio de Materiales.
Fecha de ensaye:	2007-Oct-22.
Fecha de reporte:	2007-Oct-29.
Compañía:	PROYECTO DE INVESTIGACIÓN UNIVERSIDAD DE QUÉBEC-FICIRA-UAEM
Obra:	**DETERMINAR LOS VALORES DE COMPRESIBILIDAD DE LAS ARCILLAS DEL VALLE DE TOLUCA.**
Ubicación:	RIO LERMA, TEMOAYA, ESTADO DE MÉXICO.

LÍMITE LÍQUIDO.

Número de golpes	Vidrio de reloj No.	Masa húmeda + vidrio Wm + T (1) g	Masa seca + vidrio Wd + T (2) g	Masa del vidrio de reloj T (3) g	Contenido de agua Ww (4) 4 = 1 - 2 g	Masa de suelo seca Ws (5) 5 = 2 - 3 g	Contenido de Agua w (6) 6 = 4 / 5 x 100 %
40							
25	8	42,72	36,03	23,28	6,69	12,75	52,5
20							
10							

	Vidrio de reloj No.	Masa húmeda + vidrio Wm + T (7) g	Masa seca + vidrio Wd + T (8) g	Masa del vidrio de reloj T (9) g	Contenido de agua Ww (10) 10 = 7 - 8 g	Masa de suelo seca Ws (11) 11= 8 - 9 g	Contenido de Agua w (12) 12 = 10 /11 x 100 %
LÍMITE PLÁSTICO	24	28,53	27,03	23,26	1,50	3,77	39,8
	24	28,53	27,03	23,26	1,50	3,77	39,8

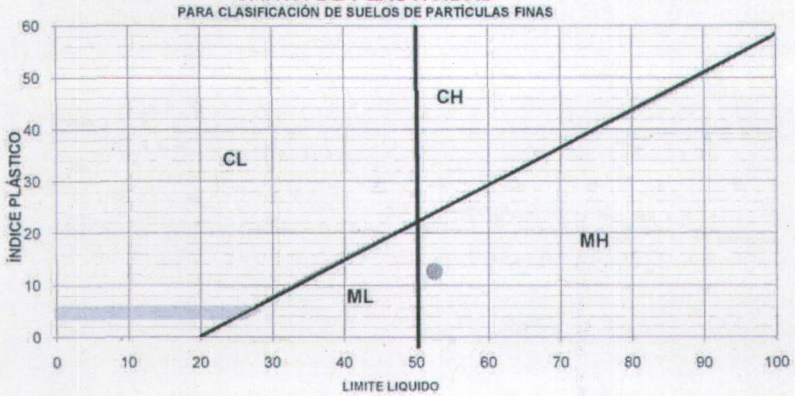


CONTRACCIÓN LINEAL	
MOLDE No.	23
Lectura inicial mm (13)	99,8
Lectura final mm (14)	95,3
% CL = 100 - ((14)/(13) x 100)	4,5

RESULTADOS	
Limite Líquido LL (%)	**52,5**
Limite Plástico LP (%)	**39,8**
Índice Plástico LP (%)	**12,7**
Contracción lineal (%)	**4,5**
CLASIFICACIÓN DEL SUELO FINO:	**MH**

CARTA DE PLASTICIDAD

PARA CLASIFICACIÓN DE SUELOS DE PARTÍCULAS FINAS



Método de ensaye incluido en el proceso "SERVICIOS DE EXTENSIÓN DEL LABORATORIO DE MATERIALES", CERTIFICADO CON LA NORMA ISO 9001:2000

NMX–C–416–ONNCCE–2003. INDUSTRIA DE LA CONSTRUCCIÓN–GEOTECNIA- Muestreo de estructuras térreas y métodos de prueba. Capítulo 6: Determinación de los límites de consistencia. Capítulo 7: Determinación de la contracción lineal.

OBSERVACIONES: Material color gris en condición húmeda.

Notas: **Los resultados son válidos sólo para los elementos ensayados.**
Este informe sólo es válido en su forma original. No debe ser reproducido, sin la aprobación por escrito, del Laboratorio de Materiales de la Facultad de Ingeniería de la UAEM.

Jefe de Sección	Responsable de Servicios de Extensión	Jefe del Laboratorio de Materiales
C. Efraín Vallejo Toledano	Ing. José Saturnino Pérez Fajardo	M. en I. Sergio Alejandro Díaz Camacho.

Universidad Autónoma del Estado de México.
Facultad de Ingeniería.
Laboratorio de Materiales.
Cerro de Coatepec S/N, Ciudad Universitaria, Toluca México. C.P. 50130.
Tel. (722) 2 14 08 55, 2 14 05 34 Ext. 260. Fax Ext. 110.

INFORME DE CLASIFICACION DE MATERIALES TERREOS.

No. Ord. Trab.: INVEST-01 Ensaye No. CIRA-03 No. Informe: IDEN-0CIRA-03-2007 Hoja: 4/16

Muestra No:	02, Tipo: Alterada; Sondeo SPT-1; Profundidad: 15 m .
Fecha de toma de la muestra:	2007-Oct-15. Muestreo realizado por personal del Laboratorio de Materiales.
Fecha de realización de ensayes:	2007-Oct-22.
Fecha de Reporte:	2007-Oct-29.
Compañía:	PROYECTO DE INVESTIGACIÓN UNIVERSIDAD DE QUÉBEC-FICIRA-UAEM
Obra:	**DETERMINAR LOS VALORES DE COMPRESIBILIDAD DE LAS ARCILLAS DEL VALLE DE TOLUCA.**
Ubicación:	RIO LERMA, TEMOAYA, ESTADO DE MÉXICO.

FRAGMENTOS DE ROCA (PORCIENTO EN PESO)	GRANDES (75 cm a 200 cm)	0%
	MEDIANOS (de 20 cm a 75 cm)	0%
	CHICOS (de 7,6 cm a 20 cm)	0%
SUELOS (PORCIENTO EN PESO)	PASA LA MALLA DE 7,6 cm (3")	100%

Tabla 1. Resultados del análisis granulométrico

Pulg.	mm	% parcial retenido	% que pasa
2"	50,0	0,0	100,0
1 ½"	37,5	0,0	100,0
1"	25,0	0,0	100,0
¾"	19,0	0,0	100,0
½"	12,7	0,0	100,0
⅜"	9,50	0,0	100,0
No. 4	4,75	0,0	100,0
No. 10	2,000	2,0	98,0
No. 20	0,850	6,5	91,5
No. 40	0,425	6,7	84,8
No. 60	0,250	5,4	79,4
No.100	0,150	2,6	76,8
No.200	0,075	4,7	72,1

D_{10} = Sin Dato D_{30} = Sin Dato
D_{60} = Sin Dato **en mm**

Cu = No aplica Cc = No aplica

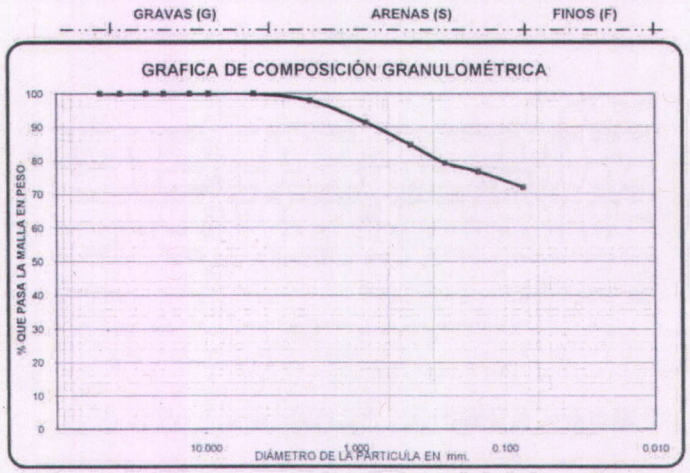


Tabla 2: Caracteristicas del material retenido hasta la malla 4,75 mm (No. 4)

Tamaño Máximo:	No aplica	Aristas:	No aplica	Grado de alteración:	No aplica
Forma:	No aplica	Dureza:	No aplica	Textura superficial:	No aplica

Tabla 3: Resultados de los límites de consistencia

Límite Líquido (%)	52,5
Límite Plástico (%)	39,8
Índice Plástico (%)	12,7
Contracción Lineal (%)	4,5

Tabla 4: Resultados de la masa Volumétrica.

Masa Volumétrica Seca Suelta kg/m^3	No se determinó

Contenido de agua del lugar: **63,0%**

Clasificación S.U.C.S	MH

Métodos de ensaye incluidos en el proceso "SERVICIOS DE EXTENSIÓN DEL LABORATORIO DE MATERIALES", CERTIFICADO CON LA NORMA ISO 9001:2000

NMX–C–416–ONNCCE–2003. INDUSTRIA DE LA CONSTRUCCIÓN–GEOTECNIA- Muestreo de estructuras térreas y métodos de prueba. Capítulo 2: Muestreo Capítulo 3: Procedimiento para la preparación de muestras. Capítulo 4. Determinación del contenido de agua. Capítulo 5. Determinación del análisis granulométrico. Capítulo 6: Determinación de los límites de consistencia. Capítulo 7: Determinación de la contracción lineal.

Notas: Los resultados son válidos sólo para los elementos ensayados.
Este informe sólo es válido en su forma original. No debe ser reproducido, sin la aprobación por escrito, del Laboratorio de Materiales de la Facultad de Ingeniería de la UAEM.

OBSERVACIONES:	Material color gris en condición húmeda.

Jefe de sección.	Responsable de Servicios de Extensión	Jefe del Laboratorio de Materiales
C. Efraín Vallejo Toledano	Ing. José Saturnino Pérez Pajardo	M. en I. Sergio Alejandro Díaz Camacho.

Universidad Autónoma del Estado de México.
Facultad de Ingeniería.
Laboratorio de Materiales.
Cerro de Coatepec S/N, Ciudad Universitaria, Toluca Méx., C.P. 50130
Tel. (722) 2 14 08 55, 2 15 45 12 Ext. 256-254. Fax: Ext. 110

INFORME DE LOS ENSAYES DE LÍMITES DE CONSISTENCIA Y CONTRACCIÓN LINEAL.

PRUEBA EN MATERIAL TAMIZADO POR LA MALLA No. 40

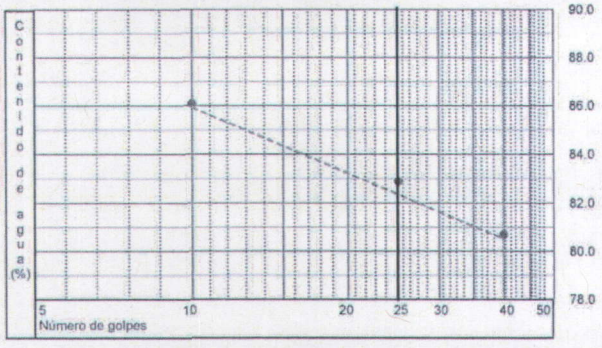
Ord. Trab.: INVEST-01 Ensaye No. CIRA-04 No. Informe: LIMI0CIRA-04-2008 Hoja: 5/16

Muestra No:	01, Tipo: Alterada; Sondeo SPT-1; Profundidad: 7,00-7,50 m .
Fecha de toma de la muestra:	2007-Ago-27. Muestreo realizado por personal del Laboratorio de Materiales.
Fecha de ensaye:	2007-Sep-11.
Fecha de reporte:	2007-Sep-18.
Compañía:	PROYECTO DE INVESTIGACIÓN UNIVERSIDAD DE QUÉBEC-FICIRA-UAEM
Obra:	DETERMINAR LOS VALORES DE COMPRESIBILIDAD DE LAS ARCILLAS DEL VALLE DE TOLUCA.
Ubicación:	RIO LERMA, SAN MATEO ATENCO, ESTADO DE MÉXICO.

LÍMITE LÍQUIDO.

Número de golpes	Vidrio de reloj No.	Masa húmeda + vidrio Wm + T (1) g	Masa seca + vidrio Wd + T (2) g	Masa del vidrio de reloj T (3) g	Contenido de agua Ww (4) 4 = 1 - 2 g	Masa de suelo seca Ws (5) 5 = 2 - 3 g	Contenido de Agua w (6) 6 = 4 / 5 x 100 %
40	5	51,56	40,53	26,87	11,03	13,66	80,7
25	4	47,77	36,49	22,89	11,28	13,60	82,9
20							
10	6	46,61	35,83	23,31	10,78	12,52	86,1

LÍMITE PLÁSTICO	Vidrio de reloj No.	Masa húmeda + vidrio Wm + T (7) g	Masa seca + vidrio Wd + T (8) g	Masa del vidrio de reloj T (9) g	Contenido de agua Ww (10) 10 = 7 - 8 g	Masa de suelo seca Ws (11) 11= 8 - 9 g	Contenido de Agua w (12) 12 = 10 /11 x 100 %
	7	52,81	38,75	20,15	14,06	18,60	75,6
	7	52,81	38,75	20,15	14,06	18,60	75,6

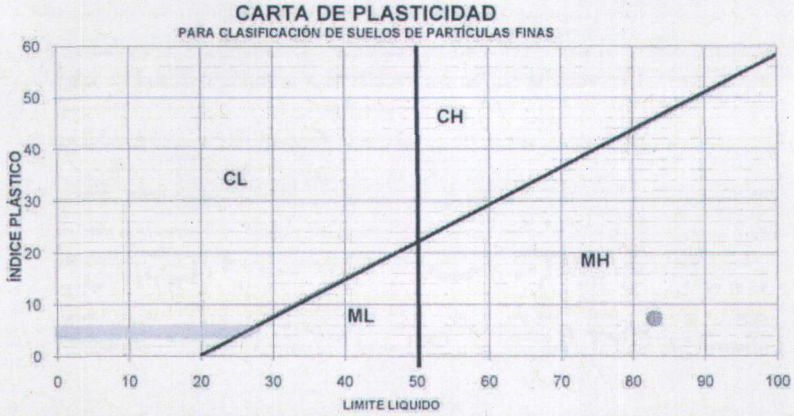


CONTRACCIÓN LINEAL	
MOLDE No.	1
Lectura inicial mm (13)	99,3
Lectura final mm (14)	96,6
% CL = 100 - ((14)/(13) x 100)	2,7

RESULTADOS	
Límite Líquido LL (%)	**82,9**
Límite Plástico LP (%)	**75,6**
Índice Plástico LP (%)	**7,3**
Contracción lineal (%)	**2,7**
CLASIFICACIÓN DEL SUELO FINO:	**OH**

CARTA DE PLASTICIDAD

PARA CLASIFICACIÓN DE SUELOS DE PARTÍCULAS FINAS



Método de ensaye incluido en el proceso "SERVICIOS DE EXTENSIÓN DEL LABORATORIO DE MATERIALES", CERTIFICADO CON LA NORMA ISO 9001:2000

NMX–C–416–ONNCCE–2003. INDUSTRIA DE LA CONSTRUCCIÓN–GEOTECNIA- Muestreo de estructuras térreas y métodos de prueba.
Capítulo 6: Determinación de los límites de consistencia. Capítulo 7: Determinación de la contracción lineal.

OBSERVACIONES: Material color negro en condición húmeda.

Notas: **Los resultados son válidos sólo para los elementos ensayados.**
Este informe sólo es válido en su forma original. No debe ser reproducido, sin la aprobación por escrito, del Laboratorio de Materiales de la Facultad de Ingeniería de la UAEM.

Jefe de Sección	Responsable de Servicios de Extensión	Jefe del Laboratorio de Materiales
C. Bicain Vallejo Toledano	Ing. José Saturnino Pérez Fajardo	M. en I. Sergio Alejandro Díaz Camacho.

Universidad Autónoma del Estado de México.
Facultad de Ingeniería.
Laboratorio de Materiales.
Cerro de Coatepec S/N, Ciudad Universitaria, Toluca México. C.P. 50130.
Tel. (722) 2 14 08 55, 2 14 05 34 Ext. 260. Fax Ext. 110.

INFORME DE CLASIFICACION DE MATERIALES TERREOS.

No. Ord. Trab.: INVEST-01 Ensaye No. CIRA-04 No. Informe: IDEN-0CIRA-04-2007 Hoja: 6/16

Muestra No:	01, Tipo: Alterada; Sondeo SPT-1; Profundidad: 7,00-7,50 m .
Fecha de toma de la muestra:	2007-Ago-27. Muestreo realizado por personal del Laboratorio de Materiales.
Fecha de realización de ensayes:	2007-Sep-11.
Fecha de Reporte:	2007-Sep-18.
Compañía:	PROYECTO DE INVESTIGACIÓN UNIVERSIDAD DE QUÉBEC-FICIRA-UAEM
Obra:	**DETERMINAR LOS VALORES DE COMPRESIBILIDAD DE LAS ARCILLAS DEL VALLE DE TOLUCA.**
Ubicación:	RIO LERMA, SAN MATEO ATENCO, ESTADO DE MÉXICO.

FRAGMENTOS DE ROCA (PORCIENTO EN PESO)	GRANDES (75 cm a 200 cm)	0%
	MEDIANOS (de 20 cm a 75 cm)	0%
	CHICOS (de 7,6 cm a 20 cm)	0%
SUELOS (PORCIENTO EN PESO)	PASA LA MALLA DE 7,6 cm (3")	100%

Tabla 1. Resultados del análisis granulométrico

Pulg.	mm	% parcial retenido	% que pasa
2"	50,0	0,0	100,0
1 ½"	37,5	0,0	100,0
1"	25,0	0,0	100,0
¾"	19,0	0,0	100,0
½"	12,7	0,0	100,0
⅜"	9,50	0,0	100,0
No. 4	4,75	0,0	100,0
No. 10	2,000	6,9	93,1
No. 20	0,850	9,7	83,4
No. 40	0,425	6,8	76,6
No. 60	0,250	4,7	71,9
No.100	0,150	3,8	68,1
No.200	0,075	4,7	63,4

D_{10} = Sin dato D_{30} = Sin dato
D_{60} = Sin dato en mm

Cu = No aplica Cc = No aplica

GRAVAS (G) ARENAS (S) FINOS (F)

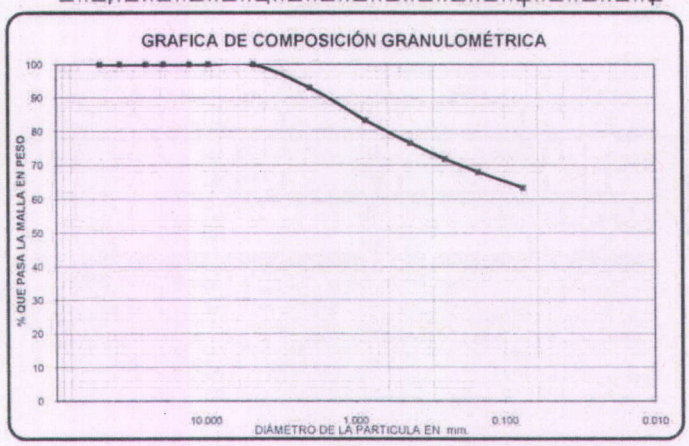


Tabla 2: Características del material retenido hasta la malla 4,75 mm (No. 4)

Tamaño Máximo:	No aplica	Aristas:	No aplica	Grado de alteración:	No aplica
Forma:	No aplica	Dureza:	No aplica	Textura superficial:	No aplica

Tabla 3: Resultados de los límites de consistencia

Límite Líquido (%)	82,9
Límite Plástico (%)	75,6
Índice Plástico (%)	7,3
Contracción Lineal (%)	2,7

Tabla 4: Resultados de la masa Volumétrica.

Masa Volumétrica Seca Suelta kg/m^3	No se determinó

Contenido de agua del lugar: 230,0%

Clasificación S.U.C.S	OH

Métodos de ensaye incluidos en el proceso "SERVICIOS DE EXTENSIÓN DEL LABORATORIO DE MATERIALES", CERTIFICADO CON LA NORMA ISO 9001:2000

NMX–C–416–ONNCCE–2003. INDUSTRIA DE LA CONSTRUCCIÓN–GEOTECNIA- Muestreo de estructuras térreas y métodos de prueba. Capítulo 2: Muestreo Capítulo 3: Procedimiento para la preparación de muestras. Capítulo 4. Determinación del contenido de agua. Capítulo 5. Determinación del análisis granulométrico. Capítulo 6: Determinación de los límites de consistencia. Capítulo 7: Determinación de la contracción lineal.

Notas: Los resultados son válidos sólo para los elementos ensayados.
Este informe sólo es válido en su forma original. No debe ser reproducido, sin la aprobación por escrito, del Laboratorio de Materiales de la Facultad de Ingeniería de la UAEM.

OBSERVACIONES:	Material color negro en condición húmeda.

Laboratorista	Responsable de Servicios de Extensión	Jefe del Laboratorio de Materiales
P.P		
C. Eloy Estrada Ramírez	Ing. José Saturnino Pérez Fajardo	M. en I. Sergio Alejandro Díaz Camacho.

Universidad Autónoma del Estado de México.
Facultad de Ingeniería.
Laboratorio de Materiales.
Cerro de Coatepec S/N, Ciudad Universitaria, Toluca Méx., C.P. 50130
Tel. (722) 2 14 08 55, 2 15 45 12 Ext. 256-254. Fax: Ext. 110

INFORME DE LOS ENSAYES DE LÍMITES DE CONSISTENCIA Y CONTRACCIÓN LINEAL.

PRUEBA EN MATERIAL TAMIZADO POR LA MALLA No. 40

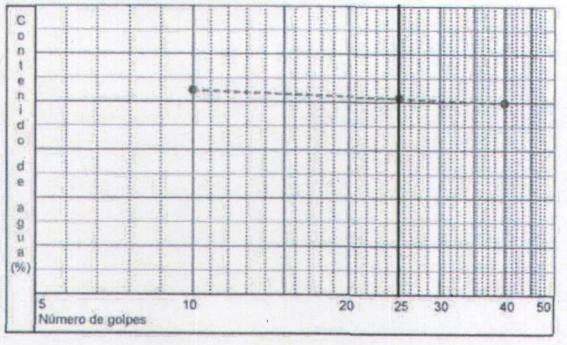
Ord. Trab.: INVEST-01 Ensaye No. CIRA-05 No. Informe: LIMI0CIRA-05-2008 Hoja: 7/16

Muestra No:	02, Tipo: Alterada; Sondeo SPT-1; Profundidad: 28,00-28,20 m .
Fecha de toma de la muestra:	2007-Ago-27. Muestreo realizado por personal del Laboratorio de Materiales.
Fecha de ensaye:	2007-Oct-11.
Fecha de reporte:	2007-Oct-18.
Compañía:	PROYECTO DE INVESTIGACIÓN UNIVERSIDAD DE QUÉBEC-FICIRA-UAEM
Obra:	DETERMINAR LOS VALORES DE COMPRESIBILIDAD DE LAS ARCILLAS DEL VALLE DE TOLUCA.
Ubicación:	RIO LERMA, SAN MATEO ATENCO, ESTADO DE MÉXICO.

LIMITE LIQUIDO.

Número de golpes	Vidrio de reloj No.	Masa húmeda + vidrio Wm + T (1) g	Masa seca + vidrio Wd + T (2) g	Masa del vidrio de reloj T (3) g	Contenido de agua Ww (4) 4 = 1 - 2 g	Masa de suelo seca Ws (5) 5 = 2 - 3 g	Contenido de Agua w (6) 6 = 4 / 5 x 100 %
40	10	50,56	46,11	26,80	4,45	19,31	23,0
25	16	52,84	47,93	26,78	4,91	21,15	23,2
20							
10	1	49,70	45,33	26,75	4,37	18,58	23,5

LÍMITE PLÁSTICO	Vidrio de reloj No.	Masa húmeda + vidrio Wm + T (7) g	Masa seca + vidrio Wd + T (8) g	Masa del vidrio de reloj T (9) g	Contenido de agua Ww (10) 10 = 7 - 8 g	Masa de suelo seca Ws (11) 11= 8 - 9 g	Contenido de Agua w (12) 12 = 10 /11 x 100 %
	37	34,80	34,04	29,49	0,76	4,55	16,7
	37	34,80	34,04	29,49	0,76	4,55	16,7

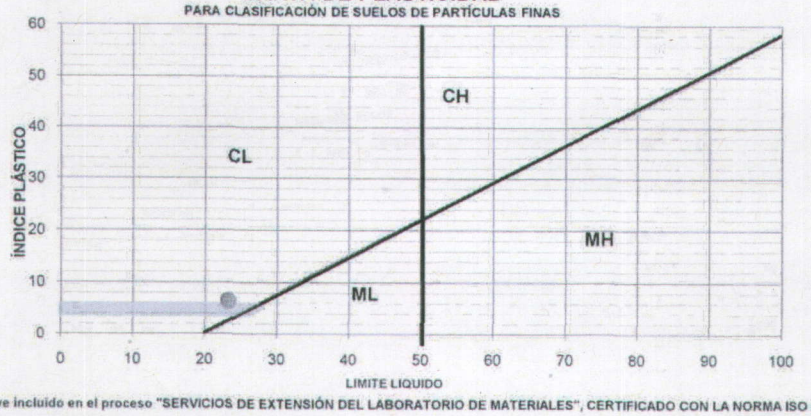


CONTRACCIÓN LINEAL	
MOLDE No.	29
Lectura inicial mm (13)	99,7
Lectura final mm (14)	96,8
% CL = 100 - ((14)/(13) x 100)	2,9

RESULTADOS	
Límite Líquido LL (%)	23,2
Límite Plástico LP (%)	16,7
Índice Plástico LP (%)	6,5
Contracción lineal (%)	2,9
CLASIFICACIÓN DEL SUELO FINO:	CL-ML

CARTA DE PLASTICIDAD

PARA CLASIFICACIÓN DE SUELOS DE PARTÍCULAS FINAS



Método de ensaye incluido en el proceso "SERVICIOS DE EXTENSIÓN DEL LABORATORIO DE MATERIALES", CERTIFICADO CON LA NORMA ISO 9001:2000

NMX–C–416–ONNCCE–2003. INDUSTRIA DE LA CONSTRUCCIÓN–GEOTECNIA- Muestreo de estructuras térreas y métodos de prueba.
Capítulo 6: Determinación de los límites de consistencia. Capítulo 7: Determinación de la contracción lineal.

OBSERVACIONES: Material color gris en condición húmeda.

Notas: **Los resultados son válidos sólo para los elementos ensayados.**
Este informe sólo es válido en su forma original. No debe ser reproducido, sin la aprobación por escrito, del Laboratorio de Materiales de la Facultad de Ingeniería de la UAEM.

Jefe de Sección	Responsable de Servicios de Extensión	Jefe del Laboratorio de Materiales
C. Efraín Vallejo Toledano	Ing. José Saturnino Pérez Fajardo	M. en I. Sergio Alejandro Díaz Camacho.

Universidad Autónoma del Estado de México.
Facultad de Ingeniería.
Laboratorio de Materiales.
Cerro de Coatepec S/N, Ciudad Universitaria, Toluca México, C.P. 50130.
Tel. (722) 2 14 08 55, 2 14 05 34 Ext. 260. Fax Ext. 110.

INFORME DE CLASIFICACION DE MATERIALES TERREOS.

No. Ord. Trab.: INVEST-01 Ensaye No. CIRA-05 No. Informe: IDEN-0CIRA-05-2007 Hoja: 8/16

Muestra No:	02, Tipo: Alterada; Sondeo SPT-1; Profundidad: 28,00-28,20 m .
Fecha de toma de la muestra:	2007-Ago-27. Muestreo realizado por personal del Laboratorio de Materiales.
Fecha de realización de ensayes:	2007-Oct-06.
Fecha de Reporte:	2007-Oct-13.
Compañía:	PROYECTO DE INVESTIGACIÓN UNIVERSIDAD DE QUÉBEC-FICIRA-UAEM
Obra:	**DETERMINAR LOS VALORES DE COMPRESIBILIDAD DE LAS ARCILLAS DEL VALLE DE TOLUCA.**
Ubicación:	RIO LERMA, SAN MATEO ATENCO, ESTADO DE MÉXICO.

FRAGMENTOS DE ROCA (PORCIENTO EN PESO)	GRANDES (75 cm a 200 cm)	0%
	MEDIANOS (de 20 cm a 75 cm)	0%
	CHICOS (de 7,6 cm a 20 cm)	0%
SUELOS (PORCIENTO EN PESO)	PASA LA MALLA DE 7,6 cm (3")	100%

Tabla 1. Resultados del análisis granulométrico

Pulg.	mm	% parcial retenido	% que pasa
2"	50,0	0,0	100,0
1 ½"	37,5	0,0	100,0
1"	25,0	0,0	100,0
¾"	19,0	0,0	100,0
½"	12,7	0,0	100,0
⅜"	9,50	0,0	100,0
No. 4	4,75	0,9	99,1
No. 10	2,000	0,6	98,5
No. 20	0,850	3,1	95,4
No. 40	0,425	6,3	89,1
No. 60	0,250	15,2	73,9
No.100	0,150	14,3	59,6
No.200	0,075	18,8	40,8

D_{10} = Sin dato D_{30} = Sin dato
D_{60} = Sin dato **en mm**

Cu = No aplica Cc = No aplica

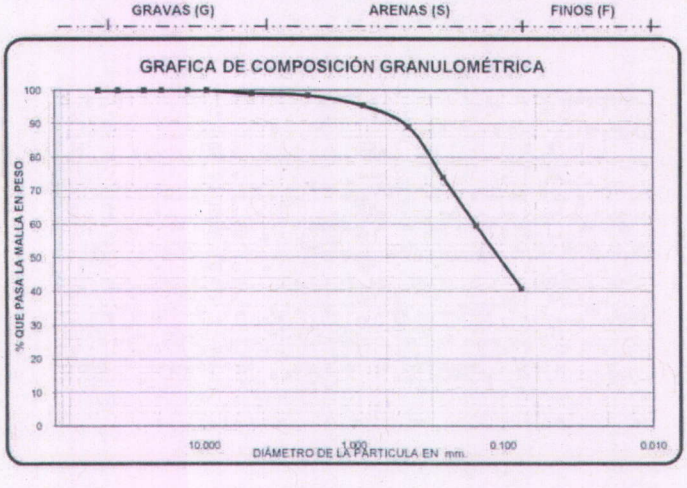


Tabla 2: Características del material retenido hasta la malla 4,75 mm (No. 4)

Tamaño Máximo:	No aplica	Aristas:	No aplica	Grado de alteración:	No aplica
Forma:	No aplica	Dureza:	No aplica	Textura superficial:	No aplica

Tabla 3: Resultados de los límites de consistencia

Límite Líquido (%)	23,2
Límite Plástico (%)	16,7
Índice Plástico (%)	6,5
Contracción Lineal (%)	2,9

Tabla 4: Resultados de la masa Volumétrica.

Masa Volumétrica Seca Suelta kg/m^3	No se determinó

Contenido de agua del lugar: **28,8%**

Clasificación S.U.C.S	SC-SM

Métodos de ensaye incluidos en el proceso "SERVICIOS DE EXTENSIÓN DEL LABORATORIO DE MATERIALES", CERTIFICADO CON LA NORMA ISO 9001:2000

NMX–C–416–ONNCCE–2003. INDUSTRIA DE LA CONSTRUCCIÓN–GEOTECNIA- Muestreo de estructuras térreas y métodos de prueba. Capítulo 2: Muestreo Capítulo 3: Procedimiento para la preparación de muestras. Capítulo 4. Determinación del contenido de agua. Capítulo 5. Determinación del análisis granulométrico. Capítulo 6: Determinación de los límites de consistencia. Capítulo 7: Determinación de la contracción lineal.

Notas: Los resultados son válidos sólo para los elementos ensayados.
Este informe sólo es válido en su forma original. No debe ser reproducido, sin la aprobación por escrito, del Laboratorio de Materiales de la Facultad de Ingeniería de la UAEM.

OBSERVACIONES:	Material color gris en condición húmeda.

Laboratorista	Responsable de Servicios de Extensión	Jefe del Laboratorio de Materiales
C. Eloy Estrada Ramírez	Ing. José Sacramino Pérez Fajardo	M. en I. Sergio Alejandro Díaz Camacho.

Universidad Autónoma del Estado de México.
Facultad de Ingeniería
Laboratorio de Materiales.

INFORME DEL ENSAYE DE DENSIDAD DE SÓLIDOS

Compañía :	PROYECTO DE INVESTIGACIÓN UNIVERSIDAD DE QUÉBEC-FICIRA-UAEM	Reporte No.	DENS-CIRA-02
Obra:	**DETERMINAR LOS VALORES DE COMPRESIBILIDAD DE LAS ARCILLAS DEL VALLE DE TOLUCA.**	No. de Orden:	INVEST-01
		Fecha de Muestreo:	2007-10-15
Ubicación:	RIO LERMA, TEMOAYA, ESTADO DE MÉXICO.	Fecha de Reporte:	2007-11-28

MATERIAL QUE PASA LA MALLA No. 4				
ENSAYE No.	CIRA-02			
Sondeo No:	SPT-1			
Profundidad:	9,00			
MATRAZ No.	1			
Temperatura t °C	19			
Wmws gr	696,9			
Wmw gr	667,1			
Ws gr	50,4			
Ws + Wmw - Wmws	20,6			
K	0,9984			
Ss	2,44			

DENSIDAD DE SUELOS (promedio) **2,44**

Ws : Peso del suelo seco

Wmw : Peso del matraz + agua a t

Wmws : Peso del matraz + agua + muestra a t

$$Ss = \frac{Ws\ K}{Ws + Wmw - Wmws}$$

K : Densidad del agua a t

Observaciones:	Muestra obtenida con tubo shelby.

Notas: **Los resultados son válidos sólo para los elementos ensayados.**
Este informe sólo es válido en su forma original. No debe ser reproducido, sin la aprobación por escrito del Laboratorio de Materiales de la Facultad de Ingeniería de la UAEM.

Jefe de sección	Responsable de los Servicios de Extensión	Jefe del Laboratorio de Materiales
C. Efraín Vallejo Toledano	Ing. José Saturnino Pérez Fajardo	M. en I. Sergio Alejandro Díaz Camacho

Universidad Autónoma del Estado de México.
Facultad de Ingeniería
Laboratorio de Materiales.

INFORME DEL ENSAYE DE DENSIDAD DE SÓLIDOS

Compañía :	PROYECTO DE INVESTIGACIÓN UNIVERSIDAD DE QUÉBEC-FICIRA-UAEM	Reporte No.	DENS-CIRA-03
Obra:	**DETERMINAR LOS VALORES DE COMPRESIBILIDAD DE LAS ARCILLAS DEL VALLE DE TOLUCA.**	No. de Orden:	INVEST-01
		Fecha de Muestreo:	2007-10-15
Ubicación:	RIO LERMA, TEMOAYA, ESTADO DE MÉXICO.	Fecha de Reporte:	2007-11-28

MATERIAL QUE PASA LA MALLA No. 4				
ENSAYE No.	CIRA-03			
Sondeo No:	SPT-1			
Profundidad:	15,00			
MATRAZ No.	2			
Temperatura t °C	20			
Wmws gr	672,5			
Wmw gr	654,7			
Ws gr	29,8			
Ws + Wmw - Wmws	12			
K	0,9982			
Ss	2,48			

DENSIDAD DE SUELOS (promedio) **2,48**

Ws : Peso del suelo seco

Wmw : Peso del matraz + agua a t

Wmws : Peso del matraz + agua + muestra a t

$$Ss = \frac{Ws\ K}{Ws + Wmw - Wmws}$$

K : Densidad del agua a t

Observaciones:	Muestra obtenida con tubo shelby.

Notas: **Los resultados son válidos sólo para los elementos ensayados.**
Este informe sólo es válido en su forma original. No debe ser reproducido, sin la aprobación por escrito del Laboratorio de Materiales de la Facultad de Ingeniería de la UAEM.

Jefe de sección	Responsable de los Servicios de Extensión	Jefe del Laboratorio de Materiales
C. Efraín Vallejo Toledano	Ing. José Saturnino Pérez Fajardo	M. en I. Sergio Alejandro Díaz Camacho

Universidad Autónoma del Estado de México.
Facultad de Ingeniería
Laboratorio de Materiales.

INFORME DEL ENSAYE DE DENSIDAD DE SÓLIDOS

Compañía :	PROYECTO DE INVESTIGACIÓN UNIVERSIDAD DE QUÉBEC-FICIRA-UAEM	Reporte No.	DENS-CIRA-04
Obra:	**DETERMINAR LOS VALORES DE COMPRESIBILIDAD DE LAS ARCILLAS DEL VALLE DE TOLUCA.**	No. de Orden:	INVEST-01
		Fecha de Muestreo:	2007-08-27
Ubicación:	RIO LERMA, SAN MATEO ATENCO, ESTADO DE MÉXICO.	Fecha de Reporte:	2007-11-28

MATERIAL QUE PASA LA MALLA No. 4				
ENSAYE No.	CIRA-04	CIRA-04		
Sondeo No:	SPT-1	SPT-1		
Profundidad:	7,00-7,50	7,00-7,50		
MATRAZ No.	2	4		
Temperatura t °C	19	19		
Wmws gr	685,7	683,3		
Wmw gr	669,2	667,2		
Ws gr	28,9	28,4		
Ws + Wmw - Wmws	12,4	12,3		
K	0,9984	0,9984		
Ss	2,33	2,31		

DENSIDAD DE SUELOS (promedio) **2,32**

Ws : Peso del suelo seco

Wmw : Peso del matraz + agua a t

Wmws : Peso del matraz + agua + muestra a t

$$Ss = \frac{Ws\ K}{Ws + Wmw - Wmws}$$

K : Densidad del agua a t

Observaciones:	Muestra obtenida con tubo shelby.

Notas: **Los resultados son válidos sólo para los elementos ensayados.**
Este informe sólo es válido en su forma original. No debe ser reproducido, sin la aprobación por escrito del Laboratorio de Materiales de la Facultad de Ingeniería de la UAEM.

Jefe de sección	Responsable de los Servicios de Extensión	Jefe del Laboratorio de Materiales
C. Efraín Vallejo Toledano	Ing. José Saturnino Pérez Fajardo	M. en I. Sergio Alejandro Díaz Camacho

Universidad Autónoma del Estado de México.
Facultad de Ingeniería
Laboratorio de Materiales.

INFORME DEL ENSAYE DE DENSIDAD DE SÓLIDOS

Compañía :	PROYECTO DE INVESTIGACIÓN UNIVERSIDAD DE QUÉBEC-FICIRA-UAEM	Reporte No.	DENS-CIRA-05
Obra:	**DETERMINAR LOS VALORES DE COMPRESIBILIDAD DE LAS ARCILLAS DEL VALLE DE TOLUCA.**	No. de Orden:	INVEST-01
		Fecha de Muestreo:	2007-08-27
Ubicación:	RIO LERMA, SAN MATEO ATENCO, ESTADO DE MÉXICO.	Fecha de Reporte:	2007-11-28

MATERIAL QUE PASA LA MALLA No. 4				
ENSAYE No.	CIRA-05	CIRA-04		
Sondeo No:	SPT-1	SPT-1		
Profundidad:	28,00-28,50	28,00-28,50		
MATRAZ No.	2	4		
Temperatura t °C	20	20		
Wmws gr	699,2	697,4		
Wmw gr	668,9	667,1		
Ws gr	49,2	48,8		
Ws + Wmw - Wmws	18,9	18,5		
K	0,9982	0,9982		
Ss	2,60	2,63		

DENSIDAD DE SUELOS (promedio) **2,62**

Ws : Peso del suelo seco

Wmw : Peso del matraz + agua a t

Wmws : Peso del matraz + agua + muestra a t

$$Ss = \frac{Ws\ K}{Ws + Wmw - Wmws}$$

K : Densidad del agua a t

Observaciones:	Muestra obtenida con tubo shelby.

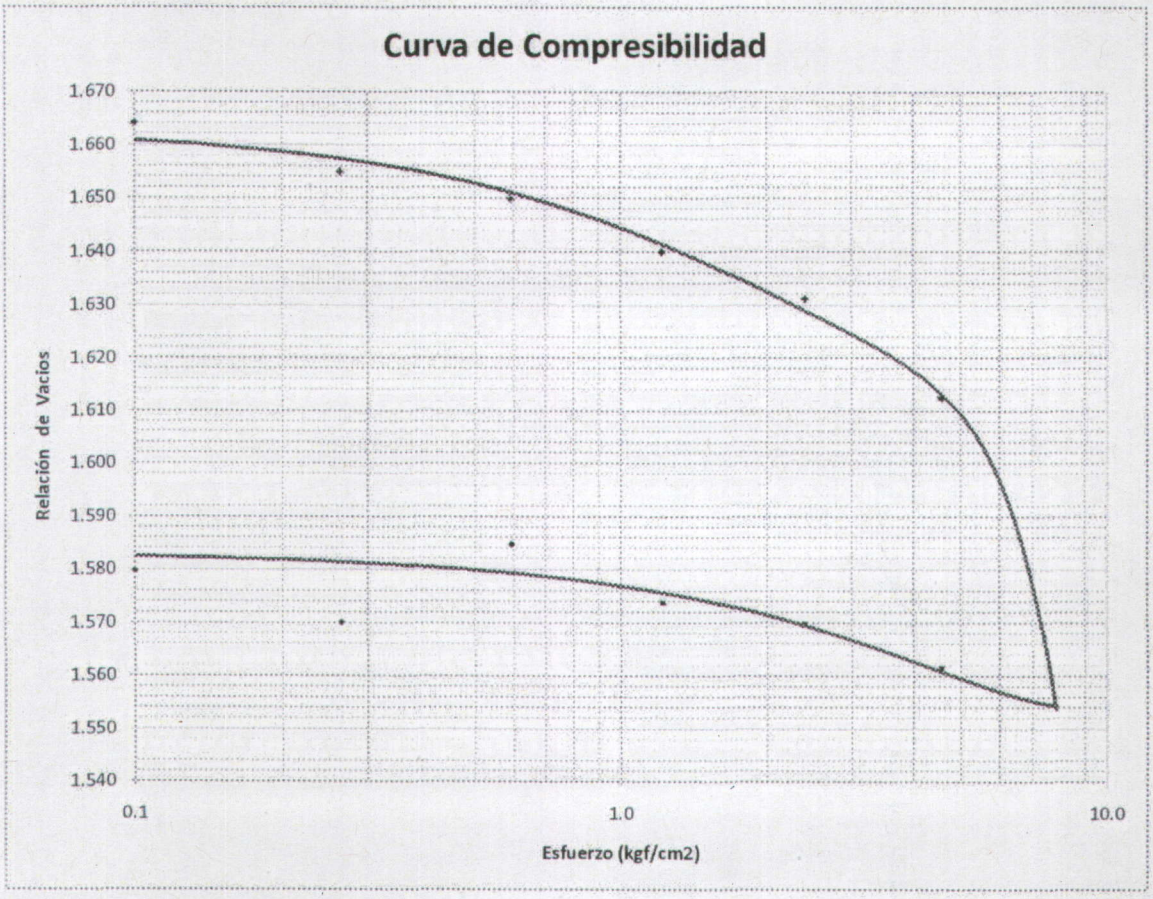
Notas: **Los resultados son válidos sólo para los elementos ensayados.**
Este informe sólo es válido en su forma original. No debe ser reproducido, sin la aprobación por escrito del Laboratorio de Materiales de la Facultad de Ingeniería de la UAEM.

Jefe de sección	Responsable de los Servicios de Extensión	Jefe del Laboratorio de Materiales
C. Efraín Vallejo Toledano	Ing. José Saturnino Pérez Fajardo	M. en I. Sergio Alejandro Díaz Camacho

CURVA DE COMPRESIBILIDAD

Compañía:	PROYECTO DE INVESTIGACIÓN UNIVERSIDAD DE QUÉBEC-FICIRA-UAEM	No. Orden:	CONS-CIRA-03
Nombre:	**DETERMINAR LOS VALORES DE COMPRESIBILIDAD DE LAS ARCILLAS DEL VALLE DE TOLUCA.**	Fecha muestreo:	2007-Oct-15
		Fecha prueba:	2007-Nov-05
Ubicación:	RIO LERMA, TEMOAYA, ESTADO DE MÉXICO.	Fecha reporte:	2007-Nov-30

No. de ensaye	S.P.T. No.	Muestra No.	Profundidad muestreo (m)	δ_s	ω_i (%)	ω_f (%)	e_i	e_f	Gw_i (%)	Gw_f (%)	Presión efectiva (kg/cm^2)
CIRA-02	1	2	15,0	2,48	62,97	63,60	1,67	1,593	93,47	98,99	5,7



MÉTODOS DE ENSAYE UTILIZADOS:

ASTM D 4186-89: STANDART TEST METHOD FOR ONE-DIMENSIONAL CONSOLIDATION PROPERTIES OF SOILS USING CONTROLLED - STRAIN LOADING.

Notas: **Los resultados son válidos sólo para los elementos ensayados.**
Este informe sólo es válido en su forma original. No debe ser reproducido sin la aprobación por escrito del Laboratorio de Materiales de la Facultad de Ingeniería de la U.A.E.M.

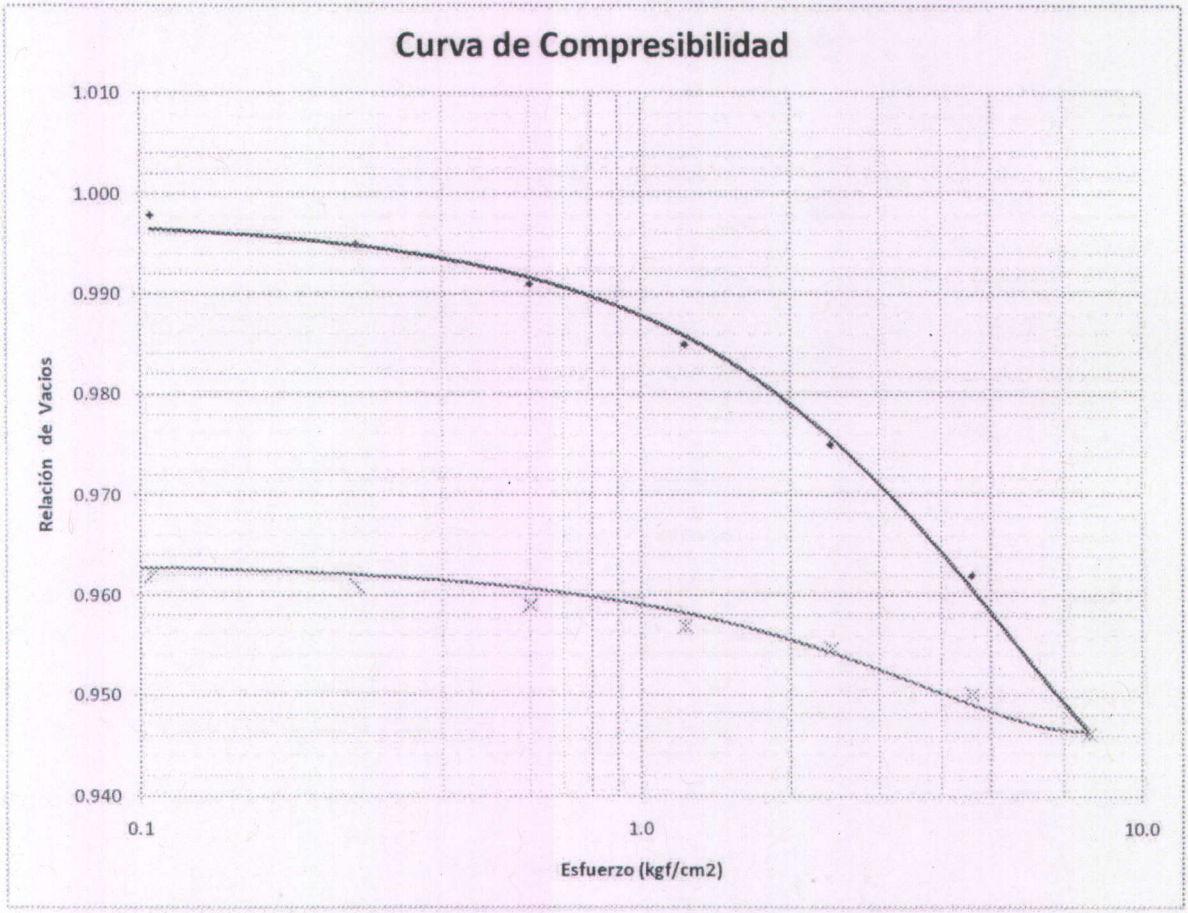
OBSERVACIONES:

JEFE DE SECCIÓN	RESPONSABLE DE LOS SERVICIOS DE EXTENSIÓN	JEFE DEL LABORATORIO
C. EFRAIN VALLEJO TOLEDANO	ING. SATURNINO PÉREZ FAJARDO	M. EN I. SERGIO ALEJANDRO DIAZ CAMACHO

CURVA DE COMPRESIBILIDAD

Compañía:	PROYECTO DE INVESTIGACIÓN UNIVERSIDAD DE QUÉBEC-FICIRA-UAEM	No. Orden:	CONS-CIRA-02
Nombre:	DETERMINAR LOS VALORES DE COMPRESIBILIDAD DE LAS ARCILLAS DEL VALLE DE TOLUCA.	Fecha muestre	2007-Oct-15
		Fecha prueba:	2007-Oct-22
Ubicación:	RIO LERMA, TEMOAYA, ESTADO DE MÉXICO.	Fecha reporte:	2007-Nov-30

No. de ensaye	S.P.T. No.	Muestra No.	Profundidad muestreo (m)	δ_s	ω_i (%)	ω_f (%)	e_i	e_f	Gw_i (%)	Gw_f (%)	Presión efectiva (kg/cm^2)
CIRA-02	1	1	9,00	2,44	38,56	42,08	1,01	0,971	93,19	100,00	1,65



MÉTODOS DE ENSAYE UTILIZADOS:
ASTM D 4186-89: STANDART TEST METHOD FOR ONE-DIMENSIONAL CONSOLIDATION PROPERTIES OF SOILS USING CONTROLLED - STRAIN LOADING.

Notas: **Los resultados son válidos sólo para los elementos ensayados.**
Este informe sólo es válido en su forma original. No debe ser reproducido sin la aprobación por escrito del Laboratorio de Materiales de la Facultad de Ingeniería de la U.A.E.M.

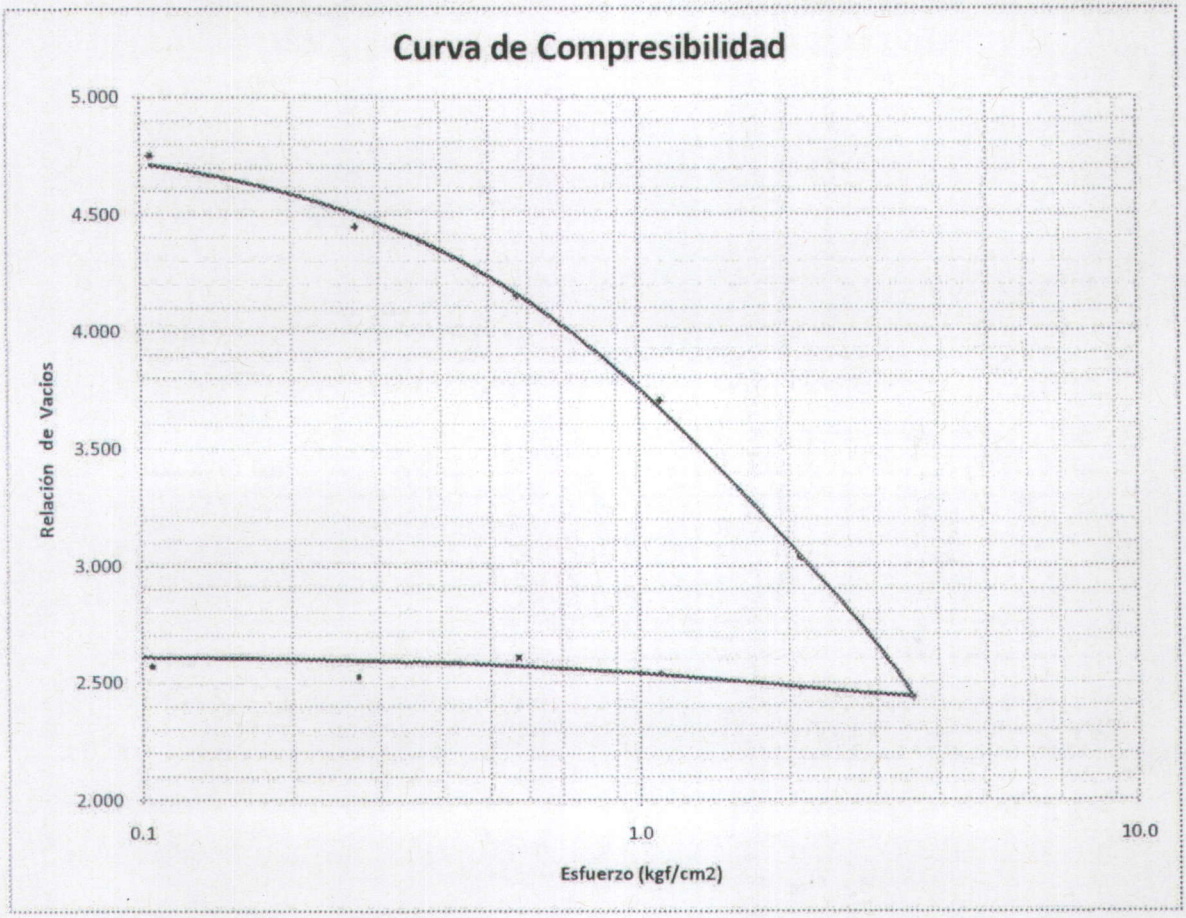
OBSERVACIONES:

JEFE DE SECCIÓN	RESPONSABLE DE LOS SERVICIOS DE EXTENSIÓN	JEFE DEL LABORATORIO
C. EFRAÍN VALLEJO TOLEDANO	ING. SATURNINO PEREZ PAJARDO	M. EN I. SERGIO ALEJANDRO DIAZ CAMACHO

CURVA DE COMPRESIBILIDAD

Compañía:	PROYECTO DE INVESTIGACIÓN UNIVERSIDAD DE QUÉBEC-FICIRA-UAEM	No. Orden:	CONS-CIRA-04
Nombre:	**DETERMINAR LOS VALORES DE COMPRESIBILIDAD DE LAS ARCILLAS DEL VALLE DE TOLUCA.**	Fecha muestre	2007-Ago-27
		Fecha prueba:	2007-Sep-09
Ubicación:	RIO LERMA, SAN MATEO ATENCO, ESTADO DE MÉXICO.	Fecha reporte:	2007-Nov-30

No. de ensaye	S.P.T. No.	Muestra No.	Profundidad muestreo (m)	δ_s	ω_i (%)	ω_f (%)	e_i	e_f	Gw_i (%)	Gw_f (%)	Presión efectiva (kg/cm^2)
CIRA-03	1	1	7,00-7,50	2,32	191,96	113,57	5,00	2,690	89,05	97,96	0,54



MÉTODOS DE ENSAYE UTILIZADOS:
ASTM D 4186-89: STANDART TEST METHOD FOR ONE-DIMENSIONAL CONSOLIDATION PROPERTIES OF SOILS USING CONTROLLED - STRAIN LOADING.

Notas: **Los resultados son válidos sólo para los elementos ensayados.**
Este informe sólo es válido en su forma original. No debe ser reproducido sin la aprobación por escrito del Laboratorio de Materiales de la Facultad de Ingeniería de la U.A.E.M.

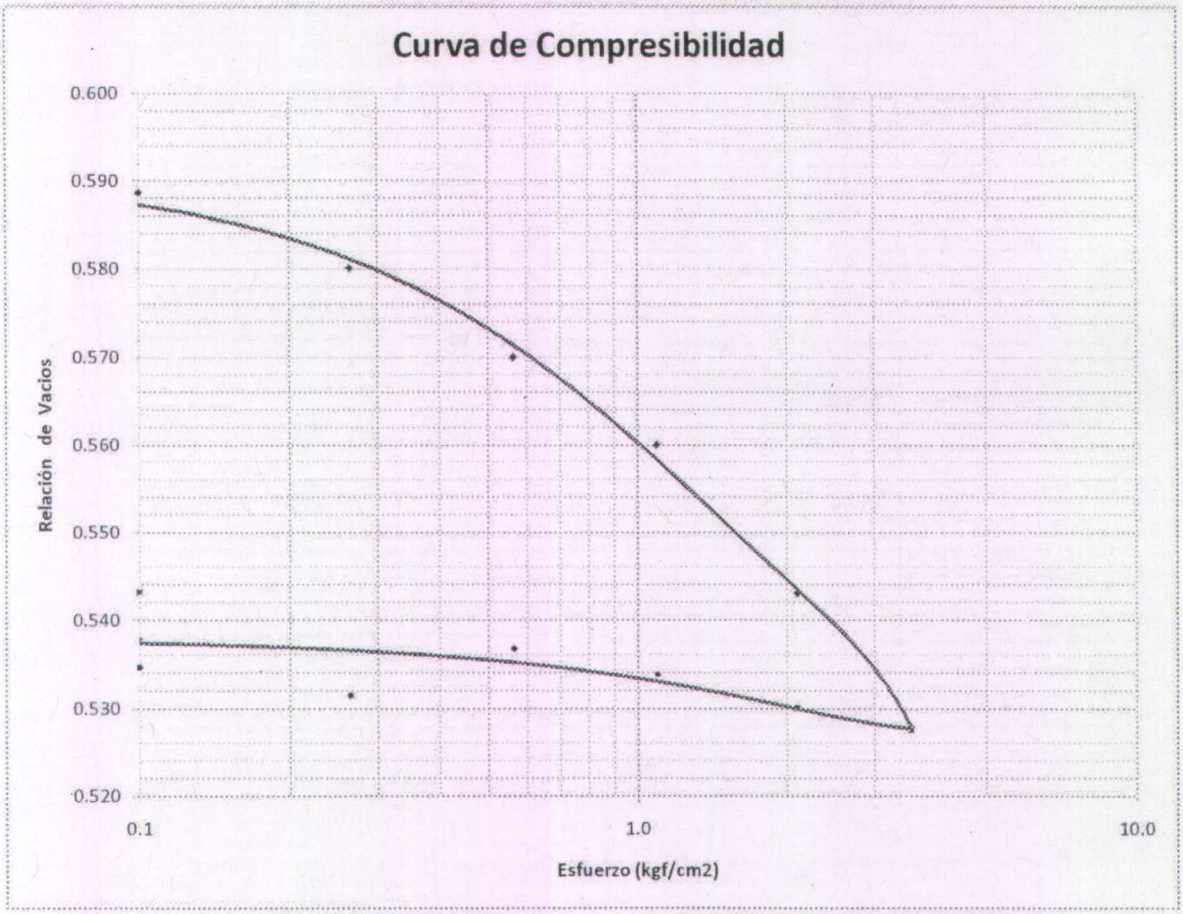
OBSERVACIONES:

JEFE DE SECCIÓN	RESPONSABLE DE LOS SERVICIOS DE EXTENSIÓN	JEFE DEL LABORATORIO
C. EFRAIN VALLEJO TOLEDANO	ING. SATURNINO PÉREZ FAJARDO	M. EN I. SERGIO ALEJANDRO DÍAZ CAMACHO

CURVA DE COMPRESIBILIDAD

Compañía:	PROYECTO DE INVESTIGACIÓN UNIVERSIDAD DE QUÉBEC-FICIRA-UAEM	No. Orden:	CONS-CIRA-05
Nombre:	**DETERMINAR LOS VALORES DE COMPRESIBILIDAD DE LAS ARCILLAS DEL VALLE DE TOLUCA.**	Fecha muestre	2007-Ago-27
		Fecha prueba:	2007-Sep-17
Ubicación:	RIO LERMA, SAN MATEO ATENCO, ESTADO DE MÉXICO.	Fecha reporte:	2007-Nov-30

No. de ensaye	S.P.T. No.	Muestra No.	Profundidad muestreo (m)	δ_s	ω_i (%)	ω_f (%)	e_i	e_f	Gw_i (%)	Gw_f (%)	Presión efectiva (kg/cm^2)
CIRA-04	1	2	28,0-28,2	2,62	23,96	22,53	0,604	0,548	100,00	100,00	0,46



MÉTODOS DE ENSAYE UTILIZADOS:
ASTM D 4186-89: STANDART TEST METHOD FOR ONE-DIMENSIONAL CONSOLIDATION PROPERTIES OF SOILS USING CONTROLLED - STRAIN LOADING.

Notas: **Los resultados son válidos sólo para los elementos ensayados.**
Este informe sólo es válido en su forma original. No debe ser reproducido sin la aprobación por escrito del Laboratorio de Materiales de la Facultad de Ingeniería de la U.A.E.M.

OBSERVACIONES:

JEFE DE SECCIÓN	RESPONSABLE DE LOS SERVICIOS DE EXTENSIÓN	JEFE DEL LABORATORIO
C. EFRAIN VALLEJO TOLEDANO	ING. SATURNINO PÉREZ FAJARDO	M. EN I. SERGIO ALEJANDRO DIAZ CAMACHO

ANNEXE E – Modèles d'évapotranspiration

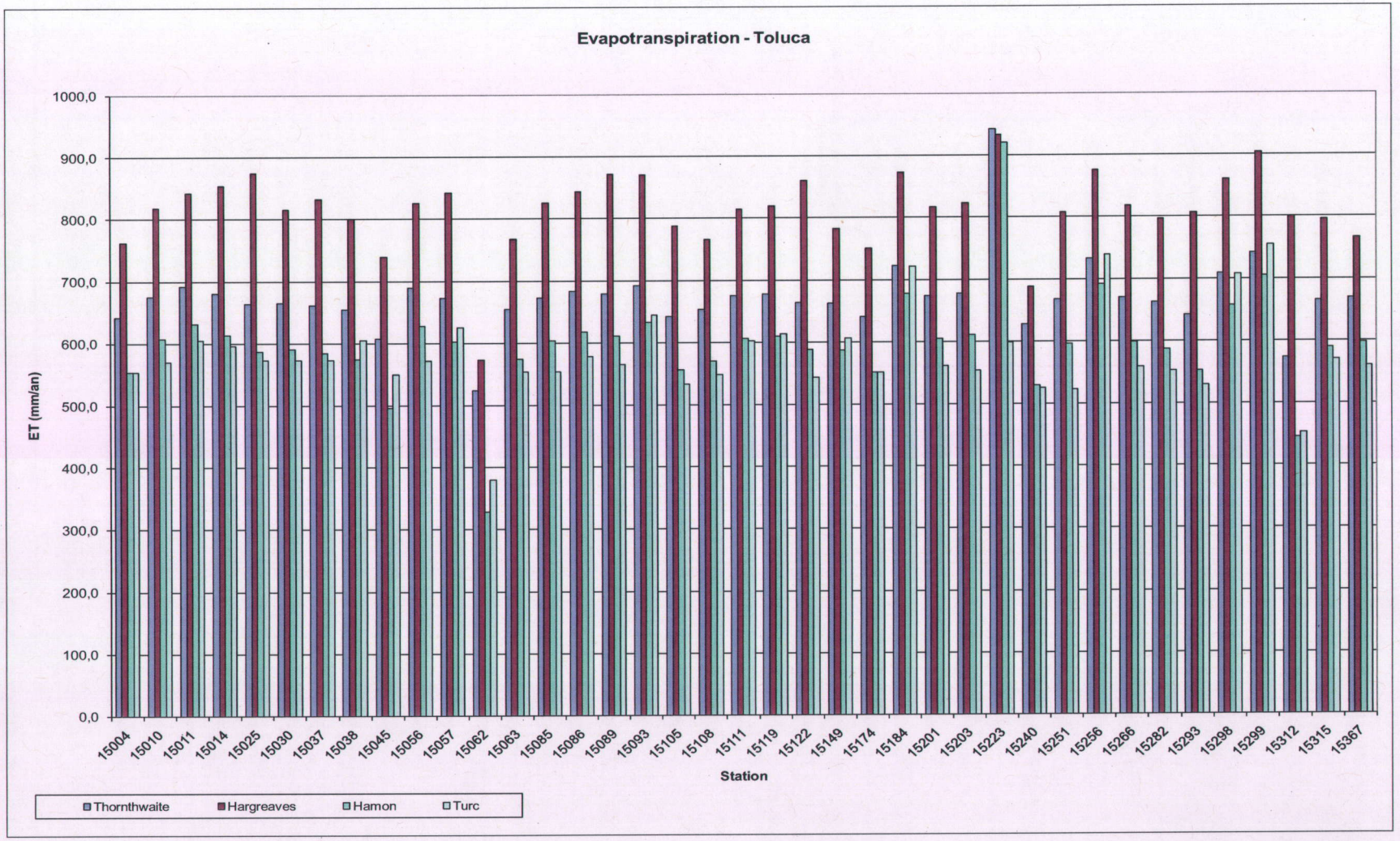


Figure 1: Etude comparative de l'évapotranspirations (Thornthwaite, Hargreaves, Hamon, Turc) à 39 stations météorologique dans la vallé de Toluca.

ANNEXE F - D-InSAR description and discussion on limitations

Annexe F: D-InSAR description and discussion on limitations

D-InSAR description

The basic D-InSAR geometry is highlighted in the following diagram:

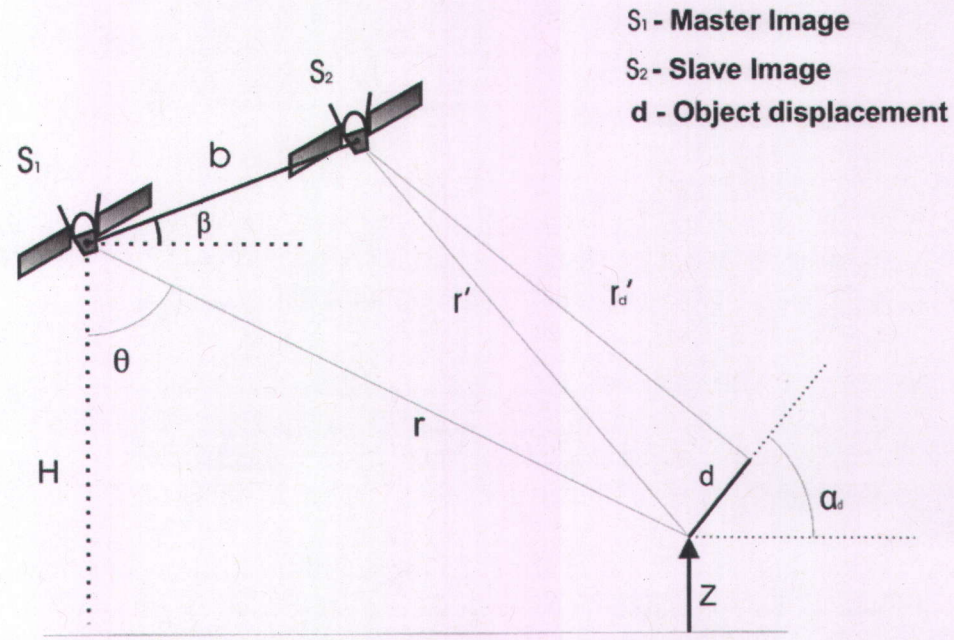


Figure 1: D-InSAR geometry to calculate surface displacement (Modified from Raisinghani, 2007)

In figure 1, the surface point with height z is displaced a distance d in the α_d direction. Hence, the target range for the slave image is now r_d'.

To estimate error, let the following relation apply:

$$\Phi(x,r) = \frac{4\pi}{\lambda}\delta r \qquad (1)$$

Where $\Phi(x,r)$ is the phase difference for each image pixel. Thus From the phase information obtained by radar satellites, the slant range difference can be obtained.

$$\delta r = \frac{\lambda}{4\pi}\Delta\Phi(x,r) \qquad (2)$$

$$\Delta(\delta r) = \frac{\lambda}{4\pi}\Delta\Phi(x,r) \qquad (3)$$

Taking, for example, a system operating with C-band (λ = 5.6 cm) and the error in the phase difference $(\Delta\Phi(x,r))$ of 30°, gives $\Delta(\delta r)$ = 2.3mm.

In the figure above, the surface point with height z is displaced a distance d in the α_d direction. Hence, the target range for the slave image is now r_d'. From equation (2) above, the following relation is obtained:

$$\Phi = \frac{4\pi}{\lambda}(r_d - r) = \frac{4\pi}{\lambda}(r_d' - r' + r' - r) = \frac{4\pi}{\lambda}(\delta r_d + \delta r) \qquad (4)$$

$$\frac{\lambda\Phi}{4\pi} = \delta r_d + \delta r \qquad (5)$$

Hence, the phase has contributions from both the target slant range displacement values and the topography δr; the latter contribution arising due to the presence of a baseline b. Thus, in the ideal case where the master and slave image passes occur on exactly the same orbit (b = 0), there are no topographic contributions and from the above geometry:

$$\delta r_d \approx d\cos(90° - \theta + \alpha_d) = d\sin(\theta - \alpha_d) \qquad (6)$$

Essentially, using D-InSAR, one can obtain the slant range displacement values δr_d' from which they can then determine *d* by prior knowledge of the landscape slope α_d.

However, the assumption that b= 0 is not realistic, so there will be some topographical displacement contribution. This is why small baselines are sought when using the D-InSAR technique to minimize that contribution. In addition, higher-resolution DEM's lead to better accuracy in determining δr which then leads to greater accuracy in determining δr_d.

Consider the following equation:

$$\varepsilon_z = \frac{r\sin\vartheta}{b_\perp} \cdot \varepsilon_{\delta r} \qquad (7)$$

Where ε_z represents the height accuracy of the object and $\varepsilon_{\delta r}$ is the corresponding accuracy on the topographic height profile (the negative sign is omitted since dealing with just the magnitude). If one uses the SRTM DEM, then ε_z = 90m and from the above equation, $\varepsilon_{\delta r}$ =1.6cm. This error is then transferred to δr_d when the δr contribution is subtracted (Franceschetti and Lanari, 1999).

Limitations of D-InSAR

Several factors influence the quality of an interferogram and the output products such as a deformation map. Five important points to consider are:

1- Perpendicular baselines between acquisitions have upper limits. Typical values for maximum usable baseline separation are less than 600 m for ERS-1/2, ENVISAT ASAR, and RADARSAT-1. In certain conditions RADARSAT-1 can have up to 800 m of perpendicular baseline. JERS-1 and ALOS allow for larger baseline however normally the baselines should be less than 1.5 km (Wegmüller et al., 2006). RADARSAT-2 is expected to have relatively small perpendicular baselines – suitable for InSAR processing (MDA, 2009).

2- Atmospheric effects - The main error term concerning the deformation rate accuracy achievable for areas of sufficient coherence, is related to the heterogeneity of the atmospheric path delay (Zebker et al., 1997). Spatial variability of the atmosphere changes with time thus fringes produced by atmospheric effects (essentially in the ionosphere and in the troposphere – i.e. clouds) should not have fixed geographic position in interferometric pairs taken at different times.

3- The terrain being imaged may change between passes of the SAR. This may result in one of two types of effects on the phase information:

- Systematic phase effects caused by large-scale motion during the time interval between the passes, for example: a city may subside. In this case if movement of the terrain between the acquisitions is larger than $\lambda/2$ (equal to interferometric fringe) only the phase between 0 and 2π of the deformation is obtained and not the whole $n2\pi+\phi$. Thus in the case of C-band (λ = 5.6 cm) the maximum detectable movement in the LOS between acquisitions is 2.8 cm. This restricts the applicability of D-InSAR to relative slow moving deformation.

- Random phase effects caused by decorrelation of the phase contributions of scatterers within the resolution cells. We call this *temporal decorrelation*. This often results in cells or entire areas being of little use for interferometry (MDA, 2007). Vegetation growth or movement is a common cause of the random phase effect.

4- As with all SAR imagery, high spatial resolution greatly influences the utility of the imagery for a particular application. With respect to the sensors, RADARSAT-2 (3.0 metres) and TerraSAR-X (1.0 metre) have among the finest resolutions. The DEM resolution is also an important factor in properly removing the topographic phase component. A higher resolution DEM will lead to proper removal of the topographic phase, and thus better deformation information.

5- Band type and wavelength - Differences in sensor wavelength have a varying effect on InSAR results. Several band types exist from different sensors (Table 1). C-Band is a mid-spectrum frequency, where the midsized wavelength enables better resolution than L-band yet worse than X-band. However, C-Band tolerates higher vegetative cover than X-band yet less than L-band. Incomplete spatial coverage caused by temporal decorrelation and problems in resolving high spatial phase gradients are limitations of C-band and X-

band INSAR (Wegmüller et al., 2006). With L-band these limitations are reduced due to the longer wavelength. Strozzi et al. (2003) demonstrated that L-band coherence over forest can be high enough to permit interpretation of the interferometric phases, not possible with C-band. X-band has an even smaller wavelength than C-band, thus for longer acquisition intervals, its use is limited to areas with minimal vegetation. However, assuming ideal conditions (minimal vegetative cover, small spatial/temporal decorrelation), higher resolution is obtained by the shorter wavelength. Advantages and disadvantages are found for all wavelengths, and each wavelength might be more suitable for a particular application. Due to the availability of data, this study uses C-Band radar data from ERS-1, ERS-2, ENVISAT ASAR, and RADARSAT-1.

References:

Franceschetti, G. and Lanari, R., (1999). *Synthetic Aperture Radar Processing.* CRC Press, Boca Raton, FL, USA.

Raisinghani, H. (2007) Differential Interferometric SAR for Geohazard Analysis Individual Project Report. International Space University.

MDA, 2009 Radarsat-2 information website, http://www.radarsat2.info/ - Frequently Asked Questions section.

Strozzi T., Wegmüller, U., Werner, C., Wiesmann, A. and Spreckels, V. (2003) JERS SAR interferometry for land subsidence monitoring, IEEE Trans. Geosci. Remote Sensing, 41, 1702-1708

Wegmüller, U., Werner, C., Strozzi, T., & Wiesmann, A. (2006). APPLICATION OF SAR INTERFEROMETRIC TECHNIQUES FOR SURFACE DEFORMATION MONITORING. In, *3rd IAG / 12th FIG Symposium*. Baden, Austria: May 22-24

Zebker, H.A.; Rosen, P.A. & Hensley, S. (1997), "Atmospheric effects in inteferometric synthetic aperture radar surface deformation and topographic maps", *Journal of Geophysical Research* 102: 7547–75

ANNEXE G – Supplementary data for the HELP3 Model

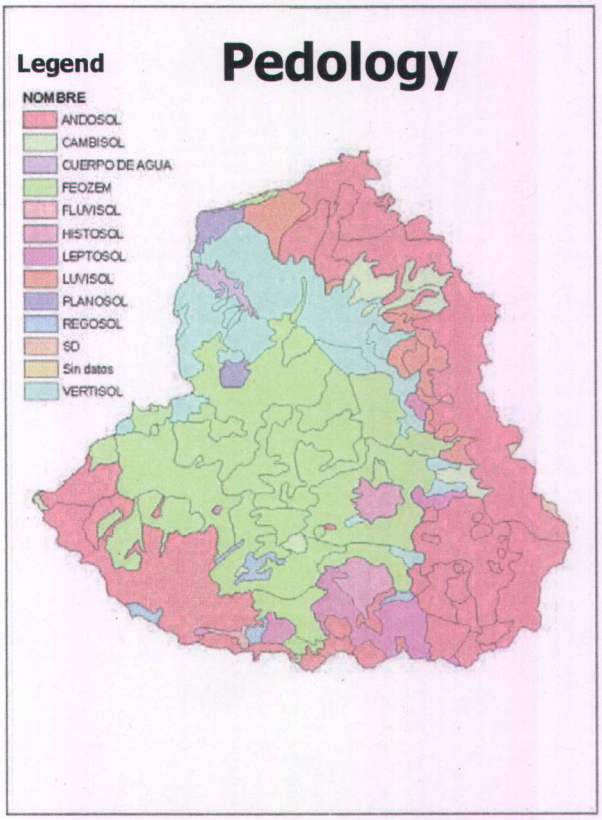


Figure 1: 2D Pedology of the Toluca Valley used for the HELP3 Model.

Table 1: Pedology values used for porosity, Field Capacity, Wilting point, K_{sat}, and SCS Curve number.

Soil name	code	Code #	Help code	porosity	Field Capacity	Wilting Point	Ksat	SCS Curve # Type (A,B,C,D)
ANDOSOL	T	0	3	0.457	0.083	0,033	3,1E-03	B
PLANOSOL	W	1	24	0,365	0,305	0.202	2,7E-06	C
LUVISOL	L	2	26	0,445	0,393	0.277	1,9E-06	C
FEOZEM	H	3	6	0,453	0,19	0.085	7,2E-04	B
VERTISOL	V	4	28	0,452	0,411	0.311	1,2E-06	D
CAMBISOL	B	5	3	0.457	0.083	0,033	3,1E-03	B
water		6	na	na	na	na	na	na
LEPTOSOL	I	7	1	0,417	0,045	0.018	1,0E-02	A
HISTOSOL	O	8	29	0,451	0,419	0.332	6,8E-06	D
REGOSOL	R	9	4	0,437	0,105	0.047	1,7E-03	A
FLUVISOL	J	10	2	0,437	0,062	0.024	5,8E-03	A

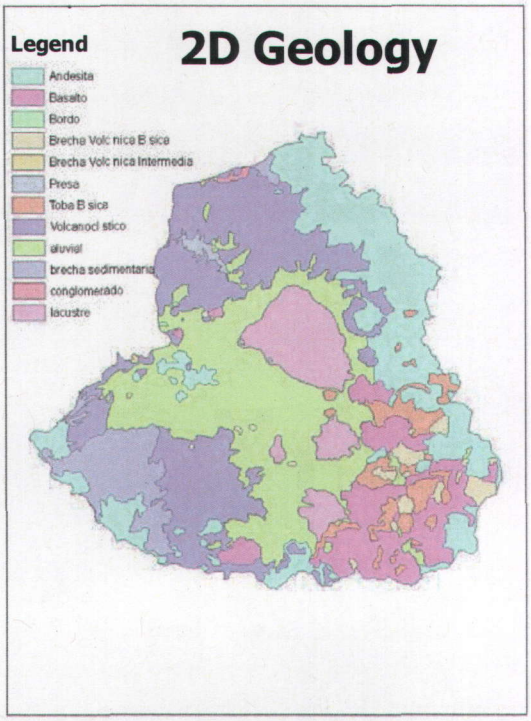


Figure 2: 2D Geology of the Toluca Valley used for the HELP3 Model. Included are values for porosity, Field Capacity, Wilting point, K_{sat}, and SCS Curve number.

Table 2: Geology values used for porosity, Field Capacity, Wilting point, K_{sat}, and SCS Curve number.

	Code #	Total Porosity	Field Capacity	Wilting Point	Ksat	SCS Curve #
Volcanoclasts	0	0,3	0,45	0,1	7,00E-04	B
Andesite	1	0,3	0,45	0,1	2,00E-04	C
Sedimentary Brechia	2	0,3	0,45	0,1	5,00E-03	C
Alluvial	3	0,437	0,062	0,024	3,00E-03	A
Conglomerate	4	0,3	0,45	0,1	2,00E-04	B
PRESA	5	0,2	0,5	0,4	2,00E-05	C
Lacustrial	6	0,451	0,419	0,332	2,00E-07	D
BORDO	7	0,3	0,45	0,1	2,00E-04	B
Basalt	8	0,3	0,5	0,4	5,00E-04	C
Toba Basico	9	0,3	0,45	0,1	2,00E-04	B
Basic Volcanic Brecia	10	0,35	0,45	0,1	2,00E-04	C
Intermediate Volcanic Brecia	11	0,3	0,45	0,1	2,00E-04	C

Annexe H – Sources of Uncertainty

In this appendix, the uncertainty in the quantification of land subsidence of the Toluca Valley is examined. There are several sources of uncertainty ranging from field data, remote sensing methods, and numerical modeling. With field data, the quality of the data gathered is a source of uncertainty, uncertainty can be attributed to measured parameters such as *h, Ss S'skv, S'ske, K, θ, compaction* (Chapters 2, 3, 4), in turn uncertainty can be attributed to the quality of the generated products: 3D geological model (Chapter 4), the the water balance (recharge, discharge, deficit) (Chapter2).

With InSAR generated results, there are also several sources of uncertainty. The quality of the satellite image gathered, the method for generating the interferogram, the quality of the subsidence maps (unwrapping techniques used) are all sources of uncertainty. It should be noted that the quality of the DEM can reduce uncertainty. In Chapter 3 it is noted that a higher resolution DEM was not available for the Toluca Valley, thus an SRTM 90 m was used.

In addition to the above uncertainties, the modeling aspect of the work presented in this thesis is also a source of uncertainty. Using an instantaneous compaction approach to modeling the behaviours of the Toluca Valley clays are also a source of uncertainty. Incorporating other physical characteristics, such as time delays, hydraulic conductivity dependence, and other could improve the uncertainty. Additionally, the numerical method used to solve the equations: finite difference vs. finite element or implicit vs. explicit solution techniques are sources of uncertainty. .

Thus, the choice of the parameters chosen to analyze uncertainty in the subsidence of the Toluca Valley is arbitrary. Since pumping scenarios for future simulations (best case, worst case, average case) (Chapter 5), and climate change (Chapter 2) were examined, the focus of this uncertainty analysis focuses on the material properties and more specifically on varying the elastic skeletal specific storage (S'_{skv}). This parameter is by far the most sensitive material property parameter to compaction representation.

Based on table 1, the S'_{skv} for the clay layers were varied by both 0.5 and 1 order of magnitude. That is to say that the clay layers (layers 1, 4, 9, and 12) were varied upward and downward by half an order of magnitude. The values were varied based on field observation.

Table 1: Description of material properties for the Toluca Valley.

Clay layer	Average case	Best case	Worst case
Clay layer 1	3,7E-6	8,7E-7	8,7E-6
Clay layer 2	4,2E-7	9,2E-8	9,2E-6
Clay layer 3	4,4E-7	9,4E-8	9,4E-7
Clay layer 4	7,5E-7	2,5E-7	2,5E-6

The results of the simulations are presented in Figure 1. As predicted, results show that S'skv is a very sensitive parameter. There are very

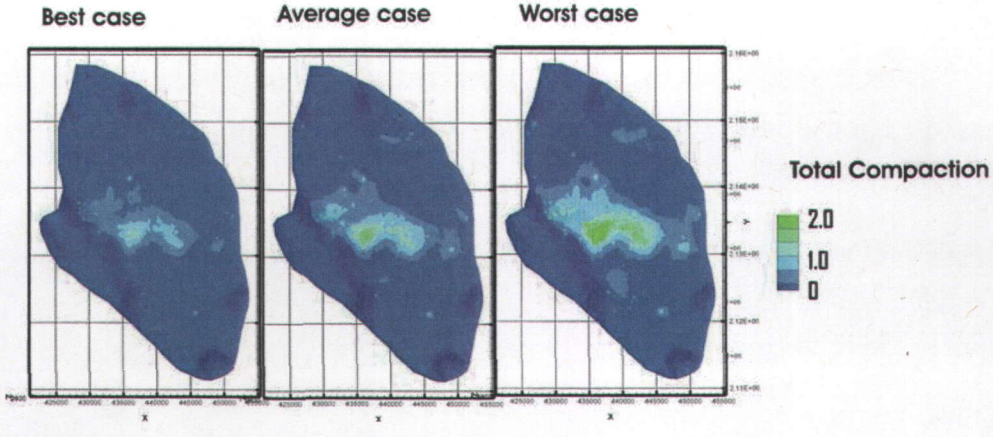


Figure 1 Total compaction (m) for the best case, average case and worst case, varying S'_{skv}

The average expected subsidence is 1.3 m. Maximum subsidence in the best case and worst case scenarios are 0.9 m and 2.0 m respectively. The exercise has shown the importance of accurate and a large quantity of field data. A better characterization of the geological structure and better estimates for S'skv will decrease uncertainty in the results and improve predictions.